

On Discovering New Facets of Cholesterol in Model Cell Membranes: the Molecular Interplay with Biological Water

M. Eng. Hanna Orlikowska-Rzeźnik



supervisor: Dr. habil. Eng. Łukasz Piątkowski, Prof. PUT

Poznan University of Technology
Faculty of Materials Engineering and Technical Physics
Institute of Physics

September 2024

*A thesis submitted in partial fulfillment of the requirements for the degree
of Doctor of Philosophy*

Dla wszystkich mieszkańców Leśnej, stałych i tymczasowych

Contents

Abstract	7
Streszczenie	9
Funding	11
Abbreviations	13
Preface	15
1 Introduction	17
1.1 Motivation	17
1.2 Outline	18
2 Cell membranes	21
2.1 Membrane organelles and their functions	21
2.2 Membrane lipid composition and structure	24
2.3 Cell membrane models	26
2.3.1 Lipid vesicles	27
2.3.2 Solid-supported lipid bilayers	28
2.3.3 Lipid monolayers	29
3 Cholesterol and membrane fluidity	31
3.1 Lipid movements	31
3.2 Impact of cholesterol on phospholipid membranes	32
3.2.1 Lipid phases	33
3.2.2 Lipid rafts	34
4 Biological water	37
4.1 Water chemistry	37
4.2 Hydrogen bond network	37
4.3 Hydrophobic effect	38
4.4 Interactions between membrane and interfacial water	40
4.4.1 Properties of interfacial water	40
4.4.2 Impact of biological water on biomembranes	40
4.4.3 Cellular membrane dehydration events	41

5	Molecular spectroscopy and imaging	43
5.1	Fluorescence spectroscopy	43
5.1.1	Jablonski diagram	43
5.1.2	Solvent relaxation	45
5.2	Fluorescence microscopy	45
5.2.1	Fluorescent membrane probes	47
5.3	Sum-frequency generation spectroscopy	49
5.3.1	Origin of sum-frequency generation	49
5.3.2	Resonant vibrational sum frequency generation	50
6	Laurdan discerns lipid membrane hydration and cholesterol content	53
7	Dehydration of lipid membrane drives redistribution of cholesterol between lateral domains	77
8	Cholesterol changes interfacial water alignment in model cell membranes	95
9	Summary	113
10	Scientific achievements	117
10.1	Education	117
10.2	Internships	117
10.3	Publications	118
10.4	Published, indexed conference materials	120
10.5	Participation in conferences	121
10.6	Patent activity	123
10.7	Scientific grants	123
10.8	Scholarships	124
10.9	Other prizes and awards	125
	Bibliography	126
	Declarations of co-authors	141
	Acknowledgments	151

Abstract

Biological cell membranes are intricate structures influenced by interactions among diverse membrane constituents and surrounding water. These biomembranes exhibit significant heterogeneity in both lipid phases and interfacial water structure and dynamics, which is crucial for cellular biochemical activity. While cholesterol is known to regulate membrane structure and dynamics, its impact on membrane hydration remains elusive. This thesis explores these interactions at a molecular level to enhance our understanding of the origin and function of the membrane physico-chemical heterogeneities.

Fluorescent environmentally sensitive probes like Laurdan are commonly used to study membrane heterogeneity. Laurdan's emission spectrum shifts are linked to changes in water molecule concentration and mobility near the probe. However, the lack of direct hydration measurements has often led to misinterpretations. In this doctoral thesis, I investigated Laurdan's spectral response to biomimetic membrane dehydration and cholesterol content, revealing the molecular mechanisms behind these changes. Dehydration induces lipid conformational ordering, restricts lipid motions, and slows hydrogen bond dynamics, impeding dipolar relaxation around Laurdan. Cholesterol incorporation, on the other hand, affects the fluorescence mainly by hindering the lipid glycerol backbone dynamics.

Fluorescence spectroscopy and microscopy experiments lead to a novel finding of the redistribution of cholesterol in phase-separated membranes under dehydration, which likely counteracts extensive fluidity changes in specific membrane regions. My results show that cholesterol's affinity for different lipid phases reverses as membrane hydration decreases. Dehydration causes lipid tails to straighten, reducing hydrophobic mismatch and aligning lipid packing, which facilitates cholesterol interaction with fluid-phase-forming lipids.

Finally, using broad-band heterodyne-detected sum frequency generation spectroscopy I probed the vibrational signatures of lipids and nanoscopic water layer hydrating the membrane. The study revealed that cholesterol disrupts the interheadgroup hydration shell in unsaturated lipid environment, depolarizing water orientation. In saturated lipid membranes, cholesterol increases lipid packing and orders headgroups, increasing water molecule orientational anisotropy. In sphingomyelin environment, due to strong condensing effect, cholesterol stabilizes highly anisotropic net orientation of interfacial water molecules.

These findings highlight the importance of cholesterol-lipid-water interplay in defining the membrane architectural and dynamical heterogeneities, including the hydration water layer.

Streszczenie

Błony komórkowe to skomplikowane struktury, na które wpływają interakcje między różnorodnymi składnikami oraz otaczającą je wodą. Biomembrany wykazują znaczną heterogeniczność zarówno jeśli chodzi o fazy lipidowe, jak i strukturę i dynamikę hydratującej je wody, co jest kluczowe dla ich aktywności biochemicznej. Choć wiadomo, że cholesterol reguluje strukturę i dynamikę błon, jego wpływ na ich uwodnienie nie jest jeszcze w pełni zrozumiany. Niniejsza praca doktorska bada te interakcje na poziomie molekularnym, aby lepiej zrozumieć pochodzenie i funkcję fizykochemicznych heterogeniczności błon.

Fluorescencyjne sondy wrażliwe na środowisko, takie jak Laurdan, są często stosowane do badania heterogeniczności błon. Zmiany w widmie emisji Laurdanu są związane ze zmianami stężenia i ruchliwości cząsteczek wody w pobliżu sondy. Jednak brak bezpośrednich pomiarów uwodnienia często prowadził do błędnych interpretacji. W ramach niniejszej pracy doktorskiej, dokonałam analizy odpowiedzi spektralnej Laurdanu na odwodnienie błon biomimetycznych oraz na zawartość cholesterolu, ujawniając mechanizmy molekularne stojące za tymi zmianami. Odwodnienie powoduje uporządkowanie konformacyjne lipidów, spowalnia ich dynamikę oraz dynamikę wiązań wodorowych, co utrudnia relaksację dipolową wokół Laurdanu. Z kolei obecność cholesterolu wpływa na fluorescencję głównie przez hamowanie dynamiki szkieletu glicerolowego lipidów.

Eksperymenty z wykorzystaniem spektroskopii i mikroskopii fluorescencyjnej ujawniły nowy efekt dotyczący redystrybucji cholesterolu w błonach fazowo rozdzielonych pod wpływem odwodnienia, co prawdopodobnie przeciwdziała znacznym zmianom płynności w określonych regionach błony. Wyniki pokazują, że powinowactwo cholesterolu do różnych faz lipidowych zmienia się w miarę zmniejszania uwodnienia błony. Odwodnienie prowadzi do prostowania ogonów lipidowych, co redukuje niedopasowanie hydrofobowe i wyrównuje upakowanie lipidów, ułatwiając w ten sposób interakcję cholesterolu z lipidami w fazie płynnej.

Stosując spektroskopię generacji sumy częstotliwości, zbadałam wibracyjne sygnatury lipidów oraz nanoskopowej warstwy wody bezpośrednio hydratującej błonę. Badania wykazały, że będąc w środowisku lipidów nienasyconych, cholesterol przerywa warstwę hydratacyjną między grupami polarnymi lipidów, depolaryzując orientację cząsteczek wody. W błonach z lipidów nasyconych, cholesterol zwiększa upakowanie lipidów i porządkuje grupy polarne, co prowadzi do wzrostu anizotropii orientacyjnej cząsteczek wody. W środowisku sfingomieliny, z powodu silnego efektu kondensacji, cholesterol stabilizuje wysoce anizotropową orientację cząsteczek wody.

Odkrycia te podkreślają istotną rolę interakcji cholesterolu, lipidów i wody w kształtowaniu architektonicznych i dynamicznych heterogeniczności błon, włączając warstwę hydratacyjną.

Funding

The research presented in this thesis was funded by:

Diamond Grant, Ministry of Science and Higher Education, *Stimulated emission microscopy for imaging of systems with very low fluorescence efficiency, in particular selected components of model biological membranes*, grant number: 0042/DIA/2019/48, principal investigator: M. Eng. Hanna Orlikowska-Rzeźnik.

Opus, National Science Centre (Poland), *Seeing the invisible – elucidating the nature of sterol aggregates in biomimetic cell membranes using modulation transfer microscopy*, grant number: 2020/37/B/ST4/01785, principal investigator: Dr. habil. Eng. Łukasz Piątkowski, Prof. PUT.

Preludium, National Science Centre (Poland), *Unraveling the effect of steroid hormones on biophysical properties of biomimetic cell membranes*, grant number: 2022/45/N/ST4/01442, principal investigator: M. Eng. Hanna Orlikowska-Rzeźnik.

EMBO Installation Grant, European Molecular Biology Organization, *Biological water: the role of hydration in cell membrane organization*, grant number: IG 4147, principal investigator: Dr. habil. Eng. Łukasz Piątkowski, Prof. PUT.

INPUTDoc Project 'Towards Internationalization of Poznan University of Technology Doctoral School' (2022-2024) within the STER Programme, co-financed by Polish National Agency for Academic Exchange (NAWA).



Ministry of Science and Higher Education
Republic of Poland



NATIONAL SCIENCE CENTRE
POLAND



Abbreviations

AC	alternating current
APD	avalanche photodiode
ATP	adenosine triphosphate
BmP	bis(monoacylglycero)phosphate
CL	cardiolipin
CCD	charge-coupled device
Chol	cholesterol
D	lateral diffusion coefficient
DFG	difference frequency generation
DNA	deoxyribonucleic acid
EPR	electron paramagnetic resonance
ER	endoplasmic reticulum
FRAP	fluorescence recovery after photobleaching
GPI	glycophosphatidylinositol
GPMV	giant plasma membrane vesicle
GUV	giant unilamellar vesicle
HD-VSFG	heterodyne-detected vibrational sum frequency generation
HDL	high-density lipoprotein
HIV	human immunodeficiency virus
IR	infrared
ITO	indium tin oxide
L_d	Liquid disordered
LDL	low-density lipoprotein
L_o	Liquid ordered

ABBREVIATIONS

LUV	large unilamellar vesicle
MD	molecular dynamics
MHC	major histocompatibility complex
MLV	multilamellar vesicle
MVV	multivesicular vesicle
NA	numerical aperture
NMR	nuclear magnetic resonance
OR	optical rectification
PC	phosphatidylcholine
PE	phosphatidylethanolamine
PS	phosphatidylserine
PSM	plasma membrane spheres
RER	rough endoplasmic reticulum
S	order parameter
SARS-CoV-2	severe acute respiratory syndrome coronavirus 2
SER	smooth endoplasmic reticulum
SFG	sum frequency generation
SHG	second harmonic generation
SLB	supported lipid bilayer
SM	sphingomyelin
SNARE	soluble N-ethylmaleimide-sensitive factor activating protein receptor
SUV	small unilamellar vesicle
UV	ultraviolet
VSFG	vibrational sum frequency generation
VIS	visible

Preface

The cell is the most fundamental unit of any form of life, capable of carrying out all basic life processes such as metabolism, growth and reproduction. Whether as standalone entities in single-cell organisms or contributing to multicellular organisms, all living cells exhibit a unifying trait—their genetic material is encapsulated within a plasma membrane. In prokaryotes, which are always unicellular, such as bacteria and archaea, the plasma membrane is the only membranous structure within the cell. Their genetic blueprint—deoxyribonucleic acid (DNA) is freely floating in the cytoplasm.

Prokaryotes dominated the Earth for about 1.5 billion years since the origin of life (from 3.5 to 2 billion years ago). Then, around two billion years ago, a remarkable evolutionary event may have occurred. While the exact details remain unclear and will most likely forever be shrouded in mystery, it is speculated that one of those primitive cells—an archaea—swallowed a bacterium. Much like the tale of Jonah and the whale, the ingested bacterium survived and adapted within the archaea. Over time, the host and its internal guest developed a symbiotic relationship, leading to the emergence of a new type of cell with a complex internal membrane system. Eukaryotes, which can be either unicellular or multicellular, include organisms such as plants, fungi, and animals. Their cells contain membrane bound organelles, including the nucleus (enclosing the DNA), the endoplasmic reticulum, the Golgi apparatus, mitochondria, lysosomes (found in animal cells), and vacuoles and chloroplasts (found in plant cells).

Therefore, it can be stated without fail that the structure and function of all forms of existence rely vastly on membranes. While membranes are pivotal in all kingdoms of life, the focus of this thesis is on the eukaryotic cell membranes or to be even more precise—vertebrate animal cell membranes, as they contain cholesterol as the main sterol (most animals synthesize cholesterol, but there are exceptions—some invertebrate animals, such as certain insects and nematodes, rely on other sterols like ergosterol or sitosterol for similar functions in their cellular membranes).

During my internship at AMOLF, we had a lively and off-the-wall discussion with colleagues (Aswathi, Balazs, Alex, I am waving to you), during which my dear friend—Alex Korotkevich—asked a geeky question: which molecule would you like to be? I do not remember the answers of others, but I do remember mine—a lipid molecule (surprise, surprise). So, I invite you to dive in with me as lipid molecules into a membrane, into the world I have been immersed in for the last five years, where we will explore the molecular interactions among key cellular membrane components—phospholipids, cholesterol, and biological water.

1

Introduction

1.1 Motivation

Cholesterol plays a multifaceted role in biological systems. Its actions reflect a balance of light and shadow, resisting easy categorization as good or bad. In public discourse, cholesterol is frequently viewed negatively due to its association with high blood levels and atherosclerosis, often linked to overeating. It must be emphasized, however, that cholesterol is indispensable for proper functioning of humans and other animals. It is primarily a crucial and abundant component of vertebrate cell membranes.

Cholesterol is synthesized through a complex series of enzymatic steps in the endoplasmic reticulum and is subsequently transported through the Golgi apparatus to the plasma membrane, where its concentration is significantly higher than in other cellular compartments [1, 2]. Cellular membranes exhibit spatial heterogeneities in dynamics, structure and physico-chemical properties, e.g. membrane dipole potential [3]. Cholesterol plays a fundamental role in modulating these heterogeneities, particularly through the formation of lipid rafts—specialized nano- and microdomains enriched in cholesterol and sphingomyelin. These rafts are hypothesized to facilitate efficient signaling, trafficking of proteins and lipids, and control host-pathogen interactions [4]. Cholesterol influences membrane dynamics and structure by integrating into the phospholipid bilayer, affecting the ordering of lipid fatty acids, thereby stabilizing membrane fluidity [5]. It has a bilateral role here – depending on the membrane phospholipid composition and temperature, it either orders or disorders the fatty acids of lipids, further highlighting its unique and nuanced character. Additionally, cholesterol modulates membrane permeability, affecting the passage of molecules across the membrane, which further ensures optimal membrane function and cellular homeostasis [6].

The structural integrity of cellular membranes relies not only on phospholipids and cholesterol but also on the thin layer of water that hydrates the membrane. This biological water is vital for preserving cell structure, regulating biochemical activities, and controlling interactions at the membrane interface. While the interactions between cholesterol and phospholipids are well documented, their interplay with biological water remains less understood. Enhanced membrane dipole potential, a key property in ion channel activity, protein binding, and aggregation, has been shown to correlate with membrane cholesterol content and phase separation (abundance of raft-like domains rich in sphingomyelin and cholesterol) [7]. Membrane dipole potential arises from the anisotropic orientation of lipid dipolar moieties and the preferential alignment of interfacial water molecules. Mapping the membrane structure, including hydration, with a focus

on cholesterol's effect, could provide a clear molecular picture of the origin of composition-specific spatial heterogeneity at the lipid-water interface.

Large reservoirs of cholesterol are also found in blood serum in the form of high-density lipoprotein (HDL), and low-density lipoprotein (LDL) particles, commonly referred to as good and bad cholesterol, respectively, due to their contrasting roles in cholesterol transport and their effects on cardiovascular health. In brief, HDL particles collect excess cholesterol from tissues and transport it to the liver for excretion, reducing plaque buildup and promoting cardiovascular health. In contrast, LDL particles transport cholesterol from the liver to other tissues where it is used in membrane synthesis, hormone production, and other vital functions. Excess LDL cholesterol can accumulate in the walls of arteries, leading to the formation of atherosclerotic plaques, leading to cardiovascular disease. In cells, LDL particles are internalized through endocytosis, involving membrane fusion to form endosomes that eventually merge with lysosomes to release cholesterol. HDL particles facilitate the efflux of excess cholesterol from cells through membrane fusion with cell membranes. The intracellular transport of cholesterol involves vesicles and membrane organelles fusion, ensuring proper distribution and utilization [8]. Consequently, cholesterol cycles within cells and between cells, with many of these transport functions involving fusion between different membranes.

Membrane fusion involves transient, local membrane dehydration, integral not only to inter- and intracellular transport but also to various biological processes such as neurotransmission, fertilization, and viral entry (e.g., HIV, SARS-CoV-2, influenza) [9]. Mechanistic understanding of these processes thus requires revealing how reduced hydration affects the membrane structure and dynamics. Clearly, elucidating the phospholipid-cholesterol-water interactions is of paramount importance for understanding how membranes organize and regulate complex biological functions.

1.2 Outline

In this thesis, I present the results of investigations of the molecular-level interplay between phospholipids, cholesterol, and biological water in model cell membranes using visible and infrared light. The dissertation is based on three original, peer-reviewed articles:

1. **Hanna Orlikowska-Rzeznik***, Emilia Krok, Madhurima Chattopadhyay, Agnieszka Lester, Lukasz Piatkowski*,
Laurdan discerns lipid membrane hydration and cholesterol content
The Journal of Physical Chemistry B 127(15), 3382-3391 (2023)
doi: 10.1021/acs.jpcc.3c00654
IF: 3.5
2. **Hanna Orlikowska-Rzeznik***, Emilia Krok, Maria Domanska, Piotr Setny, Anna Łągowska, Madhurima Chattopadhyay, Lukasz Piatkowski*
Dehydration of lipid membrane drives redistribution of cholesterol between lateral domains
The Journal of Physical Chemistry Letters 15(16), 4515-4522 (2024)
doi: 10.1021/acs.jpclett.4c00332
IF: 5.7
3. **Hanna Orlikowska-Rzeznik***, Jan Versluis, Huib J. Bakker, Lukasz Piatkowski*
Cholesterol changes interfacial water alignment in model cell membranes
Journal of the American Chemical Society 146(19), 13151-13162 (2024)
doi: 10.1016/j.bbamem.2023.184194
IF: 15.0

*corresponding author(s)

The chapters, including full-length versions of the articles and their supplementary information (Chapters 6-8), are preceded by a theoretical background of bio- and biomimetic systems, effect of cholesterol on lipid membranes and the techniques employed in the studies (Chapters 2-5).

Chapter 2 introduces cell membranes, discussing their types, functions, composition, structural and dynamical properties, and the models used to study them.

Chapter 3 focuses on lipid membrane fluidity and the interactions of cholesterol with phospholipids.

Chapter 4 addresses the properties of biological water and its interactions with lipid membranes.

Chapter 5 introduces the basic principles of the experimental techniques used in the investigations—fluorescence spectroscopy and microscopy, and vibrational sum frequency generation spectroscopy.

Chapter 6 (publication 1), encompasses the first-time investigation of the spectral response of the environmentally-sensitive fluorescent probe Laurdan to the dehydration of model cell membranes, comparing it with the effect of increasing cholesterol content, and elucidation of the molecular mechanisms governing the observed changes in Laurdan's photophysics.

Chapter 7 (publication 2), reports that alteration in the interfacial hydration layer of a biomimetic membrane results in a significant intra-membranous redistribution of cholesterol between lateral domains and a restructuring of the inter-lipid hydrogen bond network.

Chapter 8 (publication 3) reveals that cholesterol, by modulating inter-lipid interactions in biomimetic membrane, alters the alignment of membrane interfacial water.

The final chapters provides the summary of the most important results of the thesis (Chapter 9) followed by my scientific path and achievements (Chapter 10).

2

Cell membranes

2.1 Membrane organelles and their functions

A hallmark of eukaryotic cells is their compartmentalized cytoplasm, housing various membrane organelles with specialized functions. The cell with this elaborate internal membrane system forms a network of distinct reaction vessels and pipelines, optimized for the efficient synthesis of specific chemical compounds and biochemical processes. Given the focus of this thesis on the models of vertebrate animal cell membranes (containing cholesterol), I feel the necessity to outline the membranous structures within the cells of these organisms along with their fundamental roles. There are the plasma membrane, endoplasmic reticulum, nuclear envelope, Golgi apparatus, endosomes, lysosomes, autophagosomes, lipid droplets, peroxisomes, and mitochondria (see Figure 2.1).

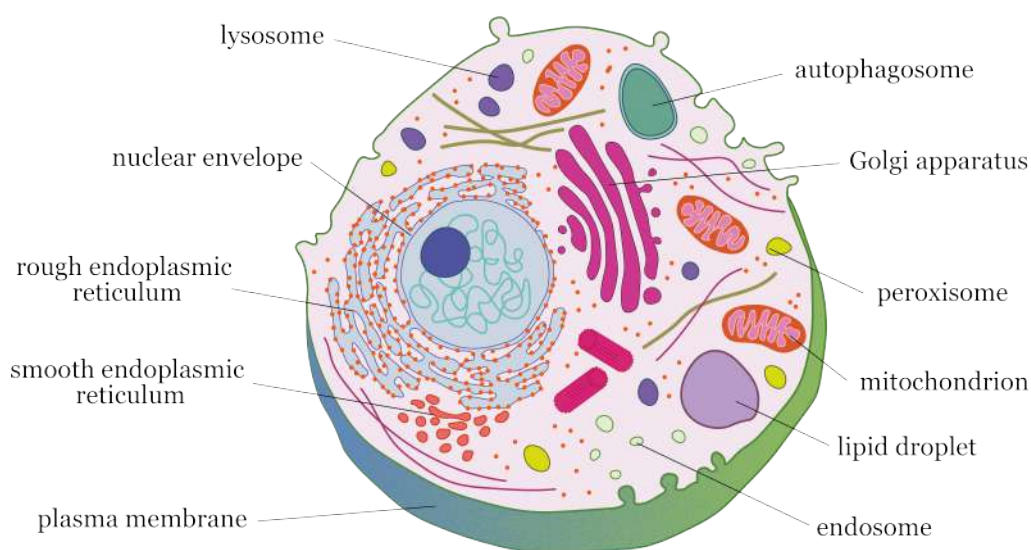


Figure 2.1: Membrane organelles found in all eukaryotic cells. The non-membranous organelles such as ribosomes, nucleolus, centrioles and cytoskeletal elements (microtubules) are shown for visual purposes.

Plasma Membrane. Being the outermost of cellular membranes, the plasma membrane has more diverse and complex functions compared to intracellular membranes. Serving as the primary interface between the cell and its microenvironment, it functions as both a physical and electrical barrier, controlling both the entry of materials into the cell and leakage of cellular contents, thereby preserving the appropriate internal conditions for cellular function. Plasma membrane plays an integral role in communication with neighbouring cells and the extracellular matrix through various integral or peripheral receptor proteins [10]. Binding of specific signaling molecules such as hormones, neurotransmitters, and growth factors from the external environment to the membrane embedded receptors initiates signal transduction pathways, where receptor activation leads to intracellular signaling cascades. These pathways regulate diverse cellular responses including gene expression, metabolism, growth, differentiation, and apoptosis.

Through integral tag molecules, e.g. glycoproteins and glycolipids, the plasma membrane facilitates cell-cell recognition, essential for the formation of tissues during embryonic development and its maintenance [11]. Plasma membrane proteins such as Major Histocompatibility Complex (MHC) molecules present fragments of foreign antigens to immune cells, enabling the immune system to distinguish between self and non-self molecules [12]. This recognition is critical for immune surveillance and the initiation of immune responses against pathogens while maintaining tolerance to the body's own cells.

Furthermore, the plasma membrane is crucial in maintaining the cell's mechanical integrity. It shapes the cell by adapting to the underlying cytoskeletal framework and supports cell motility through synchronized restructuring with cytoskeletal changes [13].

Endoplasmic reticulum (ER); rough ER (RER) and smooth ER (SER). The ER is the most expansive organelle, forming a tubular, sacs network that extends from the nuclear envelope to the cell's periphery. RER is studded with ribosomes and its primary function is to produce proteins destined to secretion into the extracellular matrix, or association with the cell membrane e.g. receptors and channels or to membrane-bound vesicles e.g. enzymes of lysosomes. Specialized receptors and channels on the RER's surface facilitate the transfer of proteins across the ER membrane. SER lacks ribosomes and is involved in the synthesis of lipids that form the membranes of all internal organelles and the plasma membrane. SER is involved also in detoxification, and calcium storage [14].

Nuclear Envelope. It is formed from two membrane bilayers, the inner and outer nuclear membrane, surrounding the nucleus. The outer membrane is continuous with the ER. Nuclear envelope protects genetic material and controls molecular traffic between the nucleus and cytoplasm via nuclear pores.

Golgi Apparatus. It consists of a series of flattened, interconnected membrane sacs arranged in a stack. Within the Golgi apparatus, hundreds of enzymes modify the entering proteins and lipids (derived primarily from ER). After modification, this organelle sorts these molecules into pathways directing them to the plasma membrane, lysosomes, endosomes, or back to the ER. Sphingolipids produced in the Golgi assist in this sorting process by forming raft domains that facilitate the export of cargo from the Golgi [15].

Mitochondria. Mitochondria consist of two bilayer membranes: an inner and an outer membrane separated by an intermembrane space. The inner membrane encloses the matrix containing a highly concentrated mixture of enzymes, mitochondrial DNA, ribosomes, and other components necessary for the mitochondrial functions. The matrix is the site of major energy-related activities. These activities encompass the Krebs cycle, which processes glycolytic products from the cytosol; β oxidation, which breaks down fatty acids into usable components; and oxidative phosphorylation, where adenosine triphosphate (ATP) is produced via the electron transport chain [16]. The inner membrane is highly convoluted, forming folds called cristae that project into the matrix of the mitochondrion. These cristae greatly increase the surface area

available for the production of ATP. Besides being a ‘powerhouse of the cell’, mitochondria also have a role to help maintain the intracellular environment as they store caspases responsible for triggering apoptosis and transiently store calcium contributing to calcium homeostasis [17].

Lipid droplets. They are unique among organelles, as they are enclosed by a single monolayer of lipids instead of bilayers. Inside, they store high concentrations of lipids, mainly cholesterol esters (cholesterol attached to various fatty acids) and triglycerides (three fatty acids linked to glycerol). These stored lipids are used for membrane formation and maintenance or as an energy source during starvation. Lipid droplets originate from ER bilayers. Proteins on the surface of lipid droplets regulate their functions, including the transfer of lipids to mitochondria and peroxisomes [18].

Endosomes. They are spherical, membrane-bound vesicles formed by the budding of the plasma membrane during endocytosis. This process internalizes extracellular cargo, such as membrane receptors and proteins, sorts and transports this endocytosed material to various destinations, including lysosomes. During the endocytic pathway, the initial vesicles, known as early endosomes, mature into late endosomes through a series of processes, including changes in protein composition, lipid content, and gradual acidification of the lumen [19].

Lysosomes. They are spherical membrane-bound vesicles containing hydrolytic enzymes. They act as the digestive system of the cell; break down waste materials and cellular debris. Lysosomes are formed by the fusion of transport vesicles budded from the Golgi complex with endosomes.

Peroxisomes. They contain essential enzymes that convert very long chain fatty acids and branched fatty acids into simpler substrates usable by mitochondria for energy production. Additionally, peroxisomes house enzymes like catalase that detoxify harmful substances and reduce reactive oxygen species. While the membrane of peroxisomes originates from the ER, their enzymes are imported from the cytosol. Furthermore, peroxisomes are involved in synthesizing plasmalogens, a major type of phospholipid found in high levels in the brain, essential for forming myelin—the insulating layer around nerves that enhances the speed of electrical signal transmission [20].

Autophagosomes. They are formed with a double bilayer membranes. Autophagosomes engulf damaged proteins and/or deliver them to lysosomes (by fusion) for degradation. They are formed *de novo* by budding from various organelles such as the ER, mitochondria, or endosomes. This process not only clears damaged components from the cytoplasm but also serves as a survival mechanism during starvation, as the breakdown products can be recycled to provide building blocks for essential synthesis or energy needed for cell survival [21].

Organelles do not operate completely independently; their functions are coordinated to benefit the entire cell. This coordination is achieved through mechanisms that facilitate the exchange of materials between organelles. One such mechanism is vesicular transport, which involves the following steps. Initially, a transient transport vesicle forms by the assembly of a protein coat on the donor membrane. This coat facilitates vesicle budding and selectively incorporates specific cargos. Once separated from the donor membrane, the vesicle sheds its coat and travels through the cytoplasm toward an acceptor membrane. Tethering factors associated with the acceptor membrane capture the vesicle. Soluble N-ethylmaleimide-sensitive factor activating protein receptor (SNARE) proteins then bring the two membranes into close proximity, initiating fusion. This fusion integrates the bilayers of the vesicle and acceptor membrane, completing cargo delivery into the acceptor compartment. The specificity of this vesicular transport relies on different types of SNARE proteins that mediate fusion with specific target membranes [22].

The movement of cargo on a specific pathway (e.g., from ER to Golgi to plasma membrane, and from plasma membrane to endosome to lysosome) is balanced by recycling pathways. These pathways are essential for retrieving materials, ensuring organelles maintain their distinct lipid

and protein compositions over time. Without such recycling mechanisms, organelles would not sustain their functional integrity [23].

2.2 Membrane lipid composition and structure

Plasma membranes and different intracellular membranes vary in their exact chemical composition. Although they exhibit a remarkable molecular diversity, they share a common and fundamental architectural feature: lipid bilayer with associated proteins (with the exception of lipid droplets surrounded by a lipid monolayer), schematically illustrated in Figure 2.2). The structural scaffold of cellular membranes is built from three major classes of lipids: glycerophospholipids, sphingolipids, and sterols (cholesterol in vertebrate). The first two classes together are called phospholipids.

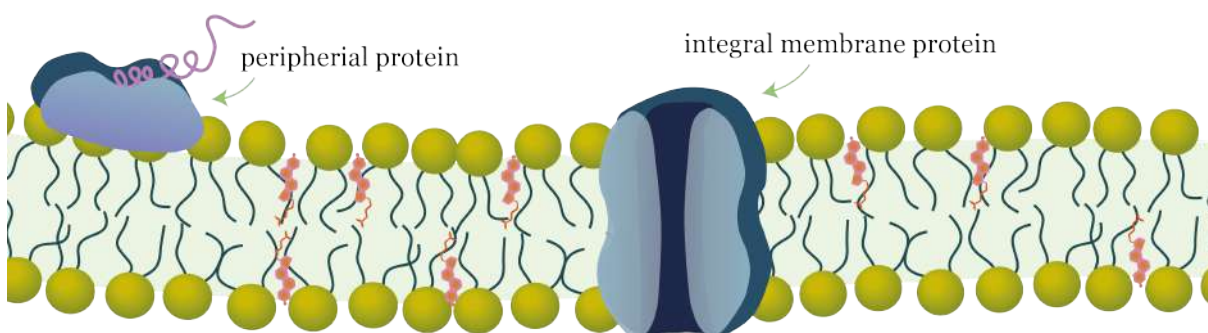


Figure 2.2: Schematic illustration of a lipid bilayer with associated proteins.

Glycerophospholipids. They are the most abundant type of lipids in cell membranes. Glycerophospholipid has two fatty acids attached to two of the three carbon atoms in glycerol. The third carbon, however, is connected to a phosphate group, which often binds to another small polar molecule such as choline, ethanolamine, or serine, to form phosphatidylcholine (PC), phosphatidylethanolamine (PE), or phosphatidylserine (PS), respectively (see Figure 2.3).

Sphingolipids. They contain one long-chain amino alcohol called sphingosine, attached to a long-chain fatty acid with or without other polar groups or sugars. As such, these lipids exhibit a wide variety of headgroup sizes; they can contain just a hydroxyl group, as seen in ceramide, a medium-sized phosphocholine headgroup found in the highly abundant sphingomyelin (SM), shown in Figure 2.3 or more complex sugar-modified headgroups collectively known as glycosphingolipids.

Phospholipid class includes also lipids unique to specific membrane organelles. For example, cardiolipins (CLs) found in the inner mitochondrial membrane [24]. CL is composed of four fatty acid chains and three glycerol molecules bound to them. This structure makes it a tetra-acyl lipid, distinct from the more common diacyl phospholipids like glycerophospholipids and sphingolipids. Another example is bis(monoacylglycero)phosphate (BmP) found predominantly in the inner leaflet of the lipid bilayer that makes up the membrane of late endosomes [25]. BmP consists of two glycerol molecules each attached to one fatty acid chain and connected by a phosphate group.

Fatty acids found in the structure of phospholipids are composed of long chains made up of nonpolar C—H bonds and typically a carboxyl group (COO⁻) at one end. Fatty acyl chains vary in both length and degree of saturation (number of double bonds). Saturated fatty acids have all carbon atoms bonded to the maximum number of hydrogen atoms. Unsaturated fatty acids can have one (monounsaturated) or more double bonds (polyunsaturated) between carbon atoms.

The double bond creates a kink in the hydrocarbon chain, affecting the membrane packing and fluidity. Most membrane fatty acyl chains contain 14 to 24 carbons [26].

Cholesterol. Cholesterol (Chol) is the only endogenous sterol found in vertebrate animal cell membranes. Unlike phospholipids, it is a polycyclic molecule with a rigid four interconnected hydrocarbon rings (three six-membered rings A-C and one five-membered ring D), forming a rigid planar structure (see Figure 2.3). A flexible short hydrocarbon tail consisting of eight carbon atoms is attached to the D-ring, while on the other end, attached to the A-ring is a single hydroxyl (OH) group. Furthermore, two methyl groups are attached at specific positions on the rings.

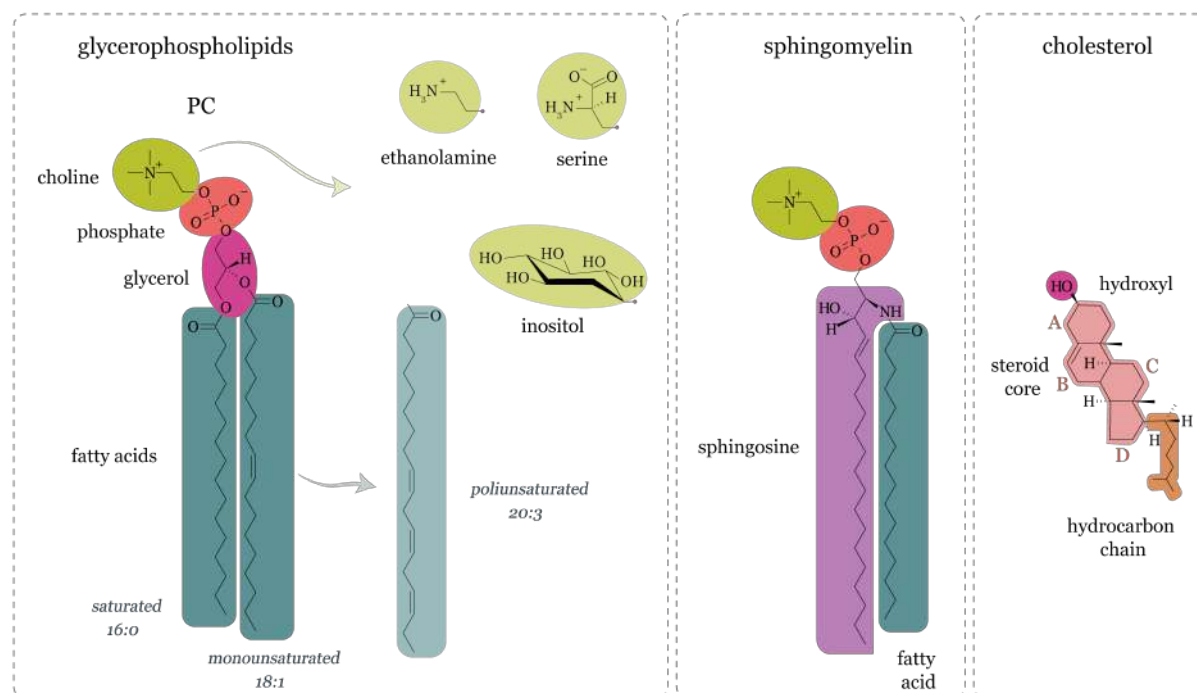


Figure 2.3: Major structural lipids of cellular membranes. Examples of polar moieties attached to a phosphate group and fatty acids are depicted in the group of glycerophospholipids.

The formation of biological membranes is fundamentally based on the unique properties of phospholipids. Their asymmetric structure, consisting of two regions of extremely different polarity yields the amphipathic character of these molecules. The dual nature of phospholipids underlies the formation of biological membranes, as will be explored later in Chapter 4. The hydrophobic hydrocarbon tails of phospholipids orient themselves towards each other, creating an interior hydrophobic core, while the hydrophilic head groups face outward towards the aqueous surroundings.

Lipids are distributed uniquely across different organelle membranes, exhibiting variations in composition and concentration that are essential for cellular function. This lipid distribution is influenced by tightly regulated pathways of lipid synthesis and transport. These pathways ultimately determine the physicochemical properties and, consequently, the biological functions of the specific cellular membrane component.

Most membrane lipids are synthesized in the ER and the Golgi apparatus, from where they are transported to their final destinations within the cell [2]. A lipid gradient is observed among various organelles in the secretory pathway, reflecting the differing functional requirements of each compartment. For instance, cholesterol is found in low quantities in the ER but is highly concentrated in the plasma membrane, with the Golgi complex acting as a crucial intermediary in this process (see Figure 2.4). Additionally, sphingomyelin and other lipids display similar

trends, highlighting the intricate regulation of lipid distribution. Early endosomes exhibit a lipid composition that closely resembles that of the plasma membrane, as they originate from it. However, upon maturation, their composition undergoes significant changes, including the acquisition of new lipids such as BmP. The steady-state lipid composition of distinct organelles is presented in Figure 2.4.

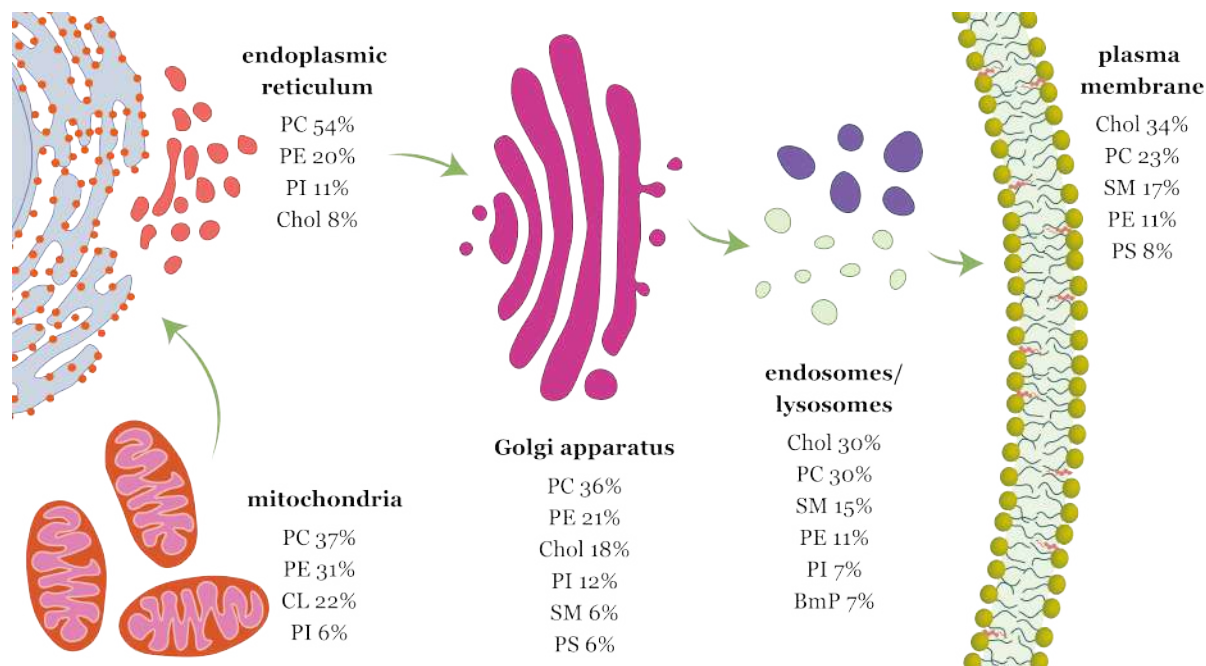


Figure 2.4: Steady-state lipid distribution in membrane organelles. The primary lipid components for specific organelle are listed based on their percentage contribution to the total lipid content, ordered from most to least abundant. Only lipids that constitute at least 5% of the total lipids in each organelle are included. Arrows indicate direction of increase in cholesterol content. Adapted from [27].

The uneven distribution of lipids is also present between the inner and outer leaflets of cellular membranes. Cytosolic leaflet of the mammalian plasma membrane, facing the cell interior, is enriched in anionic phospholipids like PS and PI [28]. In contrast, the outer leaflet, facing the extracellular matrix, is richer in PC, SM, and cholesterol [29]. Three membrane enzymes are responsible for catalyzing the transverse diffusion of compounds [30]. Flippases transport membrane glycerophospholipids and sphingolipids from the outer leaflet to the inner leaflet (cytoplasmic side) of the cell membrane. In contrast, floppases move membrane lipids from the inner leaflet to the outer leaflet. Scramblases facilitate the bidirectional movement of lipids across the membrane. In contrast, cholesterol does not require enzymes to flip-flop between the leaflets of the membrane. Maintaining the transbilayer asymmetry is pivotal as loss of lipid asymmetry can trigger specific biological processes [31]. For instance, exposure of PS lipids on the cell surface plays a key role in blood coagulation and cell apoptosis initiation [32].

2.3 Cell membrane models

Given the intricate composition and organization of biological membranes, as discussed in the previous section, interpreting the measurements of specific aspects of a membrane often proves challenging. To facilitate this interpretation, various biomimetic systems are employed as model

membranes. Researchers have developed a wide array of representations for cell membranes, most of which can be classified either as free-standing membrane in solution or membrane on surface.

Each category requires distinct preparation protocols, and the choice of model depends on the method to be used and the property to be examined. For membranes in solution, common biophysical techniques include scattering methods such as neutron [33], X-ray [34], and light scattering [35], as well as various spectroscopy methods like fluorescence spectroscopy [36], nuclear magnetic resonance (NMR) [37], electron paramagnetic resonance (EPR) spectroscopy [35], and calorimetry [38]. Conversely, for membranes on surfaces, suitable techniques include surface-sensitive methods such as sum-frequency generation (SFG) spectroscopy [39], neutron and X-ray reflectometry [40], Langmuir isotherms [41], and microscopy methods including fluorescence microscopy [42], atomic force microscopy [43], and Brewster angle microscopy [44]. Integrating findings from various membrane models and biophysical method contributes significantly to our understanding of cellular membranes.

The following subsections explore the main characteristics of the most used cell membrane models, along with a brief overview of their respective sample preparation protocols.

2.3.1 Lipid vesicles

Lipid vesicles, also known as liposomes, are spherical supramolecular structures formed by one or more lipid bilayers separated by aqueous phase spaces. Vesicles are categorized based on their structure, specifically the number of lamellae and their size [45–47]. Vesicles can be either unilamellar or multilamellar. Unilamellar vesicles consist of a single lipid bilayer forming a spherical shape, whereas multilamellar vesicles are composed of multiple lipid bilayers variously arranged. In terms of size, unilamellar vesicles are further divided into small unilamellar vesicles (SUVs) with diameters ranging typically from 20 to 100 nm, which represent the smallest, geometrically constrained size for a given lipid or lipid mixture, large unilamellar vesicles (LUVs) with diameters between 100 and 1000 nm, and giant unilamellar vesicles (GUVs) greatly exceed 1000 nm and can reach up even to several hundred microns, sizes comparable to eucaryotic cells. Multilamellar vesicles (MLVs) and multivesicular vesicles (MVVs) have sizes comparable to GUVs. However, MLVs have an “onion” structure, where lipid bilayers are stacked concentrically, whereas in MVVs the outer bilayer encloses smaller vesicles.

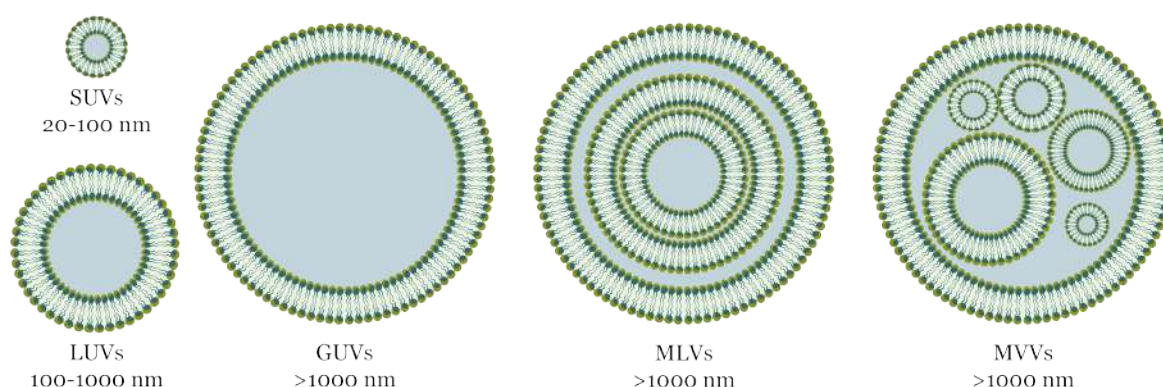


Figure 2.5: Schematic illustration of various types of lipid vesicles.

The choice of a method for producing liposomes, or a combination of several methods, is determined by the way the vesicles are used, i.e. the requirements they must meet. Depending on the technique used, more or less homogeneous suspensions of unilamellar large (LUV) or small

(SUV) or multilamellar (MLV) liposomes can be obtained. The most commonly used method is a hydration of a thin lipid film [45]. In this method, lipids are dissolved in an organic solvent, usually chloroform or a mixture of chloroform and methanol. The solvent is then evaporated under reduced pressure, so that a dry and thin lipid film forms on the walls of the vessel. The dry film undergoes hydration in aqueous solution by intense shaking. The result is a heterogeneous mixture of vesicles. The mixture can be squeezed through a membrane of known pore size to produce a more homogeneous LUV suspension, or ultrasound can be used to produce SUV liposomes. SUVs might be precursor for solid-supported lipid bilayers, which was the case in the experiments described in chapters 6 and 7.

To produce GUVs, different method is typically used, namely electroformation [47, 48]. In this approach, a thin layer of the desired lipid mixture is applied onto a conductive surface, such as glass coated with indium tin oxide (ITO), or onto two metal wires made of platinum (titanium or stainless steel can also be used). These ITO surfaces or metal wires are placed within a custom-built chamber, where the lipid film is hydrated using a sucrose buffer with a defined osmolarity. The lipid swelling process is facilitated by the use of an alternating current (AC).

2.3.2 Solid-supported lipid bilayers

While vesicles are suspended and free standing in solution, solid-supported lipid bilayers (SLBs) are deposited on a solid substrate, typically glass, mica, or silicon, and thus providing a flat membrane surface for study [49]. Lipids are arranged such that the headgroups of the lipids in one leaflet face the support surface with a very thin layer of water (0.5-1.5 nm) between them, whereas the headgroups of the lipids in the opposite leaflet are exposed to the bulk aqueous solvent [50]. The two-dimensionally confined water layer between the solid support and lipid bilayer is assumed to function as a lubricant, enabling the lipids to easily move along the plane of the surface [49]. SLB is schematically illustrated on the left panel of Figure 2.6

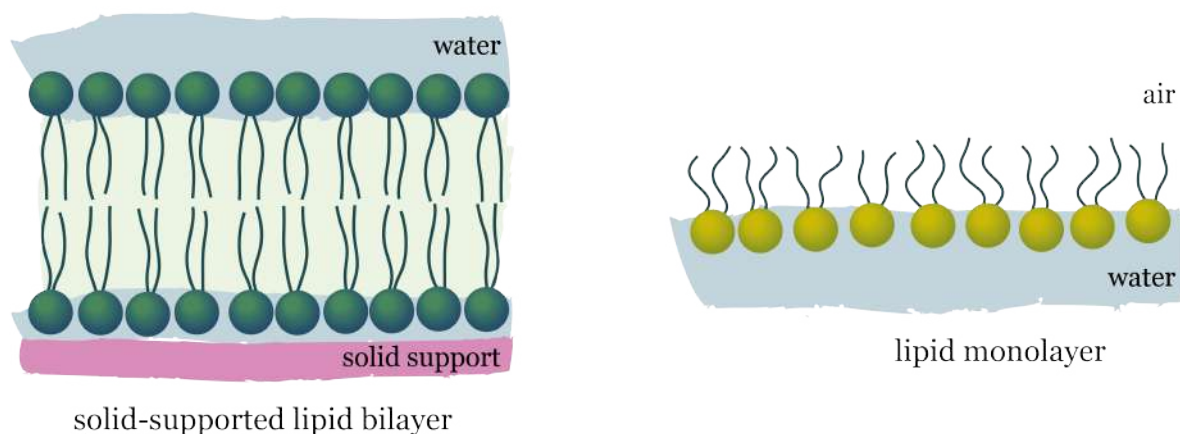


Figure 2.6: Schematic illustration of a solid-supported lipid bilayer and a lipid monolayer at the air-water interphase.

The vesicle fusion method is currently the most widely used technique for fabricating supported lipid bilayers (SLBs) [51]. This method involves the adsorption and spontaneous rupture of lipid vesicles (SUVs or LUVs) on a hydrophilic solid surface. The SLB formation is primarily governed by electrostatic interactions between a vesicle and a substrate as well as vesicle-vesicle and intrabilayer interactions [52]. Depending on the strength of these interactions, a vesicle may not adsorb onto the surface, or adsorb, become deformed and either remain intact or rupture to

further form a continuous planar lipid bilayer. The vesicle-substrate, and inter- and intrabilayer interactions are modulated by several factors: the nature of the support (including its surface charge, chemical composition, and roughness), the properties of the lipid vesicles (such as their composition, charge, size, and physical state), and the characteristics of the aqueous environment (including its composition, pH, and ionic strength) [53]. Furthermore, divalent ions, particularly calcium, have a considerable influence on SLB formation. These ions not only screen charges, modifying electrostatic interactions, but also interact directly with surfaces and lipids. Calcium ions generally promote vesicle adsorption, rupture, and SLB formation, with strongest effects observed on mica [53].

Alternative methods for SLBs formation include solvent-assisted lipid bilayer [54], bicelle adsorption [55], spin coating [56] and the Langmuir-Blodgett/Schaefer deposition methods [57], the latter often used to create asymmetrical bilayers [58]. SLBs offer a stable, flat two-dimensional surface for detailed biophysical analysis and functional studies of membrane components. These models are particularly valuable for studying membrane composition and bilayer morphology, such as the detection of microdomains or other heterogeneities [59, 60].

2.3.3 Lipid monolayers

Lipid monolayers, commonly referred to as Langmuir monolayers are another example of membrane on surfaces, however in contrast to SLBs, produced on the surface of a liquid. Typically, they are formed at the air-water interface (see the right panel of Figure 2.6). They serve as models for lipid droplets or one leaflet of the cellular bilayer membranes, providing insights into monolayer behaviours. Lipid monolayers are created by spreading lipid molecules in an organic solvent on an aqueous surface, where the lipid headgroups immerse in the water and the acyl chains orient towards the air [61, 62]. In contrast to the above-described model bilayer systems, the two-dimensional lipid density can be controlled, either by the amount of overspread lipids or by compressing the monolayer, which offers advantages for specific biophysical and biochemical assays to study the intermolecular interactions within the membrane and the surface properties.

3

Cholesterol and membrane fluidity

A fundamental property of biological membranes is their fluid, dynamic nature, enabling the cellular machinery to fulfill its functions. This fluid-like behavior allows the membrane to adapt, rearrange, and facilitate the movement of lipids and proteins. Fluidity influences the permeability of the phospholipid bilayer to small solutes [6], aids cell movement, growth and division, and modulates the activity of membrane-bound proteins [63]. The fluid nature of biomembranes enables proteins and lipids to move across the cell (or organelle) surface and locate interaction partners, influencing signaling and other cellular activities. A striking example of this was demonstrated in a study by Budin et al., which showed the clear dependence between the fluidity of the inner mitochondrial membrane (energy-transducing membrane) with the rate of cellular respiratory metabolism [64]. The fluidity of membranes is influenced by several interlinked factors, such as temperature, membrane composition, phase state, with cholesterol concentration playing a critical role. The lipid bilayer can be described as fluid in several ways, depending on the observed aspect of membrane dynamics, or rather the scales of length and time. Before describing the effect of cholesterol on membrane fluidity, let me set the stage by introducing the types of lipid movements that contribute to the fluid nature of biomembranes.

3.1 Lipid movements

Molecular motions occur across a spectrum of time and length scales, spanning from femtoseconds to seconds, and from angstroms to a few micrometers. Each type of motion contributes critically to membrane structure, dynamics, and function.

Lipid segmental motions occur at the shortest time scales. Lipid molecules undergo rapid vibrational motions of their chemical bonds, including bending and stretching, taking place in femtoseconds [65]. Moving to slightly longer time scales (picoseconds), lipid molecules experience chains and head groups isomerization or rotation. Rotational diffusion and fluctuation of the whole molecule takes place in nanoseconds [66, 67].

Coordinated motion of multiple molecules represent the longest timescale fluctuations in the system. The membrane components (lipid, proteins, and other biomolecules) unless anchored to cytoskeletal structures, the extracellular matrix, or to other biomolecules, are free to diffuse laterally along the plane of the bilayer, which occur on a time scale of microseconds to milliseconds [68]. This lateral movement allows lipids to exchange places while maintaining the overall integrity of the membrane structure.

At longer time scales, lipid molecules undergo flip-flop motions, also known as transverse diffusion, between the outer and inner leaflets of the bilayer. The literature presents significant discrepancies in reported flip-flop rates even for the same system, ranging from sub-seconds to days [69]. Despite these variations, there is a general agreement that the process is orders of magnitude faster for species with small head groups, such as cholesterol [70]. The probability of spontaneous (passive) flip-flop is low due to the high energy barrier involved in crossing the hydrophobic core of the membrane. Consequently, this process primarily occurs in the presence of enzymatic activity. As briefly described in the previous section, this type of movement is essential for lipid asymmetry in the membrane and plays a role in various cellular processes such as membrane repair and signaling.

Additionally, membrane undergoes undulations, which occur over time scales ranging from milliseconds to seconds [65]. These undulations represent collective movements of the membrane surface that facilitate e.g. membrane fusion during processes like exocytosis and endocytosis.

3.2 Impact of cholesterol on phospholipid membranes

Cholesterol, at varying concentrations in cell membranes, plays a crucial role in modulating phospholipid bilayer fluidity. Although it doesn't form bilayers independently, its amphipathic nature—combining a hydrophilic hydroxyl group with a hydrophobic planar fused ring backbone and tail—enables it to interact effectively with membrane lipids. This unique structure imposes cholesterol's orientation within the lipid membrane: the hydroxyl group aligns near the adjacent lipid headgroups, while the rigid sterol ring structure is immersed among the fatty acid chains of the lipid molecules, with its acyl chain extending toward the bilayer center [71]. Cholesterol's tilt angle relative to the membrane normal typically ranges between 10-30°, depending on the lipid environment [72–74].

The hydroxyl group of cholesterol can function as both a proton donor and acceptor, allowing it to participate in hydrogen bonding in the interfacial region with the polar moieties of phospholipids and water [75]. However, its interaction with phospholipids is primarily driven by van der Waals forces which arise from the attraction between cholesterol's rigid, planar fused-ring structure and the lipid acyl chains. This interaction is stronger with fully saturated acyl chains, which cholesterol preferentially associates with, rather than unsaturated ones [75–78]. Although cholesterol can still interact with mono- and di-unsaturated phospholipids, the presence of unsaturation significantly diminishes its affinity and activity [79, 80].

The rigid, planar steroid backbone of cholesterol restricts the conformational flexibility of the hydrocarbon chains in membrane lipids. This restriction increases the prevalence of *trans* conformations (with torsion angles of $180\pm 30^\circ$) at the expense of *gauche* conformations ($60\pm 30^\circ$) in the carbon-carbon single bonds of phospholipid acyl chains, leading to a more ordered state [75]. This also results in cholesterol exerting a condensing effect, reducing the lateral cross-sectional area of phospholipids. The diminished ability of cholesterol to condense and order membranes when mixed with unsaturated lipids likely stems from the kinks introduced by double bonds, which hinder the optimization of van der Waals forces.

Cholesterol's ordering and condensing effects also impact membrane thickness, though the outcome is complex and depends on factors such as lipid chain saturation [81, 82] and chain length [83]. Cholesterol typically increases bilayer thickness, either through chain ordering or in tandem with reducing the tilt of the phospholipid chains, a phenomenon observed primarily in lipids with 12-16 carbon chains. However, when mixed with lipids containing chains longer than 18 carbons, the effect can be the opposite [83]. This may be due to cholesterol's shorter hydrophobic portion, which forces longer chains to bend or kink in order to maximize interactions

with the cholesterol molecule [83, 84].

3.2.1 Lipid phases

The molecular interactions between cholesterol and phospholipids directly influence the membrane's phase state and, consequently, its fluidity. Membrane phases are often characterized by the order parameter (S), which measures the alignment of fatty acid chain segments (or averaged over the whole chain), and the lateral diffusion coefficient (D), which together captures both structural and dynamic membrane properties.

The membrane's phase state and resulting fluidity are highly temperature-dependent. Figure 3.1 illustrates the phase transition of a membrane as it is heated, transitioning from a rigid to fluid state, as lipid molecules gain kinetic energy with increasing temperature. The midpoint of this transition, known as the T_m , is affected mainly by the fatty acid composition of the lipid bilayer [85]. Longer and more saturated fatty acids tend to increase T_m values, while unsaturated and shorter fatty acids tend to lower T_m values. This explains why cold-adapted species, such as fish, have higher levels of unsaturated fatty acids in their membranes, allowing them to maintain fluidity at low ocean temperatures [86].

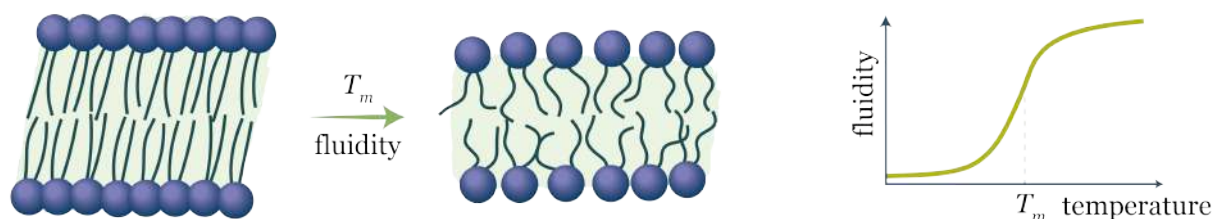


Figure 3.1: Schematic illustration of a lipid bilayer fluidity below and above T_m .

In the absence of cholesterol, pure phospholipids in the bilayer adopt one of two lamellar phases. Below T_m , lipids organize into a solid-like gel phase (L_β), where the acyl chains are tightly packed. In many cases, the acyl chains are tilted relative to the membrane normal, forming the tilted gel phase ($L_{\beta'}$). This tilt optimizes packing, particularly in lipids with longer acyl chains or asymmetrical molecular structures. For instance, SM, which contains long, saturated hydrocarbon chains, tends to form gel phases at ambient and physiological temperatures. This phase is characterized by maximal packing, ordered arrangement, where most carbon-carbon single bonds are in the *trans* configuration, and slow lipid diffusion (high S , low D), overall implying low fluidity.

Above T_m , lipids transition into a liquid crystalline phase (L_α), often referred to as the liquid-disordered (L_d) phase. However, I believe the term 'liquid-disordered' should be reserved for membranes with low cholesterol content for clarity. In this phase, *gauche* conformers are introduced into the acyl chains, leading to bilayer thinning. Unsaturated hydrocarbon chains, common in most biomembrane glycerophospholipids, favor the L_α phase at ambient and physiological temperatures. This phase is characterized by low packing, high disorder (including kinks from double bonds), and high lipid diffusion (low S , high D), resulting in high fluidity.

The phases described above represent extremes in membrane fluidity, but the incorporation of cholesterol moderates these differences. Cholesterol induces the formation of two fluid phases: L_d and liquid-ordered (L_o). When combined with high-melting lipids like SM, which typically contain long saturated fatty acids, cholesterol's rigid ring structure orders adjacent phospholipid acyl chains. At the same time, by inserting itself between lipid molecules, cholesterol disrupts the tight packing of the gel phase, increasing mobility and forming the intermediate L_o phase. This phase exhibits high molecular order along with relatively fast lateral diffusion (high S , high D).

When mixed with unsaturated glycerophospholipids, such as PC, marked by low T_m , cholesterol's rigid ring limits the rotational freedom of the fatty acid chains and elongates them, reducing the number of *gauche* conformers. This results in the formation of the L_d phase, which has higher order than the L_α phase but lower order than the L_o phase, while maintaining relatively fast translational diffusion (low S , high D). Elevation of cholesterol concentration in the bilayer formed by unsaturated lipids might lead to the transformation of L_d into L_o phase.

Various lamellar phases formed in lipid membranes are illustrated in Figure 3.2.

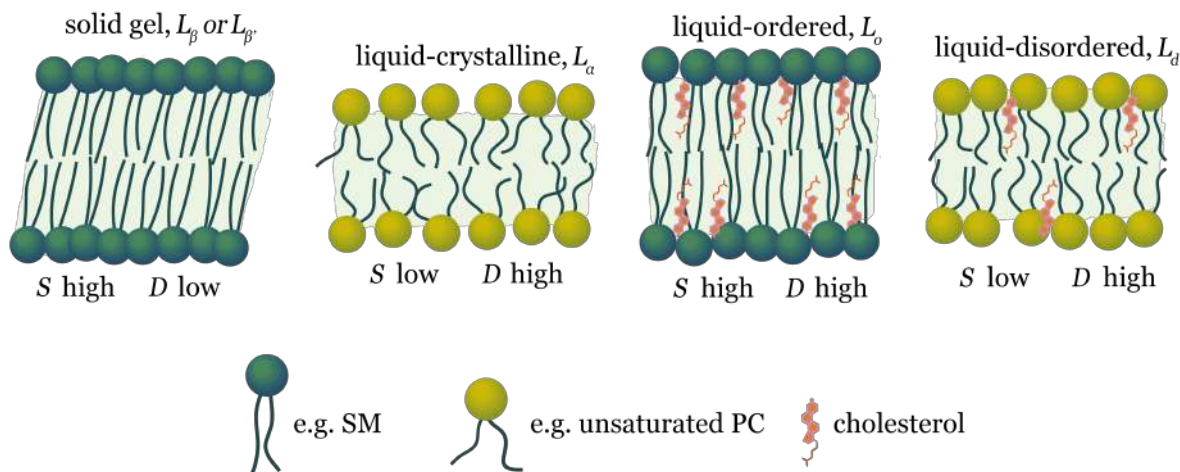


Figure 3.2: Schematic illustration of various lamellar phase states of a lipid bilayer.

The high cholesterol content in vertebrate biomembranes, particularly in the plasma membrane, prevents these membranes from adopting phases with extreme biophysical characteristics. Instead, they tend to exhibit phases with intermediate degrees of order and lateral mobility, resembling either the L_d or L_o phase, depending on local conditions. Different phases may coexist in both model membrane systems and native biomembranes, as discussed in the following section.

3.2.2 Lipid rafts

Lipids are asymmetrically distributed not only between the two leaflets of a bilayer but also within a single leaflet. Dynamic interactions among the three main types of lipids (glycerophospholipids, sphingolipids, and cholesterol) and between lipids and proteins significantly affect the distribution of these molecular components in cell membranes. This tendency of clustering together of certain molecules enables cells to create distinct subdomains of varied fluidity and biochemical characteristics in their membranes.

An example of such a subdomain is a lipid raft within the plasma membrane [4]. According to the lipid raft hypothesis, these subdomains form when sphingolipids and cholesterol become concentrated together, as cholesterol has a preference for interacting with the long, saturated acyl chains of sphingolipids [87]. These lipid subdomains are thicker, with enhanced molecular packing, less fluid, and less permeable to water molecules compared to membranes consisting only of glycerophospholipids. Lipid rafts represent a more ordered lipid phase (L_o) compared to the more disordered surrounding phase (L_d). The schematic illustration of such lipid raft is presented in Figure 3.3.

The existence of domains with different structural and physicochemical properties in the biological membranes is increasingly recognized as an important regulatory mechanism of cellular

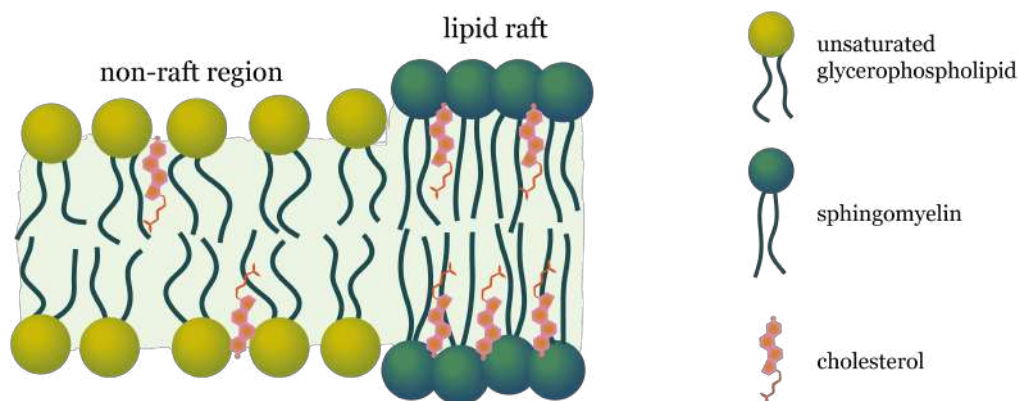


Figure 3.3: Schematic illustration of a lipid raft surrounded by more fluid phase.

physiology [88, 89].

The characteristic nanoenvironment of lipid rafts likely facilitates co-localization of specific molecules, leading to the formation of functional catalytic platforms [90]. This recruitment can bring enzymes and substrates into closer proximity, increasing the likelihood of their interaction and initiating reactions, such as those involved in signal transduction. Additionally, the distinct physicochemical properties of lipid rafts may directly influence a raft-resident protein conformation, thereby modulating its activity [91, 92]. The precise functions of lipid rafts are still under discussion, but they have been implied in cell signalling, in particular the signal transduction across the plasma membrane, mediated by glycosylphosphatidylinositol (GPI)-anchored receptors [93] and immune response (e.g. immunoglobulin E-mediated signalling) [94]. Furthermore, increasing evidence highlights the importance of cholesterol-rich lipid rafts in facilitating the entry of various viruses into target cells, including SARS-CoV-2 [95], dengue [96], ebola [97], influenza A [98], and HIV [99–102].

The coexistence of distinct lipid phases has been demonstrated in model cell membrane systems composed of simplified lipid mixtures [103]. The nonideal mixing of membrane components arises primarily as a result of different lengths of hydrophobic tails of lipids forming a bilayer. The longer tails may become exposed to the aqueous solution. To reduce this energetically unfavorable exposure, lipids self-organize based on the length of their acyl chains. The greater the height mismatch between phases, the larger the average size of the resulting domain [104]. The coexistence of L_o phase enriched in cholesterol and sphingolipids and cholesterol-poor L_d phase, considered to be the most biologically relevant, has been demonstrated in model cell membranes composed of ternary lipid mixtures of sphingomyelin, unsaturated phosphatidylcholine, and cholesterol at appropriate ratios [42, 105, 106]. Such bilayers exhibit microscopic phase separation into L_o domains surrounded by a sea of L_d phase. This size of domains enables their convenient investigation using diffraction-limited optical imaging techniques, such as fluorescence microscopy, which I describe in Chapter 5. The microscopic study of phase separation in model membranes has provided valuable insights into the role of hydrophobic mismatch and other biophysical interactions in driving lipid raft formation, stability and potential function.

Studies using model membrane systems derived from cells, cell-derived giant plasma membrane vesicles (GPMV) and plasma membrane spheres (PSM) exhibiting the coexisting phases show that the difference in the order of the two phases is smaller than for L_d and L_o , likely due to their complex lipid and protein content [107, 108].

4

Biological water

4.1 Water chemistry

The chemistry of water is pivotal to the biochemistry and physiology of all living organisms [109]. Water molecule consists of two hydrogen atoms covalently bound to the central oxygen atom through a shared pair of electrons. The remaining four valence electrons of oxygen organize into two non-bonding pairs. The repulsion between bonding and lone pairs of electrons results in the H-O-H angle of 104.5° (see left panel of Figure 4.1).

The distribution of partial positive and negative charges within water molecule is non-uniform; the electronic (negative) charge is concentrated at the oxygen end of the molecule, while each hydrogen atom carries a partial positive charge. This charge separation results in the formation of a molecular dipole (see right panel of Figure 4.1).

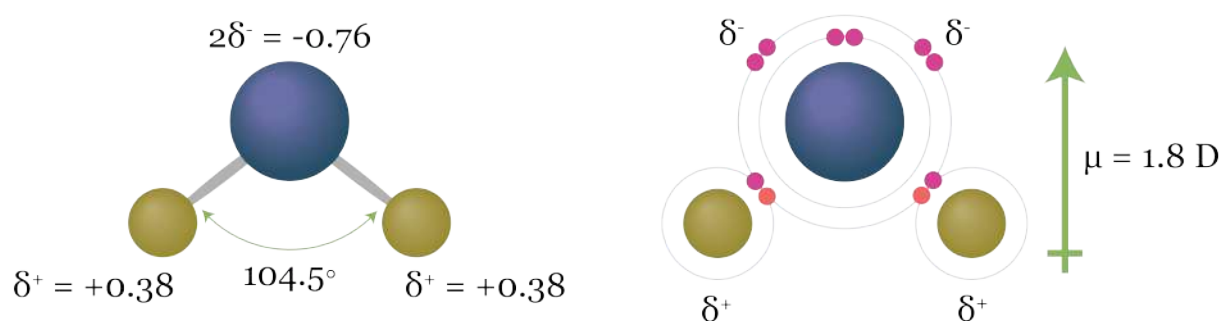


Figure 4.1: Water is a polar molecule, featuring a partial negative charge (δ^-) localized on the oxygen atom and partial positive charges (δ^+) on each of the two hydrogen atoms.

4.2 Hydrogen bond network

Water's exceptional properties and its ability to strongly interact with various biomolecules stem from its ability to form an intricate three-dimensional hydrogen bonding network. Polarity of the water molecule prompts attraction between the partially positive charge on the hydrogen atom of one water molecule and the partial negative charge on the oxygen atom of adjacent water

molecule, resulting in a hydrogen bond between them (left panel of Figure 4.2). Intermolecular hydrogen bonds are longer (ca. 3 Å) than the covalent O-H bonds (ca. 1 Å) within a water molecule [110]. They are also much weaker, with a binding energy of approximately $23 \text{ kJ} \cdot \text{mol}^{-1}$, equivalent to around $10 k_B T$ at room temperature (25°C), compared to the covalent O-H bond strength of $492 \text{ kJ} \cdot \text{mol}^{-1}$ [111]. Strengthening of the hydrogen bond occurs as the distance between oxygen atoms of adjacent water molecules and/or the angle between O-H and O-O coordinates decrease [110].

Because each water molecule contains two hydrogen atoms and two lone pairs of electrons, it can both donate and accept two hydrogen bonds; the two hydroxyl groups act as donors, and the two lone pairs on oxygen atom act as acceptors. The four hydrogen bonds optimally arrange themselves tetrahedrally around each water molecule; it maximizes the number of hydrogen bonds that can be formed (right panel of Figure 4.2). In ice, this arrangement is nearly flawless. Conversely, liquid water, due to the constant motion of water molecules, forms a disordered hydrogen-bonding network, where bonds continuously break and reform on a picosecond timescale (the activation energy needed for these transitions is low) [112]. Despite the transient nature of the hydrogen bond network in water, most water molecules are consistently coordinated with at least three other molecules (3.5 hydrogen bonds per water molecule on average) [113]. This rapid reorganization contributes significantly to water's solvent versatility, enabling it to promptly adapt to structural changes in biomolecules.

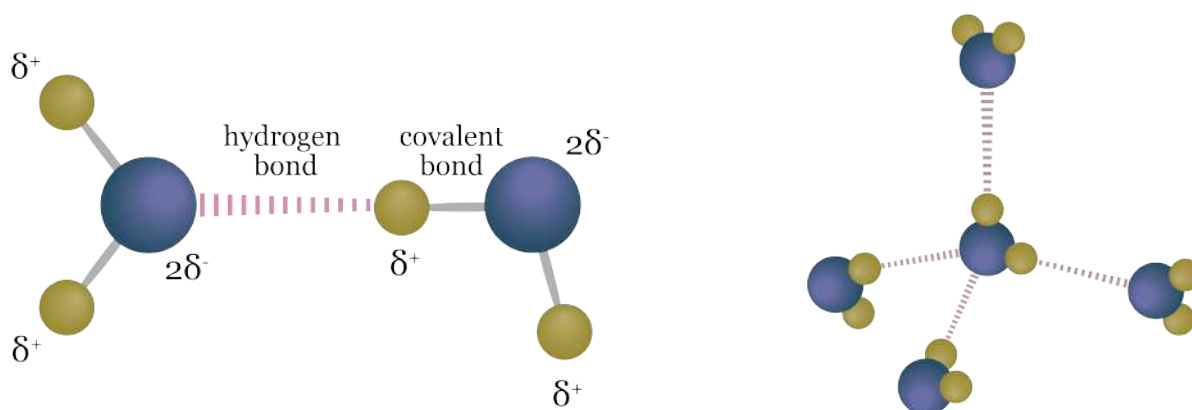


Figure 4.2: Hydrogen bond between two water molecules (left panel). Tetrahedral arrangement of hydrogen-bonded water molecules (right panel).

Hydrogen bonds extend beyond interactions solely among water molecules. Water can form hydrogen bonds with other polar molecules. Additionally, these bonds can arise between various organic molecules or within different segments of a single large molecule, like a protein [114]. Despite being around tens of times weaker than covalent bonds, hydrogen bonds exert significant influence, shaping the structures of numerous macromolecules such as proteins and nucleic acids, and regulating molecular interactions within cellular environments [115].

4.3 Hydrophobic effect

The localized structuring facilitated by hydrogen bonding in water accounts for various fascinating phenomena in biological systems, such as the self-assembly of lipid bilayers in aqueous environments. The strong propensity of water molecules to interact with each other leads to the exclusion of hydrophobic molecules (or hydrophobic parts of molecules) from the aqueous

phase, promoting an arrangement where hydrophobic molecules (or their parts) aggregate to minimize disruption to hydrogen bonding between water molecules. This phenomenon is called the *hydrophobic effect*.

From the thermodynamic standpoint, the dispersal of molecules, such as lipids, in an aqueous environment, creates an unfavourable system condition both in terms of enthalpy and entropy. For convenience, let me use the Gibbs free energy formula (4.1) [116]:

$$\Delta G = \Delta H - T\Delta S, \quad (4.1)$$

where ΔG , ΔH , ΔS and T stand for the change in Gibbs free energy, change in enthalpy, change in entropy, and temperature, respectively. The hydrophobic lipid tails disrupt the hydrogen bonding network within water and entail reorganization of water molecules around them, increasing the total enthalpy of the system; therefore $\Delta H > 0$. It entails the formation of cage-like structures around the hydrophobic regions, thereby locally increasing the order of water molecules and restricting their movement. This leads to a significant decrease of the total entropy of the system; therefore $\Delta S < 0$. To minimize the resulting increase in free energy, lipid molecules tend to cluster together.

Lipid assembly in water increases disorder among water molecules, reducing the aligned surface area around them, thus $\Delta S > 0$. The change in ΔH of the system can be either negative, zero, or positive as the formation of new hydrogen bonds can partially, fully, or over compensate for the hydrogen bonds broken by the entrance of the hydrophobic molecules' moieties. The change in enthalpy (contribution from bonds), however, is typically insignificant compared to change in entropy.

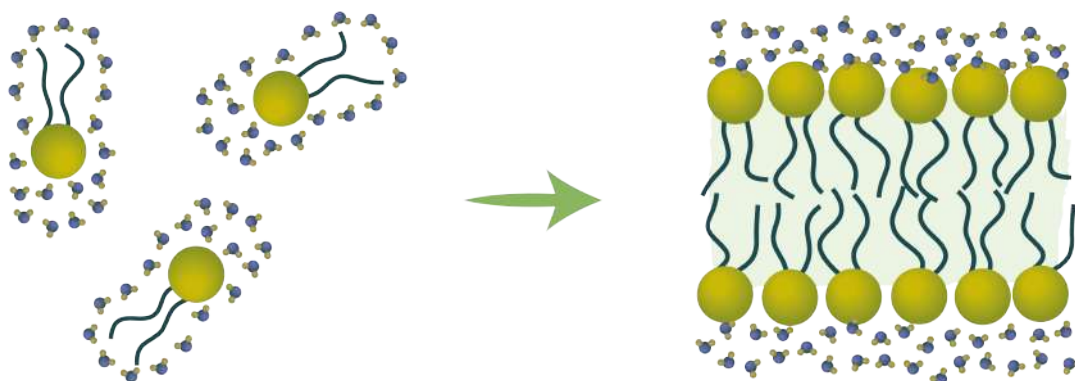


Figure 4.3: The dispersion of lipid molecules in water leads to the structuring of water molecules around each lipid molecule (left panel), which entails decrease in entropy of the system. The aggregation of lipid molecules into a lipid bilayer structure (right panel) leads to the overall order decrease, resulting in a state that is more entropically favored.

Depending on factors such as the difference in width between the lipid head group and tails, various structures like micelles or bilayers can form. For instance, phosphatidylcholines, which have relatively equal widths between head group and tails, tend to form bilayers, while more conical-shaped lipids like phosphatidylethanolamine tend to form micelles [117].

4.4 Interactions between membrane and interfacial water

The nanoscopic layer of water, with a thickness corresponding to a couple of molecular diameters ($\sim 1\text{-}2.4$ nm), that directly hydrates biological systems is often referred to as *biological water* or hydration water [118]. Biological water not only does serve as an entropic driving force for the structural self-assembly process of the lipid membranes and other biomolecular aggregates (hydrophobic effect), but also significantly influences their dynamics and bioactivity [42, 109, 119, 120]. It also mediates the interactions between biomolecules and biomolecular ensembles such as membranes and solutes (such as proteins, DNA, and ions) [121, 122]. Given the focus of this thesis, considerations regarding interfacial water around biomolecules in the following sections primarily concern lipid membranes.

Investigations regarding water in the vicinity of biomembranes can be generally divided into two main areas: (i) the properties of hydration water (e.g. structural and dynamical), and (ii) the influence of the hydration water on the structure, dynamics, and function of lipid membranes. Researchers have investigated these aspects through diverse methodologies, including fluorescence spectroscopy [123], NMR spectroscopy [124], dielectric relaxation [125], neutron and X-ray scattering [126–128], molecular dynamics (MD) simulations [129–132], infrared spectroscopy [133–135], and vibrational sum frequency generation spectroscopy [136–138].

4.4.1 Properties of interfacial water

The properties of biological water are significantly different from that of bulk water, owing to confinement effects and partially disrupted hydrogen-bond network near the polar moieties of the lipid headgroups [124, 129, 139]. Biological water next to lipid membranes displays a more rigid water structure with a notably slowed translational and rotational motion and a concomitant increase of H-bond lifetimes [125, 140]. However, the extent of this retardation remains debated, as various perspectives have been inferred based on different experimental and computational methods.

The lipid assemblies in water not only influence the water dynamics but also impact the structure of biological water. Recent advancements in interface-selective vibrational sum frequency generation spectroscopy, incorporating heterodyne detection, have enabled the direct measurement of the complex second-order nonlinear susceptibility ($\chi^{(2)}$). The imaginary component ($\text{Im}\chi^{(2)}$) yields unequivocal insights into the orientation of interfacial water molecules. This technique along with other experimental and computational approaches have provided compelling evidence of water molecules exhibiting preferential orientation at interfaces with not only anionic and cationic lipids but also with neutral (zwitterionic) lipids [130–132, 136, 141, 142]. However, the mechanisms governing the preferential water orientation differ between these lipid groups. In the case of cationic and anionic lipids, water alignment is driven by monopolar effects induced by their charges. Conversely, for zwitterionic lipids—the ones used in the experiments described in this thesis, water orientation arises from dipolar effects, attributed to the significant dipole fields between oppositely charged moieties within the headgroup [143].

4.4.2 Impact of biological water on biomembranes

Hydration water does not only serve as an entropic driving force for the structural self-assembly of lipid membranes but also significantly affects their dynamic, structural, and functional

properties. This influence becomes particularly evident in both experimental [42, 43, 144, 145] and computational [146, 147] studies conducted across varying degrees of hydration.

The number of water molecules hydrating the membrane drastically affects lipid dynamics [42, 146]. Using the fluorescence recovery after photobleaching (FRAP) technique, Chattopadhyay et al. found that the lateral diffusion of phosphatidylcholine lipids in solid-supported lipid bilayers is highly sensitive to membrane water content [42, 144]. Lower membrane hydration results in a reduced lipid diffusion coefficient and a smaller mobile fraction of lipids. It was concluded that the water molecules forming the hydration shell around the phosphocholine moiety facilitate lipid diffusion by reducing electrostatic repulsion between neighbouring lipid headgroups. When hydration levels drop and these shielding water molecules are depleted, repulsive interactions increase, raising the activation energy for diffusion. At a constant temperature, fewer lipids have sufficient energy to overcome this barrier, leading to a significant reduction in lipid mobility and lateral lipid diffusion coefficient [42]. In a follow-up study, Chattopadhyay et al. demonstrated that maintaining the hydration shell around the phosphocholine moiety, and thus the lipid mobility, at reduced hydration is affected by the type of biologically relevant ions present [145]. Both sodium (Na^+) and potassium (K^+) ions stabilize the hydration shell, thereby enhancing lipid mobility under low hydration conditions. In contrast, magnesium (Mg^{2+}) and calcium (Ca^{2+}) ions destabilize the hydration shell, impeding lipid mobility when bulk water is depleted.

Results from MD simulations by Malik and Debnath also indicate that as membrane dehydration progresses, the fraction of mobile lipids decreases, while the fraction of caged (immobile) lipids increases [146]. Furthermore, dehydration of the membrane leads to bilayer ordering, evidenced by a decrease in the area per lipid head group, an increase in bilayer thickness, and higher lipid order parameters. These structural changes in the bilayers correlate with the changes in biological water dynamics as the number of water molecules decreases. The translational and rotational movements of water molecules near the membrane slow down, and dynamical heterogeneities emerge [146].

Confocal fluorescence microscopy investigations revealed that the overall structure of membranes exhibiting coexisting L_d and L_o phases remains unaffected by decreased water content, provided that changes in hydration are applied gradually [42]. However, substantial structural reorganization was detected at the nanoscale [43]. Atomic force microscopy measurements by Krok et al. showed that lowering hydration levels causes lipids to migrate from the L_d phase to the L_o phase, resulting in the formation of L_d nanodomains within the more ordered L_o phase [43]. Furthermore, the height difference between the L_d and L_o phases decreased linearly with reduced membrane hydration. This process was found to be reversible, with increasing environmental humidity restoring the height mismatch to its original state.

4.4.3 Cellular membrane dehydration events

While it is widely acknowledged that biomembranes typically reside within a fully hydrated environment, it is important to recognize that cellular processes also entail localized and transient membrane dehydration events. These events include the adsorption of biomacromolecules onto the membrane surface and the fusion of lipid bilayers. The latter, in particular, constitutes a pivotal phenomenon in various cellular processes such as neurotransmission, fertilization, viral entry, and exocytosis [148–151].

Despite the evolutionary and structural diversity of the proteins involved in these processes, they follow a common pathway characterized by a sequence of distinct intermediates (see Figure 4.4) [150, 152, 153]. Initially, loose protein-mediated membrane contacts occur, followed by the tight apposition of membranes, resulting in local and transient membrane dehydration, while still preserving bilayer integrity. To achieve this state, repulsive forces between lipid headgroups and

the energy barrier associated with dehydration at the fusing zone must be overcome. Subsequently, membrane structure is perturbed by the merging of the proximal leaflets, leading to the formation of a fusion stalk or a hemifusion diaphragm. This stage is succeeded by the rupture of the diaphragm, resulting in the formation of a fusion pore that subsequently expands, completing the process of membrane merger.

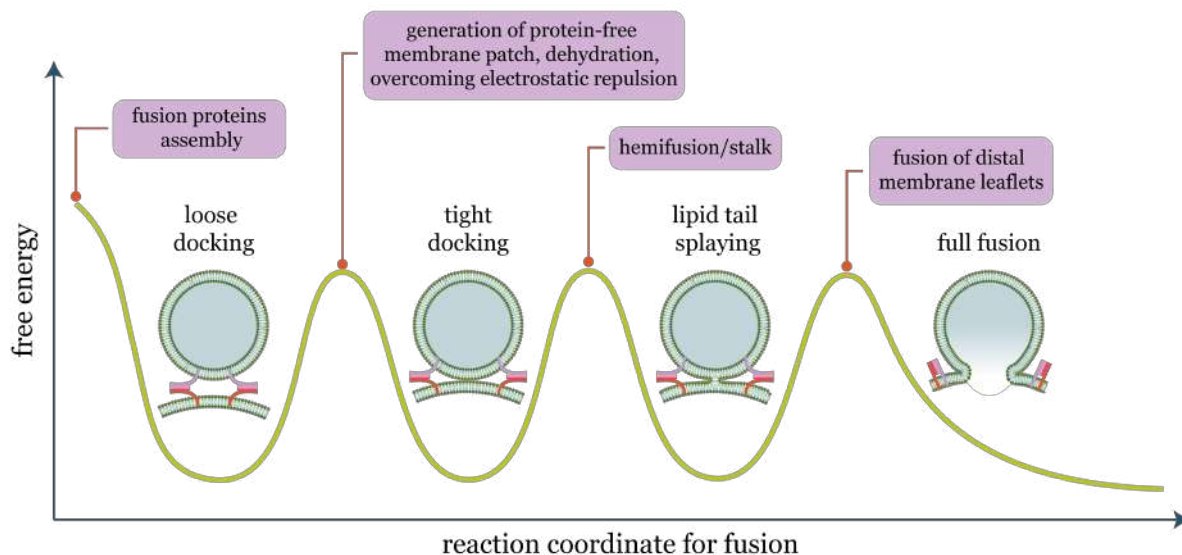


Figure 4.4: Schematic of the free energy profile for the membrane fusion process. The phenomena occurring while overcoming energy barriers and those corresponding to local minima in the energy landscape are indicated. Fusion intermediates are depicted at local minima. The scaling on the axes is arbitrary. Adapted from [152].

In addition to instances of the biomacromolecules adsorption onto the membrane surface and the lipid bilayers fusion, a water-depleted environment is created in the endoplasmic reticulum and Golgi apparatus, where lipid membranes are closely interleaved with each other.

The unambiguous information about exact hydration state of the membrane in native conditions are hard to find. Its determination is nontrivial due to the transient nature of such cellular events and the modulation of the extent to which water interacts with different segments of the lipid bilayer by factors such as temperature, the type of lipid headgroup, acyl chain composition, and the phase state of a lipid bilayer. Therefore, studying this phenomenon both *in vivo* and *in vitro* presents significant challenges.

5

Molecular spectroscopy and imaging

To characterize the cholesterol-phospholipid-water interplay in biomimetic lipid membranes I employed a set of molecular spectroscopy and imaging techniques, namely: fluorescence spectroscopy, fluorescence microscopy, and vibrational sum-frequency generation (VSFG) spectroscopy. In this section, we delve into the fundamental physical concepts that underpin these methods.

At the heart of all the experimental techniques used in this thesis are light-matter interactions. Atoms and molecules, being much smaller than the wavelength of light, interact with the oscillating electric field of light. The molecules are polarized in a rhythmic manner, experiencing a uniform time-varying electric field that alternately moves their positive and negative charges in opposite directions. When a molecule is rhythmically driven at its resonant frequency, it effectively absorbs energy from the incoming waves. This is crucial for spectroscopy and microscopy because the resonance of molecular components dictates, which frequencies of electromagnetic radiation are absorbed, creating the unique spectra of different molecules.

5.1 Fluorescence spectroscopy

5.1.1 Jablonski diagram

According to quantum mechanics, a molecule can only take on certain discrete values of energy, called energy levels. The overall energy state of a molecule is a combination of its electronic, vibrational, and rotational states. A molecule can transition between energy levels by absorbing or emitting photons, or through non-radiative energy exchanges within a molecule or with its environment. Molecular energy levels and various transitions are commonly illustrated using a Jablonski diagram [154], such as the one shown in Figure 5.1.

In a molecule, which consists of a set of atoms, the respective atomic orbitals (probability density of finding an electron in a selected region of space around the nucleus) can overlap, leading to the formation of molecular orbitals, which have specific spatial charge distributions. The arrangement of delocalized electrons in these molecular orbitals defines the molecule's electronic configuration and thus the energy levels. The electronic energy levels are denoted on Jablonski diagram by S (singlet state, with electrons having antiparallel spins) and T (triplet state, with electrons having parallel spins).

Each electronic state has its own set of vibrational energy levels, resulting from the quantized vibrational modes of the molecule. These modes are due to the periodic motion of atoms within

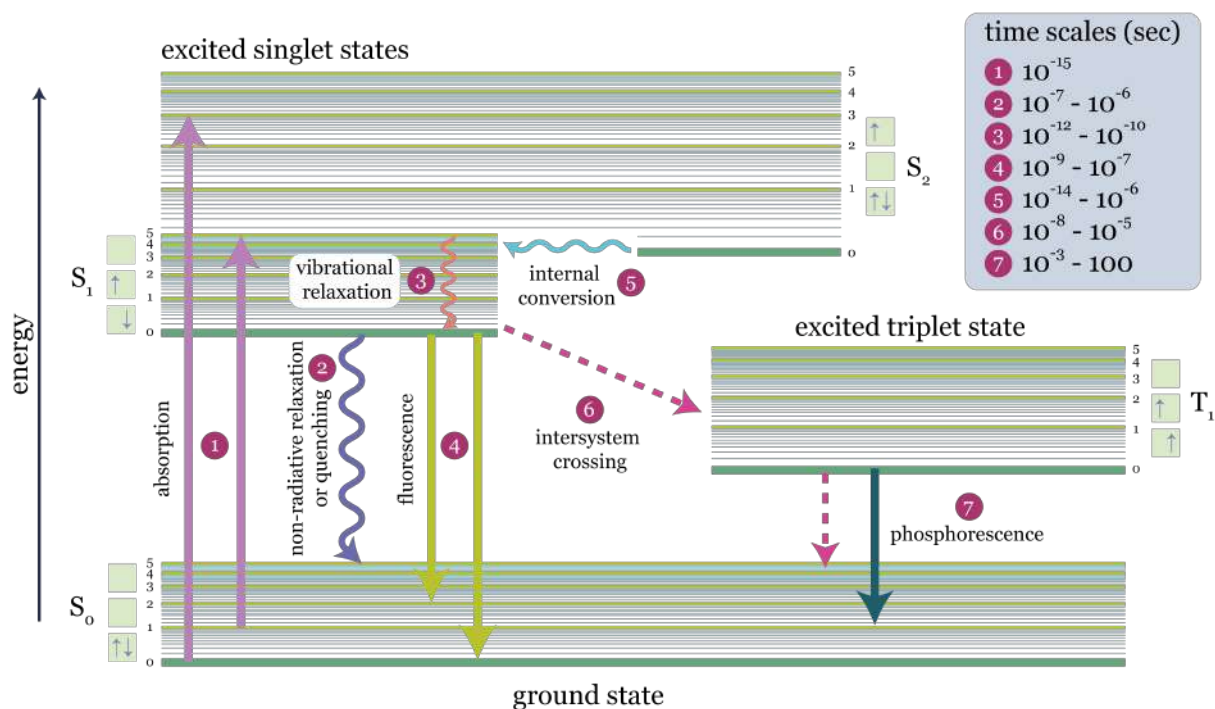


Figure 5.1: Jablonski diagram representing the exemplary molecular energy levels along with the timescale of various transitions between energy levels. Thicker lines represent electronic energy levels, while thinner and the thinnest lines indicate various vibrational and rotational energy states, respectively. Solid lines represent radiative transitions between the energy states, while wavy and dashed lines indicate non-radiative transitions.

the molecule, such as stretching and bending of chemical bonds. Each vibrational level, in turn, has its own set of rotational levels, associated with the overall rotation of the molecule. Generally, the energy associated with electronic transitions is the highest, followed by vibrational transitions, and then rotational transitions. This hierarchy is due to the relative magnitudes of the energy associated with these various degrees of freedom: electronic transitions typically involve energies corresponding to ultraviolet (UV) or visible (VIS) light, vibrational transitions involve energies corresponding to infrared (IR) light, whereas rotational transitions involve energies corresponding to microwave radiation.

The lowest energy arrangement of a molecule is in the lowest vibrational level of its electronic ground state, which is usually a singlet state (S_0). Upon absorbing a photon, one electron is quickly promoted to a higher orbital, typically the first excited singlet state (S_1), without flipping its spin. This means the excited electron's spin remains antiparallel to the electron left behind in the original orbital. The absorption is considered as an instantaneous process occurring at time scales of femtoseconds ($\sim 10^{-15}$ s) [155]. The energy of the absorbed photon must equal the energy difference between the ground and excited states. In the excited state, the electrons' spatial charge distribution changes almost instantaneously, within femtoseconds ($\sim 10^{-15}$ s), while the heavier atomic nuclei adjust more slowly, over picoseconds ($\sim 10^{-12}$ s). The excited electron moves to an orbital further from the nuclei, causing the molecule to relax and vibrate around the new equilibrium positions of the atoms. This vibrational energy is quickly dissipated as kinetic energy through intra- or intermolecular energy transfer, in a process called vibrational relaxation, eventually settling the molecule into the lowest vibrational energy level of the excited state S_1 (a process occurring within 10^{-12} s - 10^{-10} s) [155]. If change in the electronic state occurs, the

process is called internal conversion (10^{-14} s - 10^{-6} s) [155].

Despite this relaxation, the molecule still has more energy than in the S_0 state and eventually returns to the ground state. Several pathways exist for a molecule to return to the ground state. One possibility is relaxation through the spontaneous emission of a photon (fluorescence), occurring within $\sim 10^{-9}$ s - 10^{-7} s) or through non-radiative decay (occurring within $\sim 10^{-7}$ s - 10^{-6} s) [155]. Because of the rapid relaxation to the lowest vibrational level of the excited state, emission spectra of molecules are usually independent of the excitation wavelength, known as Kasha's rule [156]. This energy dissipation during the vibrational relaxation governs the difference in wavelengths between absorbed and emitted photons, known as Stokes shift [157]. The Stokes shift is the phenomenon enabling the fluorescence imaging, which is described in Chapter 5.2.

Alternatively, the molecule may undergo intersystem crossing, where the excited electron flips its spin, entering the triplet state (T_1). Returning from T_1 to S_0 requires another spin flip, a rare and slow process, resulting either in phosphorescence or non-radiative decay (both occurring within ($\sim 10^{-3}$ s - 100 s) [155].

5.1.2 Solvent relaxation

Upon absorption of a photon, a molecule may transition from its vibrational ground state to various higher vibrational states. The lowest-energy transition in an absorption spectrum is the transition, which occurs from the ground state ($S_{0,n}$) to the first vibrational level of the first electronically excited state ($S_{1,0}$). Since vibrational relaxation and internal conversion happen faster than fluorescence, fluorescence predominantly occurs from the electronically excited vibrational ground state ($S_{1,0}$) to one of the vibrational states of the electronic ground state ($S_{0,n}$), as depicted in Figure 5.1. As a result, this transition in a fluorescence spectrum exhibits the largest energy difference. Therefore, the $S_{0,n}$ - $S_{1,0}$ transitions in absorption and fluorescence spectra should be equivalent. However, if the solvent molecules surround the molecule of interest, they adjust their orientations according to the molecule's ground state electronic configuration (see Figure 5.2). Upon absorption, the molecule's electronic structure changes, but the solvent molecules do not instantly follow it. This leaves the excited molecule in a Franck-Condon state (S_{1FC}), surrounded by solvent molecules still arranged for the ground state. Solvent relaxation then occurs as the solvent adapts to the molecule's new electronic structure, creating a more energetically favourable state (S_{1REL}). After fluorescence, the solvent molecules have not yet adapted to the molecule's new ground state. Consequently, the Franck-Condon state post-fluorescence is at a higher energy compared to the initial ground state before absorption (S_{0FC}). Therefore, the $S_{0,n}$ - $S_{1,0}$ transitions in an absorption spectrum are associated with higher energies compared to those in an emission spectrum $S_{1,0}$ - $S_{0,n}$. The magnitude of this shift depends on the solvent - the higher the polarity of the solvent, the higher the strength of the effect [158].

5.2 Fluorescence microscopy

Fluorescence microscopy builds upon the principles of fluorescence spectroscopy but adds the critical advantage of spatial resolution, allowing for the visualization of the distribution and/or dynamics of fluorescent molecules within the biological environments *in vitro* or *in vivo* or other samples. The fundamental feature of any fluorescence microscopy setup is to illuminate and excite the specimen with a specific band of wavelengths and then isolate the much weaker emitted fluorescence (of a longer wavelength) from the excitation light for detection. In a well-configured microscope, only the emission light reaches the detector so that the resulting fluorescent structures are superimposed with high contrast against a very weak background signal for the formation of

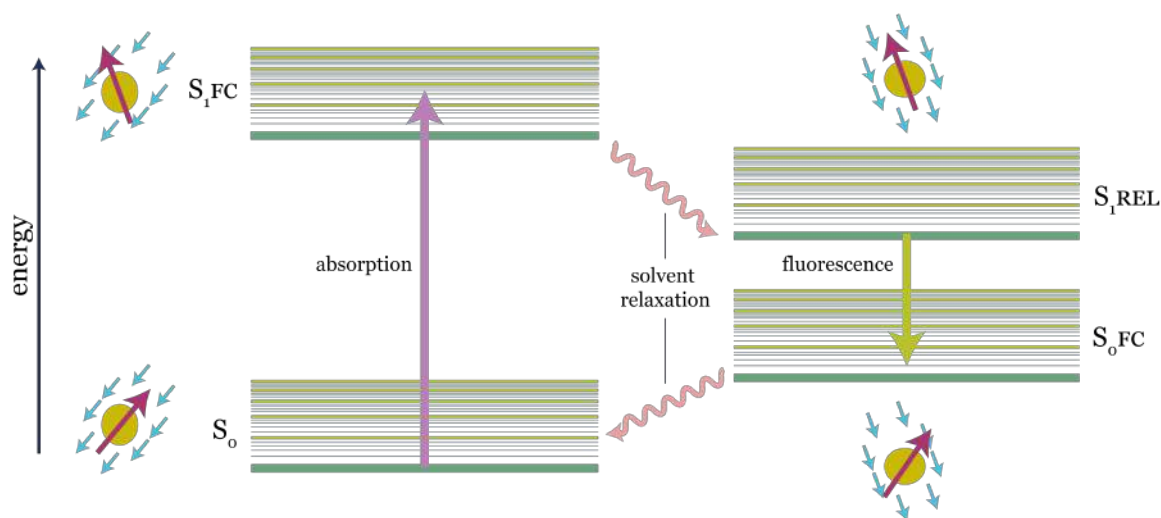


Figure 5.2: The effect of solvent relaxation on the molecular energy levels.

an image. The detection limits are generally determined by the dark counts of the detector.

The most basic form of fluorescence microscopy is widefield fluorescence microscopy, in which the entire field of view is illuminated by the light source (see the left panel of Figure 5.3). The excitation beam is propagated and introduced at the back focal plane of the objective in such a way to create a large, collimated beam with a Gaussian intensity profile uniformly illuminating the entire sample within the field of view. In most widefield fluorescence microscopes, the excitation light (e.g., mercury lamp or laser) passes through a wavelength-selective excitation filter and then is reflected off the surface of a dichroic mirror that only allows certain wavelengths to pass (or wavelength-non-selective beamsplitter) and subsequently passes through the microscope objective to illuminate the sample. When the fluorescent probes in the sample are excited, they emit fluorescence, which is collected by the same objective and passes back through the dichroic mirror (or beamsplitter). This technique is known as epifluorescence microscopy. On its way to the detector, the light usually passes through additional wavelength-selective emission filter, to suppress further the excitation light. The filtered fluorescence signal originating from the entire field of view is then directly projected on a camera.

A significant limitation of widefield fluorescence microscopy is the illumination of multiple planes within the sample, which creates a high background, obscures features in the specimen plane of interest, ultimately reducing axial resolution. To address this issue, confocal microscopy was developed and patented by Marvin Minsky in 1961 [159]. While preparing this text, I had a thought, that it was a time of remarkable events, as my parents were born in the same year (smile highly appreciated).

Instead of illuminating the entire sample as in widefield microscopy, in confocal approach the excitation laser is focused onto the sample to a diffraction-limited spot using a high numerical aperture (NA) objective (see the right panel of Figure 5.3). Similarly, the emitted fluorescence is collected by the same objective, however, before reaching the detector, in the conjugate focal plane of the microscope objective, a pinhole is positioned, to spatially filter out the out-of-focus light and restrain it from being detected. This configuration allows for three-dimensional imaging of biological specimens without the need for physical sectioning.

Fluorescence signal is typically detected by an avalanche photodiode (APD) due to its low dark current, high quantum efficiency, and single-photon sensitivity. Large-area images are generated by scanning the sample (or the objective) point-by-point and recording the fluorescence intensity at each point. Since a confocal microscope collects fluorescence from only one focal spot at

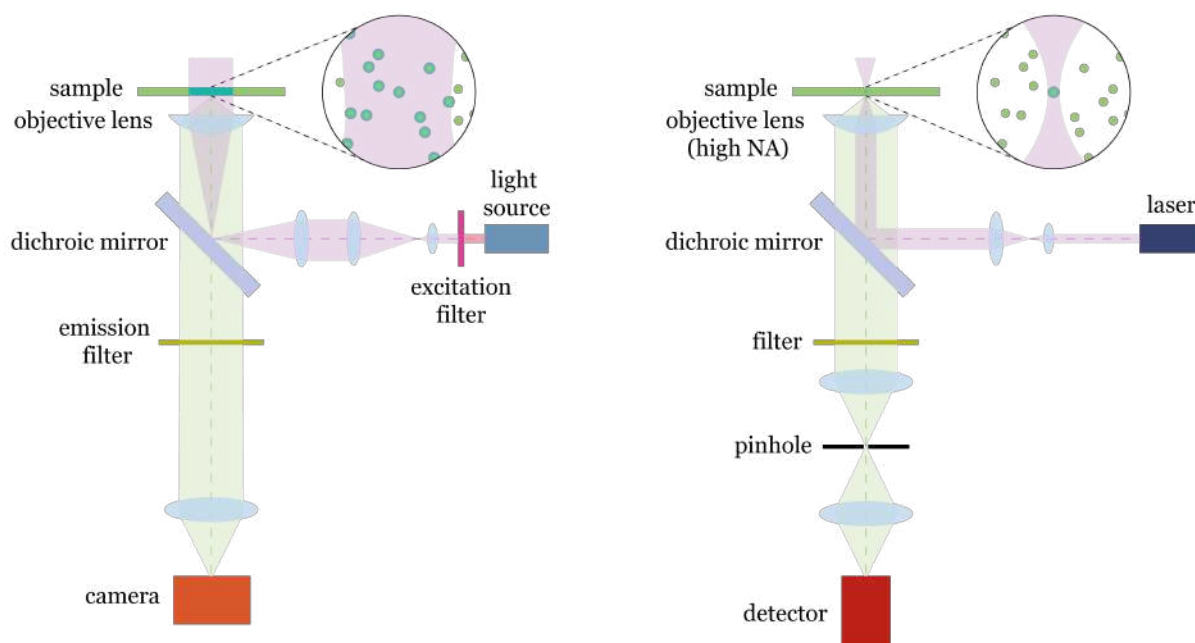


Figure 5.3: Schematic representation of widefield (left panel) and confocal (right panel) microscope setups.

a time, either the sample or the focal spot must be moved to create a large-area image. Moving the sample can be accomplished with a motorized stage, such as a piezoelectric scanning stage, but this method results in relatively slow scanning speeds. Alternatively, the focus can be shifted by using scanning mirrors to change the incident angle at the back focal plane, as is done in confocal laser scanning microscopes. For the collection of the results presented in this thesis, I used both types of scanning – in the home-built fluorescence microscope, the sample was moved using a piezoelectric scanning stage, in the commercial confocal microscope, the laser spot was moved using scanning mirrors.

The emission spectra from specific locations and various fluorescent probes within the sample can also be captured with a spectrally resolved detection based on a charge-coupled device (CCD) paired with a spectrometer, which I utilized in this thesis to monitor the Laurdan fluorescence.

5.2.1 Fluorescent membrane probes

Organic molecules that are considered fluorescent typically contain conjugated double bonds (in aromatic or extended systems) within their chemical structure. Conjugated double bonds involve alternating single and double bonds, creating a system of overlapping atomic p-orbitals. This overlap leads to the formation of delocalized molecular orbitals, allowing π -electrons to be shared across the conjugated system [160, 161]. This delocalization lowers the energy gap between the ground and excited states, making it easier for the molecule to absorb UV or VIS light and subsequently emit it as fluorescence.

Most of the structural components of cell membranes, such as phospholipids and cholesterol, are inherently non-fluorescent. The lack of conjugated double bonds in their structure is a key reason for the absence of suitable electronic transitions that would allow for fluorescence in the UV/VIS range. The accurate understanding of their organization, physicochemical properties and finally their function is therefore closely related to the selection and development of suitable fluorescent analogues that faithfully mimic their properties while allowing detection by spectroscopic or

microscopic methods [162].

The most widely used fluorescent probes in biomembrane studies, and in the measurements forming the base for this thesis, can be categorized into two groups: phase-specific lipid analogues, which are useful due to their preferential distribution between coexisting domains, and phase-sensitive probes, whose photophysical properties change in response to different lipid environments.

Phase-specific probes. These probes can be used to map the lateral organization of membranes, study phase separation, and investigate the dynamics of lipids in coexisting domains. This group of molecules includes primarily fluorescently labeled lipids, most commonly cholesterol [163–165], sphingomyelin [165–167], PC and PE [168], in which the synthetic fluorescent dye is typically covalently attached to the lipid molecule. This stable bond ensures that the fluorescent tag remains associated with the lipid during experiments, providing reliable and consistent labeling. The dye can be attached to different parts of the lipid molecule, such as the head group or one of the acyl chains. These lipid analogues may preferentially partition into different lipid phases, such as the L_o or L_d phase. However, their partitioning behavior is complex and influenced by factors such as the size, polarity, charge, and position of the label, as well as the lipid head group and membrane composition [107]. This is especially evident in the studies showing that the magnitude of the preference between different membrane phases may change or even revert depending on the cell membrane model used [107].

Experimental studies show that the majority of the fluorescently-labeled lipids tend to partition into the more fluid L_d phase, even the 'raft lipids' ones, such as sphingolipids and sterols, with few exceptions [107, 168–170]. The molecular sizes of lipids and their fluorescent tags are typically of the same order (~ 1 kDa). This, along with the tight packing of saturated lipids in the L_o or gel phase likely prevent the insertion of raft lipids tagged with bulky fluorescent dyes.

For instance, head group-tagged PE lipids with unsaturated fatty acid chains (e.g., Atto 633-DOPE) exclusively localize in the L_d phase in model membranes [42], in line with intuition. On the other hand, the labeled PE lipids with saturated fatty acid chains (e.g., DPPE) display less predictable partitioning behavior. DPPE lipids bearing rhodamine-derived fluorophores, such as Lissamine Rhodamine or Texas Red, prefer the L_d phase [171, 172]. Both head group and acyl chain-labeled SM (saturated lipid) fluorescent analogues (e.g. Atto 532-SM, TopFluor-SM, respectively) were shown to partition more into the L_d phase in GUVs [107]. Among the few, chain-labeled TopFluor-cholesterol partitions preferentially in raft-like L_o phase, regardless of the membrane model used [107].

Phase-Sensitive Probes. In contrast to phase-specific probes, the phase-sensitive probes, or alternatively environment-sensitive probes, may partition equally into distinct phase domains in lipid membranes [173]. Nevertheless, they can still provide contrast in fluorescence microscopy, which is governed by the change in their photophysical properties, such as fluorescence emission wavelength (spectral shift), intensity, or fluorescence lifetime, in response to their molecular environment [174]. These probes can provide information about the physicochemical properties of the lipid membranes, such as lipid order (packing) [175], polarity [176], dipole potential [177], and membrane tension [178], just to mention a few. The most common phase-sensitive probes include Laurdan (6-dodecanoyl-2-dimethylaminonaphthalene), which exhibits a spectral shift (solvatochromic probe) depending on the lipid order, and thereby can differentiate between L_o and L_d phase. Its sensitivity to the phase state of the membrane stems from the solvent relaxation phenomenon, which I described in the Chapter 5.1.2. The other example of environment-sensitive probe capable of discerning different membrane phases is di-4-ANEPPDHQ, for which spectral shifts depending on the environment are also observed. However, the underlying physical mechanism of its spectral changes is different. Di-4-ANEPPDHQ is an electrochromic dye, i.e. its fluorescence emission spectrum is sensitive to the transmembrane potential, meaning that

any change in the electric field across the membrane will induce a spectral shift in fluorescence emission. This shift occurs due to a direct interaction between the membrane electric field and the dipole moments of the dye's electronic states [179].

5.3 Sum-frequency generation spectroscopy

5.3.1 Origin of sum-frequency generation

Light is an electromagnetic wave, and as such it is influenced by both the electronic and magnetic properties of the matter it encounters. However, since electronic forces and interactions are significantly stronger than magnetic ones, the description of sum-frequency generation (SFG) spectroscopy in this thesis will be limited to the electric dipole approximation. For a more comprehensive understanding of the quantum mechanical principles underlying SFG, please refer to the textbooks [180–183].

When a molecule interacts with light via weak oscillating electric field \vec{E} , the electron cloud of the molecule will follow this oscillation, resulting in an electric polarization proportional to the electric field:

$$\vec{P} = \alpha \vec{E}, \quad (5.1)$$

where the constant α represents the molecule's polarizability (a measure of how easily its electron cloud can be distorted by an external electric field). In a condensed state with many molecules, their individual polarizabilities can be summed to determine the macroscopic polarizability, known as the susceptibility. This property dictates the overall polarization \vec{P} induced in a material by an electric field:

$$\vec{P} = \epsilon_0 \chi \vec{E}, \quad (5.2)$$

where ϵ_0 is the permittivity of free space. However, for the intense, coherent fields generated by high-power pulsed lasers, two above equations (5.1 and 5.2) no longer hold. At the molecular level, the electron cloud can no longer follow the oscillation, introducing anharmonicity into its response. This anharmonicity, on a macroscopic scale, appears as a nonlinearity in the susceptibility χ . We can express this nonlinearity by representing χ as a sum of components:

$$\chi = \chi^{(1)} + \chi^{(2)} + \chi^{(3)} + \dots \quad (5.3)$$

Here, $\chi^{(1)}$, the first-order susceptibility, represents the linear relationship between P and E . The second-order nonlinear susceptibility, $\chi^{(2)}$, captures the quadratic relationship between \vec{P} and \vec{E} , and the third-order nonlinear susceptibility, $\chi^{(3)}$, describes the cubic relationship between \vec{P} and \vec{E} , and so on, with the nonlinear terms being significantly smaller than the linear term. Equation 5.2 thus becomes:

$$\vec{P} = \epsilon_0 (\chi^{(1)} \vec{E} + \chi^{(2)} \vec{E}^2 + \chi^{(3)} \vec{E}^3 + \dots) \quad (5.4)$$

To explore the origins of the sum-frequency generation, we must consider an incident electric field consisting of electric fields \vec{E}_1 and \vec{E}_2 , oscillating at frequencies ω_1 and ω_2 , overlapped in time and space. The time dependence of the total electric field experienced by a material can be then written as the sum of the respective electric fields:

$$\vec{E}(t) = \vec{E}_1(e^{-i\omega_1 t} + e^{i\omega_1 t}) + \vec{E}_2(e^{-i\omega_2 t} + e^{i\omega_2 t}) \quad (5.5)$$

The resulting second-order polarization $\vec{P}^{(2)}$ response of a material with a non-zero $\chi^{(2)}$ is given by:

$$\vec{P}^{(2)}(t) = \epsilon_0 \chi^{(2)} \vec{E}(t)^2 = \epsilon_0 \chi^{(2)} [\vec{E}_1(e^{-i\omega_1 t} + e^{i\omega_1 t}) + \vec{E}_2(e^{-i\omega_2 t} + e^{i\omega_2 t})]^2 \quad (5.6)$$

Using the binomial theorem, the expression in the brackets can be written as:

$$[\vec{E}_1(e^{-i\omega_1 t} + e^{i\omega_1 t})]^2 + [\vec{E}_2(e^{-i\omega_2 t} + e^{i\omega_2 t})]^2 + 2(\vec{E}_1(e^{-i\omega_1 t} + e^{i\omega_1 t})\vec{E}_2(e^{-i\omega_2 t} + e^{i\omega_2 t})) \quad (5.7)$$

Using the binomial theorem again, and that $e^m e^n = e^{m+n}$, for the first term we get:

$$[\vec{E}_1(e^{-i\omega_1 t} + e^{i\omega_1 t})]^2 = \vec{E}_1^2(e^{-i2\omega_1 t} + e^{i2\omega_1 t} + 2e^0) = \vec{E}_1^2(e^{-i2\omega_1 t} + e^{i2\omega_1 t}) + 2\vec{E}_1^2 \quad (5.8)$$

By an analogy, for the second term we get:

$$[\vec{E}_2(e^{-i\omega_2 t} + e^{i\omega_2 t})]^2 = \vec{E}_2^2(e^{-i2\omega_2 t} + e^{i2\omega_2 t}) + 2\vec{E}_2^2 \quad (5.9)$$

And calculating the third term and combining like terms, leads to:

$$\begin{aligned} 2\vec{E}_1(e^{-i\omega_1 t} + e^{i\omega_1 t})\vec{E}_2(e^{-i\omega_2 t} + e^{i\omega_2 t}) &= 2\vec{E}_1\vec{E}_2(e^{-i\omega_1 t} + e^{i\omega_1 t})(e^{-i\omega_2 t} + e^{i\omega_2 t}) = \\ &= 2\vec{E}_1\vec{E}_2(e^{-i(\omega_1+\omega_2)t} + e^{i(\omega_1+\omega_2)t}) + 2\vec{E}_1\vec{E}_2(e^{-i(\omega_1-\omega_2)t} + e^{i(\omega_1-\omega_2)t}) \end{aligned} \quad (5.10)$$

Combining all terms, we obtain various components of the second-order nonlinear polarization response of a material:

$$\begin{aligned} \vec{P}^{(2)}(t) &= \epsilon_0 \chi^{(2)} \vec{E}(t)^2 = \epsilon_0 \chi^{(2)} [\vec{E}_1(e^{-i\omega_1 t} + e^{i\omega_1 t}) + \vec{E}_2(e^{-i\omega_2 t} + e^{i\omega_2 t})]^2 = \\ &= \epsilon_0 \chi^{(2)} [\vec{E}_1^2(e^{-i2\omega_1 t} + e^{i2\omega_1 t}) + \vec{E}_2^2(e^{-i2\omega_2 t} + e^{i2\omega_2 t}) + \quad \text{(SHG)} \\ &+ 2\vec{E}_1\vec{E}_2(e^{-i(\omega_1+\omega_2)t} + e^{i(\omega_1+\omega_2)t}) + \quad \text{(SFG)} \quad (5.11) \\ &+ 2\vec{E}_1\vec{E}_2(e^{-i(\omega_1-\omega_2)t} + e^{i(\omega_1-\omega_2)t}) + \quad \text{(DFG)} \\ &+ 2(\vec{E}_1^2 + \vec{E}_2^2)] \quad \text{(OR)} \end{aligned}$$

This expression shows all contributions of the second-order nonlinear susceptibility to the polarization. There is a constant term, responsible for the process called optical rectification (OR), which leads to the creation of a static field proportional to \vec{E}_1^2 and \vec{E}_2^2 . Two terms oscillating at twice the original frequencies $2\omega_1$ and $2\omega_2$ are due to second harmonic generation (SHG), and the terms oscillating at the sum frequency $\omega_1+\omega_2$ and at the difference frequency $\omega_1-\omega_2$ result from sum frequency generation (SFG) and difference-frequency generation (DFG) processes, respectively.

5.3.2 Resonant vibrational sum frequency generation

In this thesis, I present the results of resonant VSFG spectroscopy measurements (Chapter 8). In this technique, one of the incident beam frequencies is selected to match the vibrational modes of the investigated sample. This can be achieved when the frequency of the excitation beam lies in the IR spectral range (ω_{IR}). The second beam is set to a visible frequency (ω_{VIS}), typically not-resonant with the material. The beams originating from a VIS and IR pulsed laser source, interact within the sample to generate a sum-frequency pulse ($\omega_{SFG} = \omega_{VIS} + \omega_{IR}$). When ω_{IR} approaches the resonant frequencies of vibrational transitions, the second-order susceptibility $\chi^{(2)}$ is enhanced, and thus the SFG signal intensity.

For VSFG, the second-order polarization component in the frequency domain can be expressed as follows:

$$\vec{P}^{(2)}(\omega_{SFG}) = \epsilon_0 \chi^{(2)} \vec{E}(\omega_{VIS}) \vec{E}(\omega_{IR}) \quad (5.12)$$

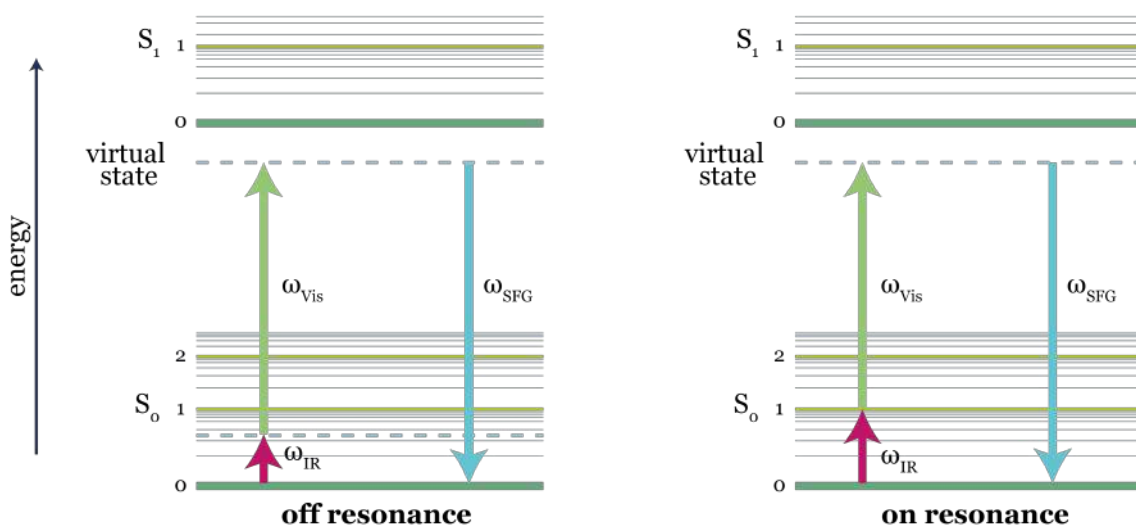


Figure 5.4: Energy level schemes for exemplary paths responsible for non-resonant and resonant process. In the first scenario the incoming beam energies do not match any molecular transitions, resulting in minimal SFG. In the second scheme, the IR beam energy matches the molecular vibration, leading to a resonant enhancement of SFG signal.

It can be demonstrated that in centrosymmetric media, $\chi^{(2)}$ equals zero, meaning that SFG can only occur when inversion symmetry is broken [184]. This condition is naturally met at material interfaces, enabling sum-frequency light to be produced solely from these interfacial regions. This feature is key to the surface specificity observed in SFG spectroscopy. Nevertheless, SFG can also occur within the bulk of non-centrosymmetric crystals. An example of such a crystal is α -quartz, which was used for reference measurements in the experiments presented in Chapter 8.

The second-order susceptibility, comprises both resonant (R) and non-resonant (NR) components, and is given by:

$$\chi^{(2)}(\omega) = \chi_{NR}^{(2)} + \chi_R^{(2)}(\omega) = A_{NR} + \sum_n \frac{A_{R,n}}{\omega_n - \omega_{IR} - i\Gamma_n} \quad (5.13)$$

In this formula, $\chi_{NR}^{(2)}$ and $\chi_R^{(2)}$ denote the effective non-resonant and resonant second-order susceptibilities, respectively. A_{NR} and A_R are the amplitudes of the non-resonant and resonant susceptibilities, while ω_n and Γ_n represent the resonant frequency and the width of the n -th vibrational mode. From equation 5.13, it can be inferred that as ω_{IR} approaches the resonant frequency of a vibrational mode at ω_n , the second-order susceptibility $\chi^{(2)}$ exhibits a resonance with an amplitude $A_{R,n}$ and a linewidth Γ_n .

The resonant second-order nonlinear susceptibility, denoted as $\chi_R^{(2)}$, is a complex quantity. It is often represented by plotting its squared magnitude (intensity spectrum), which correlates directly with the intensity of the SFG signal [143]. For a more detailed analysis of the spectral characteristics of $\chi_R^{(2)}$, it can be decomposed into its real and imaginary components. In the case of a single resonance, the expression is given by:

$$\begin{aligned}
\chi_{R,n}^{(2)} &= \frac{A_{R,n}}{\omega_n - \omega_{IR} - i\Gamma_n} \frac{\omega_n - \omega_{IR} + i\Gamma_n}{\omega_n - \omega_{IR} + i\Gamma_n} = \frac{A_n(\omega_n - \omega_{IR} + i\Gamma_n)}{(\omega_n - \omega_{IR})^2 + \Gamma_n^2} = \\
&= \frac{A_{R,n}(\omega_n - \omega_{IR})}{(\omega_n - \omega_{IR})^2 + \Gamma_n^2} + i \frac{A_{R,n}\Gamma_n}{(\omega_n - \omega_{IR})^2 + \Gamma_n^2} \equiv \\
&\equiv \text{Re}\chi_{R,n}^{(2)} + i\text{Im}\chi_{R,n}^{(2)}
\end{aligned} \tag{5.14}$$

Equation 5.14 indicates that for the real part of the second-order resonant susceptibility ($\text{Re}\chi_R^{(2)}$), the frequency dependence is contained both in the numerator and the denominator. As a result of the intricate frequency dependence, $\text{Re}\chi_R^{(2)}$ is rather challenging to interpret. In contrast, for the imaginary part of the second-order resonant susceptibility ($\text{Im}\chi_R^{(2)}$), the frequency dependence is confined to the denominator only. As such, $\text{Im}\chi_R^{(2)}$ mirrors the key spectral characteristics of the intensity SFG spectrum while also providing information about the absolute amplitude of the resonances, whether positive or negative. For this reason, examining $\text{Im}\chi_R^{(2)}$ is often more insightful when analyzing an SFG spectrum. This is illustrated in Figure 5.5, where the real and imaginary components of $\chi_R^{(2)}$ for an arbitrary resonance are plotted.

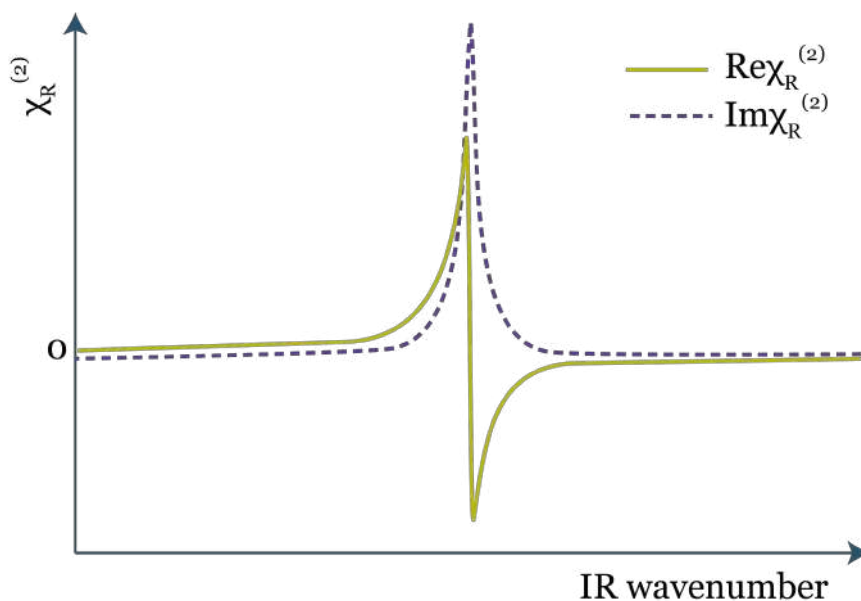


Figure 5.5: The real and imaginary components of $\chi_R^{(2)}$ for an arbitrary resonance. The real component has a dispersive profile, whereas the imaginary component is symmetric around the resonance frequency. Reproduced from [184].

6

Laurdan discerns lipid membrane hydration and cholesterol content

Laurdan is one of the most widely used fluorescent environment-sensitive probes in membrane research, particularly for studying lateral fluidity heterogeneities. Its fluorescence characteristics respond to changes in membrane fluidity due to its sensitivity to the polarity and dipolar relaxation rates of its immediate environment. In the study presented in this chapter, I investigated, for the first time, the spectral response of Laurdan to varying membrane hydration levels and compared these findings to the effect of changes in cholesterol content. While both modulators influence membrane fluidity, their effects are distinct, albeit subtle. I propose a molecular mechanism to explain these differences. Furthermore, by monitoring Laurdan's fluorescence spectrum in the fluid phase of both a phase-separated membrane and a one-phase membrane at full hydration, I discovered that dehydration produces different outcomes in each system. In the phase-separated membrane, fluidity changes were more moderate, suggesting an additional mechanism absent in the one-phase system. I demonstrated that cholesterol redistribution between phases likely accounts for this difference.

Laurdan Discerns Lipid Membrane Hydration and Cholesterol Content

Hanna Orlikowska-Rzeznik,^{*} Emilia Krok, Madhurima Chattopadhyay, Agnieszka Lester, and Lukasz Piatkowski^{*}Cite This: *J. Phys. Chem. B* 2023, 127, 3382–3391

Read Online

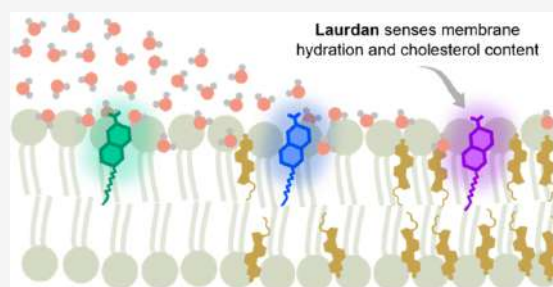
ACCESS |

Metrics & More

Article Recommendations

Supporting Information

ABSTRACT: Studies of biological membrane heterogeneity particularly benefit from the use of the environment-sensitive fluorescent probe Laurdan, for which shifts in the emission, produced by any stimulus (e.g., fluidity variations), are ascribed to alterations in hydration near the fluorophore. Ironically, no direct measure of the influence of the membrane hydration level on Laurdan spectra has been available. To address this, we investigated the fluorescence spectrum of Laurdan embedded in solid-supported lipid bilayers as a function of hydration and compared it with the effect of cholesterol—a major membrane fluidity regulator. The effects are illusively similar, and hence the results obtained with this probe should be interpreted with caution. The dominant phenomenon governing the changes in the spectrum is the hindrance of the lipid internal dynamics. Furthermore, we unveiled the intriguing mechanism of dehydration-induced redistribution of cholesterol between domains in the phase-separated membrane, which reflects yet another regulatory function of cholesterol.



INTRODUCTION

Water hydrating biological membranes are unequivocally essential for the maintenance of cell viability. Living in peculiar physicochemical cooperation, water stabilizes the structure and dynamics of the lipid bilayer¹ and mediates its interactions with other biomolecules,² while lipids affect the spatial arrangement and dynamics of adjacent water molecules.³ It is generally accepted that biomembranes exist in a fully hydrated environment; however, it should be noted that cell life also involves the local, temporary membrane dehydration events, such as adsorption of biomacromolecules or lipid bilayer fusion, the latter being a key phenomenon to subcellular compartmentalization, cell growth, neurotransmission, fertilization, viral entry, or exocytosis.^{4,5} Hence, it is clear that the mechanistic understanding of such events requires detailed insights into the local membrane hydration state. Yet, its determination is nontrivial, since the extent to which water interacts with different segments of the lipid bilayer is modulated by various factors such as temperature, the type of lipid headgroup, acyl chain composition, and the phase state of a lipid bilayer.^{6,7} Membrane phase is largely governed by cholesterol (Chol) content, which is a key regulator of acyl chains' conformational order and lipid dynamics.⁸ Pure phospholipid bilayers are known to exist either in the solid (gel) or liquid-disordered (L_d) phase. At sufficient concentration, cholesterol promotes the formation of the intermediate phase known as the liquid-ordered (L_o) phase, which may

coexist with the other two.⁹ The L_o/L_d coexistence, manifested as lateral heterogeneity on a nanometer and micrometer scale, is considered to be the most relevant from the biological perspective.^{10,11} One of the approaches to assess membrane heterogeneity is to employ a fluorescent environmentally sensitive probe immersed in a bilayer, such as the most commonly used Laurdan.¹² Upon electronic excitation, the Laurdan dipole moment significantly increases, giving rise to dipolar relaxation of the surrounding molecules. The rearrangement of the immediate environment consumes the energy of the excited Laurdan molecule, manifested as a red shift of the emission spectrum.¹³ This accounts for the extreme sensitivity of Laurdan to the polarity and rate of dipolar relaxation of its immediate environment. In the literature, Laurdan is used to probe the membrane heterogeneity referring, often interchangeably, to different membrane physicochemical properties, including lipid order,¹⁴ hydration,¹⁵ or the general term fluidity,¹⁶ and although these features are related to each other, they are not equivalent. Nevertheless, regardless of the property, any shift in the

Received: January 30, 2023

Revised: March 13, 2023

Published: April 6, 2023



emission spectrum has been taken as a consequence of alterations in the number and/or mobility of water molecules near Laurdan's fluorescent moiety, below the glycerol backbone of the phospholipids. Ironically, despite widespread use for more than four decades, no direct measure of the influence of the membrane hydration state on Laurdan spectra has been available.

Here, we investigated, for the first time, the spectral response of Laurdan to dehydration of biomimetic cell membranes, directly compared it with the effect of increasing cholesterol content, and elucidated the molecular mechanisms that govern the observed changes. By monitoring the fluorescence spectral characteristics of Laurdan during dehydration of the membrane with L_o/L_d coexistence, we unveiled an intriguing mechanism of interphase cholesterol redistribution, that is of relevance for membrane-centered cellular events. Our results have important implications for the proper interpretation of data obtained with this and other environmental probes, especially when assessing membrane heterogeneity in living systems, where numerous effects, including local variations in hydration and cholesterol content, can be encountered, often simultaneously.

METHODS

Materials. Lipids 1,2-dimyristoleoyl-glycero-3-phosphocholine (di14:1- $\Delta 9_{cis}$ -PC), egg yolk sphingomyelin (eggSM), cholesterol (Chol), 1,2-dipalmitoyl-*sn*-glycero-3-phosphocholine (DPPC), and 23-(dipyrrometheneborondifluoride)-24-norcholesterol (TopFluor-Chol) were supplied by Avanti Polar Lipids (Alabaster, AL). Fluorescent probe 6-dodecanoyl-2-dimethylaminonaphthalene (Laurdan), phospholipid 1,2-dioleoyl-*sn*-glycero-3-phosphoethanolamine labeled with Atto 633 (Atto 633-DOPE), monosialoganglioside (GM1) from bovine brain, and chloroform (HPLC grade) were purchased from Merck KGaA (Darmstadt, Germany). Alexa Fluor 594 conjugated with cholera toxin subunit B (Alexa Fluor 594-CTxB) was obtained from Molecular Probes, Life Technologies (Grand Island, NY). Buffer reagent 4-(2-hydroxyethyl)piperazine-1-ethanesulfonic acid (HEPES PUFFERAN) was obtained from Carl Roth GmbH + Co., KG (Karlsruhe, Germany). Calcium chloride (CaCl_2) was purchased from Chempur (Piekary Slaskie, Poland). Sodium chloride (NaCl) was supplied by PPH STANLAB Sp. z o.o. (Lublin, Poland). All compounds were used without further purification. Ultrapure water was acquired using the Milli-Q Direct Water Purification System from Merck KGaA (Darmstadt, Germany). Optical adhesive UV-activated glue Norland 68 was purchased from Thorlabs Sweden AB (Mölnådal, Sweden). The sheets of mica used for the preparation of solid supports for the lipid membranes were obtained from Shree GR Exports Private Limited (Kolkata, India). Glass coverslips No. 0 were purchased from Paul Marienfeld GmbH & Co., KG (Lauda-Königshofen, Germany).

Solid-Supported Lipid Bilayers Fabrication. Solid-supported lipid bilayers (SLBs) were prepared using vesicle deposition on a solid substrate procedure as described previously¹ with appropriate modifications. SLBs of different compositions were examined: (i) pure di14:1- $\Delta 9_{cis}$ -PC, (ii) binary mixtures di14:1- $\Delta 9_{cis}$ -PC/Chol with varying Chol molar ratio ($x_{\text{Chol}} = 0.1; 0.2; 0.25; 0.3; 0.4; 0.5; 0.6$), (iii) equimolar ternary mixture di14:1- $\Delta 9_{cis}$ -PC/Chol/eggSM, (iv) pure DPPC, and (v) binary mixtures di14:1- $\Delta 9_{cis}$ -PC/DPPC

with two DPPC molar ratios ($x_{\text{DPPC}} = 0.1; 0.9$). First, the membrane components were mixed along with the fluorescent probe(s) to form a chloroform solution of the specified composition with a final lipid concentration of 10 mM. The lipid to each fluorescent probe molar ratio was 1000:1. For the fluorescence spectral measurements, two probes—Laurdan and Atto 633-DOPE—were used, whereas, for the confocal microscopy experiments three probes—Atto 633-DOPE, TopFluor-Chol, and Alexa Fluor 594-CTxB-GM1 complex—were used to label the membrane. The appropriate solution was then dried under nitrogen gas, followed by desiccation in the vacuum chamber for at least 2 h. The lipid film was then hydrated in buffer solution (10 mM HEPES and 150 mM NaCl, pH adjusted to 7.4) to obtain a 10 mM lipid concentration. The lipid suspension was subjected to four cycles of heating to 60°C and vortexing, with each heating and vortexing step taking 1 min, producing multilamellar vesicles (MLVs). The lipid mixture was diluted 10-fold in a buffer to yield a 1 mM MLV suspension, and then distributed into sterilized glass vials and stored at -20°C for further use. The aliquoted MLV suspension of the desired composition was bath-sonicated for at least 10 min until the solution became transparent, indicating the formation of small unilamellar vesicles (SUVs). To prepare a solid support for SUV deposition, a small amount of immersion oil was deposited onto glass coverslip No. 0, over which a thin sheet of freshly cleaved mica, cut beforehand as round plates with a diameter of 9.53 mm (3/8 inches), was placed and adhered with UV-activated glue around the periphery of the substrate. A microcentrifuge tube's lid and bottom were cut off and the resulting cylinder was placed on a coverslip and sealed with silicone to form a reservoir with mica at the bottom. 100 μL of SUVs suspension was deposited on the mica surface followed by the immediate addition of 2 μL of 0.1 M CaCl_2 solution. After 30 s, 600 μL of the previously used buffer solution was added to prevent the hydration layer from drying out. After 30 min of incubation at ambient temperature, the SLB was rinsed 10 times with 2 mL of buffer solution to wash out the excess, unburst vesicles. Finally, the remaining volume of the tube was filled with the buffer solution, and this condition is called the fully hydrated state of the membrane throughout the paper.

SLB Hydration-State Control. To perform a direct measurement of the effect of the hydration state of the lipid bilayer on the Laurdan fluorescence spectrum, we employed our home-built humidity control setup,^{1,17} assuring a controlled drying process with a slow and sequential decrease in the relative humidity (RH) of the membrane environment. The setup consists of a nitrogen gas (N_2) cylinder, three flow meters, three manual valves, a reservoir with water (for water-vapor saturation), and an electronic hygrometer. In brief, to reduce the SLB hydration, bulk water was first removed with a micropipette from the sample container until no buffer droplets on the mica surface were visible to the naked eye. Nitrogen gas of 95% RH was then immediately, and gently blown into the sample container. The relative humidity of N_2 was regulated by mixing wet (water-vapor-saturated, 95% RH) and dry (0% RH) gas streams. Wet and dry N_2 gas flows were individually regulated by two manual valves while monitoring the readings of two flow meters connected to the flow paths. A third flowmeter and manual valve were used to keep the final N_2 gas flow rate constant at ~ 1.2 L/min throughout the experiment. The electronic hygrometer allowed monitoring of the relative humidity and temperature of the final gas flow,

indicating the possible need for adjustment. The dehydration was performed from 95 to 80% RH and further in steps of ~ 10 to 0% RH. The SLB atmosphere was equilibrated to the specified relative humidity after about 10 min, and only then were the sample imaged and Laurdan emission spectra recorded.

SLB Imaging and Steady-State Emission Spectra Acquisition. The main experiments were carried out on a manual, inverted microscope (Carl Zeiss, Axiovert 200). The excitation beam at 370 nm was provided by a pulsed supercontinuum laser (NKT Photonics, SuperK FIANIUM FIU-15) equipped with a UV extension unit (NKT Photonics, SuperK EXTEND-UV). In all of the experiments described, we used nonpolarized excitation. A 50/50 beam splitter was used to reflect the excitation light into an oil immersion objective (Carl Zeiss, EC Plan-Neofluar 40x/1.30), which focused the beam to a diffraction-limited spot in the sample plane. The epifluorescence signal was spectrally filtered using a 380 nm long-pass filter (Semrock, FF01-380/LP-25) and guided to a single photon counting module (Hamamatsu Photonics, C11202-100) for imaging purposes or to a spectrograph (Andor, Kymera 328I-C), where it was spectrally dispersed with a 150 lines/mm grating and subsequently detected with an electron multiplying charge-coupled device camera (Andor, iXon 888 UCS-BB), precooled to -70°C , for spectral measurements. One or the other detection path was selected with the help of a remotely controlled mirror. Single photon counting module counts were read and converted to a digital signal by data acquisition card (National Instruments Corporation, NI USB-6363). The sample was scanned across the fixed laser foci with a piezoelectric nanopositioning stage (Mad City Labs, Nano-LPS200) in the x - y dimension. Nano-Drive 3 controller (Mad City Labs) was used for controlling the scanning stage. Image reconstruction and positioning of the sample were controlled using a home-made LabVIEW program. To avoid excessive photobleaching, sample illumination was synchronized with data acquisition using an optical beam shutter (Thorlabs, SHB1T).

Monitoring of the cholesterol distribution in the SLB with multiple probes as a function of membrane hydration was realized using a laser-scanning confocal upright microscope (Carl Zeiss, LSM 710) with an oil immersion objective (Carl Zeiss, EC Plan-Neofluar 40x/1.30). Lasers of wavelengths 633, 488, and 543 nm were used for the excitation of Atto 633-DOPE, TopFluor-Chol, and Alexa Fluor 594-CTxB-GM1, respectively. The laser power was adjusted during imaging to avoid excessive photobleaching of the sample.

Fluorescence Spectra Analysis. Laurdan generalized polarization (GP) was calculated from the equation introduced by Parasassi et al.¹⁸ and most commonly used in the literature:

$$\text{GP} = \frac{I_{440} - I_{490}}{I_{440} + I_{490}}$$
 where I_{440} and I_{490} are fluorescence intensities averaged over five data points (~ 2 nm) around 440 and 490 nm, respectively. The averaging was done to compensate for the noise present in the spectra. Each GP value demonstrated in the figures is averaged over at least 10 different spots from each of the samples at a particular membrane hydration state or each cholesterol molar fraction (the number of samples varies from experiment to experiment and ranges from 1 to 4). The uncertainties were calculated as standard deviations.

Spectral decomposition of the fluorescence spectra acquired for the samples with specific composition and at specific

conditions was done using two log-normal functions in the form¹⁹

$$\begin{cases} I = I_m \exp\left[-\frac{\ln 2}{\ln^2(\rho)} \ln^2\left(\frac{a-v}{a-v_m}\right)\right] & \text{if } v < a \\ I = 0 & \text{if } v > a \end{cases} \quad (1)$$

where I represents the fluorescence emission intensity, I_m is the maximum of intensity, v is the wavenumber, v_m is the spectral position of the maximum intensity of the log-normal function, $\rho = \frac{v_m - v_{\min}}{v_{\max} - v_m}$ is the asymmetry of the function (v_{\max} and v_{\min} represent the wavenumber values at half intensity), and a is the limiting wavenumber: $a = v_m + \frac{(v_{\max} - v_{\min})\rho}{\rho^2 - 1}$. First, fluorescence spectra (averaged from at least five spots from each of the samples at a particular membrane hydration state or each cholesterol molar fraction) were fitted to a sum of two log-normal functions, independently for each sample and for each hydration/cholesterol content. In the fitting procedure, performed in Matlab, emission intensity I_m , spectral position of the maximum intensity of the log-normal function v_m , as well as spectral positions determining the asymmetry of the function v_{\max} and v_{\min} were all kept as free parameters. The values for all of the parameters were restricted to take up physically meaningful values. To ensure that the two log-normal functions do not exhibit excessive asymmetry, we restricted $v_m - v_{\min}$ to take up values no larger than 1.5 times $v_{\max} - v_m$. All fitted parameters took values within the imposed bounds for over 90% of the fitted spectra. We point out that throughout the manuscript and the Supporting Information, all spectral data are presented in the wavelength space—experimental data are acquired in the wavelength space—thus, such a representation is more intuitive and also can be easily compared with other literature data showing Laurdan fluorescence spectra.

From the individual spectral fits, it was evident that the two log-normal functions (referred to as short-wavelength and long-wavelength bands in the main text) describe all of the acquired spectra very well (see Figure S1a,b), yielding high values of the coefficient of determination ($R^2 > 0.993$ for all fitted spectra). Moreover, we note that the spectral position of the maximum intensity (v_m) of each fitted function did not exhibit significant changes as a function of hydration/cholesterol content, clearly pointing at the interconversion of the two (short wavelength/long wavelength) populations (see Figure S1c,d). The observed frequency shifts of the two bands for all hydration/cholesterol conditions are small (~ 5 – 10 cm^{-1}) with respect to the separation between the bands (> 50 cm^{-1}) and are random rather than showing a specific trend.

Next, we performed global fits (n spectra for all hydration conditions or cholesterol content for each sample with the specific composition) in which v_m was kept as a global parameter for each of the two bands. All other parameters were allowed to vary for each sample condition. We used averaged parameter values from individual fits as starting parameters for the global fit. An exemplary result of the global fit is shown in Figure S2.

The populations of Laurdan experiencing solvent relaxation and of Laurdan embedded in a nonrelaxing environment were obtained by integrating the short-wavelength and long-wavelength bands, respectively, and represented as band

areas relative to the area of the entire fluorescence spectrum [%].

It should be emphasized that dehydration of the lipid membrane does not affect its integrity and does not lead to the introduction of structural defects. The collected fluorescence emission spectra are highly reproducible (see Note 1 in the Supporting Information), both within the same sample as well as between different samples. Typically, 10–30 emission spectra from distinct spots were measured at each hydration condition for each sample and, importantly, the minute differences (mainly in absolute intensity) are much smaller (see Figure S3) than the differences between emission spectra for different hydration states.

RESULTS AND DISCUSSION

Changes in the steady-state fluorescence spectrum of Laurdan embedded in the solid-supported lipid bilayers (SLBs) composed of a pure phospholipid (di14:1- $\Delta 9$ cis-PC) resulting from membrane dehydration are depicted in Figure 1a. The membrane hydration state was varied by applying a drying process with a slow and sequential reduction in the sample environment's relative humidity (RH).¹

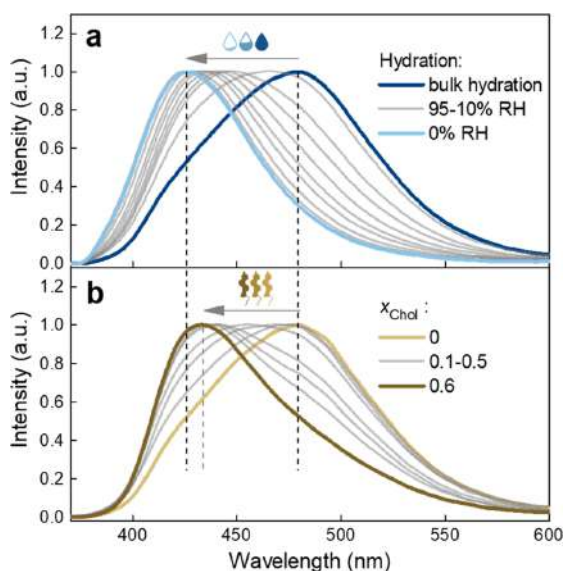


Figure 1. Changes in the fluorescence spectrum of Laurdan embedded in the di14:1- $\Delta 9$ cis-PC SLB induced by (a) decreasing hydration state from bulk hydration down to 0% RH of the atmosphere surrounding the membrane (the intermediate hydrations are 95, 80, 70, 60, 50, 40, 30, 20, and 10% RH) and (b) increasing cholesterol molar fraction x_{Chol} from 0 up to 0.6 (the intermediate molar fractions are 0.1, 0.2, 0.25, 0.3, 0.4, and 0.5). Laurdan emission spectrum for each hydration step and each x_{Chol} is averaged over two different samples, smoothed using a fast Fourier transform filter, and normalized.

The fluorescence spectrum of Laurdan in the fully hydrated SLBs is characterized by a broad band with its maximum centered at ~ 480 nm, a value that is typically attributed to the L_d phase,²⁰ congruent with the report that at room temperature di14:1- $\Delta 9$ cis-PC lipids form the disordered phase.²¹ As the hydration decreases, the spectrum exhibits a

progressive blue shift. After drastic dehydration (0% RH), the probe's emission spectrum resembles that characteristic of ordered membranes (in the gel phase) with the maximum centered at ~ 430 nm.²² Consequently, the observed changes are reflected in the Laurdan generalized polarization (GP), which is a commonly used parameter to assess the overall membrane order (Figure 2a, blue part).¹⁹ It is defined as $GP = (I_{440} - I_{490}) / (I_{440} + I_{490})$, where I_{440} and I_{490} are the fluorescence emission intensities at 440 and 490 nm, respectively.¹⁸

Theoretically, GP can assume values between 1 and -1 ; however, in the lipid membranes, it does not reach its extreme values and typically scales from 0.6 (the most ordered) to below -0.1 (the least ordered).²³ As can be seen from Figure 2a (blue part), for a fully hydrated membrane, GP has a negative value, indicative of a disordered bilayer. Upon removal of bulk water and equilibrating the membrane with an atmosphere of 95% RH, the GP takes on a value close to zero and gradually increases with a further reduction of water content, reaching a maximum of 0.62 ± 0.04 for a water-depleted membrane (0% RH), a characteristic of a gel phase. We note here that the collected fluorescence emission spectra are highly reproducible, both when acquired within the same sample from multiple spots as well as between different samples, and that the minute spectral variation is much smaller than the differences between emission spectra for different hydration states (see Note 1 in the Supporting Information and Figure S3).

Interestingly, we verified whether pure Laurdan deposited on a solid support spectrally responds to changes in hydration by exposing its dry layer to bulk water (see Note 2 in the Supporting Information and Figure S4). However, it neither shifts the spectrum nor changes its shape. We infer that water molecules do not permeate the dried tightly packed aggregates/crystals of Laurdan and that the intermolecular interactions between the probe's molecules dominate over interactions with the interfacial water that would decrease the emitted energy by dipolar relaxation.

To confront the pure effect of membrane dehydration with the influence of cholesterol on the Laurdan response, we examined the membranes composed of a binary mixture of di14:1- $\Delta 9$ cis-PC with varying molar fraction of cholesterol (x_{Chol}). Changes in the probe's emission spectrum resulting from the increasing x_{Chol} are depicted in Figure 1b. The emission peak is significantly affected by the sterol concentration, exhibiting the shift in the same direction as in the case of decreasing hydration. At first glance, changes due to membrane dehydration and due to addition of cholesterol appear very similar. Nevertheless, a few significant differences can be pointed out. Up to $x_{\text{Chol}} = 0.2$, the long-wavelength shoulder of the spectrum (~ 490 – 550 nm) virtually does not change. Only at $x_{\text{Chol}} = 0.25$ and above is a progressive decrease in its intensity observed. In contrast, the lower wavelength part of the spectrum initially exhibits drastic shift and then stops changing above $x_{\text{Chol}} = 0.3$. These were not observed in the case of membrane dehydration, for which gradual change of the spectral position was observed throughout the entire dehydration trajectory. Another characteristic feature, evident when analyzing the change in the spectral shape with increasing x_{Chol} is a spectral shoulder (~ 480 nm) that stands out over a wide range of cholesterol concentrations. Most importantly, comparing the extent of the blue shift, it is apparent that membrane dehydration down to

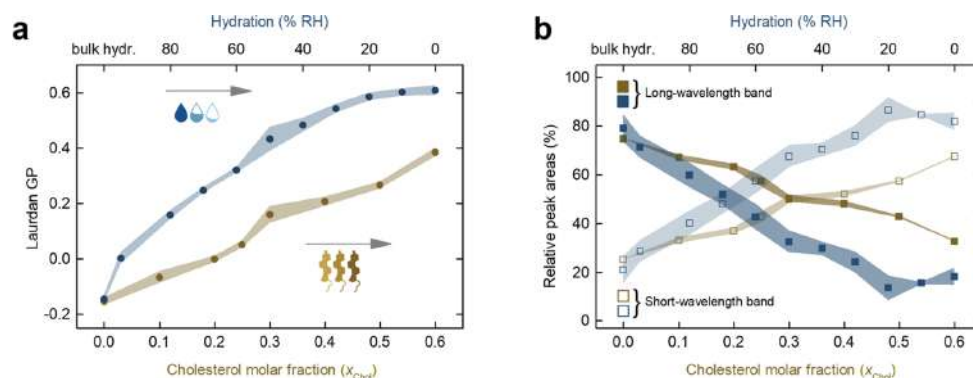


Figure 2. (a) Laurdan GP as a function of membrane hydration and cholesterol molar fraction in a di14:1- $\Delta 9$ cis-PC SLB. (b) Relative area of the two log-normal components that give the best fit to the Laurdan emission spectra in the same membrane system. The uncertainties are standard deviations, denoted as shadows around mean values.

0% RH causes greater changes than the highest cholesterol content, $x_{\text{Chol}} = 0.6$. The same conclusions can be derived by analyzing the course of the GP parameter (Figure 2a, brownish part). The increase in cholesterol is accompanied by an increase in Laurdan GP, but to a much lesser extent compared to the pure effect of water depletion, as it reaches a maximum of 0.38 ± 0.03 for the highest x_{Chol} . We also verified higher molar fractions of cholesterol (0.7 and 0.8), but as expected, they did not produce further changes in the fluorescence spectrum, which is reasonable given the limited solubility of cholesterol in the phospholipid membrane.²⁴ To evaluate whether the other ordering lipid, such as the saturated DPPC, produces a similar spectral response of the probe, we measured Laurdan's fluorescence spectrum in SLBs composed of pure DPPC as well as mixtures of DPPC with di14:1- $\Delta 9$ cis-PC at molar fractions of DPPC equal to 0.1 and 0.9. Intermediate molar fractions were omitted to avoid phase separation.²⁵ Data are presented in Figure S5 and discussed in Supporting Information Note 3. In a nutshell, at a very low molar fraction $x_{\text{DPPC}} = 0.1$, DPPC has a comparable effect on Laurdan's fluorescence spectrum to cholesterol at $x_{\text{Chol}} = 0.1$. However, when higher molar fractions of these molecules are considered, it is clear that cholesterol has a stronger effect on Laurdan's spectral response than DPPC, which highlights the unique character of this sterol molecule.

It can be noted that the Laurdan fluorescence spectrum has a complex line shape, indicative of a heterogeneous local environment. Although due to the dynamic nature of the phospholipid bilayer with existing packing defects,²⁶ and the nonuniform, to some extent, insertion depth²⁷ and orientation²⁸ of Laurdan in the membrane, there may be different subpopulations of Laurdan molecules experiencing distinct environments, we consider that the ability of the local environment to adapt to the excited Laurdan molecule (dipolar relaxation) is the major determinant of Laurdan's fluorescence spectral properties. In the simplest approach, the Laurdan emission can be modeled in terms of a simple two-state model, assuming that the steady-state spectrum contains two contributions, a short-wavelength band reflecting Laurdan population experiencing little or no dipolar relaxation and a long-wavelength band associated with Laurdan within the readily relaxing environment. Thus, to gain further insight into the probe's local molecular environment upon membrane dehydration and addition of cholesterol, we performed spectra

decomposition using two log-normal line shapes as proposed by Bacalun et al.¹⁹ (Figure S2 and Methods Section). The results of such an analysis are plotted in Figure 2b as the relative areas of the short-wavelength and long-wavelength bands, reflecting the percentages of Laurdan populations associated with the nonrelaxed and relaxed local solvent environment, respectively, as a function of the membrane hydration (blue part) and cholesterol content (brownish part). The exemplary extracted spectra for different cholesterol molar fractions are shown in Figure S2.

The Laurdan fluorescence spectra, at all degrees of hydration, can be well described by a superposition of two log-normal line shapes, with peaks around 475 and 427 nm, confirming that the fluorescence decay is mainly due to transitions from only two different excited energy levels. In a pure phospholipid bilayer under fully hydrated conditions, most ($\sim 79\%$) of the fluorescence emission is due to the long-wavelength transition of Laurdan residing in hydrated, relaxed environment (Figure 2b, blue part). As water content is lowered, the population of Laurdan molecules that experiences a dipolar relaxation starts decreasing, giving rise to the short-wavelength transition. A steady decrease of the population within a relaxed environment (and a concomitant increase of the population experiencing the nonrelaxed medium) is observed from a fully hydrated state to around 20% RH. Below this value, the band fractions reach a plateau with the relative populations of the two Laurdan populations accounting for ~ 18 and $\sim 82\%$, respectively, and hence the opposite of full hydration.

Noticeably, cholesterol produces more subtle changes (Figure 2b, brownish part). Analogously to the dehydration process, the Laurdan fluorescence spectra, at all x_{Chol} , can be well reconstructed by a superposition of two log-normal lines, with maxima around 482 and 430 nm (Figure S2). Throughout the analyzed range of cholesterol concentrations, the differences in the proportion of the populations emitting from within the relaxed and nonrelaxed solvent environments are not as pronounced compared to the effect of decreasing membrane hydration. In other words, compared to dehydration, even at high x_{Chol} , a considerable number of Laurdan molecules experience a dipolar relaxation.

Now, let us consider the physical origin of the observed changes. Golfetto et al.²⁹ presented an interesting approach combining the fluorescence lifetime detection and phasor

analysis and showed for Laurdan in solution and Laurdan embedded in model and live cell membranes the ability to disentangle the effects of the extent of hydration versus cholesterol content. However, it should be noted that in this work, the membrane hydration level has not been altered directly. The only variables that were controlled were cholesterol content (in both lipid vesicles and live cells) and epidermal growth factor stimulation (in the case of live cells), and none of them change the membrane hydration state directly and in a specific way. The observed shortening of Laurdan's fluorescence lifetime resulting from collisional quenching has been assigned solely to the reduction of the number of water molecules around the probe without considering other effects. Indeed, the first thing that comes to mind, when observing the shift of the spectrum toward shorter wavelengths as the membrane is dehydrated, is the gradual reduction in the amount of water molecules around the fluorophore. It must be emphasized, however, that there is compelling evidence pointing that the rationale behind dehydration-induced Laurdan's spectral response must be different.

1. First of all, the Laurdan fluorescent moiety localizes below the glycerol backbone of phospholipids, near the *sn*-1 carbonyls,³⁰ where water molecules are scarce and strongly bound via hydrogen bonds to the lipid carbonyl oxygen atoms.^{31–33} Naturally, Laurdan emission is mostly sensitive to the changes in its direct vicinity, rather than at the level of phosphates or even the more outer parts of the membrane. In the lipid membrane interphase region, beyond the carbonyls, water is distributed around the phosphate and choline groups. The carbonyl and phosphate regions involve on average six hydrogen-bonded water molecules.³¹ The choline moiety, on the other hand, due to the nonpolar character of methylenes, cannot form H-bonds with adjacent water molecules. Instead, it organizes the water molecules via weak electrostatic and van der Waals interactions so that they form a clathrate structure around it, containing, in the case of a zwitterionic phosphocholine lipid, about six water molecules.³⁴ In total, these twelve water molecules are considered a first hydration shell. Subsequent hydration shells exclusively incorporate water molecules that are unbound to lipids and are assumed to be localized mostly in the outer parts of the membrane.³⁵ During dehydration, it is the strength of intermolecular interactions that governs the order of desorption of water molecules. As such, loose water molecules interacting only with each other, through relatively weak hydrogen bonds, along with the water molecules directly associated with phospholipids via the weak van der Waals interactions are removed first. These are followed by desorption of water molecules bound more strongly to polar residues of phospholipids.³⁵ It has been shown that upon removal of bulk water and exposing the lipid bilayers to 95% RH, the first solvation shell is largely preserved and only further reduction of hydration degree breaks it down.¹ However, even extreme dehydration does not remove water strongly bound to lipids, particularly those associated with the carbonyls.³⁴ Having this molecular picture in mind, we infer that upon membrane dehydration, the most drastic changes in hydration

occur in the outer regions of the phospholipid bilayer, while the number of water molecules in the vicinity of Laurdan fluorophore barely changes. Thus, the rationale behind Laurdan's response and the change in the local dipolar relaxation properties cannot result solely from the reduction of the number of water molecules in the vicinity of Laurdan. This points toward changes in the kinetics of Laurdan's local environment.

2. In fact, the nanosecond solvent relaxation kinetics, revealed by the time-dependent fluorescence shift measurements of Laurdan in phospholipid bilayers, is associated with the collective rearrangement of the hydrated *sn*-1 carbonyls and not water molecules themselves.³⁶ In addition, in the same work, it was demonstrated that GP calculated from the steady-state Laurdan emission spectra correlates well with rearrangement kinetics of the immediate vicinity of the fluorophore and not the total spectral shift (which mirrors the polarity and thus the number of water molecules).³⁶ This implies that Laurdan GP primarily reflects the mobility of hydrated functional groups of lipids at the Laurdan level rather than the extent of water penetration.
3. The mobility of lipid carbonyls, in turn, has been found to be dependent on the local hydrogen bond network dynamics.³⁷ Noteworthy, a number of experimental^{38–40} and molecular dynamics (MD) simulation³² studies unveiled the slowdown of interfacial water dynamics induced by membrane dehydration.^{32,38} These results indicate an increased residence time of bound water molecules within the lipid polar groups as the water content decreases. The more persistent the hydrogen bonds between water molecules and carbonyl oxygens, the more restricted dynamics of hydrated carbonyls, and consequently, the lower ability of these oscillators to adapt to the excited state of Laurdan.
4. In addition to the slowdown of interfacial water dynamics, both the structural and dynamical properties of lipid bilayers have been found to be affected by the water content.^{1,38,41,42} Membrane dehydration results in a decrease in the area and volume per lipid and a concomitant increase in membrane thickness, as well as a slowdown in the lipid translational and rotational mobility, ultimately leading to a liquid-disordered to gel-phase transition.

Our results of the log-normal decomposition reinforce the idea that during membrane dehydration, there is no significant change in the hydration level at the Laurdan site. Had the number of water molecules aligning around the Laurdan dipole decreased, indicating a decrease in the polarity of the immediate vicinity of the fluorophore, a shift in the peak wavelength would have been observed. Instead, we obtained stable positions of the peaks (see Figure S1).

When interpreting the steady-state Laurdan emission spectrum, it is important to keep in mind that it is the resultant not only of the extent of dipolar relaxation but also of the interplay between its rate and the probe's fluorescence lifetime. In other words, Laurdan emission can be red-shifted only if solvent dipolar realignment occurs while Laurdan is in its excited state. If the dipolar relaxation completes within Laurdan fluorescence lifetime, the steady-state spectrum captures the fully solvent-relaxed state. On the other hand,

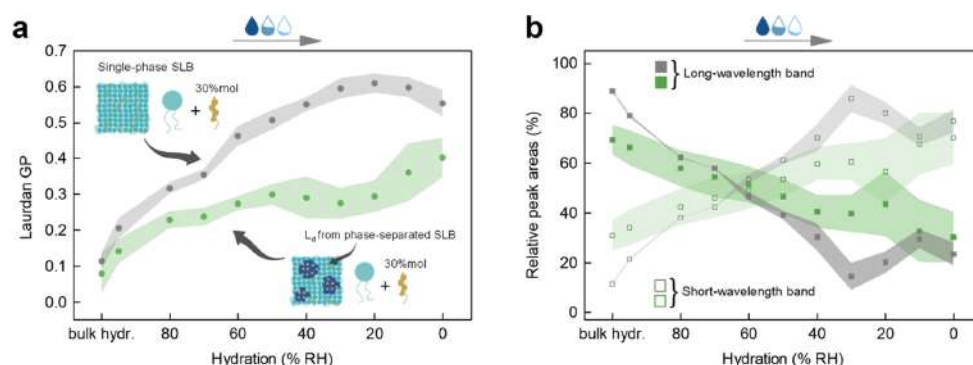


Figure 3. (a) Laurdan GP for L_d domains from phase-separated SLB composed of an equimolar mixture of di14:1- $\Delta 9$ cis-PC/Chol/eggSM and for the counterpart from SLB without phase separation composed of a binary mixture of di14:1- $\Delta 9$ cis-PC/Chol with $x_{\text{Chol}} = 0.3$ as a function of the hydration level. (b) Relative area of the two log-normal components that give the best fit of the Laurdan emission spectra in the same membrane systems as a function of hydration. The uncertainties are standard deviations, denoted as shadows around mean values.

when the fluorescence occurs before the probe's polar environment responds, the Laurdan steady-state spectrum appears as if dipolar relaxation has not occurred. It should be noted, however, that the main process that shortens the fluorescence lifetime of Laurdan is the collisional quenching by water molecules within the bilayer.²⁹ Therefore, the excited-state lifetime is expected to be the shortest at fully hydrated conditions. Yet, at this hydration level, we observe a substantial red shift. Thus, while we do not assert that we capture the fully solvent-relaxed state, the emission occurs at least from a partially solvent-relaxed state. We assume that as the membrane hydration level decreases, Laurdan fluorescence lifetime does not change or at most increases.

Altogether, the above reasoning based on our observations as well as compelling evidence from previous studies show that the observed changes in the Laurdan fluorescence emission spectrum result from the hampered dipolar relaxation of Laurdan's immediate environment. Therefore, we interpret the decrease in the area of the long-wavelength band as a diminishing population of Laurdan molecules for which the collective relaxation of the hydrated lipid groups completes within Laurdan's fluorescence lifetime. In other words, as the water depletion in the bilayer progresses, the number of localized sites where hydrogen bond network and lipid dynamics allow for the hydrated carbonyls to reorient along the Laurdan excited-state dipole decreases.

The influence of membrane dehydration and the effect of cholesterol on the Laurdan emission spectrum are illusively similar, but not equivalent. Importantly, congruent with our spectral decomposition results, as suggested by Amaro et al.,⁴³ based on the time-resolved emission spectra measurements, the presence of cholesterol does not significantly affect the polarity (number of water molecules) in the vicinity of the Laurdan fluorophore. Therefore, cholesterol-induced changes in the probe's emission spectrum must also be associated with the reduced kinetics of dipolar relaxation. Intriguingly, both experimental and theoretical investigations revealed that contrary to dehydration, an increase in cholesterol content in the membrane leads to a rupturing of rigid interlipid H-bonds bridging two adjacent phospholipids, and an accompanying increase in the fraction of lipid–water H-bonds, which are faster and more mobile, thus overall leading to an enhancement in the water mobility at the interface.^{44–46} This effect

would rather promote the dipolar relaxation around the Laurdan fluorescent moiety. On the other hand, cholesterol is known to induce phospholipid bilayer ordering, as manifested by a significant increase in the C–H bond order parameter of different segments in the acyl chains of lipids in nuclear magnetic resonance experiments.^{47–49} Interestingly, as reported by Warschawski and Devaux,⁴⁷ the effect of cholesterol is much more pronounced than temperature or even the degree of unsaturation of the acyl chains. However, it should be emphasized that this relates only to the hydrophobic core of the membrane. The structural order parameters of the interfacial regions of the phospholipid bilayer, namely, the choline, phosphate, and glycerol backbone of the lipid headgroups along with the carbonyl region, remain virtually unaffected by the presence of cholesterol.^{48,49} Therefore, it is highly unlikely that it is the structural conformational ordering that causes such drastic changes in the Laurdan spectrum upon addition of cholesterol. It is worth noting, however, that the conformational order reflects the orientation of the C–H bond vector with respect to the bilayer normal averaged over the lipid ensemble and over time,⁵⁰ but does not carry information about its dynamics. Importantly, recent work by Antila et al.⁴⁹ unveiled that although cholesterol causes only marginal changes in the structural order of the membrane region where Laurdan resides, it significantly impedes the dynamics of the glycerol backbone and the associated carbonyls. This implies that the predominant phenomenon governing the cholesterol-induced blue shift of the Laurdan fluorescence spectrum is the slowing down of intralipid dynamics.

After determining both the effect of dehydration of a pure phospholipid bilayer and cholesterol incorporation, we evaluated the Laurdan response to dehydration of a phase-separated membrane, which is considered a much better mimic of biological membranes. To this end, we used an equimolar ternary mixture of di14:1- $\Delta 9$ cis-PC, cholesterol, and egg sphingomyelin (eggSM), which at room temperature exhibits the L_o/L_d phase coexistence (Figure S6). The use of SLBs as samples and fluorescence microscopy coupled with spectral detection enabled collection of spectra separately from the L_d and L_o domains. Under fully hydrated conditions, the emission of Laurdan in L_o is blue-shifted and significantly narrower than for Laurdan in the L_d phase (Figure S7), consistent with the previous observations.⁵¹ As expected, as the hydration level

decreases, the fluorescence spectrum of Laurdan in L_d shifts toward shorter wavelengths (Figure S7a). Changes for L_o phase are much less pronounced (Figures S7b and S8); therefore, we focus here on the L_d . The discussion on the insensitivity of Laurdan to dehydration of the L_o phase can be found in Supporting Information Note 4. Complete dehydration of L_d domains resulted in a smaller shift in the spectrum than dehydration of the single-component membrane, but greater than for a membrane with the maximum cholesterol content. It is worth noting that the lateral organization of the membrane was monitored between the spectra collection routes for distinct hydration states, and it was confirmed that the phase separation of the membrane remained virtually unaltered during the dehydration process (see Figure S6). Comprehensive data on this issue can be found in our previous work.¹

Analysis of the GP parameter as a function of hydration level of L_d domains reveals an interesting behavior (Figure 3a, green part).

In the range from bulk hydration to 50% RH, a gradual, small increase in GP can be observed, after which it remains constant down to 20% RH, and then it increases slightly again. It is qualitatively different than in the case of pure phospholipid SLBs dehydration. Intrigued by this, we examined whether changes in GP caused by the dehydration process of a membrane without phase separation, but with the same composition as in the L_d domains, occur in the same way. By comparing the line shape of the Laurdan fluorescence spectra acquired from the L_d domains with the ones originating from the monophasic membranes with different x_{Chol} , we inferred that under fully hydrated conditions, the x_{Chol} in L_d is in the range of ~ 0.25 – 0.3 . Therefore, to reproduce the molecular L_d composition in the membrane without phase separation, we prepared monophasic lipid membranes with $x_{\text{Chol}} = 0.3$ and yet again monitored Laurdan fluorescence during the dehydration process. It was assumed that since the two systems at bulk hydration are compositionally the same, the dehydration process would cause the same changes in Laurdan emission. Changes of the Laurdan spectrum in a membrane composed of a binary mixture of di14:1- $\Delta 9$ cis-PC and Chol due to dehydration are demonstrated in Figure S9. The course of the GP value as a function of the hydration state of this membrane (Figure 3a, gray part) qualitatively resembles that for a pure phospholipid membrane (Figure 2a), except that it starts from a slightly higher value at full hydration (indicative of increased order) and stops changing below 30% RH but reaches the same average value of 0.62. But most importantly, and surprisingly, it does not resemble the trajectory for its counterpart from the phase-separated membrane (Figure 3a, green part). For the membrane without L_o domains present, the changes are steeper and do not exhibit a plateau in the range from 50 to 20% RH. In addition, in general, GP has significantly higher values for each of the hydration levels, except for bulk hydration, compared to the L_d domains from the phase-separated membrane. The spectral global analysis further highlights these differences (Figure 3b). The results are rather intriguing and indicative of an additional mechanism that counteracts and effectively softens the changes caused by dehydration of L_d in the phase-separated membrane. The observed trajectories (whether GP or resulting from spectral decomposition) resemble those observed for changing the cholesterol content (Figure 2b) rather than those for dehydration, suggesting that perhaps the cholesterol content in

L_d phase changes. This is feasible as L_o phase contains more cholesterol ($\sim 70\%$ of all cholesterol in the membrane) and may act as a reservoir of cholesterol in the phase-separated membranes. Therefore, we reason that the peculiar dehydration-induced behavior of L_d phase in the phase-separated membrane might be due to the redistribution of components between L_o and L_d domains, most likely involving cholesterol. This would also rationalize our previous findings,¹ that with reduced hydration, the hydrophobic mismatch between the L_d and L_o domains decreases significantly (cholesterol influx to L_d phase would increase its thickness, thus lessening the hydrophobic mismatch between domains). To test our hypothesis, we conducted fluorescence microscopy experiments with fluorescently labeled cholesterol, the results of which are depicted in Figure S10. Under fully hydrated conditions, as expected, higher intensity of TopFluor-Chol emission is found in L_o domains. However, with reduced hydration, the contrast diminishes until it becomes reversed, showing that the L_d domains contain more cholesterol. Therefore, it can be concluded that cholesterol influx from L_o to L_d phase counteracts the dehydration-induced extensive changes in fluidity. However, the study of cholesterol migration was not the aim of this work and an in-depth understanding and quantification of this phenomenon require additional experiments and analysis.

CONCLUSIONS

In conclusion, we have provided a direct measure of the influence of the hydration level of the lipid bilayer on Laurdan spectra, which so far has been unattainable. We have shown that the effects of membrane dehydration and cholesterol incorporation on Laurdan's fluorescence spectrum are illusively similar, and thus interpretation of data obtained with this probe should be done with caution. We evidence that the dehydration-induced changes in Laurdan's emission spectrum result from the conformational ordering of lipids and hindrance of the lipid internal motions along with the slowdown of hydrogen bond network dynamics acting collectively to impede the dipolar relaxation around the probe's excited-state dipole. In the case of cholesterol incorporation, for which neither hydrogen bond network relaxation slowdown nor static conformational ordering of the lipid bilayer region probed by Laurdan is observed, changes in the emission are likely caused only by the hampered dynamics of the glycerol backbone and the associated carbonyls, which rationalizes more subtle changes compared to membrane dehydration.

Moreover, by varying the composition and organization of the membranes (single-component, multicomponent phase-separated), we have shown that Laurdan's spectral response to dehydration is much temperate in the presence of cholesterol. In other words, cholesterol to some extent counteracts the lowered relaxation properties of Laurdan's local environment upon dehydration.

Furthermore, our unprecedented way to obtain biomimetic cell membranes with a well-controlled hydration state without interfering with membrane composition along with the detection of the Laurdan spectral response led us to unveil that the dehydration of the phase-separated membrane drives the redistribution of cholesterol between domains. It likely acts as a regulatory mechanism to prevent excessive deviations in fluidity that may destabilize the cell membrane and hence be harmful to the cell. This intriguing finding adds to the multiple

actions of cholesterol toward the mechanochemical homeostasis of lipid membranes. Our results provide new insights at the intersection of physical chemistry, photo- and biophysics and should stimulate the design of a range of new experiments and simulations regarding the specificity and sensitivity of environmental probes.

■ ASSOCIATED CONTENT

Supporting Information

The Supporting Information is available free of charge at <https://pubs.acs.org/doi/10.1021/acs.jpcc.3c00654>.

Experimental results and information; additional results of the independent and global fitting procedure for different SLB systems, reproducibility of the measured spectra, fluorescence images and spectra of Laurdan crystals/aggregates on solid support in dry and wet conditions, fluorescence spectra of Laurdan embedded in lipid bilayers composed of pure DPPC and binary mixtures with di14:1- Δ^9 cis-PC, fluorescence microscopy images of a phase-separated SLB as a function of the membrane hydration state, fluorescence spectra of Laurdan in liquid-disordered and liquid-ordered domains from phase-separated SLB and in one-phase SLB with the molar fraction of cholesterol 0.3 as a function of the membrane hydration state, generalized polarization of Laurdan in the liquid-ordered phase as a function of membrane hydration, and confocal fluorescence microscopy images of a triple-labeled SLB composed of an equimolar mixture of di14:1- Δ^9 cis-PC, cholesterol, and egg sphingomyelin for three different membrane hydration states (PDF)

■ AUTHOR INFORMATION

Corresponding Authors

Hanna Orlikowska-Rzeznik – Faculty of Materials Engineering and Technical Physics, Poznan University of Technology, 61-138 Poznan, Poland; orcid.org/0000-0003-0697-4781; Phone: +48 61 665 31 99; Email: hanna.orlikowska@put.poznan.pl

Lukasz Piatkowski – Faculty of Materials Engineering and Technical Physics, Poznan University of Technology, 61-138 Poznan, Poland; orcid.org/0000-0002-1226-2257; Phone: +48 61 665 31 80; Email: lukasz.j.piatkowski@put.poznan.pl

Authors

Emilia Krok – Faculty of Materials Engineering and Technical Physics, Poznan University of Technology, 61-138 Poznan, Poland; orcid.org/0000-0002-4637-2729

Madhurima Chattopadhyay – Faculty of Materials Engineering and Technical Physics, Poznan University of Technology, 61-138 Poznan, Poland; orcid.org/0000-0001-8900-163X

Agnieszka Lester – Faculty of Materials Engineering and Technical Physics, Poznan University of Technology, 61-138 Poznan, Poland; orcid.org/0000-0002-4047-9672

Complete contact information is available at: <https://pubs.acs.org/doi/10.1021/acs.jpcc.3c00654>

Notes

The authors declare no competing financial interest.

■ ACKNOWLEDGMENTS

This work was financed from the budget funds allocated for science in the years 2019–2023 as a research project under the “Diamond Grant” program (Decision: 0042/DIA/2019/48). The authors acknowledge the financial support from the EMBO Installation Grant 2019 (IG 4147) and the National Science Centre (Poland) 2020/37/B/ST4/01785. L.P. acknowledges financial support from the First TEAM Grant No. POIR.04.04.00-00-5D32/18-00 provided by the Foundation for Polish Science (FNP).

■ REFERENCES

- Chattopadhyay, M.; Krok, E.; Orlikowska, H.; Schwill, P.; Franquelim, H. G.; Piatkowski, L. Hydration Layer of a Few Molecules Controls Lipid Mobility in Biomimetic Membranes. *J. Am. Chem. Soc.* **2021**, *143*, 14551–14562.
- Martelli, F.; Crain, J.; Franzese, G. Network Topology in Water Nanoconfined between Phospholipid Membranes. *ACS Nano* **2020**, *14*, 8616–8623.
- Laage, D.; Elsaesser, T.; Hynes, J. T. Water Dynamics in the Hydration Shells of Biomolecules. *Chem. Rev.* **2017**, *117*, 10694–10725.
- Aeffner, S.; Reusch, T.; Weinhausen, B.; Salditt, T. Energetics of Stalk Intermediates in Membrane Fusion Are Controlled by Lipid Composition. *Proc. Natl. Acad. Sci. U.S.A.* **2012**, *109*, E1609–E1618.
- Tian, Z.; Gong, J.; Crowe, M.; Lei, M.; Li, D.; Ji, B.; Diao, J. Biochemical Studies of Membrane Fusion at the Single-Particle Level. *Prog. Lipid Res.* **2019**, *73*, 92–100.
- Watanabe, N.; Suga, K.; Umakoshi, H. Functional Hydration Behavior: Interrelation between Hydration and Molecular Properties at Lipid Membrane Interfaces. *J. Chem.* **2019**, *2019*, No. 4867327.
- M'Baye, G.; Mély, Y.; Duportail, G.; Klymchenko, A. S. Liquid Ordered and Gel Phases of Lipid Bilayers: Fluorescent Probes Reveal Close Fluidity but Different Hydration. *Biophys. J.* **2008**, *95*, 1217–1225.
- Wydro, P.; Knapczyk, S.; Łapczyńska, M. Variations in the Condensing Effect of Cholesterol on Saturated versus Unsaturated Phosphatidylcholines at Low and High Sterol Concentration. *Langmuir* **2011**, *27*, S433–S444.
- Aguilar, L. F.; Pino, J. A.; Soto-Arriaza, M. A.; Cuevas, F. J.; Sánchez, S.; Sotomayor, C. P. Differential Dynamic and Structural Behavior of Lipid-Cholesterol Domains in Model Membranes. *PLoS One* **2012**, *7*, No. e40254.
- Levental, I.; Levental, K. R.; Heberle, F. A. Lipid Rafts: Controversies Resolved, Mysteries Remain. *Trends Cell Biol.* **2020**, *30*, 341–353.
- Sezgin, E.; Levental, I.; Mayor, S.; Eggeling, C. The Mystery of Membrane Organization: Composition, Regulation and Roles of Lipid Rafts. *Nat. Rev. Mol. Cell Biol.* **2017**, *18*, 361–374.
- Gunther, G.; Malacrida, L.; Jameson, D. M.; Gratton, E.; Sánchez, S. A. LAURDAN since Weber: The Quest for Visualizing Membrane Heterogeneity. *Acc. Chem. Res.* **2021**, *54*, 976–987.
- Malacrida, L.; Gratton, E. LAURDAN Fluorescence and Phasor Plots Reveal the Effects of a H₂O₂ Bolus in NIH-3T3 Fibroblast Membranes Dynamics and Hydration. *Free Radic. Biol. Med.* **2018**, *128*, 144–156.
- Owen, D. M.; Rentero, C.; Magenau, A.; Abu-Siniyeh, A.; Gaus, K. Quantitative Imaging of Membrane Lipid Order in Cells and Organisms. *Nat. Protoc.* **2012**, *7*, 24–35.
- Salvolini, E.; Buldreghini, E.; Lucarini, G.; Vignini, A.; Lenzi, A.; Di Primio, R.; Balercia, G. Involvement of Sperm Plasma Membrane and Cytoskeletal Proteins in Human Male Infertility. *Fertil. Steril.* **2013**, *99*, 697–704.
- Hofstetter, S.; Denter, C.; Winter, R.; McMullen, L. M.; Gänzle, M. G. Use of the Fluorescent Probe LAURDAN to Label and Measure Inner Membrane Fluidity of Endospores of *Clostridium* Spp. *J. Microbiol. Methods* **2012**, *91*, 93–100.

- (17) Chattopadhyay, M.; Orlikowska, H.; Krok, E.; Piatkowski, L. Sensing Hydration of Biomimetic Cell Membranes. *Biosensors* **2021**, *11*, No. 241.
- (18) Parasassi, T.; De Stasio, G.; d'Ubaldo, A.; Gratton, E. Phase Fluctuation in Phospholipid Membranes Revealed by Laurdan Fluorescence. *Biophys. J.* **1990**, *57*, 1179–1186.
- (19) Bacalum, M.; Zorila, B.; Radu, M. Fluorescence Spectra Decomposition by Asymmetric Functions: Laurdan Spectrum Revisited. *Anal. Biochem.* **2013**, *440*, 123–129.
- (20) Pérez, H. A.; Disalvo, A.; de los Angeles Frias, M. Effect of Cholesterol on the Surface Polarity and Hydration of Lipid Interphases as Measured by Laurdan Fluorescence: New Insights. *Colloids Surf., B* **2019**, *178*, 346–351.
- (21) Aghaaminiha, M.; Ghanadian, S. A.; Ahmadi, E.; Farnoud, A. M. A Machine Learning Approach to Estimation of Phase Diagrams for Three-Component Lipid Mixtures. *Biochim. Biophys. Acta, Biomembr.* **2020**, *1862*, No. 183350.
- (22) De Vequi-Suplicy, C. C.; Benatti, C. R.; Lamy, M. T. Laurdan in Fluid Bilayers: Position and Structural Sensitivity. *J. Fluoresc.* **2006**, *16*, 431–439.
- (23) Bagatolli, L. A. Monitoring Membrane Hydration with 2-(Dimethylamino)-6-Acyl-naphthalenes Fluorescent Probes. In *Subcellular Biochemistry*; Springer, 2015; Vol. 71, pp 105–125.
- (24) Subczynski, W. K.; Pasenkiewicz-Gierula, M.; Widomska, J.; Mainali, L.; Raguz, M. High Cholesterol/Low Cholesterol: Effects in Biological Membranes: A Review. *Cell Biochem. Biophys.* **2017**, *75*, 369–385.
- (25) Shimokawa, N.; Nagata, M.; Takagi, M. Physical properties of the hybrid lipid POPC on micrometer-sized domains in mixed lipid membranes. *Phys. Chem. Chem. Phys.* **2015**, *17*, 20882–20888.
- (26) Tripathy, M.; Thangamani, S.; Srivastava, A. Three-Dimensional Packing Defects in Lipid Membrane as a Function of Membrane Order. *J. Chem. Theory Comput.* **2020**, *16*, 7800–7816.
- (27) Jurkiewicz, P.; Sýkora, J.; Olzyńska, A.; Humpolíčková, J.; Hof, M. Solvent Relaxation in Phospholipid Bilayers: Principles and Recent Applications. *J. Fluoresc.* **2005**, *15*, 883–894.
- (28) Osella, S.; Smisdom, N.; Ameloot, M.; Knippenberg, S. Conformational Changes as Driving Force for Phase Recognition: The Case of Laurdan. *Langmuir* **2019**, *35*, 11471–11481.
- (29) Golffetto, O.; Hinde, E.; Gratton, E. Laurdan Fluorescence Lifetime Discriminates Cholesterol Content from Changes in Fluidity in Living Cell Membranes. *Biophys. J.* **2013**, *104*, 1238–1247.
- (30) Jurkiewicz, P.; Cwiklik, L.; Jungwirth, P.; Hof, M. Lipid Hydration and Mobility: An Interplay between Fluorescence Solvent Relaxation Experiments and Molecular Dynamics Simulations. *Biochimie* **2012**, *94*, 26–32.
- (31) Pasenkiewicz-Gierula, M.; Baczynski, K.; Markiewicz, M.; Murzyn, K. Computer Modelling Studies of the Bilayer/Water Interface. *Biochim. Biophys. Acta, Biomembr.* **2016**, *1858*, 2305–2321.
- (32) Calero, C.; Franzese, G. Membranes with Different Hydration Levels: The Interface between Bound and Unbound Hydration Water. *J. Mol. Liq.* **2019**, *273*, 488–496.
- (33) Zhang, R.; Cross, T. A.; Peng, X.; Fu, R. Surprising Rigidity of Functionally Important Water Molecules Buried in the Lipid Headgroup Region. *J. Am. Chem. Soc.* **2022**, *144*, 7881–7888.
- (34) Disalvo, E. A.; Lairion, F.; Martini, F.; Tymczyszyn, E.; Frias, M.; Almaleck, H.; Gordillo, G. J. Structural and Functional Properties of Hydration and Confined Water in Membrane Interfaces. *Biochim. Biophys. Acta, Biomembr.* **2008**, *1778*, 2655–2670.
- (35) Bhide, S. Y.; Berkowitz, M. L. Structure and Dynamics of Water at the Interface with Phospholipid Bilayers. *J. Chem. Phys.* **2005**, *123*, No. 224702.
- (36) Amaro, M.; Šachl, R.; Jurkiewicz, P.; Coutinho, A.; Prieto, M.; Hof, M. Time-Resolved Fluorescence in Lipid Bilayers: Selected Applications and Advantages over Steady State. *Biophys. J.* **2014**, *107*, 2751–2760.
- (37) Beranová, L.; Humpolíčková, J.; Sýkora, J.; Benda, A.; Cwiklik, L.; Jurkiewicz, P.; Gröbner, G.; Hof, M. Effect of Heavy Water on Phospholipid Membranes: Experimental Confirmation of Molecular Dynamics Simulations. *Phys. Chem. Chem. Phys.* **2012**, *14*, 14516–14522.
- (38) Malik, S.; Debnath, A. Dehydration Induced Dynamical Heterogeneity and Ordering Mechanism of Lipid Bilayers. *J. Chem. Phys.* **2021**, *154*, No. 174904.
- (39) Tielrooij, K. J.; Paparo, D.; Piatkowski, L.; Bakker, H. J.; Bonn, M. Dielectric Relaxation Dynamics of Water in Model Membranes Probed by Terahertz Spectroscopy. *Biophys. J.* **2009**, *97*, 2484–2492.
- (40) Piatkowski, L.; De Heij, J.; Bakker, H. J. Probing the Distribution of Water Molecules Hydrating Lipid Membranes with Ultrafast Förster Vibrational Energy Transfer. *J. Phys. Chem. B* **2013**, *117*, 1367–1377.
- (41) Maiti, A.; Daschakraborty, S. How Do Urea and Trimethylamine-N-Oxide Influence the Dehydration-Induced Phase Transition of a Lipid Membrane? *J. Phys. Chem. B* **2021**, *125*, 10149–10165.
- (42) Högberg, C. J.; Lyubartsev, A. P. A Molecular Dynamics Investigation of the Influence of Hydration and Temperature on Structural and Dynamical Properties of a Dimyristoylphosphatidylcholine Bilayer. *J. Phys. Chem. B* **2006**, *110*, 14326–14336.
- (43) Amaro, M.; Reina, F.; Hof, M.; Eggeling, C.; Sezgin, E. Laurdan and Di-4-ANEPPDHQ Probe Different Properties of the Membrane. *J. Phys. D: Appl. Phys.* **2017**, *50*, No. 134004.
- (44) Elola, M. D.; Rodriguez, J. Influence of Cholesterol on the Dynamics of Hydration in Phospholipid Bilayers. *J. Phys. Chem. B* **2018**, *122*, 5897–5907.
- (45) Oh, M. I.; Oh, C. I.; Weaver, D. F. Effect of Cholesterol on the Structure of Networked Water at the Surface of a Model Lipid Membrane. *J. Phys. Chem. B* **2020**, *124*, 3686–3694.
- (46) Cheng, C. Y.; Olijve, L. L. C.; Kausik, R.; Han, S. Cholesterol Enhances Surface Water Diffusion of Phospholipid Bilayers. *J. Chem. Phys.* **2014**, *141*, No. 22D513.
- (47) Warschawski, D. E.; Devaux, P. F. Order Parameters of Unsaturated Phospholipids in Membranes and the Effect of Cholesterol: A ¹H-¹³C Solid-State NMR Study at Natural Abundance. *Eur. Biophys. J.* **2005**, *34*, 987–996.
- (48) Kučerka, N.; Perlmutter, J. D.; Pan, J.; Tristram-Nagle, S.; Katsaras, J.; Sachs, J. N. The Effect of Cholesterol on Short- and Long-Chain Monounsaturated Lipid Bilayers as Determined by Molecular Dynamics Simulations and X-Ray Scattering. *Biophys. J.* **2008**, *95*, 2792–2805.
- (49) Antila, H. S.; Wurl, A.; Ollila, O. H. S.; Miettinen, M. S.; Ferreira, T. M. Rotational Decoupling between the Hydrophilic and Hydrophobic Regions in Lipid Membranes. *Biophys. J.* **2022**, *121*, 68–78.
- (50) Piggot, T. J.; Allison, J. R.; Sessions, R. B.; Essex, J. W. On the Calculation of Acyl Chain Order Parameters from Lipid Simulations. *J. Chem. Theory Comput.* **2017**, *13*, 5683–5696.
- (51) Jay, A. G.; Hamilton, J. A. Disorder Amidst Membrane Order: Standardizing Laurdan Generalized Polarization and Membrane Fluidity Terms. *J. Fluoresc.* **2017**, *27*, 243–249.

Supporting Information

Laurdan Discerns Lipid Membrane Hydration and Cholesterol Content

Hanna Orlikowska-Rzeznik*, Emilia Krok, Madhurima Chattopadhyay, Agnieszka Lester, Lukasz Piatkowski*

Faculty of Materials Engineering and Technical Physics, Poznan University of Technology, Piotrowo 3, 61-138 Poznan, Poland

*hanna.orlikowska@put.poznan.pl, tel. +48 61 665 31 99

*lukasz.j.piatkowski@put.poznan.pl, tel. +48 61 665 31 80

Supplementary Experimental Results and Information

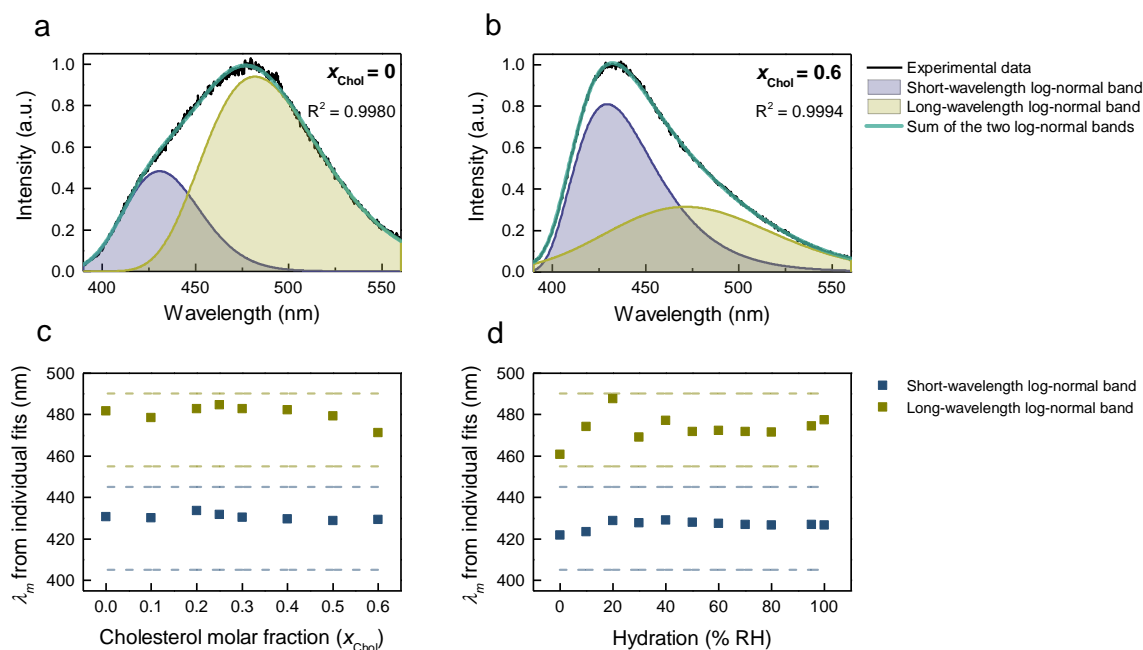


Figure S1. The exemplary results of the independent, individual spectra fitting procedure. Two-peak log-normal decomposition of the fluorescence spectra of Laurdan in an exemplary SLB composed of (a) pure di14:1- $\Delta 9$ cis-PC and (b) the binary mixture of di14:1- $\Delta 9$ cis-PC/Chol at $x_{\text{Chol}} = 0.6$ under fully hydrated conditions. Coefficients of determination R^2 are indicated in the figures. Spectral positions of the maximum intensity λ_m of the two log-normal functions as a function of (c) x_{Chol} for an exemplary single-phase SLB and (d) membrane hydration of the liquid-disordered phase for an exemplary phase-separated SLB. Blue and olive dashed lines correspond to the limiting range in the fitting procedure for short-wavelength and long-wavelength bands, respectively.

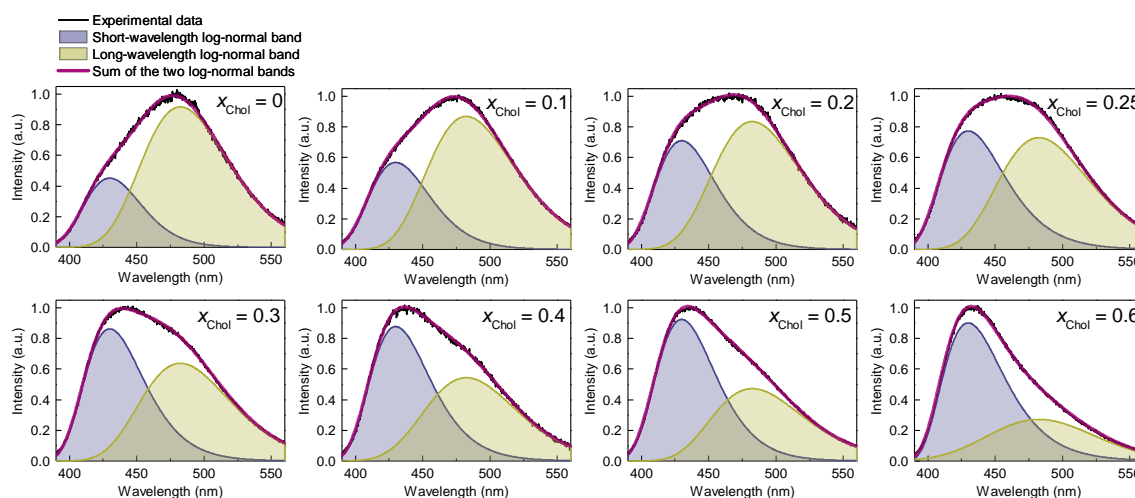


Figure S2. An exemplary result of the global fitting procedure. Two-peak log-normal decomposition of the fluorescence spectra of Laurdan in an exemplary SLB composed of di14:1- $\Delta 9cis$ -PC and different cholesterol molar ratios x_{Chol} . Coefficient of determination $R^2 = 0.9990$.

Note 1.

The collected fluorescence emission spectra are highly reproducible, both when acquired within the same sample as well as between different samples. Typically, 10 to 30 emission spectra from distinct spots, separated by a distance ranging from a few to thousands micrometers (the diameter of the mica flake is 8 mm), were measured for each membrane hydration state. As an example, in figure S1 we show 20 spectra collected at 50% RH during the dehydration and 10 during the rehydration process. First of all, spectra for a 50% RH for a given de(re)hydration process are just on top of each other, indicating negligible variability of the Laurdan environment within the sample. Secondly, changes in the spectrum are fully reversible, exhibiting only small hysteresis, resulting most probably from the inaccuracy of our humidity control system. Most importantly, the minute differences (mainly in absolute intensity) are much smaller than the differences between emission spectra for different hydration states.

Moreover, it should be emphasized that the used dehydration methodology leads to the preservation of membrane structure upon dehydration. We devoted a significant part of our previous work¹ to this topic and we are confident that, except for the deposition of a few aggregates on top of the membrane, the lipid bilayer integrity upon dehydration is not affected, provided that the membrane has been subjected to a well-controlled, gradual decrease in hydration level. Confocal images of solid-supported lipid bilayers (SLBs) labeled with multiple fluorescence probes, together with our most recent AFM studies (data not published) indicate that no significant changes occur in the quality of the phase-separated membrane structure (both in micro- as well as nano-scale, in the quality of the phase-separated membrane structure) when subjected to dehydration.

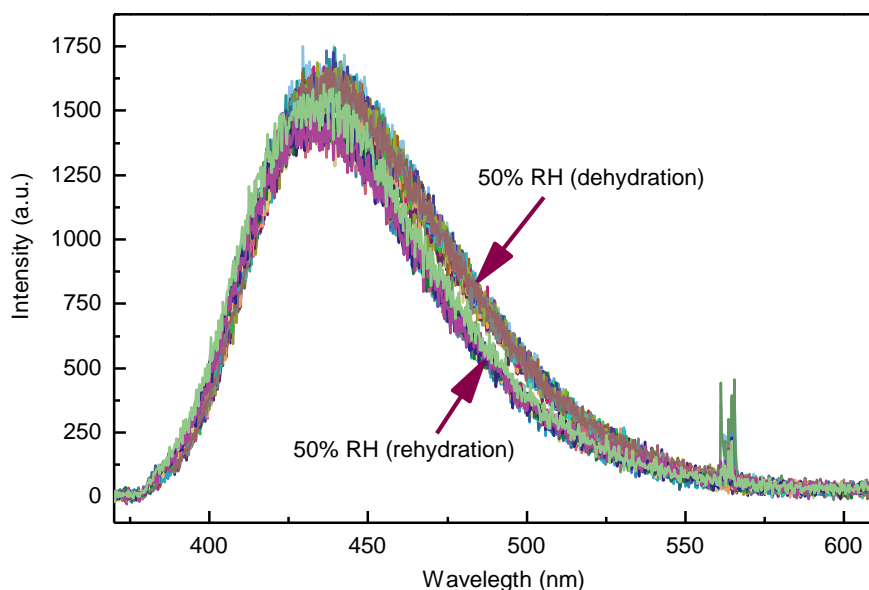


Figure S3. The fluorescence spectra of Laurdan embedded in an exemplary one-component solid supported lipid bilayer composed of di14:1- Δ 9cis-PC lipids collected for ~50% relative humidity. The spectra originate from 30 distinct spots within the sample, separated by a distance ranging from a few to thousands of micrometers (the diameter of the mica flake is 8 mm). 20 spectra were collected at 50% RH during the dehydration and 10 during the rehydration process.

Note 2.

As a control, we measured the fluorescence spectrum of Laurdan layer deposited on a solid support in extreme hydration conditions: dried and exposed to bulk water. In the first place, we verified the fluorescence spectrum of Laurdan in solvents of distinct polarity, for which the Laurdan spectrum is known – chloroform and methanol. When dissolved in chloroform, Laurdan emission exhibits the maximum intensity at ~433 nm and in methanol at ~494 nm (see Fig. S4b), which is consistent with the literature.² After drying from both organic solvents, the fluorescence spectrum of Laurdan layer is blue-shifted with a maximum intensity centered at ~415-420 nm (see Fig. S4b,c), which is most likely a manifestation of the locally excited state.³ We note that the deposition of Laurdan on solid support yields a formation of the isolated islands of aggregated and/or crystalline form of the probe (see Fig. S4a).

Intriguingly, exposure of such crystals/aggregates to bulk water neither shifts the spectrum nor changes its shape (see Fig. S4b). It is in accordance with the previously reported data demonstrating that Laurdan exhibits fluorescence emission maximum at around 410-415 nm in water.⁴ In another study on extensive photophysical characterization of Laurdan and its derivatives, Laurdan fluorescence in water was not detected at all.⁵ However, its derivative with an additional carboxymethyl group (MoC-Laurdan) was found to fluoresce in water with a very marked blue shift (maximum centered at around 410 nm), which was attributed to the fluorescence of non-hydrated aggregates. Whereas C-Laurdan (with one methyl group less with respect to Laurdan), which is highly soluble in water undergoes the expected red-shift and its fluorescence emission maximum is centered at ~520 nm.

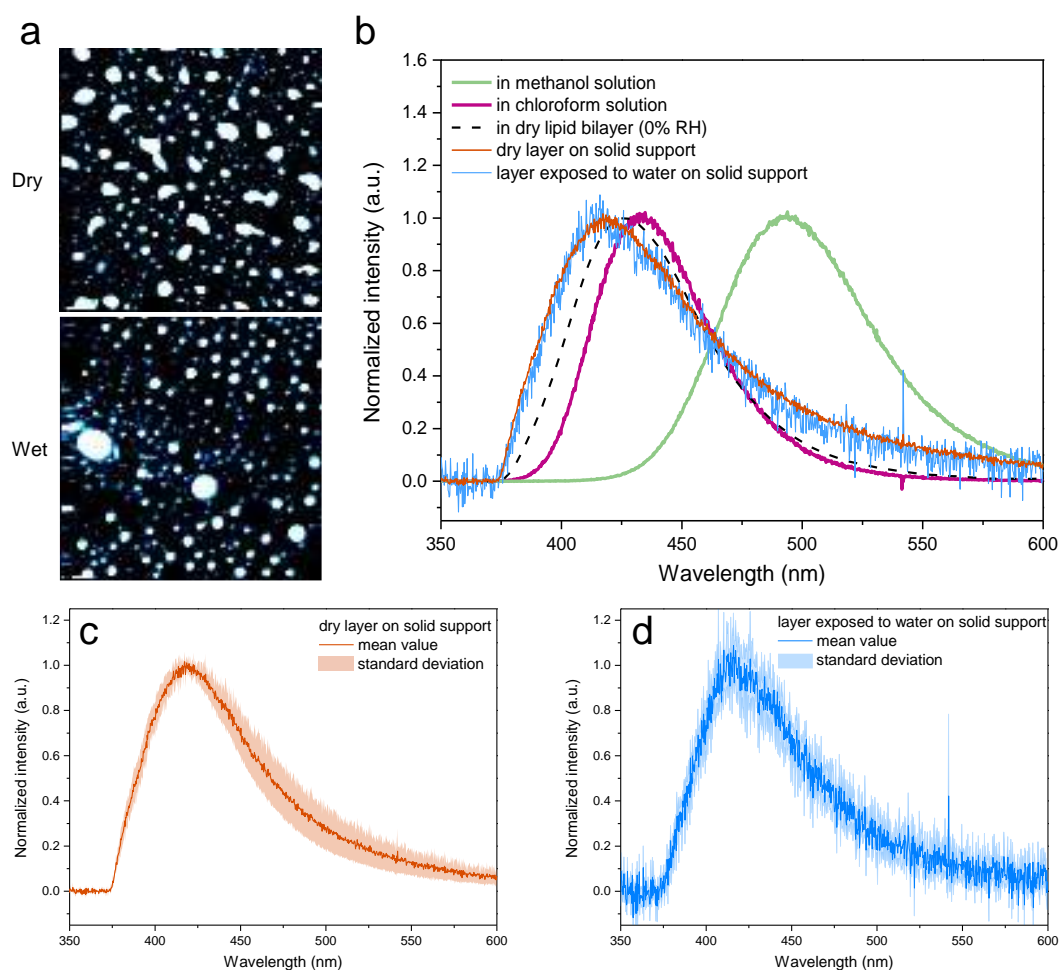


Figure S4. (a) Fluorescence microscopy images of Laurdan deposited on clean glass coverslip after drying from $\sim 1 \mu\text{M}$ chloroform solution (Dry) and after exposing it to bulk ultrapure water (Wet). Images reflect the sample area of dimensions $50 \times 50 \mu\text{m}$. Contrast was adjusted and color was added for better visualization. (b) Fluorescence spectra of Laurdan on glass coverslip in dry and wet conditions averaged over at least 9 spectra collected from distinct spots within the sample area presented on panel a as well as of Laurdan in methanol and chloroform solutions. For the reference, the fluorescence spectrum of Laurdan in dry (0% RH) solid-supported lipid bilayer composed of di14:1- $\Delta 9\text{cis}$ -PC is presented. Fluorescence spectra of Laurdan on glass coverslip in dry (c) and wet (d) conditions presented on panel c with added uncertainties are standard deviations, denoted as shadows around mean values. Spectra were normalized to better visualize the differences.

Noteworthy, we evaluated whether the fluorescence spectrum of the dried Laurdan layer exposed to pure water changes with time, but even after 17 hours, no changes were detected. Our results along with the available literature point in the direction that water molecules do not permeate the Laurdan layer, which most likely consist of tightly packed aggregates/crystals and that the intermolecular interactions between Laurdan molecules dominate over interactions with the interfacial water that would decrease the emitted energy by dipolar relaxation.

Regardless of the hydration condition (dry or wet), minor differences in the shape of the emission band between distinct spots within the sample was observed, but no clear trend regarding for instance the size of the crystal/aggregate or whether the spectrum was collected from in between the isolated

islands was found. To visualize the extent of the variability of the fluorescence spectra shape, in Figure S4c and S4d we plotted uncertainties (standard deviations), denoted as shadows around mean values. We infer that the Laurdan fluorescence spectrum depends on the state of aggregation and or whether it is in a crystalline form. Compared to its emission in a dried lipid membrane, it is blue-shifted by 5-10 nm (see Figure S4b, dashed black line). It must be emphasized however, that Laurdan in lipid membrane is expected to exist in its monomeric form, while on the support we deal with crystals and/or aggregates, for which probe-probe intermolecular interactions such as van der Waals forces and π - π interactions have to be taken into account.

More noise is evident to the normalized averaged spectrum of Laurdan layer exposed to bulk water because in wet conditions the overall fluorescence intensity decreased when compared to dry conditions, possible because of the collisional quenching with water molecules (see Fig. S4b-d).

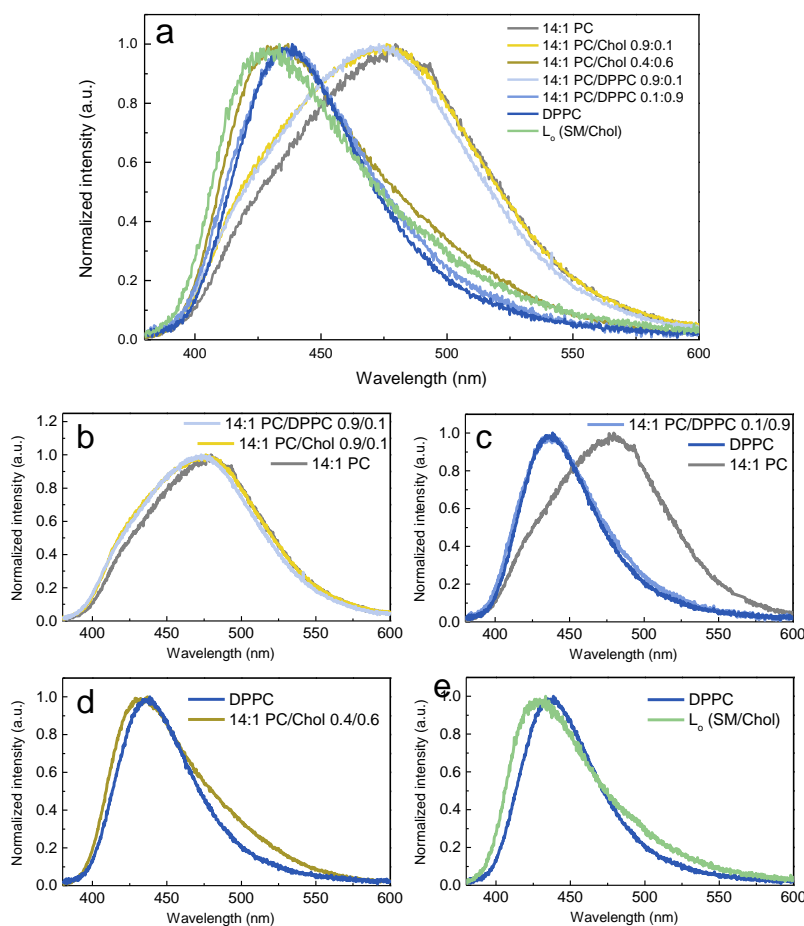


Figure S5. Fluorescence spectra of Laurdan embedded in exemplary solid-supported lipid bilayers composed of pure DPPC and binary mixtures of di14:1- Δ 9cis-PC and DPPC at $x_{\text{DPPC}} = 0.1$ and 0.9 (blue shades, panels a-e). For each membrane composition the spectrum is averaged from 30 background-corrected spectra collected from distinct spots within the sample. For the comparison, exemplary fluorescence spectra of Laurdan in solid-supported lipid bilayers composed of pure di14:1- Δ 9cis-PC (gray, panels a-c) as well as its mixtures with cholesterol at molar fractions $x_{\text{Chol}} = 0.1$ (yellow shade, panel a) and 0.6 (yellow shade, panels a and d) and in liquid-ordered phase (L_o) from the phase-separated membrane (green, panels a and e) are presented. Spectra were normalized to better visualize the differences.

Note 3.

At a very low molar fraction of DPPC ($x_{\text{DPPC}} = 0.1$), the Laurdan fluorescence spectrum is slightly blue-shifted with respect to pure di14:1- $\Delta 9$ cis-PC bilayer (Fig. S5b), similarly as for $x_{\text{Chol}} = 0.1$, indicative of a minor increase of the membrane rigidity in both cases. At very high molar fractions of DPPC, namely $x_{\text{DPPC}} = 0.9$ and 1.0, the Laurdan fluorescence spectrum is prominently blue-shifted, as expected for the gel phase (Fig. S5c). Molecular movements in the gel phase are relatively constrained due to the high degree of order and packing of the lipid molecules, therefore dipolar relaxation around the Laurdan probe is strongly hampered. The possibility that the local environment of the Laurdan probe in gel-phase DPPC bilayer might be characterized by slightly decreased polarity with respect to the di14:1- $\Delta 9$ cis-PC bilayer, due to reduced water penetration down to lipid carbonyl level, also cannot be ruled out. No significant differences in the fluorescence spectrum can be observed between pure DPPC and di14:1- $\Delta 9$ cis-PC/DPPC 0.1/0.9 bilayers, although for the bilayer with very low molar fraction of di14:1- $\Delta 9$ cis-PC, the spectrum seems to be a bit broader, which can be a manifestation of a disrupted tight gel-phase packing of DPPC introducing a broader distribution of Laurdan's local environments (Fig. S5c). When the fluorescence spectrum of Laurdan in DPPC matrix is compared to the di14:1- $\Delta 9$ cis-PC bilayer with cholesterol at molar fraction $x_{\text{Chol}} = 0.6$ (Fig. S5d), it can be seen that for the sample with cholesterol, the spectrum is slightly blue-shifted (by ~5 nm) but at the same time has a higher contribution of a long-wavelength band associated with Laurdan within a readily relaxing environment. Given almost half of the concentration of cholesterol when compared to DPPC and the observed changes, it is clear that cholesterol has a stronger effect on the Laurdan's spectral response than a saturated phospholipid such as DPPC. This highlights further the unique character of this sterol molecule. In the figure above we presented also Laurdan's spectrum in L_o phase from the phase-separated SLB. Interestingly, when the newly acquired data are apposed to the probe's fluorescence spectrum in L_o phase (Fig. S5e), it is clear that although both phases – gel (DPPC) and L_o (SM/Chol) are considered rigid, Laurdan can distinguish them. It is in accordance with the results presented in the previous study employing different environment-sensitive probes demonstrating that gel and L_o phases exhibit similar fluidity but the latter is less hydrated.⁶

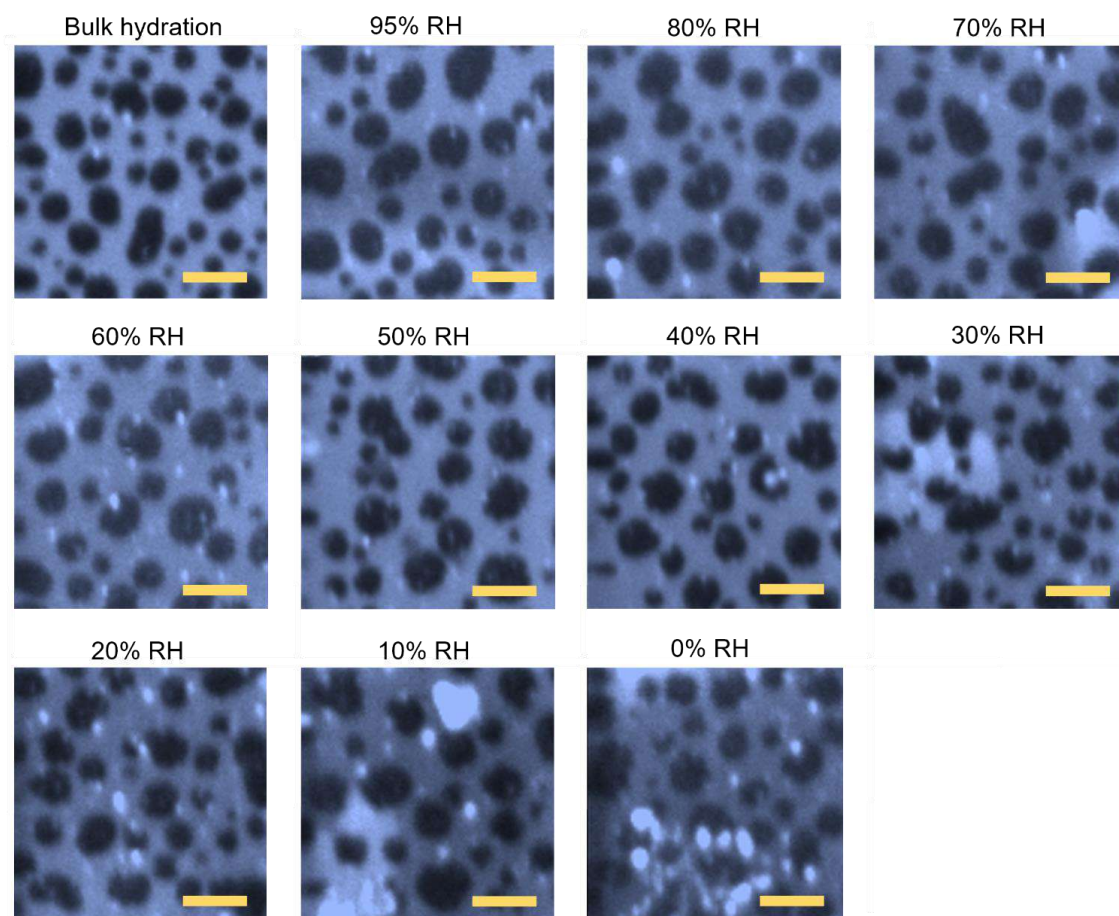


Figure S6. Fluorescence microscopy images of an exemplary phase-separated solid-supported lipid bilayer composed of an equimolar mixture of di14:1- $\Delta 9$ cis-PC, cholesterol, and egg sphingomyelin as a function of membrane hydration state. The membrane exhibits phase separation into liquid-disordered (bright regions) and liquid-ordered (dark regions) domains. The membrane was labeled with Laurdan, which distributes evenly in the membrane regardless of phase, and Atto 633-DOPE, which localizes mainly in the liquid-disordered phase, and from this comes the contrast. The concentration of each dye was 0.1% mol. Each image represents a different area within the sample. The images shown originate from one of the four phase-separated samples analyzed in this work. The scale bar corresponds to 5 μ m.

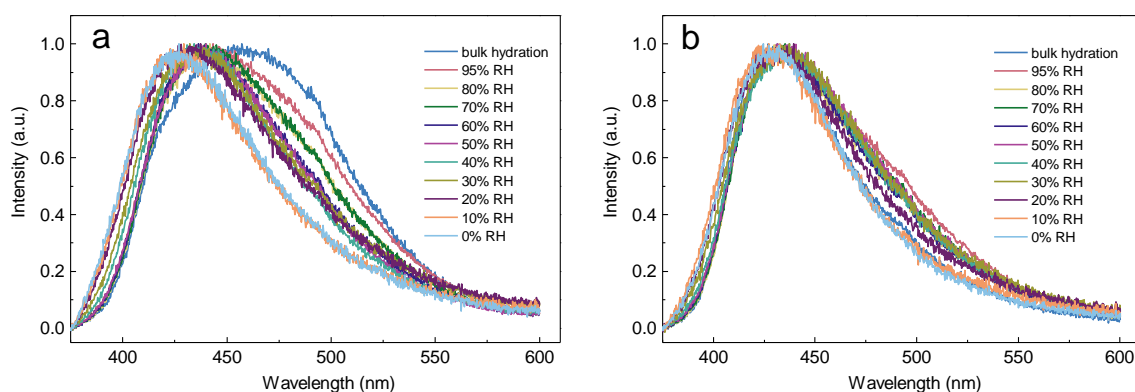


Figure S7. Fluorescence spectrum of Laurdan embedded in an exemplary phase-separated solid supported lipid bilayer composed of an equimolar mixture of di14:1- $\Delta 9cis$ -PC, cholesterol, and egg sphingomyelin as a function of membrane hydration state collected from (a) liquid-disordered domains and (b) liquid-ordered domains. The spectra shown on both panels originate from one of the four phase-separated samples analyzed in this work (same sample as in Fig. S6). For each hydration state and each phase, the spectrum is averaged from at least 10 background-corrected spectra collected from distinct domains within the $20 \times 20 \mu\text{m}$ sample area. The resulting spectra were normalized to better visualize the changes.

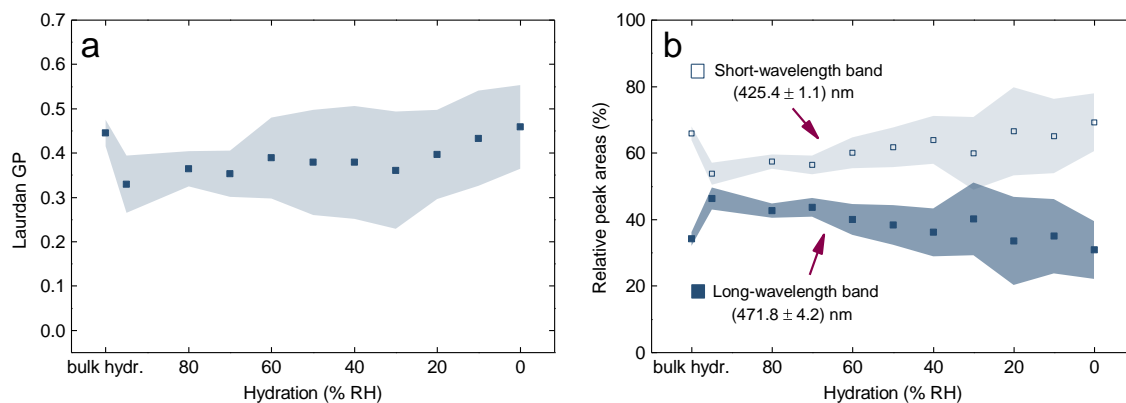


Figure S8. (a) Laurdan GP as a function of hydration level of liquid-ordered domains from phase-separated solid supported lipid bilayer composed of an equimolar mixture of di14:1- $\Delta 9cis$ -PC, cholesterol, and egg sphingomyelin. (b) The relative area of the two log-normal functions that give the best fit to the Laurdan emission spectra in the same SLB system as a function of membrane hydration state. Open and full symbols are used for short- and long-wavelength bands, respectively. The data shown on both panels are averaged over four different samples. The uncertainties are standard deviations, denoted as shadows around mean values.

Note 4.

The insensitivity of Laurdan's emission spectrum in the liquid-ordered phase to changes in hydration over a fairly wide range is unlikely to indicate that no changes are occurring within this phase, but rather that Laurdan is not the appropriate dye to probe them. The liquid-ordered phase composed of saturated phospholipids (egg sphingomyelin in our case) and a high proportion of cholesterol is found to be the least hydrated and the most ordered among all the possible phases.^{6,7} It is also reflected in the log-normal decomposition results (Fig. S7b), which revealed the considerably low contribution of long-

wavelength band in the Laurdan emission even at fully hydrated conditions compared to liquid-disordered domains or pure phospholipid bilayer. Even if the functional groups of sphingomyelin at the membrane depth where Laurdan resides are partially hydrated, its dipolar relaxation is slow compared to Laurdan's fluorescence timescale.⁸ The stiff lipid acyl chains implicate the negligible contribution of Laurdan population surrounded by the relaxable environment to the emission spectrum over a wide range of membrane hydration states. Hence, in the main text we focused on the changes occurring within the liquid-disordered phase, for which the rate of dipolar relaxation is comparable to Laurdan fluorescence lifetime.⁸

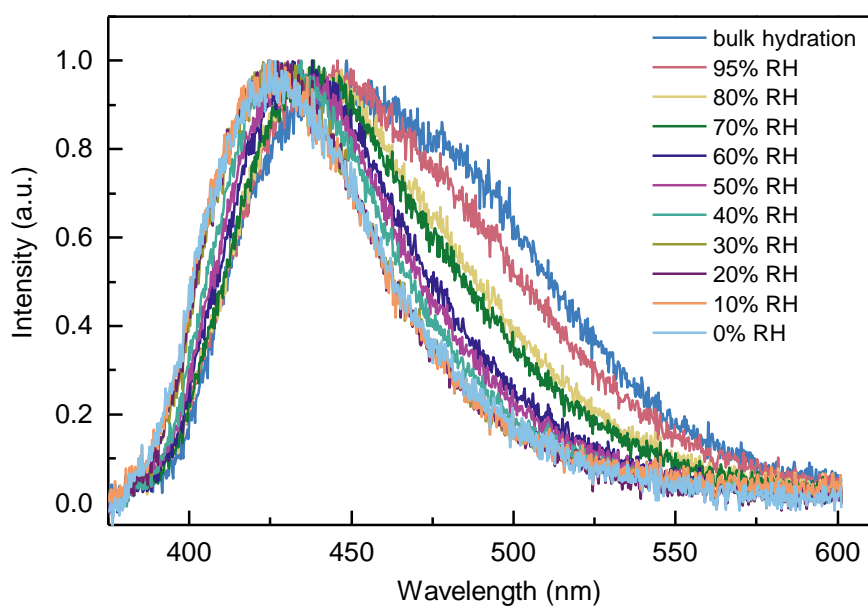


Figure S9. Fluorescence spectrum of Laurdan embedded in an exemplary solid-supported lipid bilayer composed of a binary mixture of di14:1- Δ 9cis-PC and cholesterol at $x_{\text{Chol}} = 0.3$ as a function of membrane hydration state. For each hydration state, the spectrum is averaged from at least 10 background-corrected spectra collected from distinct spots within the 20 x 20 μm sample area. The resulting spectra were normalized to better visualize the changes.

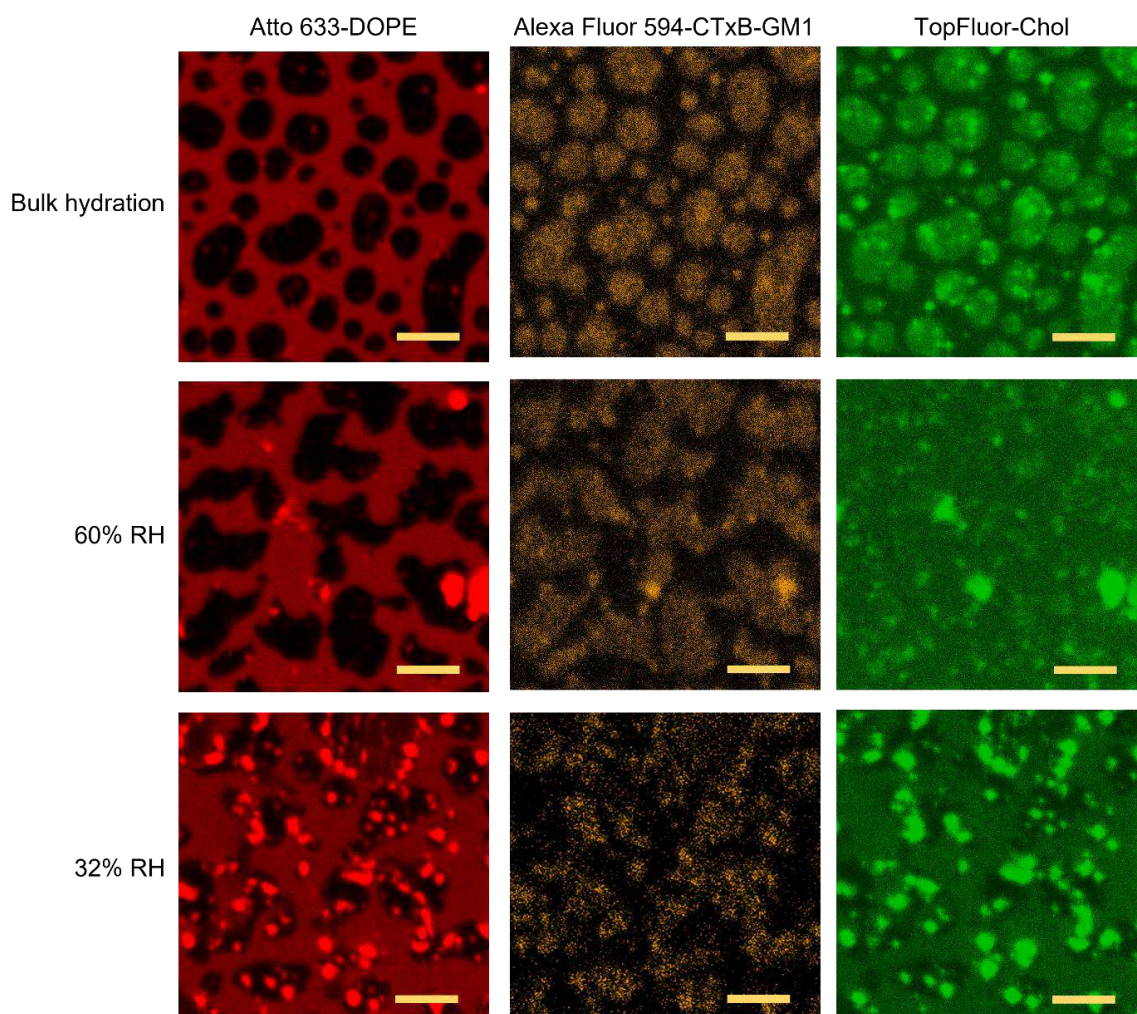


Figure S10. Confocal fluorescence microscopy images of a triple-labeled phase-separated solid-supported lipid bilayer composed of an equimolar mixture of di14:1- $\Delta 9$ cis-PC, cholesterol, and egg sphingomyelin for three different membrane hydration states. Liquid-disordered phase is labeled with Atto 633-DOPE (red, left column), liquid-ordered phase is labeled with Alexa Fluor 594-CTxB-GM1 complex (yellow, middle column) and cholesterol, which partitions in both phases is labeled with TopFluor-Chol probe (green, right column). Images for each hydration state originate from different sample area. Under fully hydrated conditions higher intensity of TopFluor-Chol is found in liquid-ordered domains, denoting that liquid-ordered phase contains more cholesterol than liquid-disordered phase, in accordance with the previous reports. At 60% RH the contrast virtually vanishes, indicative of homogenous distribution of cholesterol between distinct phases. At 32% RH the contrast is reversed with respect to the fully hydrated conditions, denoting that at low hydration conditions liquid-disordered phase contains more cholesterol than liquid-ordered phase. The concentration of each dye was 0.1% mol. The scale bar corresponds to 5 μ m.

References

- (1) Chattopadhyay, M.; Krok, E.; Orlikowska, H.; Schwille, P.; Franquelim, H. G.; Piatkowski, L. Hydration Layer of Only a Few Molecules Controls Lipid Mobility in Biomimetic Membranes. *J. Am. Chem. Soc.* **2021**, *143* (36), 14551–14562.
- (2) Hornum, M.; Kongsted, J.; Reinholdt, P. Computational and Photophysical Characterization of a Laurdan Malononitrile Derivative. *Phys. Chem. Chem. Phys.* **2021**, *23* (15), 9139–9146.
- (3) Owen, D. M.; Rentero, C.; Magenau, A.; Abu-Siniyeh, A.; Gaus, K. Quantitative Imaging of Membrane Lipid Order in Cells and Organisms. *Nat. Protoc.* **2012**, *7* (1), 24–35.
- (4) Hu, S.; Yao, Z.; Ma, X.; Yue, L.; Chen, L.; Liu, R.; Wang, P.; Li, H.; Zhang, S. T.; Yao, D.; Cui, T.; Zou, B.; Zou, G. Pressure-Induced Local Excitation Promotion: New Route toward High-Efficiency Aggregate Emission Based on Multimer Excited State Modulation. *J. Phys. Chem. Lett.* **2022**, *13* (5), 1290–1299.
- (5) Mazeres, S.; Joly, E.; Lopez, A.; Tardin, C. Characterization of M-Laurdan, a Versatile Probe to Explore Order in Lipid Membranes. *F1000Research* **2014**, *3*, 172.
- (6) M'Baye, G.; Mély, Y.; Duportail, G.; Klymchenko, A. S. Liquid Ordered and Gel Phases of Lipid Bilayers: Fluorescent Probes Reveal Close Fluidity but Different Hydration. *Biophys. J.* **2008**, *95* (3), 1217–1225.
- (7) Warschawski, D. E.; Devaux, P. F. Order Parameters of Unsaturated Phospholipids in Membranes and the Effect of Cholesterol: A ¹H-¹³C Solid-State NMR Study at Natural Abundance. *Eur. Biophys. J.* **2005**, *34* (8), 987–996.
- (8) Leung, S. S. W.; Brewer, J.; Bagatolli, L. A.; Thewalt, J. L. Measuring Molecular Order for Lipid Membrane Phase Studies: Linear Relationship between Laurdan Generalized Polarization and Deuterium NMR Order Parameter. *Biochim. Biophys. Acta - Biomembr.* **2019**, *1861* (12), 183053.

THE JOURNAL OF PHYSICAL CHEMISTRY LETTERS

A JOURNAL OF THE AMERICAN CHEMICAL SOCIETY

April 25, 2024
Volume 15
Number 16
pubs.acs.org/JPCL



7

Dehydration of lipid membrane drives redistribution of cholesterol between lateral domains

The dehydration-induced migration of cholesterol from raft-like domains to the surrounding, more fluid phase, introduced in the previous chapter, is thoroughly examined in the publication presented in this chapter. Using fluorescence microscopy, I explored how cholesterol is distributed within the phase-separated model cell membrane under different hydration conditions. I quantified this process and found that cholesterol's affinity for specific lipid phases (raft-like L_o vs. non-raft L_d) reverses as membrane hydration decreases from approximately 12 to 6 water molecules per lipid. Atomistic molecular dynamics simulations, which revealed changes in the lipid bilayer structure and inter-lipid hydrogen bonding network, provided insights into the molecular basis for this cholesterol redistribution.

On the left, there is a cover for the article presented in this chapter. I entitled it as *Lipid sprites donating cholesterol to needy neighbours*. The graphic was designed by Katarzyna Bogdańska.

Dehydration of Lipid Membranes Drives Redistribution of Cholesterol Between Lateral Domains

Hanna Orlikowska-Rzeznik,* Emilia Krok, Maria Domanska, Piotr Setny, Anna Łągowska, Madhurima Chattopadhyay, and Lukasz Piatkowski*

Cite This: *J. Phys. Chem. Lett.* 2024, 15, 4515–4522

Read Online

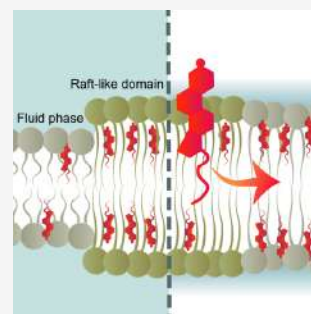
ACCESS |

Metrics & More

Article Recommendations

Supporting Information

ABSTRACT: Cholesterol-rich lipid rafts are found to facilitate membrane fusion, central to processes like viral entry, fertilization, and neurotransmitter release. While the fusion process involves local, transient membrane dehydration, the impact of reduced hydration on cholesterol's structural organization in biological membranes remains unclear. Here, we employ confocal fluorescence microscopy and atomistic molecular dynamics simulations to investigate cholesterol behavior in phase-separated lipid bilayers under controlled hydration. We unveiled that dehydration prompts cholesterol release from raft-like domains into the surrounding fluid phase. Unsaturated phospholipids undergo more significant dehydration-induced structural changes and lose more hydrogen bonds with water than sphingomyelin. The results suggest that cholesterol redistribution is driven by the equalization of biophysical properties between phases and the need to satisfy lipid hydrogen bonds. This underscores the role of cholesterol–phospholipid–water interplay in governing cholesterol affinity for a specific lipid type, providing a new perspective on the regulatory role of cell membrane heterogeneity during membrane fusion.



Cell membranes extend well beyond their role as mere physical barriers, serving to maintain cellular integrity. Hydrated lipid bilayer assemblies, abundant in proteins, sustain a far-from-equilibrium state crucial for the energetic and dynamic nature of cells. This enables cells to execute essential biochemical processes for life, adaptation, and response to their environment.

Expanding upon the fundamental fluid mosaic model,¹ our understanding of cell membrane architecture has evolved. The current perspective describes it as an intricate, asymmetric lipid bilayer structure with nonrandomly distributed components.² Cell membranes exhibit lateral heterogeneity, marked by transient nanodomains, known as relatively ordered “lipid rafts”, which are enriched in cholesterol and sphingolipids.³ These rafts are surrounded by a fluid phase, characterized by the abundance of unsaturated phospholipids.³ The prevailing consensus is that the molecular structure of the lipid rafts closely resembles that of the liquid ordered (L_o) phase, while the fluid regions are effectively modeled as the liquid disordered (L_d) phase, coexisting in biomimetic cell membranes composed of ternary lipid mixtures (saturated and unsaturated phospholipids and cholesterol).⁴

Lipid rafts have been suggested to be pivotal in various cellular processes, including signal transduction,⁵ membrane protein trafficking,⁶ and host–pathogen interactions.⁷ A growing body of evidence emphasizes the role of cholesterol-rich lipid rafts in the entry of various viruses into target cells, such as acute respiratory syndrome coronavirus 2 (SARS-CoV-2),⁸ dengue,⁹ ebola,¹⁰ influenza A,¹¹ and human immunode-

ficiency virus (HIV).^{12–16} Most of these viruses utilize the endocytic route for cell entry, whereas HIV enters T lymphocytes through membrane fusion at the cell surface.¹⁷ Notably, the HIV fusion peptide exhibits structural changes dependent on the target membrane cholesterol level, adopting mostly an α -helical conformation in the low cholesterol condition but shifting toward a β -sheet secondary structure with increasing cholesterol content.¹⁸ This observation raises the intriguing possibility that membrane regions differing in cholesterol content may be sequentially engaged in the fusion process, or alternatively, that the cholesterol level is actively regulated at the fusion site. Further studies using the mimics of HIV envelope and target T cell membrane revealed that high content of cholesterol, and particularly the phase separation into fluid L_d and raft-like L_o domains, facilitates the membrane fusion process.^{14,15} Intriguingly, the L_o – L_d phase boundaries have been unveiled to serve as preferential binding sites for the HIV fusion peptide.^{14,15}

Membrane fusion is a central phenomenon not only in viral entry, which leads to the pathological condition, but also in a whole palette of biological processes such as fertilization¹⁹ or

Received: February 1, 2024

Revised: March 30, 2024

Accepted: April 10, 2024

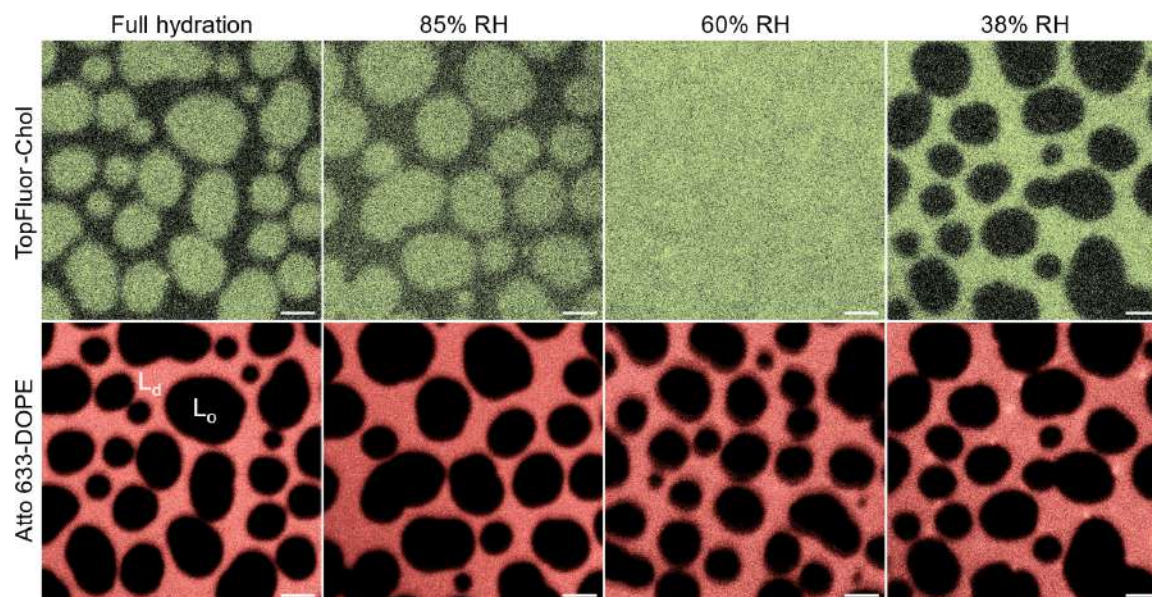


Figure 1. Exemplary confocal fluorescence microscopy images of a double-labeled, phase-separated SLB composed of an equimolar mixture of 14:1 PC, Chol, and SM at four membrane hydration states. Chol, which partitions in both the L_o and L_d phases, is labeled with the TopFluor probe (green, upper row), while the L_d phase is labeled with Atto 633-DOPE (pink, bottom row). Images for each hydration state originate from distinct sample areas. The concentration of each fluorescent probe was 0.1 mol %. The scale bar corresponds to 2.5 μm .

neurotransmitter release by exocytosis,²⁰ which have also been shown to be affected by membrane cholesterol content. Despite the evolutionary and structural diversity of the proteins involved, these processes share a common pathway characterized by a series of distinct intermediates. The initial loose protein-mediated membrane contact is followed by tight apposition of the membranes, leading to local, transient membrane dehydration.²¹

In a quest to gain a more detailed picture of the role of cholesterol and lipid rafts in the membrane fusion process at the stage of dehydration, we pose the questions: What is the specific organization of cholesterol in the membrane fusion dehydration intermediate, and why might the boundaries of raft-like domains promote the fusion process? To address these queries, we employed confocal fluorescence microscopy and molecular dynamics (MD) simulations. We focused on the lateral distribution of cholesterol between coexisting L_o and L_d phases in planar solid-supported lipid bilayers (SLBs) under varying hydration conditions, which were precisely controlled by slow and sequential changes in the relative humidity (RH) of the membrane environment.

We investigated the membranes composed of an equimolar mixture of the unsaturated lipid 1,2-dimyristoleoyl-glycero-3-phosphocholine (14:1 PC), egg sphingomyelin (SM), and cholesterol (Chol). The 14:1 PC:SM:Chol (1:1:1) SLBs exhibit microscopic phase separation at room temperature into L_o domains and the surrounding L_d phase. The L_o domains consist of sphingomyelin and a high fraction of cholesterol and are characterized by a high degree of ordering of fatty acid chains, and consequently dense molecular packing and decreased intramolecular dynamics. In contrast, the surrounding L_d phase is composed of the unsaturated lipid 14:1 PC and a lower cholesterol fraction. The L_d phase is less tightly packed

and exhibits greater fluidity due to steric constraints arising from the unsaturated acyl chains.

The lateral distribution of cholesterol was monitored as a function of membrane hydration state using a fluorescently labeled cholesterol derivative, modified at the terminus of the alkyl backbone, TopFluor-cholesterol, often referred to as BODIPY-cholesterol.²² For control purposes, the L_d phase was labeled with the unsaturated lipid 1,2-dioleoyl-*sn*-glycero-3-phosphoethanolamine (DOPE) labeled at the headgroup with the Atto 633 fluorescent probe. Exemplary fluorescence microscopy images of a double-labeled SLB at four membrane hydration states (bulk hydration, 85%, 60%, and 38% RH) are depicted in Figure 1.

As shown in Figure 1, under fully hydrated conditions, TopFluor-Chol preferentially localizes in SM and Chol-rich L_o domains, evident from the higher fluorescence intensity in L_o compared to L_d regions. This observation aligns with previous findings for hydrated giant unilamellar vesicles (GUVs) and cell-derived giant plasma membrane vesicles (GPMVs), which exhibited analogous phase separation.²³ However, we note that as membrane hydration decreases, the contrast diminishes, then completely disappears, and eventually reverses. In contrast, the distribution of Atto 633-DOPE remains constant regardless of the membrane hydration state, maintaining a strong preference for the L_d phase. Consequently, the overall membrane structure remains unaltered during dehydration (and rehydration) of the phase separated membrane. Neither does phase separation disappear, nor does phase inversion occur at any membrane hydration state. Our previous research provides extensive information on this matter.²⁴

To quantify the hydration-dependent distribution of TopFluor-Chol between distinct phases, we extracted fluorescence intensities (I_{L_o} and I_{L_d}) of the respective phases, using the green channel of the confocal images. Given that previous

findings demonstrated the fluorescence quantum yield of TopFluor-Chol to be virtually independent of the lipid environment, specifically in the L_o and L_d phases,²³ we assumed that the fluorescence intensity is proportional to the relative concentration of fluorescently labeled cholesterol in the membrane phases. Consequently, to calculate the partitioning coefficient of TopFluor-Chol in the L_o and L_d phases, we employed the following equations: $xL_o = I_{L_o}/(I_{L_o} + I_{L_d})$, $xL_d = I_{L_d}/(I_{L_o} + I_{L_d})$, respectively. According to this definition, $0.5 < xL_o \leq 1$ implies that the affinity of TopFluor-Chol for the L_o phase is stronger than for the L_d , whereas a value in the range $0 \leq xL_o < 0.5$ means that TopFluor-Chol favors the L_d phase over the L_o environment. xL_o equal to 0.5 is indicative of no lipid phase-selectivity. The values of xL_d should be interpreted analogously. The resulting partitioning coefficients xL_o and xL_d as a function of membrane hydration state are depicted in Figure 2.

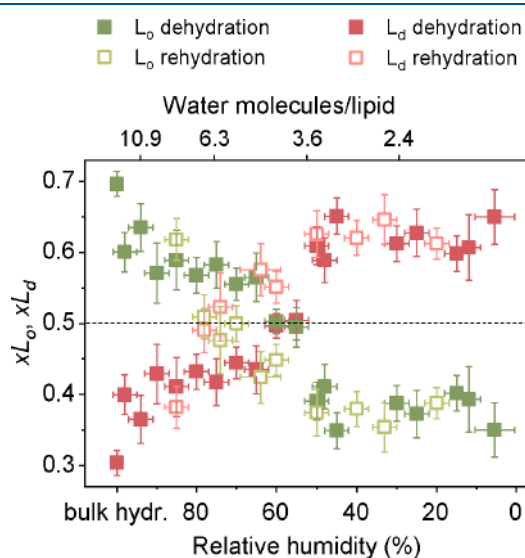


Figure 2. Partitioning coefficients (xL_o , xL_d) of TopFluor-Chol in the L_o and L_d phases within the 14:1 PC:SM:Chol (1:1:1) SLBs equilibrated in atmosphere of different relative humidity levels during dehydration (solid squares) and rehydration (open squares). Each data point represents the partitioning coefficient calculated based on the average fluorescence intensities from at least 6 spots of distinct phase from each sample at a specific membrane hydration state. The number of samples varies with membrane hydration state, ranging from 1 to 3.

As shown in Figure 2, under bulk membrane hydration, the partitioning coefficient of TopFluor-Chol in L_o domains equals to 0.70 ± 0.02 , and correspondingly 0.30 ± 0.02 in the L_d phase, indicating its preference for an SM-rich environment. We note here that the partitioning coefficient of TopFluor-Chol for the L_o phase has been reported to be equal to 0.80 ± 0.03 in GUVs and 0.66 ± 0.60 in cell-derived GPMVs.²³ Importantly, the values we report here are in full quantitative agreement with the partitioning coefficient of native cholesterol between coexisting L_o and L_d phases (~ 0.7 and ~ 0.3 , respectively) in fully hydrated SLBs of the same composition.²⁵ Consequently, it can be inferred that, under these specific conditions, TopFluor-Chol accurately mimics native chole-

sterol in terms of its lateral distribution in the phase-separated lipid bilayer.

Surprisingly, upon removal of bulk water and equilibration of the membrane with an atmosphere of high relative humidity ($\sim 95\%$ RH), the xL_o drops to a value slightly above 0.6. Then, it gradually decreases with further reduction in water content, ultimately reaching a plateau with an average value of 0.38 within the hydration range of 5–50% RH. Notably, this effect is reversible, as demonstrated during the rehydration of the SLB (see Figure 2).

To ascertain whether the lateral distribution of TopFluor-Chol accurately reflects the native behavior of Chol, not only under fully hydrated conditions but also under reduced hydration, we first had to rule out the possibility that Chol migration toward surrounding unsaturated lipids was solely due to the expulsion of the relatively bulky TopFluor moiety, aiming to escape tight SM-rich regions during dehydration. To address this concern, we repeated the dehydration/rehydration experiment, replacing TopFluor-Chol with analogously labeled SM (TopFluor-SM). The results of this experiment are demonstrated in the Supporting Information in Figure S1. In brief, the partitioning coefficients of labeled SM in the L_o and L_d phases remain unchanged regardless of the membrane hydration state. However, it is noteworthy that the SM tagged with TopFluor favors the L_d phase, with xL_o and xL_d averaging 0.39 and 0.61, respectively. Despite this, there remains a considerable amount of TopFluor-SM molecules in the L_o domains, which could potentially diffuse into the surrounding L_d phase upon membrane dehydration. However, such migration does not occur.

To gain a detailed molecular level insight into the dehydration-driven cholesterol redistribution between lipid raft and nonraft environment, we employed atomistic molecular dynamics simulations of three kinds of systems: (i) fully hydrated SM:Chol (3:2) and 14:1 PC:Chol (3:1) bilayers to represent experimentally resolved, fully hydrated L_o and L_d phases with their respective cholesterol content, (ii) fully hydrated 14:1 PC:SM:Chol (1:1:1) membrane, initialized with randomly mixed lipid molecules to confirm that we can observe the onset of phase separation and Chol migration toward SM-rich regions, and (iii) gradually dehydrated 14:1 PC:SM:Chol (1:1:1) system down to hydration level corresponding to 8 water molecules per lipid, to check the reversal of Chol preference from SM to phosphatidylcholine (PC) lipids and to analyze membrane organization under low water availability. We note that, although lower hydration levels were achievable, lipid bilayer became increasingly unstable which manifested itself in isolated, random events (single occurrences per hundreds of ns of simulation time) of irreversible surface penetration by lipid hydrocarbon chains. Accordingly, we decided to limit dehydration at the level allowing for stable runs of desired length.

Our simulations of fully hydrated, initially randomly mixed 14:1 PC:SM:Chol bilayer indicated a gradual separation of 14:1 PC and SM into membrane patches (Figure S2), with Chol exhibiting the expected tendency to colocalize with SM rather than PC lipids as the simulation progressed (Figures 3 and S3, fully hydrated condition). This observation validates the force field used for simulations, and notably, it demonstrates that the experimentally observed partitioning of TopFluor-Chol between L_o and L_d phases is indeed driven by the Chol moiety. Remarkably, gradual dehydration of the system down to 8 water molecules per lipid led to the inversion

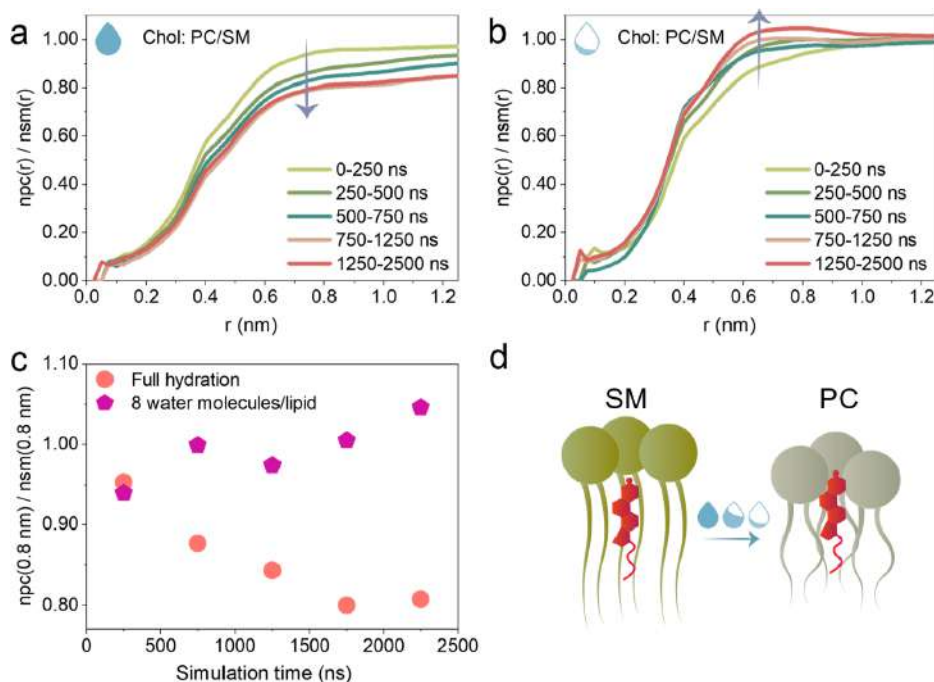


Figure 3. (a, b) Ratio of cumulative radial distribution functions of PC and SM lipids around cholesterol at different simulation times for lipid bilayer in fully hydrated and partially dehydrated (8 water molecules per lipid) conditions, respectively. (c) Evolution of PC/SM ratio within 0.8 nm distance around cholesterol over simulation time for 14:1 PC:SM:Chol lipid bilayer under fully hydrated and partially dehydrated conditions. (d) Cartoon representation of a cholesterol colocalization trend.

of Chol preference from the SM to PC phase (Figures 3 and S3, partially dehydrated condition), again in agreement with experimental findings.

The transition from fully hydrated PC:Chol and SM:Chol phases to a perturbed hydration regime was accompanied by an increase in overall membrane thickness and hydrocarbon chain ordering, with the PC phase showing significantly larger effects compared to the already thick and ordered SM phase (Table S1). In either phase, the distribution of Chol across the membrane normal shifted outward from the midplane, following the trends observed for its neighboring lipid head distributions (Figure S4). In the case of Chol in the PC phase, however, the effect of dehydration was further augmented by an additional ~ 0.1 nm displacement toward the bilayer surface, relative to the displacement of PC phosphate groups, yielding a 26% reduction in the distance between the Chol's hydroxyl group and lipid's phosphate moiety (Figure 4 and Table S1).

The different response of PC and SM phases to dehydration was reflected by differences in hydrogen bond populations (Figure 5, Tables S2–S4). Overall, following limited availability of the aqueous solvent, PC lipids lost more interactions with water molecules than did SM lipids (Figure 5b). Intriguingly, while SM lipids lost similar fraction of hydrogen bonds within the interfacial region as in the headgroup region, PC lipids lost significantly more hydrogen bonds in the interfacial region compared to the headgroup region (35% vs 11%, respectively). Chol molecules, which were already better hydrated in the PC-rich compared to SM-rich phase under full solvent availability (1.2 vs 1.1 H-bonds with water per Chol molecule, respectively), were found to preserve their interaction with water more efficiently among PC than

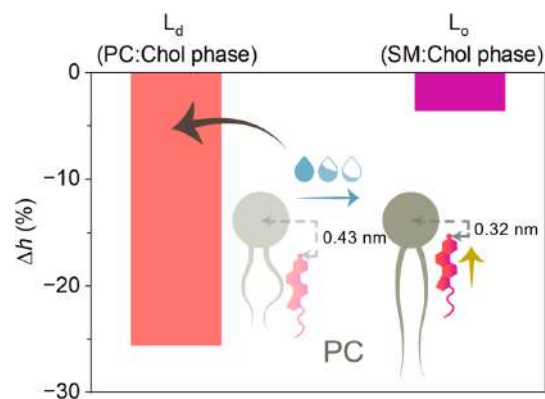


Figure 4. Percentage change in the distance (h) between the O atom in the hydroxyl group of Chol and the P atom in the phosphate of the lipid headgroup, PC or SM in the respective phase, upon dehydration down to 8 water molecules per lipid, calculated relative to fully hydrated conditions, along with a schematic representation of the observed scenario for Chol in the PC phase. The absolute values for SM can be found in Table S1.

SM lipids (loss of 9% vs 22% lipid–water hydrogen bonds per Chol molecule, respectively, Figure 5c). In both phases, the reduction of Chol interaction with water was compensated by an increase of its interaction with neighboring lipids (Table S4). Notably, however, in the case of PC-rich phase additional hydrogen bonds were formed with PC headgroups, whereas in

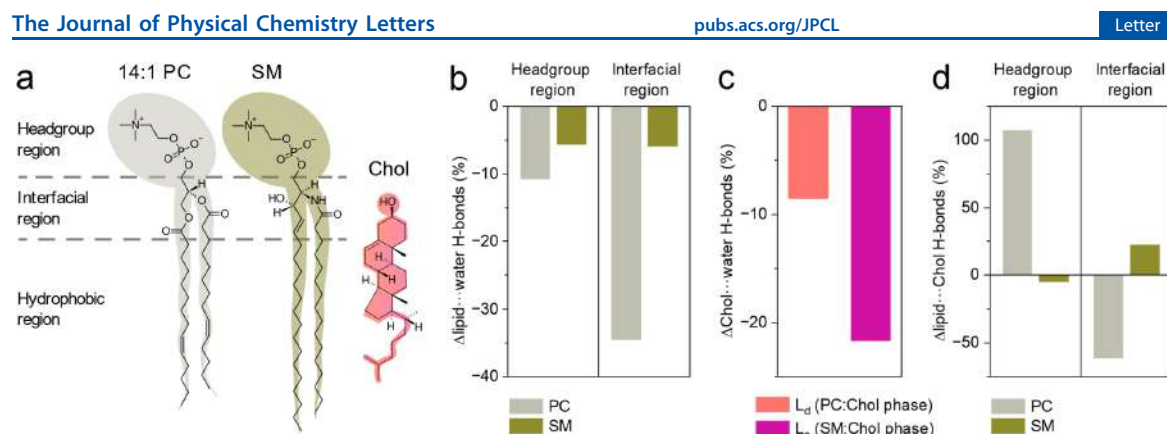


Figure 5. (a) Molecular structures of the studied lipids: 14:1 PC, SM and Chol. Percentage change in the number of hydrogen bonds (b) between lipids (PC and SM) and water (per lipid), (c) between Chol and water (per Chol), and (d) between Chol's hydroxyl and lipids (per Chol). Panels (b)–(d) depict the effects observed upon dehydration down to 8 water molecules per lipid and are calculated relative to fully hydrated conditions. See the Supporting Information for the absolute values (Tables S2–S4).

the SM-rich phase, new interactions were created within the interfacial region (Figure 5d).

The compiled experimental and computational evidence indicates that, under conditions of low membrane hydration, cholesterol exhibits a stronger affinity for unsaturated phosphatidylcholine-rich over sphingomyelin-rich regions. Moreover, the redistribution of cholesterol between coexisting domains induced by dehydration is not specific to the TopFluor-Chol probe but does occur with native, untagged Chol as well. However, a question remains: What is the driving force behind this peculiar behavior of cholesterol, unprecedented in previous observations?

Numerous studies have established that cholesterol tends to favor phospholipids featuring saturated acyl chains, as opposed to those with unsaturated acyl chains.^{26–28} Nevertheless, it is clear that factors beyond acyl chain saturation also play a significant role in cholesterol-phospholipid interactions. This is exemplified by the observation that under fully hydrated conditions cholesterol prefers interacting with SM over PC lipids, even at equal acyl chain order (and hydrophobic length).²⁹ While SM and PC share the same headgroup, they differ in the headgroup-tails linkage. Unlike the glycerol linkage present in PC lipids, the presence of a sphingosine linkage imparts SM with not only hydrogen bond acceptor groups but also with donor ones (NH and OH). These hydrogen bonding capabilities, along with acyl chain order and hydrophobic length, appear to promote the preferential association of cholesterol with sphingomyelin under full hydration.

Under fully hydrated conditions, due to a higher chain order and more carbons in the hydrophobic chains of sphingomyelin compared to unsaturated phosphatidylcholine molecules, the L_o domains exhibit greater thickness compared to the surrounding continuous L_d phase. Upon membrane dehydration, this height disparity at the interface of coexisting phases (hydrophobic mismatch) decreases linearly.³⁰ Our previous atomic force microscopy study revealed that under mild dehydration conditions (90% RH, ca. 10 water molecules/lipid), a thickness of the L_d phase equals to 3.87 nm, while the height mismatch was 1.36 nm, yielding a thickness of the L_o phase of 5.23 nm.³⁰ The hydrophobic mismatch between the raft-like and nonraft phases decreased nearly 2-fold (from 1.36 to 0.8 nm) as membrane hydration

decreased from approximately 10 to less than 1 water molecule per lipid.³⁰ The results of MD simulations presented herein indicate that the decrease in hydrophobic mismatch primarily stem from the dehydration-induced thickening of the L_d phase, resulting from the ordering of PC lipid acyl chains.

As such, the differences in lipid phase characteristics, such as thickness and ordering, become less pronounced under low solvent availability. We propose that this fosters more efficient penetration of the PC compartment by Chol. An additional driving force for Chol redistribution seems to arise from the need to satisfy lipid hydrogen bonds, particularly within highly polar and solvent-exposed phosphate groups, which become increasingly difficult to maintain with lowering water content. In this regard, PC molecules, which lose more interaction with water than SM lipids upon dehydration (likely due to the absence of H-bond donor groups in contrast to SM), offer more opportunities to interact with Chol's hydroxyl group, especially given the dehydration-induced upward shift toward the membrane surface.

The cholesterol influx from the L_o domains into surrounding unsaturated lipid-rich regions rationalizes well the phenomenon observed in our previous experimental study using the environment-sensitive fluorescent probe Laurdan.²⁵ In brief, we compared changes of the L_d phase's fluidity, determined from the Laurdan emission spectrum, as a function of the hydration state of two types of SLBs: (i) a membrane with coexisting L_d and L_o domains, identical in composition to the current study, but with only Atto 633-DOPE and Laurdan as fluorescent labels (so Chol was native, untagged), and (ii) a single-phase membrane with the same molecular composition as the L_d phase in the phase-separated membrane (containing 0.3 mol fraction of Chol). While the two systems were compositionally identical under fully hydrated conditions, dehydration yielded disparate results. A decrease in the fluidity of the L_d phase upon dehydration was observed in both systems, however, the changes in the phase-separated membrane were smaller (approximately by a factor of 2 at low hydrations). This pointed toward an additional mechanism that counteracts and moderates the effects of L_d dehydration in the phase-separated membrane. In light of our current findings, we can now unambiguously state that in the membrane with L_o domains, as dehydration progresses, Chol migrates from the L_o

domains to the surrounding unsaturated lipid-rich L_d regions, preventing excessive stiffening of the membrane. In other words, Chol fluidizes a dehydrated L_d environment.

We note that our findings have important implications for the membrane fusion process. The hydrophobic mismatch between the L_d and L_o domains gives rise to an interfacial force known as line tension at the boundary between the two phases. In prior study, we found that reduction in hydration from approximately 10 to less than 1 water molecule per lipid, in the same membrane system as studied herein, governed a 3.5-fold decline in line tension (from approximately 7 to 2 pN).³⁰ Cholesterol, in general, can either increase or decrease the thickness of a phospholipid bilayer, depending on the lipid chain length, saturation, and lipid phase. However, it has been established that for lipids containing 12–16 carbons per chain, cholesterol thickens the bilayer regardless of saturation and phase.^{31,32} Therefore, in our case, where L_d lipids have 14 carbons and L_o lipids have 16 carbons per chain, we assume that Chol increases the thickness of both 14:1 PC lipids in the L_d phase and SM lipids in the L_o phase. Consequently, the depletion of Chol in L_o domains and the associated enrichment of Chol in the surrounding L_d phase lead to a decrease in hydrophobic mismatch. Therefore, both the dehydration and the redistribution of cholesterol between domains contribute to a decrease in hydrophobic mismatch and the resulting reduction in line tension, minimizing the boundary energy of the L_o domains.

To estimate the possible energy gain associated with a reduction in line tension, we employ a simplistic model describing the boundary energy of an individual raft-like domain surrounded by a continuous fluid phase as $E = \gamma L$, where γ represents the line tension, and L denotes the domain perimeter.¹⁵ In our investigations, we did not observe notable alterations in the perimeter of the L_o domains during dehydration, leading us to assume that it is constant, with changes occurring only in line tension. Based on our previous atomic force microscopy studies, a decrease in membrane hydration from approximately 10 to fewer than 1 water molecule per lipid resulted in a reduction in line tension by around 5 pN.³⁰ Addressing a more realistic size for the raft in the cell membrane, we consider a raft with a diameter of 20 nm in calculations. Under these assumptions, the energy gain is estimated to be on the order of $70k_B T$ (detailed calculations are provided in the Supporting Information), which falls within the range of free energy barrier predicted in theoretical models for membrane fusion.^{33,34} Therefore, it seems feasible that as the two membranes get closer and the dehydration of lipid headgroups progresses, more cholesterol is released from raft domains into the continuous more fluid phase. This, in tandem with a dehydration-induced ordering of lipid acyl chains, leads to a significant reduction in line tension at the distinct environment boundary. Consequently, this reduction produces an energy gain, facilitating the formation of the subsequent stalk intermediate. Furthermore, cholesterol counteracts the dehydration-induced extensive changes in fluidity of the nonraft membrane regions,²⁵ thus creating a more favorable environment for the fusion.

In summary, we used confocal fluorescence microscopy and atomistic MD simulations to unravel cholesterol-phospholipid–water interactions and the organization of cholesterol in lipid bilayer with coexisting L_o and L_d phases under reduced hydration—a scenario reminiscent of temporal membrane dehydration during cellular events such as membrane fusion.

We unveiled that dehydration of a biomimetic lipid bilayer drives cholesterol release from raft-like L_o domains into the surrounding L_d phase. The inversion of cholesterol preference from raft-like SM-rich domains to the surrounding unsaturated PC-rich phase underscores the regulatory role of water in shaping cell membrane structure.

Our MD simulation results suggest that a molecular rationale for dehydration-induced cholesterol redistribution between lateral domains, involves two primary coacting factors. First, unsaturated PC lipids in the L_d phase exhibit greater susceptibility to structural changes upon dehydration compared to SM lipids in the L_o phase. As the membrane gets dehydrated, the acyl chains of the PC lipids undergo significant ordering and a concomitant increase in membrane thickness. Consequently, the biophysical properties of the two phases become more similar, facilitating the interaction of cholesterol with PC lipids. Second, upon membrane dehydration, unsaturated PC lipids lose more hydrogen bonds with water than SM molecules. In response to the excessive loss of hydrogen bonds by PC headgroups, cholesterol migrates toward the PC phase and shifts to the surface to form hydrogen bonds between its hydroxyl group and the phosphate moieties of the PC headgroups.

The dehydration-induced cholesterol release from lipid rafts into the surrounding phase may potentially play a role during cellular events involving membrane fusion. First, it maximizes the reduction of hydrophobic mismatch between domains of distinct phases (and thus the line tension), facilitating the energy release required for stalk formation. Second, lipid rafts likely serve as cholesterol reservoirs, releasing the sterol to regulate membrane fluidity. We emphasize the universality of the latter role, as continuous adjustments to membrane fluidity are necessary to ensure the integrity and functionality of biological membranes under diverse physiological conditions, extending beyond the context of membrane fusion.

■ ASSOCIATED CONTENT

SI Supporting Information

The Supporting Information is available free of charge at <https://pubs.acs.org/doi/10.1021/acs.jpcllett.4c00332>.

Materials and methods; partitioning coefficient of TopFluor-SM in the L_o and L_d phases within the 14:1 PC:SM:Chol (1:1:1) SLB as a function of membrane hydration; evidence of phase separation under fully hydrated conditions from MD simulations; radial lipid distribution functions around cholesterol under fully hydrated and partially dehydrated conditions; number density profiles of water O atom, PC and SM P atoms, Chol O atom along Z axis in the respective phases under fully hydrated conditions and partially dehydrated conditions; structural parameters of simulated lipid bilayers under fully hydrated and partially dehydrated conditions; number of hydrogen bonds between lipids (including cholesterol) and water and between cholesterol and lipids under fully hydrated and partially dehydrated conditions; calculation of the energy released due to reduction of line tension (PDF)

■ AUTHOR INFORMATION

Corresponding Authors

Hanna Orlikowska-Rzeznik – Faculty of Materials Engineering and Technical Physics, Poznan University of

Technology, 60-965 Poznan, Poland; orcid.org/0000-0003-0697-4781; Email: hanna.orlikowska@put.poznan.pl
Lukasz Piatkowski – Faculty of Materials Engineering and Technical Physics, Poznan University of Technology, 60-965 Poznan, Poland; orcid.org/0000-0002-1226-2257; Email: lukasz.j.piatkowski@put.poznan.pl

Authors

Emilia Krok – Faculty of Materials Engineering and Technical Physics, Poznan University of Technology, 60-965 Poznan, Poland; orcid.org/0000-0002-4637-2729
Maria Domanska – Biomolecular Modelling Group, Centre of New Technologies, University of Warsaw, 02-097 Warsaw, Poland; orcid.org/0000-0002-4691-2983
Piotr Setny – Biomolecular Modelling Group, Centre of New Technologies, University of Warsaw, 02-097 Warsaw, Poland; orcid.org/0000-0002-0769-0943
Anna Lagowska – Faculty of Materials Engineering and Technical Physics, Poznan University of Technology, 60-965 Poznan, Poland
Madhurima Chattopadhyay – Faculty of Materials Engineering and Technical Physics, Poznan University of Technology, 60-965 Poznan, Poland; Present Address: Department of Biophysics, University of Texas Southwestern Medical Center, Dallas, Texas, USA; orcid.org/0000-0001-8900-163X

Complete contact information is available at: <https://pubs.acs.org/10.1021/acs.jpclett.4c00332>

Author Contributions

H.O.-R., E.K., M.C., and L.P. conceptualization; H.O.-R., M.D., P.S., and A.L. data curation; H.O.-R., M.D., P.S. and A.L. formal analysis; H.O.-R. and L.P. funding acquisition; H.O.-R., E.K., M.D., P.S., A.L., M.C., and L.P. investigation; H.O.-R., P.S. and L.P. methodology; M.D. and P.S. software; L.P. project administration; P.S. and L.P. resources; L.P. supervision; H.O.-R., E.K., P.S. and L.P. validation; H.O.-R. visualization; H.O.-R. and P.S. writing—original draft; H.O.-R., E.K., M.S., P.S., A.L. and L.P. writing—review and editing. All authors have given approval to the final version of the manuscript.

Notes

The authors declare no competing financial interest.

ACKNOWLEDGMENTS

This work was financed from the budget funds allocated for science in the years 2019–2023 as a research project under the “Diamond Grant” program (decision: 0042/DIA/2019/48). H.O.-R. acknowledges funding from the National Science Centre (Poland) 2022/45/N/ST4/01442. L.P. acknowledges the financial support from the National Science Centre (Poland) 2020/37/B/ST4/01785. M.D. and P.S. were supported by the National Science Centre (Poland) 2020/38/E/ST4/00319.

REFERENCES

(1) Singer, S. J.; Nicolson, G. L. The Fluid Mosaic Model of the Structure of Cell Membranes: Cell Membranes Are Viewed as Two-Dimensional Solutions of Oriented Globular Proteins and Lipids. *Science* **1972**, *175*, 720–731.
 (2) Nicolson, G. L.; Ferreira de Mattos, G. The Fluid–Mosaic Model of Cell Membranes: A Brief Introduction, Historical Features,

Some General Principles, and Its Adaptation to Current Information. *Biochim. Biophys. Acta - Biomembr.* **2023**, *1865*, No. 184135.
 (3) Levental, I.; Levental, K. R.; Heberle, F. A. Lipid Rafts: Controversies Resolved, Mysteries Remain. *Trends Cell Biol.* **2020**, *30*, 341–353.
 (4) Sezgin, E.; Levental, I.; Mayor, S.; Eggeling, C. The Mystery of Membrane Organization: Composition, Regulation and Roles of Lipid Rafts. *Nat. Rev. Mol. Cell Biol.* **2017**, *18*, 361–374.
 (5) Koyama-Honda, I.; Fujiwara, T. K.; Kasai, R. S.; Suzuki, K. G. N.; Kajikawa, E.; Tsuboi, H.; Tsunoyama, T. A.; Kusumi, A. High-Speed Single-Molecule Imaging Reveals Signal Transduction by Induced Transbilayer Raft Phases. *J. Cell Biol.* **2020**, *219*, No. e202006125.
 (6) Ouweneel, A. B.; Thomas, M. J.; Sorci-Thomas, M. G. The Ins and Outs of Lipid Rafts: Functions in Intracellular Cholesterol Homeostasis, Microparticles, and Cell Membranes. *J. Lipid Res.* **2020**, *61*, 676–686.
 (7) Bukrinsky, M. I.; Mukhamedova, N.; Sviridov, D. Lipid Rafts and Pathogens: The Art of Deception and Exploitation. *J. Lipid Res.* **2020**, *61*, 601–610.
 (8) Li, X.; Zhu, W.; Fan, M.; Zhang, J.; Peng, Y.; Huang, F.; Wang, N.; He, L.; Zhang, L.; Holmdahl, R.; Meng, L.; Lu, S. Dependence of SARS-CoV-2 Infection on Cholesterol-Rich Lipid Raft and Endosomal Acidification. *Comput. Struct. Biotechnol. J.* **2021**, *19*, 1933–1943.
 (9) Diwaker, D.; Mishra, K. P.; Ganju, L.; Singh, S. B. Protein Disulfide Isomerase Mediates Dengue Virus Entry in Association with Lipid Rafts. *Viral Immunol.* **2015**, *28*, 153–160.
 (10) Miller, M. E.; Adhikary, S.; Kolokoltsov, A. A.; Davey, R. A. Ebola Virus Requires Acid Sphingomyelinase Activity and Plasma Membrane Sphingomyelin for Infection. *J. Virol.* **2012**, *86*, 7473–7483.
 (11) Audi, A.; Soudani, N.; Dbaibo, G.; Zaraket, H. Depletion of Host and Viral Sphingomyelin Impairs Influenza Virus Infection. *Front. Microbiol.* **2020**, *11*, 612.
 (12) Campbell, S. M.; Crowe, S. M.; Mak, J. Lipid Rafts and HIV-1: From Viral Entry to Assembly of Progeny Virions. *J. Clin. Virol.* **2001**, *22*, 217–227.
 (13) Popik, W.; Alce, T. M.; Au, W.-C. Human Immunodeficiency Virus Type 1 Uses Lipid Raft-Colocalized CD4 and Chemokine Receptors for Productive Entry into CD4 + T Cells. *J. Virol.* **2002**, *76*, 4709–4722.
 (14) Yang, S. T.; Kiessling, V.; Simmons, J. A.; White, J. M.; Tamm, L. K. HIV Gp41-Mediated Membrane Fusion Occurs at Edges of Cholesterol-Rich Lipid Domains. *Nat. Chem. Biol.* **2015**, *11*, 424–431.
 (15) Yang, S. T.; Kiessling, V.; Tamm, L. K. Line Tension at Lipid Phase Boundaries as Driving Force for HIV Fusion Peptide-Mediated Fusion. *Nat. Commun.* **2016**, *7*, 11401.
 (16) Leung, K.; Kim, J. O.; Ganesh, L.; Kabat, J.; Schwartz, O.; Nabel, G. J. HIV-1 Assembly: Viral Glycoproteins Segregate Quantally to Lipid Rafts That Associate Individually with HIV-1 Capsids and Virions. *Cell Host Microbe* **2008**, *3*, 285–292.
 (17) Dimitrov, D. S. Virus Entry: Molecular Mechanisms and Biomedical Applications. *Nat. Rev. Microbiol.* **2004**, *2*, 109–122.
 (18) Lai, A. L.; Moorthy, A. E.; Li, Y.; Tamm, L. K. Fusion Activity of HIV Gp41 Fusion Domain Is Related to Its Secondary Structure and Depth of Membrane Insertion in a Cholesterol-Dependent Fashion. *J. Mol. Biol.* **2012**, *418*, 3–15.
 (19) Sleight, S. B.; Miranda, P. V.; Plaskett, N. W.; Maier, B.; Lysiak, J.; Scrabble, H.; Herr, J. C.; Visconti, P. E. Isolation and Proteomic Analysis of Mouse Sperm Detergent-Resistant Membrane Fractions: Evidence for Dissociation of Lipid Rafts during Capacitation. *Biol. Reprod.* **2005**, *73*, 721–729.
 (20) Chamberlain, L. H.; Burgoyne, R. D.; Gould, G. W. SNARE Proteins Are Highly Enriched in Lipid Rafts in PC12 Cells: Implications for the Spatial Control of Exocytosis. *Proc. Natl. Acad. Sci. U. S. A.* **2001**, *98*, 5619–5624.

- (21) Witkowska, A.; Heinz, L. P.; Grubmüller, H.; Jahn, R. Tight Docking of Membranes before Fusion Represents a Metastable State with Unique Properties. *Nat. Commun.* **2021**, *12*, 3606.
- (22) Hölttä-Vuori, M.; Uronen, R. L.; Repakova, J.; Salonen, E.; Vattulainen, I.; Panula, P.; Li, Z.; Bittman, R.; Ikonen, E. BODIPY-Cholesterol: A New Tool to Visualize Sterol Trafficking in Living Cells and Organisms. *Traffic* **2008**, *9*, 1839–1849.
- (23) Sezgin, E.; Levental, I.; Grzybek, M.; Schwarzmann, G.; Mueller, V.; Honigsmann, A.; Belov, V. N.; Eggeling, C.; Coskun, Ü.; Simons, K.; Schwille, P. Partitioning, Diffusion, and Ligand Binding of Raft Lipid Analogs in Model and Cellular Plasma Membranes. *Biochim. Biophys. Acta - Biomembr.* **2012**, *1818*, 1777–1784.
- (24) Chattopadhyay, M.; Krok, E.; Orlikowska, H.; Schwille, P.; Franquelim, H. G.; Piatkowski, L. Hydration Layer of Only a Few Molecules Controls Lipid Mobility in Biomimetic Membranes. *J. Am. Chem. Soc.* **2021**, *143*, 14551–14562.
- (25) Orlikowska-Rzeznik, H.; Krok, E.; Chattopadhyay, M.; Lester, A.; Piatkowski, L. Laurdan Discerns Lipid Membrane Hydration and Cholesterol Content. *J. Phys. Chem. B* **2023**, *127*, 3382–3391.
- (26) Yasuda, T.; Tsuchikawa, H.; Murata, M.; Matsumori, N. Deuterium NMR of Raft Model Membranes Reveals Domain-Specific Order Profiles and Compositional Distribution. *Biophys. J.* **2015**, *108*, 2502–2506.
- (27) Nyström, J. H.; Lönnfors, M.; Nyholm, T. K. M. Transmembrane Peptides Influence the Affinity of Sterols for Phospholipid Bilayers. *Biophys. J.* **2010**, *99*, 526–533.
- (28) Niu, S. L.; Litman, B. J. Determination of Membrane Cholesterol Partition Coefficient Using a Lipid Vesicle-Cyclodextrin Binary System: Effect of Phospholipid Acyl Chain Unsaturation and Headgroup Composition. *Biophys. J.* **2002**, *83*, 3408–3415.
- (29) Lönnfors, M.; Doux, J. P. F.; Killian, J. A.; Nyholm, T. K. M.; Slotte, J. P. Sterols Have Higher Affinity for Sphingomyelin than for Phosphatidylcholine Bilayers Even at Equal Acyl-Chain Order. *Biophys. J.* **2011**, *100*, 2633–2641.
- (30) Krok, E.; Franquelim, H. G.; Chattopadhyay, M.; Orlikowska-Rzeznik, H.; Schwille, P.; Piatkowski, L. Nanoscale Structural Response of Biomimetic Cell Membranes to Controlled Dehydration. *Nanoscale* **2023**, *16*, 72–84.
- (31) Mielke, S.; Sorkin, R.; Klein, J. Effect of Cholesterol on the Mechanical Stability of Gel-Phase Phospholipid Bilayers Studied by AFM Force Spectroscopy. *Eur. Phys. J. E* **2023**, *46*, 77.
- (32) Chen, T.; Ghosh, A.; Enderlein, J. Cholesterol-Induced Nanoscale Variations in the Thickness of Phospholipid Membranes. *Nano Lett.* **2023**, *23*, 2421–2426.
- (33) Kawamoto, S.; Shinoda, W. Free Energy Analysis along the Stalk Mechanism of Membrane Fusion. *Soft Matter* **2014**, *10*, 3048–3054.
- (34) Rizo, J. Molecular Mechanisms Underlying Neurotransmitter Release. *Annu. Rev. Biophys.* **2022**, *51*, 377–408.

Supporting Information for

Dehydration of Lipid Membrane Drives Redistribution of Cholesterol Between Lateral Domains

Hanna Orlikowska-Rzeznik,^{1*} Emilia Krok,¹ Maria Domanska,² Piotr Setny,² Anna Łągowska,¹ Madhurima Chattopadhyay,^{1†} and Lukasz Piatkowski^{1*}

¹Faculty of Materials Engineering and Technical Physics, Poznan University of Technology, 60-965 Poznan, Poland

²Biomolecular Modelling Group, The Centre of New Technologies, University of Warsaw, 02-097 Warsaw, Poland

Correspondence: hanna.orlikowska@put.poznan.pl (H. Orlikowska-Rzeznik); lukasz.j.piatkowski@put.poznan.pl (L. Piatkowski)

Table of Content:

Materials and Methods

Supplementary Figures S1–S4

Supplementary Tables S1–S4

Calculation of the Energy Released Due to Reduction of Line Tension

CHAPTER 7. DEHYDRATION OF LIPID MEMBRANE DRIVES REDISTRIBUTION OF CHOLESTEROL BETWEEN LATERAL DOMAINS

Materials and Methods

Materials. Lipids: 1,2-dimyristoleoyl-glycero-3-phosphocholine (14:1 PC), egg yolk sphingomyelin (SM), cholesterol (Chol), and fluorescently labelled lipids: 23-(dipyrrometheneborondifluoride)-24-norcholesterol (TopFluor-Chol) and N-[11-(dipyrrometheneboron difluoride)undecanoyl]-D-*erythro*-sphingosylphosphorylcholine (TopFluor-SM) were provided by Avanti Polar Lipids (Alabaster, AL). Lipid 1,2-dioleoyl-sn-glycero-3-phosphoethanolamine labeled with Atto 633 (Atto 633-DOPE) and HPLC grade chloroform were acquired from Merck KGaA (Darmstadt, Germany). Buffer reagent 4-(2-hydroxyethyl)piperazine-1-ethanesulfonic acid (HEPES PUFFERAN) was purchased from Carl Roth GmbH + Co., KG (Karlsruhe, Germany). Calcium chloride (CaCl₂) was sourced from Chempur (Piekary Slaskie, Poland) and sodium chloride (NaCl) was supplied by PPH STANLAB Sp. z o.o. (Lublin, Poland). These compounds were used as purchased without further purification. Ultrapure water of 18.2 MΩ×cm resistivity was obtained using the Milli-Q Direct Water Purification System from Merck KGaA (Darmstadt, Germany). Optical adhesive UV-activated glue Norland 68 was purchased from Thorlabs Sweden AB (Mölnå, Sweden). Sheets of mica, which were used to prepare solid supports for the lipid bilayers, were obtained from Shree GR Exports Private Limited (Kolkata, India).

Solid-Supported Lipid Bilayers Fabrication. Solid-supported lipid bilayers (SLBs) were prepared using a vesicle deposition on a solid substrate method, as described elsewhere.¹⁻³ We investigated SLBs composed of an equimolar ternary mixture 14:1 PC:Chol:SM with 0.1 mol% of Atto 633-DOPE and 0.1 mol% of additional fluorescent label, either TopFluor-Chol or TopFluor-SM. The membrane components were mixed in chloroform with a final lipid concentration of 10 mM. Subsequently, the relevant solution was dried using nitrogen gas and then subjected to desiccation in a vacuum chamber for a minimum of 2 hours. The lipid film was hydrated using a buffer solution (containing 10 mM HEPES and 150 mM NaCl, pH adjusted to 7.4) to achieve a lipid concentration of 10 mM. The lipid suspension underwent four cycles of heating to 60°C and vortexing, with each heating and vortexing step lasting 1 minute. The lipid mixture was diluted tenfold in a buffer to obtain a 1 mM vesicle suspension, and then distributed into glass vials for storage at -20°C for subsequent use. A portion of the MLV suspension, with the desired composition, was bath-sonicated for a minimum of 10 minutes. To prepare a solid support for the deposition of vesicles, a thin sheet of freshly cleaved mica, pre-cut into round plates with a 9 mm diameter, was fixed on a glass coverslip with UV-activated glue. Subsequently, a plastic cylinder, created by removing the lid and bottom of a microcentrifuge tube was placed on mica and sealed with silicone to create a reservoir with mica at the bottom. Next, 100 μL of 1 mM vesicle suspension was deposited onto the mica surface, followed by the immediate addition of 2 μL of a 0.1 M CaCl₂ solution. After ca. 30 seconds, 600 μL of the previously mentioned buffer solution was introduced to prevent the dehydration of the membrane under formation. Following a 30-minute incubation at room temperature, the supported lipid bilayer was rinsed with 20 mL of buffer solution to remove excess unburst vesicles. Ultimately, pure buffer solution was used to fill the remaining space in the reservoir, a condition referred to as bulk hydration throughout the paper.

SLB Hydration-State Control. To control the lipid membrane hydration state, we utilized our custom-designed humidity control system, described previously.¹⁻³ The setup includes several components: a nitrogen gas (N₂) cylinder, three flow meters, three manual valves, a water reservoir (for achieving water vapor saturation), and an electronic hygrometer. Initially, to decrease the hydration of the SLB, bulk water was extracted from the sample container using a micropipette until no buffer droplets were visible on the mica surface. Subsequently, nitrogen gas with a relative humidity of 95% RH was gently introduced into the sample container. The RH of the nitrogen gas was controlled by blending streams of wet (water-vapor-saturated, 95% RH) and dry (0% RH) gases. The individual flows of wet and dry N₂ gases were regulated using two manual valves, and the flow rates were monitored with two flow meters connected to their respective paths. To maintain a constant N₂ gas flow rate of approximately 1.2 L/min throughout the experiment, a third flow meter and manual valve were employed. An electronic hygrometer allowed continuous monitoring of both the relative humidity and temperature of the final gas stream, prompting adjustments as necessary. The de(re)hydration process was carried out gradually. After allowing approximately 10 minutes for the SLB atmosphere to equilibrate to the specified relative humidity, the sample was imaged.

Fluorescence Imaging. Confocal fluorescence imaging was performed on a Carl Zeiss LSM 710 laser-scanning confocal microscope, using 488 nm and 633 nm laser lines. The samples were illuminated and fluorescence was collected through a Carl Zeiss EC Plan-Neofluar 40x/1.30 oil immersion objective. The laser power was adjusted during imaging to prevent the dyes from undergoing excessive photobleaching.

Molecular Dynamics Simulations. Simulations represented symmetric bilayers of ~81 nm² area (9 nm × 9 nm) in the XY plane, composed of lipid types used in the experiments, embedded in aqueous environment. The following systems were constructed using the CHARMM-Gui⁴ server: SM:Chol (90:60 lipids per monolayer), 14:1 PC:Chol (90:30 lipids per monolayer), 14:1 PC:SM:Chol (62:62:62 lipids per monolayer), each with 2.5 nm margin of water on both membrane sides. The systems were simulated at temperature T = 298 K, and ambient pressure, under periodic boundary conditions with default equilibration protocol provided by CHARMM-Gui and production runs of 0.5, 0.5 and 2.5 μs, respectively. After the first 0.3 μs of the simulation time, the snapshot of 14:1 PC:SM:Chol system was used to generate dehydrated bilayer: water molecules that were furthest away from the membrane were removed to leave ~13 water molecules per lipid. The system size in Z direction, perpendicular to the membrane plane, was increased from ~9 to 12 nm, in order to create ~7 nm thick water vapor layer. Following this modification, the system size in Z direction was fixed and semiisotropic barostat was applied only in X and Y directions. Effective simulation pressure in XY plane of -100 bar was adjusted by trial and error to achieve membrane area possibly close to that of the fully hydrated system (note that system cross-section along the Z axis contains lipid/liquid water phase and water vapor). After the system was equilibrated for 0.1 μs, the second, analogous dehydration stage, albeit with no further modification of the simulation box dimensions, was performed to achieve hydration level of 8 water molecules per lipid. The effective pressure was established at -30 bar and the system was simulated for 2.5 μs. All simulations were carried out with Gromacs software.⁵ Charmm36 force field was used for lipids,⁶ and TIP3P model was used for water,⁷ with default simulation parameters for the force field used, as implemented in CHARMM-Gui input generator.

CHAPTER 7. DEHYDRATION OF LIPID MEMBRANE DRIVES REDISTRIBUTION OF CHOLESTEROL BETWEEN LATERAL DOMAINS

In order to determine the presence of PC and SM rich phases in the system, membrane plane was divided into $3 \text{ nm} \times 3 \text{ nm}$ grid and lipid molar fractions were evaluated within each cell, separately for each leaflet. To increase sampling, the calculations were repeated with grid origin translated along 5×5 sub-grid spanning the reference cell of the $3 \text{ nm} \times 3 \text{ nm}$ grid. The analysis of fully hydrated L_d and L_o phases was carried out based on their dedicated simulations, whereas the analysis of dehydrated PC:Chol and SM:Chol phases was conducted over grid areas with PC fraction among PC and SM lipids >0.9 and <0.1 , respectively. Radial distribution functions were calculated between hydroxyl oxygen atoms of cholesterol and phosphorus atoms of PC and SM lipids. Lipid density profiles across the membrane, and radial distribution functions were calculated using standard Gromacs tools, hydrogen bonding and other analyses were conducted using MDAnalysis python package.⁸

Lipid Order Parameter Determination. The ordering of the lipid acyl chains was determined by calculation of the order parameter (S_{CH}). S_{CH} is a measure of the relative orientation of the carbon-hydrogen bonds with respect to the bilayer normal. It was calculated according to the formula:

$$S_{CH} = \frac{1}{2} \langle 3 \cos^2 \theta - 1 \rangle, \quad (1)$$

in which θ is the angle between the bilayer normal and the vector joining carbon atom to its hydrogen atom, and $\langle \rangle$ represents an ensemble average. Calculation of the order parameter of lipid acyl chains was carried out with `g_lomepro` software.⁹

CHAPTER 7. DEHYDRATION OF LIPID MEMBRANE DRIVES REDISTRIBUTION OF CHOLESTEROL BETWEEN LATERAL DOMAINS

Supplementary Figures S1–S4

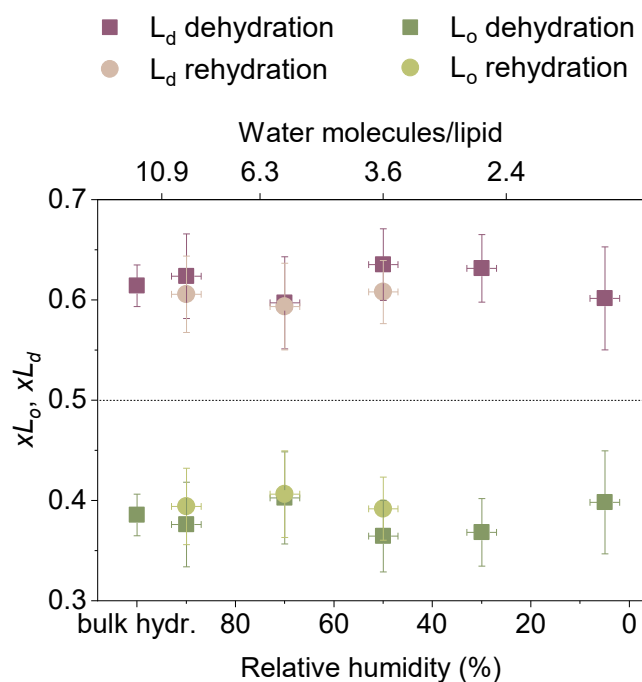


Figure S1. The partitioning coefficients of TopFluor-SM in the liquid-ordered (L_o) and liquid-disordered (L_d) phases within the 14:1 PC:SM:Chol (1:1:1) SLBs equilibrated in atmosphere of different humidity levels during both dehydration (squares, darker colours) and rehydration (circles, lighter colours). Each data point represents the partitioning coefficients calculated based on the average fluorescence intensities from at least 20 spots of distinct phase at a specific membrane hydration state from each of the two samples.

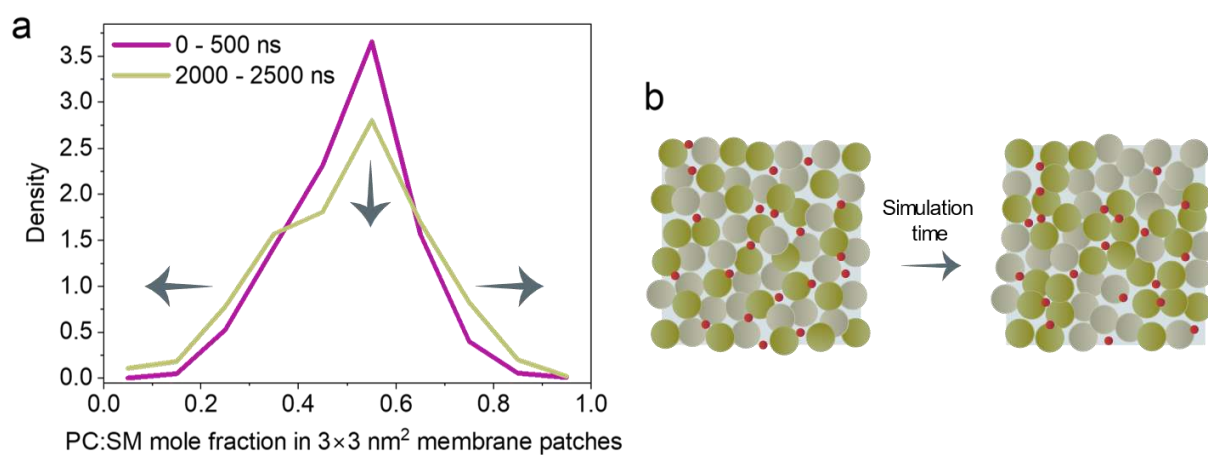


Figure S2. (a) The distribution of PC:SM mole fractions in $3 \times 3 \text{ nm}^2$ membrane patches in the simulated 14:1 PC:SM:Chol (1:1:1) lipid bilayer under bulk hydration. (b) The cartoon representation of the phase separation trend as the simulation progressed.

CHAPTER 7. DEHYDRATION OF LIPID MEMBRANE DRIVES REDISTRIBUTION OF CHOLESTEROL BETWEEN LATERAL DOMAINS

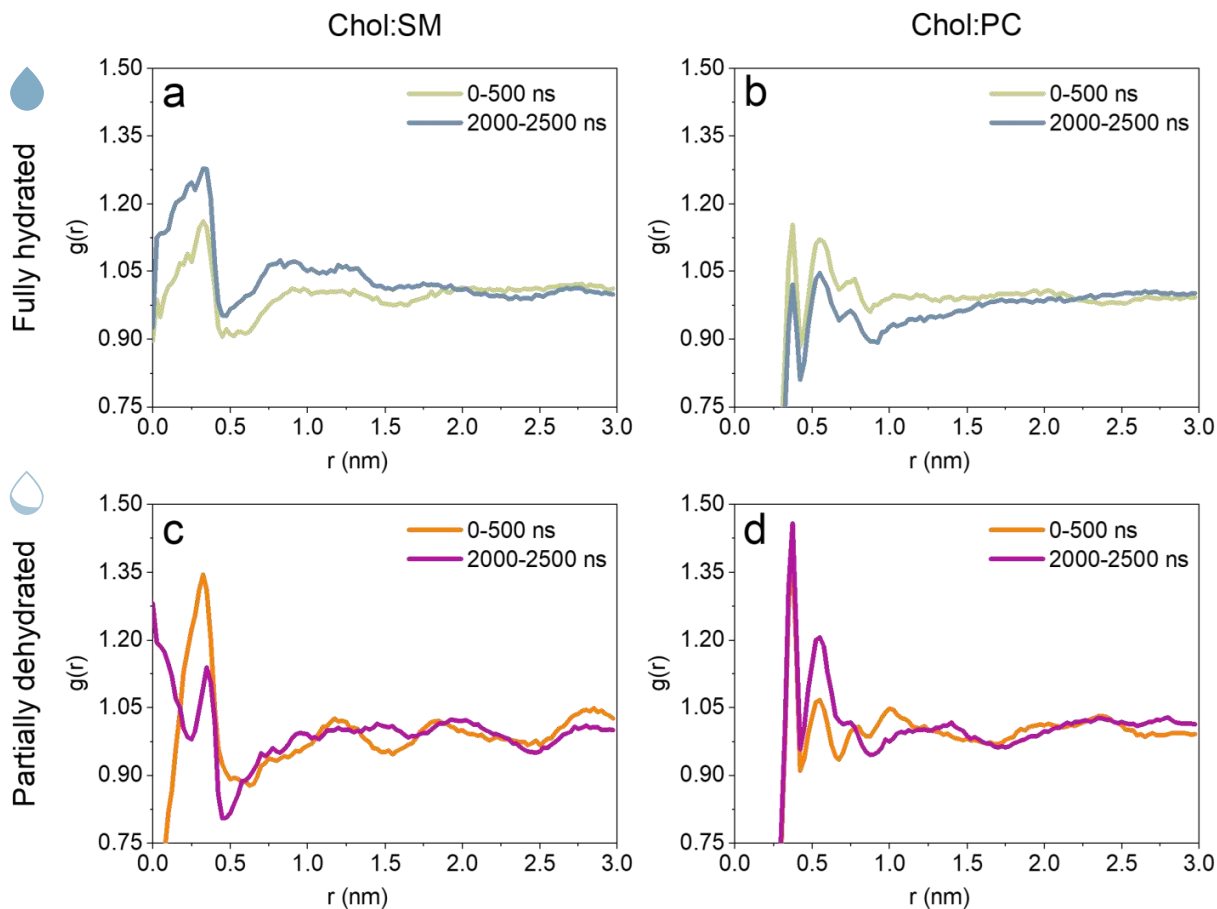


Figure S3. Radial distribution functions of 14:1 PC and SM lipids around cholesterol at the beginning (0–500 ns) and at the end (2000–2500 ns) of 14:1 PC:SM:Chol (1:1:1) lipid bilayer simulations under (a,b) fully hydrated and (c,d) partially dehydrated conditions (8 water molecules per lipid). Note that non-zero $g(r=0)$ values for Chol:SM pair result from a tendency of Chol hydroxyl groups to remain covered under SM head groups.

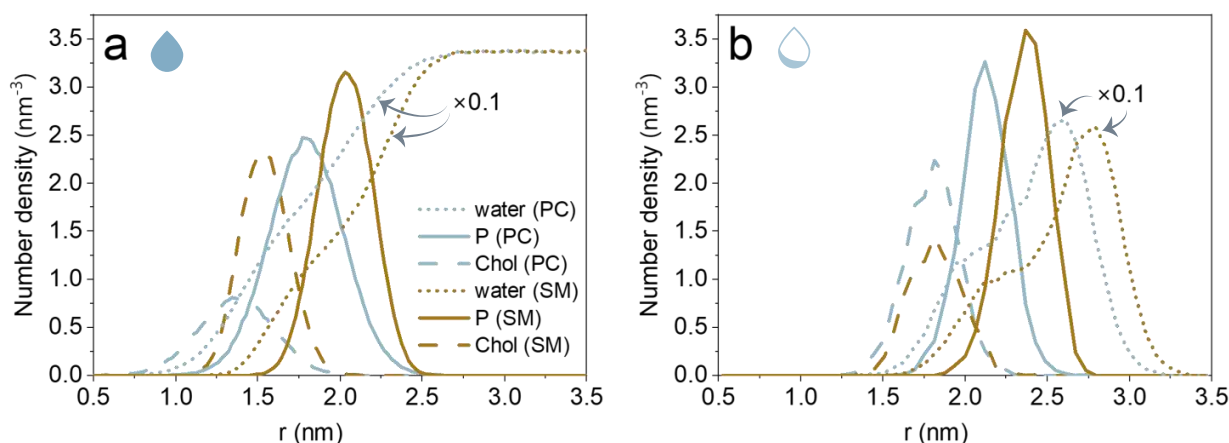


Figure S4. Number density profiles of water O atoms, PC and SM P atoms, Chol O atoms along Z axis in the respective phases in (a) fully hydrated conditions and (b) partially dehydrated conditions (8 water molecules per lipid).

CHAPTER 7. DEHYDRATION OF LIPID MEMBRANE DRIVES REDISTRIBUTION OF CHOLESTEROL BETWEEN LATERAL DOMAINS

Supplementary Tables S1–S4

Table S1. Structural parameters of simulated lipid bilayers under different hydration conditions (full hydration and partial dehydration down to 8 water molecules per lipid): membrane thickness (d), defined as averaged lipid P-P atom distance, cholesterol O atom position along bilayer normal with respect to lipid P atom position (h), and an average order parameter of the lipid acyl chains (S_{CH}).

Membrane hydration	d (nm)		h (nm)		S_{CH}	
	L_d (PC:Chol phase)	L_o (SM:Chol phase)	PC	SM	PC	SM
Full hydration	3.59	4.65	-0.43	-0.56	0.156	0.374
Partial dehydration	4.25	4.72	-0.32	-0.54	0.283	0.369

Table S2. Number of hydrogen bonds with water per lipid under different hydration conditions: full hydration and partial dehydration down to 8 water molecules per lipid. The headgroup region includes the oxygens of the phosphate group (PO_4) in both lipids, while the interfacial region involves oxygens of the carbonyl groups (CO) in PC, and oxygen and nitrogen atoms of the amide group (CO, NH) and oxygen atom of the hydroxyl group in SM.

Membrane hydration	PC...water			SM...water		
	Headgroup region	Interfacial region	In total	Headgroup region	Interfacial region	In total
Full hydration	4.33	1.24	5.56	3.89	1.55	5.44
Partial dehydration	3.86	0.81	4.67	3.67	1.46	5.13

Table S3. Number of hydrogen bonds with water per cholesterol under different hydration conditions: full hydration and partial dehydration down to 8 water molecules per lipid.

Membrane hydration	Chol...water	
	L_d (PC:Chol phase)	L_o (SM:Chol phase)
Full hydration	1.18	1.06
Partial dehydration	1.08	0.83

Table S4. Number of hydrogen bonds between cholesterol and lipids per cholesterol molecule under different hydration conditions: full hydration and partial dehydration down to 8 water molecules per lipid. The headgroup region includes the oxygens of the phosphate group (PO_4) in both lipids, while the interfacial region involves oxygens of the carbonyl groups (CO) in PC, and oxygen and nitrogen atoms of the amide group (CO, NH) and oxygen atom of the hydroxyl group in SM.

Membrane hydration	Chol...PC			Chol...SM		
	Headgroup region	Interfacial region	In total	Headgroup region	Interfacial region	In total
Full hydration	0.107	0.113	0.220	0.058	0.287	0.345
Partial dehydration	0.222	0.044	0.266	0.055	0.351	0.407

CHAPTER 7. DEHYDRATION OF LIPID MEMBRANE DRIVES REDISTRIBUTION OF CHOLESTEROL BETWEEN LATERAL DOMAINS

Calculation of the Energy Released Due to Reduction of Line Tension

To estimate changes of the energy of the system upon a reduction in line tension, we employ a simplistic model describing the boundary energy of an individual raft-like domain surrounded by a continuous fluid phase as $E = gL$, where g represents the line tension, and L denotes the domain perimeter.¹⁰ We assumed the L to be constant, as we did not observe notable alterations in the perimeter of the L_0 domains during dehydration. Consequently, in our calculations, the g is the only parameter that changes. Based on our previous atomic force microscopy study, a decrease in membrane hydration from approximately 10 to fewer than 1 water molecule per lipid (from 90% to 5% relative humidity) resulted in a reduction in line tension from around 7 pN to 2 pN.² For estimation, we consider a raft with a diameter of 20 nm. Change in the boundary energy of an individual raft is then:

$$\Delta E = E_{deh} - E_{hyd} = (\gamma_{deh} - \gamma_{hyd})L, \quad (2)$$

where subscripts *deh* and *hyd* denotes low and high hydration conditions, respectively.

$$\Delta E = (2 \text{ pN} - 7 \text{ pN}) \cdot 2\pi \cdot 10 \text{ nm} = -5 \text{ pN} \cdot 20\pi \text{ nm} = -100\pi \text{ pN} \cdot \text{nm} \approx -314 \text{ pN} \cdot \text{nm}$$

A negative value of the energy change is indicative of the reduction of the boundary energy of the system associated with the free energy release.

The thermal energy at physiological temperature of 37°C is:

$$k_B T \approx 1.38 \cdot 10^{-23} \text{ J} \cdot \text{K}^{-1} \cdot 310 \text{ K} = 427.8 \cdot 10^{-23} \text{ J} \approx 4.3 \cdot 10^{-21} \text{ N} \cdot \text{m} \approx 4.3 \text{ pN} \cdot \text{nm}$$

$$\left| \frac{\Delta E}{k_B T} \right| = \left| \frac{-314 \text{ pN} \cdot \text{m}}{4.3 \text{ pN} \cdot \text{m}} \right| \approx 73$$

Therefore, the possible free energy, released during dehydration-driven cholesterol redistribution between lipid raft and non-raft environment can be on the order of $70k_B T$.

References

- (1) Orlikowska-Rzeznik, H.; Krok, E.; Chattopadhyay, M.; Lester, A.; Piatkowski, L. Laurdan Discerns Lipid Membrane Hydration and Cholesterol Content. *J. Phys. Chem. B* **2023**, *127*, 3382–3391.
- (2) Krok, E.; Franquelim, H. G.; Chattopadhyay, M.; Orlikowska-Rzeznik, H.; Schwille, P.; Piatkowski, L. Nanoscale Structural Response of Biomimetic Cell Membranes to Controlled Dehydration. *Nanoscale* **2024**, *16*, 72–84.
- (3) Chattopadhyay, M.; Krok, E.; Orlikowska, H.; Schwille, P.; Franquelim, H. G.; Piatkowski, L. Hydration Layer of Only a Few Molecules Controls Lipid Mobility in Biomimetic Membranes. *J. Am. Chem. Soc.* **2021**, *143*, 14551–14562.
- (4) Jo, S.; Kim, T.; Iyer, V. G.; Im, W. CHARMM-GUI: A Web-Based Graphical User Interface for CHARMM. *J. Comput. Chem.* **2008**, *29*, 1859–1865.
- (5) Abraham, M. J.; Murtola, T.; Schulz, R.; Páll, S.; Smith, J. C.; Hess, B.; Lindahl, E. Gromacs: High Performance Molecular Simulations through Multi-Level Parallelism from Laptops to Supercomputers. *SoftwareX* **2015**, *1–2*, 19–25.
- (6) Klauda, J. B.; Venable, R. M.; Freites, J. A.; O'Connor, J. W.; Tobias, D. J.; Mondragon-Ramirez, C.; Vorobyov, I.; MacKerell, A. D.; Pastor, R. W. Update of the CHARMM All-Atom Additive Force Field for Lipids: Validation on Six Lipid Types. *J. Phys. Chem. B* **2010**, *114*, 7830–7843.
- (7) Jorgensen, W. L.; Chandrasekhar, J.; Madura, J. D.; Impey, R. W.; Klein, M. L. Comparison of Simple Potential Functions for Simulating Liquid Water. *J. Chem. Phys.* **1983**, *79*, 926–935.
- (8) Michaud-Agrawal, N.; Denning, E. J.; Woolf, T. B.; Beckstein, O. MDAAnalysis: A Toolkit for the Analysis of Molecular Dynamics Simulations. *J. Comput. Chem.* **2011**, *32*, 2319–2327.
- (9) Gapsys, V.; De Groot, B. L.; Briones, R. Computational Analysis of Local Membrane Properties. *J. Comput. Aided. Mol. Des.* **2013**, *27*, 845–858.
- (10) Yang, S. T.; Kiessling, V.; Tamm, L. K. Line Tension at Lipid Phase Boundaries as Driving Force for HIV Fusion Peptide-Mediated Fusion. *Nat. Commun.* **2016**, *7*, 11401.



8

Cholesterol changes interfacial water alignment in model cell membranes

In this chapter, I present a detailed study of how cholesterol affects membrane structure (lipid monolayer) and its interactions with biological water across different lipid types. To achieve this, I employed broadband heterodyne-detected vibrational sum frequency generation (HD-VSFG) spectroscopy to probe the vibrational signatures of lipids, cholesterol, and nearby water molecules. HD-VSFG is highly surface-specific and provides unique information about the absolute orientation of molecular moieties. I found that in membranes composed of unsaturated phosphatidylcholines, cholesterol disrupts the hydration shell around the lipid headgroups, leading to depolarization of water molecule orientation. In contrast, in membranes with saturated fatty acid chains, cholesterol interacts specifically with the lipids, resulting in increased lipid packing and enhanced ordering of the lipid headgroups—a phenomenon known as the condensing effect. This effect also increases the net orientation of membrane-associated water molecules that hydrate the remaining headgroups. In sphingomyelin monolayers, the cholesterol-induced condensing effect is most pronounced, with the orientation of interfacial water molecules hydrating the headgroups being the most anisotropic.

On the left, a tulip meadow seamlessly transitioning into a densely packed lipid membrane, symbolizes the intricate interactions among cholesterol, phospholipids, and biological water. The illustration reflects the setting of the measurements discussed in this chapter, which were conducted in the Netherlands, the tulip capital of the world. The graphic was designed by Katarzyna Bogdańska.

Cholesterol Changes Interfacial Water Alignment in Model Cell Membranes

Hanna Orlikowska-Rzeznik,* Jan Versluis, Huib J. Bakker, and Lukasz Piatkowski*


 Cite This: *J. Am. Chem. Soc.* 2024, 146, 13151–13162


Read Online

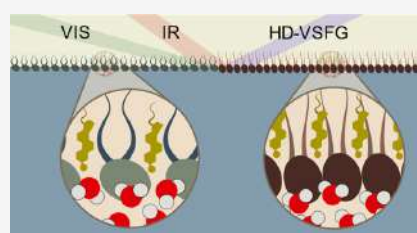
ACCESS |

Metrics & More

Article Recommendations

Supporting Information

ABSTRACT: The nanoscopic layer of water that directly hydrates biological membranes plays a critical role in maintaining the cell structure, regulating biochemical processes, and managing intermolecular interactions at the membrane interface. Therefore, comprehending the membrane structure, including its hydration, is essential for understanding the chemistry of life. While cholesterol is a fundamental lipid molecule in mammalian cells, influencing both the structure and dynamics of cell membranes, its impact on the structure of interfacial water has remained unknown. We used surface-specific vibrational sum-frequency generation spectroscopy to study the effect of cholesterol on the structure and hydration of monolayers of the lipids 1,2-dipalmitoyl-*sn*-glycero-3-phosphocholine (DPPC), 1,2-dioleoyl-*sn*-glycero-3-phosphocholine (DOPC), and egg sphingomyelin (SM). We found that for the unsaturated lipid DOPC, cholesterol intercalates in the membrane without significantly changing the orientation of the lipid tails and the orientation of the water molecules hydrating the headgroups of DOPC. In contrast, for the saturated lipids DPPC and SM, the addition of cholesterol leads to clearly enhanced packing and ordering of the hydrophobic tails. It is also observed that the orientation of the water hydrating the lipid headgroups is enhanced upon the addition of cholesterol. These results are important because the orientation of interfacial water molecules influences the cell membranes' dipole potential and the strength and specificity of interactions between cell membranes and peripheral proteins and other biomolecules. The lipid nature-dependent role of cholesterol in altering the arrangement of interfacial water molecules offers a fresh perspective on domain-selective cellular processes, such as protein binding.



INTRODUCTION

The life of eukaryotic cells relies critically on the presence and properties of lipid membranes. First, they maintain the cellular integrity by separating the cell interior from the extracellular milieu and by defining the subcellular organelles.¹ Second, they create a dynamic molecular matrix that supports the vital functions of integral membrane proteins,² thereby facilitating a wide range of biochemical processes, including neurotransmission,³ energy production,⁴ and immune response.⁵ Cell membranes exhibit a huge molecular heterogeneity of lipid compounds, as evident in the ever-evolving field of lipidomics, which aims to identify and quantify the molecular species of cellular lipids and their biological functions.⁶ Yet, it has been long recognized that the most abundant lipids found in mammalian cell membranes can be generally divided into three categories: glycerophospholipids (phosphatidylcholines in particular), sphingolipids, and cholesterol, which along with the nanoscopic layer of water directly hydrating the lipids, commonly referred to as *biological water*, define the structural scaffold of cellular membranes.⁷

The properties of biological water differ markedly from water in the bulk due to confinement effects and a perturbed interfacial H-bond donor/acceptor balance.^{8–10} Interfacial water is characterized by greatly slowed down rotational¹¹ and translational¹² dynamics as a result of the formation of

strong hydrogen bonds with the polar moieties of lipids (e.g., phosphate and carbonyl). Lipid–water interactions also affect the structure of interfacial water. Strong evidence has been found that biological water is highly polarized such that the hydrogen atoms point toward the membrane interior in the case of zwitterionic phospholipids.^{13–18} The preferential arrangement of the lipid moieties and the nonrandom orientation of the associated water molecules determine the sign and magnitude of the membrane dipole potential,¹⁹ which was shown to strongly influence a variety of membrane-centered processes, such as drug binding,²⁰ translocation of ions and macromolecules,^{21,22} clustering and binding affinity of proteins,²³ as well as the function of membrane-incorporated proteins,²⁴ and many more.^{25–27} Furthermore, the molecular structure of biological water has been postulated to dictate the fusogenic properties of lipid membranes.²⁸ In a molecular dynamics simulation study by Kasson et al., the ordering of

Received: January 11, 2024

Revised: April 20, 2024

Accepted: April 22, 2024

Published: April 30, 2024



water bound to the surface of biomembranes was found to control membrane fusion dynamics.²⁹ Consequently, any alteration in the arrangement of interfacial water has potential impact on all processes in which membrane fusion plays a fundamental role, such as neurotransmission, fertilization, viral entry, exocytosis, and intracellular transport.³⁰

The existing literature provides valuable insights into the structure and dynamics of biological water, yet it is important to note that these findings are primarily derived from studies involving pure phospholipid model systems. Given that cholesterol is a fundamental component of mammalian cell membranes and that it plays a crucial role in regulating both the structure and dynamics of lipid membranes³¹ as well as functioning of membrane proteins,³² its influence on both the dynamics and structural aspects of biological water should be explicitly acknowledged. This gains further importance considering that cholesterol, along with sphingomyelin, is associated with the formation of so-called lipid rafts,³³ i.e., transient functional domains involved in various cellular processes such as membrane trafficking, signal transduction, or host–pathogen interactions.^{34,35}

It is well documented that cholesterol's interactions with adjacent phospholipids induce conformational ordering of lipid alkyl chains, reduce the area per lipid, and increase the thickness of the lipid bilayer,^{36–38} thereby changing the permeability³⁹ and mechanical properties of the membrane.⁴⁰ In contrast, the effect of cholesterol on interfacial water properties remains largely unexplored experimentally. Cheng et al. using ¹H Overhauser dynamic nuclear polarization relaxometry found that cholesterol enhances the translational diffusivity of water at the surface of the phosphatidylcholine bilayer and attributed this finding to potential weakening or breaking of the strong hydrogen-bond network of the surface hydration layers.⁴¹ Recently, Pyne et al., by employing attenuated total reflection–Fourier transform infrared spectroscopy in the terahertz frequency domain, found evidence that cholesterol weakens the interfacial intermolecular hydrogen bonds at a lipid bilayer composed of negatively charged lipids, which eventually leads to accelerated global dynamics of water at the membrane.⁴² However, they found a negligible effect in the case of zwitterionic lipids.

These important consequences of the intimate interactions of cholesterol with the membrane prompt the question whether changes in the lipid structure and dynamics, along with affected interfacial water dynamics, are accompanied by alterations in the arrangement of biological water molecules. In a quest to gain a more detailed picture of the potential impact of cholesterol on the orientation of water molecules, which plays a pivotal role in determining the membrane dipole potential, we pose several questions: Does cholesterol influence membrane-bound water ordering? If so, to what extent, and how does this effect depend on the nature of the lipid matrix? Finally, what mechanisms are at play—does cholesterol in the membrane interact with water directly, or it exerts its effects indirectly by altering the arrangement of adjacent phospholipids?

To study how cholesterol affects the hydrogen-bonding network of biological water, we employed heterodyne-detected vibrational sum-frequency generation (HD-VSFG) spectroscopy, which is inherently an interface-specific technique, using zwitterionic lipid monolayers as a model for cell membranes. By altering the cholesterol content of the membrane, we explored its impact on the hydration characteristics of three

types of phospholipids: two phosphatidylcholines (unsaturated and saturated) and sphingomyelin. The interface was probed in two vibrational regions: The first region covers the bending vibrations of lipid methyl and methylene groups and the stretch vibration of lipid carbonyls, providing information on the lipid structure; the second region covers the stretching of lipid methyl and methylene groups, along with the stretch vibration of the water hydroxyl groups, the latter providing direct insight into the structure of the interfacial water. In the context of membrane hydration structure, phospholipid carbonyls hold particular significance as they terminate the hydrogen-bond network of biological water hydrating the membrane.⁴³ This is due to their spatial positioning within the boundary region, which separates the well-solvated polar lipid heads from the hydrophobic lipid fatty acid chains. By integrating water-centric and lipid-centric viewpoints, we were able to correlate the changes induced by cholesterol on the membrane structure with alterations in the structural arrangement of water molecules within the phospholipid headgroups.

MATERIALS AND METHODS

Materials. Lipids 1,2-dipalmitoyl-*sn*-glycero-3-phosphocholine (DPPC), 1,2-di-oleoyl-*sn*-glycero-3-phosphocholine (DOPC), egg sphingomyelin (SM), and cholesterol (Chol) were supplied by Avanti Polar Lipids. D₂O (99.9 atom % D) and spectrophotometric grade chloroform were purchased from Sigma-Aldrich. All compounds were used as received without further purification. The concentration of phospholipid stock solutions in chloroform was 0.1 mM. Deionized water was acquired using the Millipore Nanopure system (18.2 MΩ cm, pH 5.5). The molecular structures of the studied lipids, Chol and the three zwitterionic phospholipids DOPC, DPPC, and SM, are depicted in Figure 1. The structural differences between the lipids are highlighted.

Sample Preparation. Following a thorough cleaning procedure with ethanol and ultrapure water, a home-built Teflon trough (35 mm

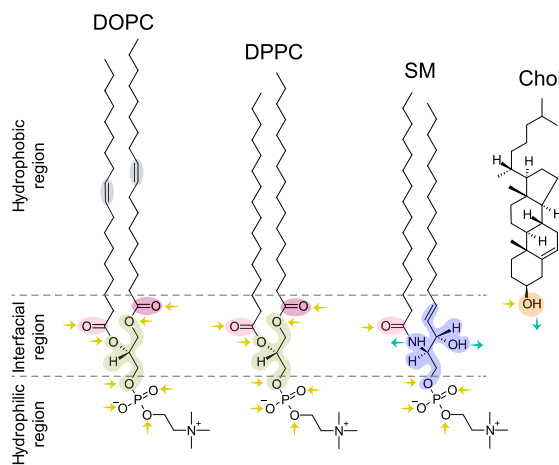


Figure 1. Molecular structures of the studied lipids: DOPC, DPPC, SM, and Chol. The glycerol linkage of phosphatidylcholines (DOPC, DPPC) is indicated in green. The sphingosine linkage of SM is indicated in blue. Carbonyl groups are indicated in pink shades. The hydroxyl group of cholesterol is indicated in orange. Double bonds in the hydrocarbon tails of DOPC are indicated in gray. Hydrogen-bond accepting and donating atoms are indicated by yellow and turquoise arrows, respectively.

diameter) was filled with either H₂O or D₂O as a subphase. H₂O was used for measurements in the CH and OH stretching vibration regions. D₂O was used for measurements in the CH bending and CO stretching vibration regions to avoid the measurements being affected by the response of the water bending mode. Self-assembled lipid monolayers were formed by dropwise spreading a lipid stock solution onto the surface of the neat subphase using a microliter Hamilton syringe. After spreading, at least 1 min was allowed for solvent evaporation and monolayer equilibration before sum-frequency generation spectroscopy measurements were taken. Lipid surface coverage (surface pressure) was controlled by the amount of lipid solution applied onto the subphase and was kept constant throughout the experiment. The HD-VSFG data presented herein correspond to the case where the surface is fully covered with lipids, indicated by the complete vanishing of the response of unbound water OH groups (see Figure S1). The amount of lipid solution applied onto the subphase to fulfill this condition corresponds to a surface pressure of around 40 mN/m for each sample (pure Chol, pure phospholipids, and phospholipid mixtures with Chol). The surface pressure was measured independently, outside the HD-VSFG experimental setup, using a Langmuir–Blodgett (KSV Nima) balance equipped with a platinum Wilhelmy plate. The measurements were conducted at a temperature of 21 °C. Under these conditions, all of the lipid monolayers were in a condensed-phase state. The studied phospholipids mix effectively with cholesterol in the entire range of the investigated molar fractions.^{44–46}

Heterodyne-Detected Vibrational Sum-Frequency Generation Spectroscopy (HD-VSFG). HD-VSFG experiments were carried out using a home-built optical setup based on an amplified Ti:sapphire laser system (oscillator: Coherent Mantis, amplifier: Coherent Legend Elite Duo). The laser system produced 35 fs pulses centered at 800 nm, with an energy of approximately 6.5 mJ and a repetition rate of 1 kHz. The laser output was divided into two parts, one of which was used to pump a commercial optical parametric amplifier (Light Conversion HE-TOPAS) to generate tunable infrared (IR) pulses with a spectral bandwidth of ~400 cm⁻¹. The IR pulses were centered at approximately 3200 and 1600 cm⁻¹ (with bandwidths at half-maximum of about 550 and 350 cm⁻¹) to probe the hydroxyl stretching and phospholipid carbonyl stretching regions, respectively. The other part of the laser output (visible, VIS) underwent spectral narrowing (using diffraction grating and spatial filtering) to a bandwidth of approximately 20 cm⁻¹, which largely determines the spectral resolution of the detected SFG signal. The IR and VIS beams were spatially and temporally overlapped at the surface of a gold mirror, leading to the generation of light at their sum frequency. This sum-frequency generation (SFG) signal, originating from the strong nonresonant second-order nonlinear susceptibility ($\chi^{(2)}$) of gold, served as a local oscillator (LO-SFG). The IR and VIS beams had incidence angles of ~55 and ~50°, respectively, relative to the surface normal. Before the sample, in the optical path of the reflected LO-SFG signal, a 1 mm thick silica plate was inserted to introduce a time delay of approximately 1.6 ps of the SFG light with respect to the IR and VIS beams. Subsequently, all three beams were focused by a spherical mirror onto the sample surface, where the IR and VIS beams overlapped spatially and temporally and generated a sample vibrational sum-frequency generation (VSFG) signal. The delayed LO-SFG and sample VSFG were subsequently coupled into a spectrograph (Princeton Instruments Acton SpectraPro SP-2300), and the spectral interference pattern of the two light signals was detected using a charge-coupled device (CCD) camera (Princeton Instruments Pixis 100). To extract the phase of the sample VSFG light, we repeated the HD-VSFG experiments using a z-cut quartz crystal instead of the sample. To obtain the extracted phase with sufficient accuracy, the quartz crystal was placed at the same height as the sample, which was controlled by monitoring the position of the signal on the CCD camera. Spectra were collected in ssp polarization combination (s: polarized SFG, s: polarized VIS, p: polarized IR). To minimize the loss of IR intensity caused by water vapor absorption along the optical path and to prevent unsaturated lipid oxidation

(DOPC), the optical setup was continuously purged with nitrogen gas.

The measured interference spectra are affected by spectral modulation effects, resulting from an etaloning effect in the CCD camera, which is particularly strong in the 1600 cm⁻¹ region (for details see Supporting Information, Note S1). To correct for this effect, we performed two separate measurements on a z-cut quartz crystal, for which crystal orientation differed by 180°. By summing two reference spectra with a 180° phase difference, we effectively eliminated the interference from LO-SFG and the quartz SFG. The remaining modulation primarily represents the structural noise. This remaining signal was then utilized to correct the measured signal from the samples for both the spectral dependence of the input IR beam and the etaloning effect, using the procedure described by Moll et al.^{47,48} The Teflon trough with water and a lipid monolayer was positioned on a rotating holder to facilitate the continuous renewal of the sample-probed area. This approach served two main purposes: (i) to average the HD-VSFG signal across distinct locations on the sample surface and (ii) to mitigate laser-induced thermal effects—specifically, the Marangoni flows resulting from steady-state laser heating, which displace lipids from the laser focal region.^{49,50} In the analysis conducted, the raw interferograms were subjected to Fourier transformation for further processing. The spectra processing was realized using a custom Python script. Each HD-VSFG spectrum presented in the figures is averaged over at least three spectra per membrane composition, unless otherwise indicated.

RESULTS AND DISCUSSION

Impact of Cholesterol on the Interfacial Monolayer Structure. First, we analyze the spectral signatures from the individual membrane constituents in the carbonyl (C=O) stretching region. The direct comparison of the $\text{Im}\chi^{(2)}$ spectra of pure cholesterol and the cholesterol-free DOPC, DPPC, and SM monolayers at the D₂O–air interface is depicted in Figure 2.

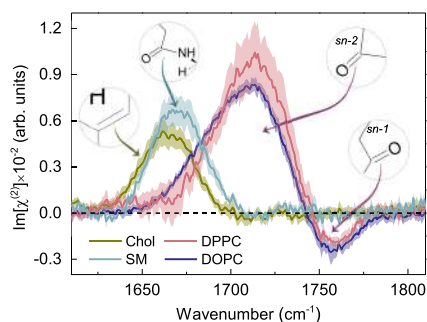


Figure 2. $\text{Im}\chi^{(2)}$ spectra of Chol, DOPC, DPPC, and SM monolayers at the D₂O subphase in the phospholipid carbonyl stretching vibration region. Curves represent the mean spectra with shaded areas indicating the standard deviation.

The $\text{Im}\chi^{(2)}$ spectrum of the pure cholesterol–D₂O interface, in the phospholipid carbonyl stretching region, is characterized by a pronounced positive peak at 1665 cm⁻¹.

In a recent study of sphingomyelin–cholesterol interactions in lipid monolayers,⁵¹ the aforementioned band has been overlooked in the intensity VSFG spectrum measured with the same polarization combination as used here (ssp). Following Genova et al.⁵² who reported Raman spectra of the neat cholesterol film, we attribute the band at 1665 cm⁻¹ to the carbon-to-carbon double-bond (C=C) stretching vibration from the steroid ring structure.

In the $\text{Im}\chi^{(2)}$ spectra of both DOPC– D_2O and DPPC– D_2O interfaces, two bands of opposite signs and different amplitudes can be distinguished: a prominent positive peak at approximately 1715 cm^{-1} and a weaker negative one at $\sim 1760\text{ cm}^{-1}$. These two partially overlapping bands are assigned to the phosphatidylcholine ester carbonyl stretching vibrations and have been previously identified by linear infrared spectroscopies.^{53,54} Consistent with previous studies, we assign the lower-frequency band to hydrogen-bonded phospholipid carbonyls and the higher-frequency band to non-hydrogen-bonded carbonyl groups.⁵³ The signs of the $\text{Im}\chi^{(2)}$ responses from the two carbonyl populations suggest that the hydrogen-bonded C=O groups are preferentially oriented with their oxygen atoms pointing toward the bulk water region (O-down), whereas the free C=O groups are preferentially oriented toward the hydrophobic part of the membrane (O-up). This interpretation of the response of the C=O vibrational modes is consistent with the molecular picture presented by Dreier et. al, arising from the analysis of the HD-VSFG data for the monolayers composed of the charged lipids (DPTAP and DPPG).⁵⁵ The positive band likely originates mainly from *sn*-2 carbonyls with a net O-down orientation, located closer to the bulk water region and thus hydrated through hydrogen bonding. On the other hand, the negative band most likely arises predominantly from *sn*-1 carbonyls, which preferentially orient with their oxygen atoms toward the hydrophobic region of the membrane (O-up), located further away from the bulk water region and, as a result, nonhydrated.

In contrast to phosphatidylcholines (PCs), the $\text{Im}\chi^{(2)}$ spectrum of the SM– D_2O interface exhibits only one pronounced band at $\sim 1670\text{ cm}^{-1}$, which originates from the stretching mode of the carbonyl group in the N-linked acyl chain (amide I).⁵⁶ The positive sign and relatively small width of the band indicates a homogeneous orientational distribution of SM C=O groups with their oxygen atoms pointing toward the bulk water region (O-down). Furthermore, its spectral position (45 cm^{-1} shift to a lower wavenumber with respect to DPPC and DOPC) suggests that these moieties are hydrated. We note here that the amide modes are typically observed at lower frequencies than carbonyl modes from PC lipids.⁵⁷

In Figure 3, we present $\text{Im}\chi^{(2)}$ spectra of the interface of mixed phospholipid/cholesterol monolayers on D_2O in the CH bending and C=O stretching regions. The $\text{Im}\chi^{(2)}$ spectra of pure components are shown for reference. The two negative peaks at 1385 and 1460 cm^{-1} , found in the $\text{Im}\chi^{(2)}$ spectra of all mixed monolayers, are ascribed to the methyl and methylene bending modes. In the case of SM, we also observe contributions from the NH bending modes in this spectral region (amide II and/or amide III).⁵⁶

As shown in Figure 3A and B, upon increasing the cholesterol content in the DOPC and DPPC monolayers, the positive and negative bands of the carbonyl stretch vibrations (1715 and 1760 cm^{-1}) decrease, while the amplitudes of the bands of the Chol C=C stretching (1665 cm^{-1}) and CH bending modes increase.

To quantify the effect and to gain a more detailed molecular-level insight into the cholesterol-induced changes at the carbonyl level of the membranes composed of DOPC and DPPC, we performed spectra decomposition using three Gaussian line shapes, to account for the contribution from cholesterol and two oppositely oriented carbonyl populations. The results of this analysis are plotted in Figure 4.

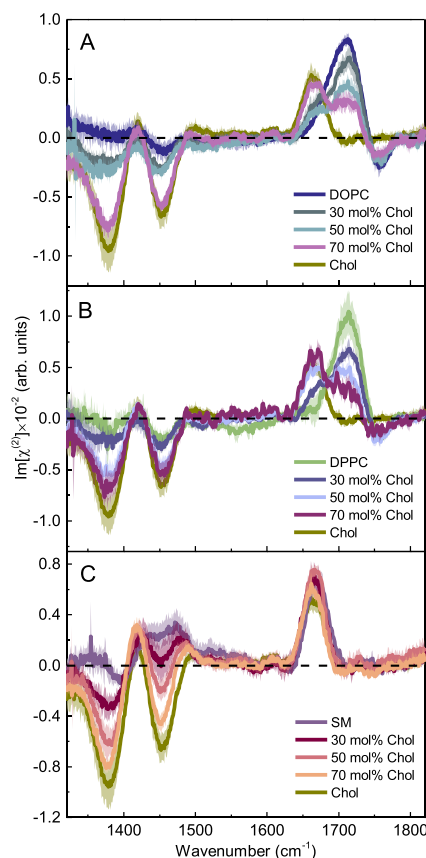


Figure 3. $\text{Im}\chi^{(2)}$ spectra of (A) DOPC, (B) DPPC, and (C) SM monolayers at the D_2O subphase in the absence and presence of cholesterol at molar fractions of 0.3, 0.5, and 0.7 in the CH bending and C=O stretching vibration regions. The $\text{Im}\chi^{(2)}$ spectrum of Chol is shown for reference. Curves represent the mean spectra with shaded areas indicating the standard deviation.

The $\text{Im}\chi^{(2)}$ spectra of the monolayers composed of DPPC and DOPC enriched with cholesterol can be well expressed as a linear combination of the bands centered at: (i) 1665 cm^{-1} with a width (full width at half-maximum) of 35 cm^{-1} , assigned to the C=C stretch vibration from the cholesterol ring structure, (ii) 1715 cm^{-1} with a width of 50 cm^{-1} , assigned to the hydrogen-bonded phospholipid carbonyls, and (iii) 1750 cm^{-1} with a width of 40 cm^{-1} , attributed to the non-hydrogen-bonded phospholipid carbonyls. The results of the fitting procedure for the Chol-DOPC and Chol-DPPC monolayers at a cholesterol content of 70 and 30 mol % are depicted in Figure 4A and D, respectively.

In Figure 4B and E, it is evident that with an increase in cholesterol content, the areas of both peaks corresponding to distinct carbonyl populations decrease with respect to the pure DOPC and DPPC monolayers. This observation aligns with expectations as the introduction of cholesterol leads to an exchange of a portion of PC lipids, resulting in an increased sterol contribution to the $\text{Im}\chi^{(2)}$ spectra, accompanied by a simultaneous decrease in the contribution from PC (dilution effect). However, the areas of the two peaks, and therefore the abundance of both detected carbonyl populations, do not

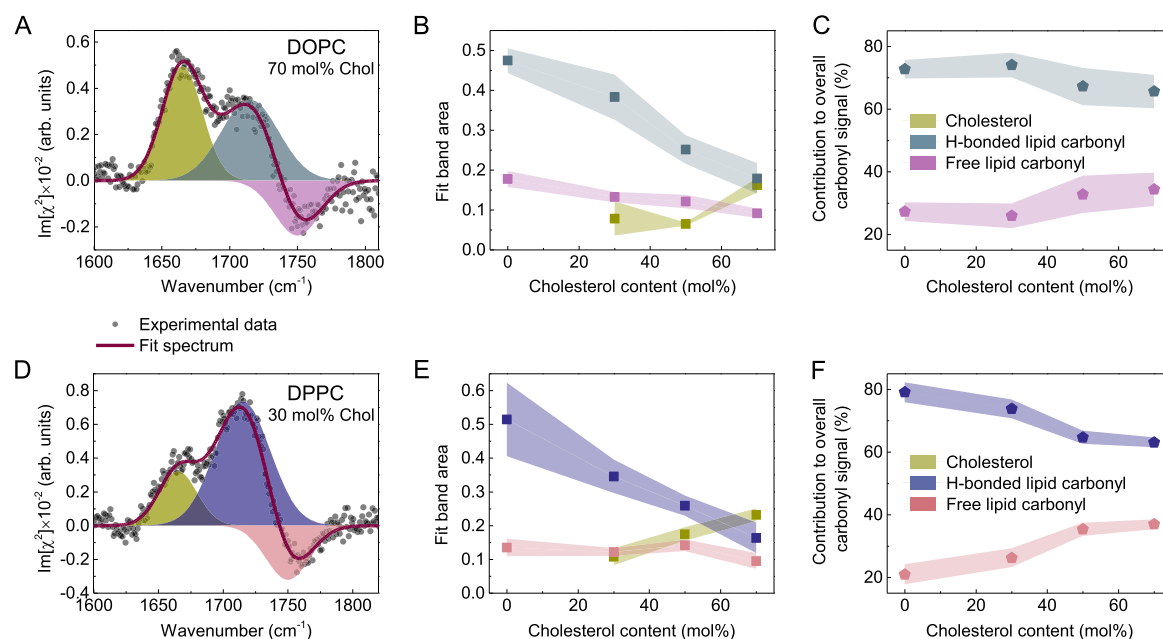


Figure 4. Results of $\text{Im}\chi^{(2)}$ spectra decomposition using three Gaussian line shapes in the lipid carbonyl stretching region for cholesterol-containing PC lipid monolayers. The upper panels (A–C) correspond to DOPC and the bottom ones (D–F) to DPPC samples. (A, D) Three peak Gaussian decomposition of the exemplary $\text{Im}\chi^{(2)}$ spectrum of the phospholipid/Chol monolayer. (B, E) The area of the distinct Gaussian components as a function of cholesterol concentration. (C, F) Contribution of the hydrogen-bonded and non-hydrogen-bonded carbonyls to the overall signal from carbonyls, calculated based on the fitted band areas, as a function of cholesterol concentration. Curves on panels B, C, E, and F represent the mean values with shaded areas indicating the standard deviation. The lines connecting the points act as a guide to the eye.

diminish at the same rate or to the same extent. Figure 4C and F demonstrates that as the cholesterol content in the membranes increases, the relative contribution of the non-hydrogen-bonded carbonyls to the HD-VSFG response increases, while the relative contribution of the hydrogen-bonded carbonyls decreases, reflecting cholesterol-induced changes in the membrane H-bond network structure.

We identify two possible explanations for the observed effect. In the first scenario, cholesterol induces conformational changes in PC carbonyl groups, leading to an apparent increase in the population of free carbonyls. However, nuclear magnetic resonance experiments have shown that the structural order parameters of the interfacial regions of the phosphatidylcholine membranes, including the carbonyl region, remain largely unaffected by the presence of cholesterol.^{36,58} Therefore, the structural conformational rearrangements of the hydrogen-bonded and non-hydrogen-bonded carbonyls induced by cholesterol appear unlikely. Alternatively, cholesterol-induced ordering of phospholipid tails results in tighter membrane packing (condensing effect), leading to the expulsion of some water molecules, particularly those located above the head-group, at the level of the carbonyl groups. This mechanism would indeed increase the relative population of free carbonyls, and we find this explanation more plausible. This effect is less pronounced in the case of DOPC, for which the difference in the hydrogen-bonded and free carbonyl populations in the membrane without cholesterol is smaller than that in the case of DPPC (see Figure 4C and F). This is likely due to the presence of unsaturation in the acyl chains of DOPC, which leads to a higher area per molecule and consequently greater separation between the interfacial moieties of the phospholi-

pids when compared to DPPC (also in the presence of cholesterol), as well as less-effective cholesterol-induced condensing effect.^{59,60} As a result, the ability of cholesterol to effectively perturb the carbonyl region of DOPC is less pronounced compared to DPPC.

It is apparent from Figures 2 and 3C that the band resulting from the sphingomyelin carbonyl stretching coincides to a great extent with the band originating from the cholesterol carbon-to-carbon double-bond stretching. Owing to this overlap, it becomes challenging to trustfully resolve and accurately fit the individual contributions in the mixtures of these two components. Nonetheless, some valuable qualitative observations can still be made.

In the extreme scenario, where cholesterol would not interact with sphingomyelin, one could expect that the $\text{Im}\chi^{(2)}$ spectra of their mixtures would be a linear combination of their respective vibrational spectra multiplied by their molar fraction in the membrane. We calculated such spectra and determined to what extent they overlap with the experimental spectra. The results of this analysis are shown in Figure S2. In brief, for all three SM/Chol systems, the amplitude of the observed $\text{C}=\text{O}/\text{C}=\text{C}$ stretching band is higher than that expected from a weighted sum of Chol and SM. Thus, the results indicate that the HD-VSFG spectra in the mixed SM/Chol systems are certainly not simply additive, indicating the presence of interactions between SM and Chol. The higher peak amplitudes can be either due to an increased membrane density or due to an enhanced orientation of the oscillators (SM $\text{C}=\text{O}$ and/or Chol $\text{C}=\text{C}$).

Effect of Cholesterol on the Interfacial Water Structure within Model Cell Membranes. After establish-

ing the impact of cholesterol on the biological water H-bond network from a phospholipid-centric perspective, we proceed to analyze its effects on the interfacial water structure. First, we examine the interfacial water structure within one-component model cell membranes. Figure 5 shows the $\text{Im}\chi^{(2)}$ spectra of the neat water and one-component phospholipid monolayers on water in the CH and OH stretch vibration region.

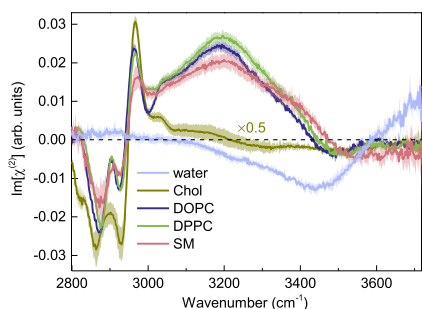


Figure 5. $\text{Im}\chi^{(2)}$ spectra of neat air–water, DOPC–water, DPPC–water, SM–water, and Chol–water interfaces in the CH and OH stretch vibration region. Curves represent the mean spectra with shaded areas indicating the standard deviation. The spectrum of the Chol monolayer was divided by two for the visualization purposes.

The $\text{Im}\chi^{(2)}$ spectrum of the neat air–water interface (Figure 5, light blue line) is characterized by two bands of opposite signs: a broad negative band with a maximum intensity centered at ca. 3450 cm^{-1} and a narrower positive band at around 3700 cm^{-1} . The former is assigned to the OH stretching vibrations of water molecules that donate hydrogen bonds to other water molecules and that have a net orientation with their hydrogen atoms pointing toward the bulk phase (H-down). The higher-frequency band is attributed to the stretching vibrations of the non-hydrogen-bonded (free) OH groups of water molecules, which orient with their hydrogen atoms facing the air (H-up).

For all studied phospholipids (DOPC, DPPC, SM), the $\text{Im}\chi^{(2)}$ spectrum of the lipid membrane in the CH stretching region ($2800\text{--}3000\text{ cm}^{-1}$) exhibits characteristic bands arising from the vibrations of methyl groups terminating the hydrophobic chains. The details of the band assignment can be found in the Supporting Information (Note S2).

Phospholipid monolayers clearly rearrange the interfacial water structure. The amplitude of the $\text{Im}\chi^{(2)}$ signal in the OH stretching region is significantly larger for all three zwitterionic lipids than for the neat water, which is in accordance with earlier studies for zwitterionic lipid monolayers.^{15,61} Regardless of the phospholipid type, the $\text{Im}\chi^{(2)}$ spectrum shows an intense broad feature with a maximum intensity at around 3200 cm^{-1} with a shoulder band at 3400 cm^{-1} . This feature is positive in sign up to approximately 3450 cm^{-1} , reflecting H-up oriented hydrogen-bonded water molecules.⁶² In the higher-frequency region, near 3500 cm^{-1} , one can observe a relatively weak negative signal that is considered a signature of weakly hydrogen-bonded water molecules buried above the lipid headgroup (H-down oriented).^{62–64} Overall, the $\text{Im}\chi^{(2)}$ spectrum of SM resembles the spectra of the other two zwitterionic phospholipids. However, two significant differences are observed. First, the doublet feature of the OH stretch band is more pronounced in the case of SM, with the peak at

3400 cm^{-1} being stronger than those in the case of DOPC and DPPC. Second, the negative band near 3500 cm^{-1} extends to the frequency region of the free OH stretch vibration of the water–air interphase. Despite the net zero surface charge of the zwitterionic lipid monolayers, there is a noticeable preferential alignment of interfacial water molecules, reminiscent of a negatively charged interface.⁶⁶ This phenomenon has been hypothesized to be due to the higher charge density and greater reorienting capability of the negatively charged phosphate group compared to the positively charged choline group, favoring an upward orientation of water dipoles.⁶⁷ However, recent HD-VSFG experiments by Dreier et al. on zwitterionic lipids, with reversed positions of phosphate and choline groups, provided evidence that the rationale is different.¹⁵ This study demonstrated that it is the electric field arising between two oppositely charged groups within the hydrophilic head that governs the net orientation of the interfacial water.¹⁵ Additionally, Saak et al. have established that the alignment of interfacial water caused by zwitterionic phospholipids is unaffected by ionic screening, thereby evidencing the charge neutrality of such membranes.⁶⁸ Collectively, these findings lead to the conclusion that the probed OH signal in the presently studied model cell membranes originates mainly from water molecules within the primary hydration shell.⁶⁸

Changes in the $\text{Im}\chi^{(2)}$ spectra of the lipid–water interfaces in the CH and OH stretch vibration regions resulting from the incorporation of cholesterol into the membranes are depicted in Figure 6. Upon an increase in cholesterol content, the amplitudes of the peaks in the CH stretch vibration region monotonically increase for all three phospholipids. We assign this effect primarily to the following. The $\text{Im}\chi^{(2)}$ spectrum of a pure cholesterol monolayer exhibits the highest peak amplitudes in the CH stretch vibration region when compared to the phospholipid–water interfaces. This is likely due to the tighter packing (lower area per molecule) and higher number of methyl groups in the cholesterol structure, which increase the effective number of CH oscillators in the probed area. Increasing the molar fraction of cholesterol at the surface thus leads to an increase of the CH signals. The changes of the area under the curve within the $2840\text{--}2990\text{ cm}^{-1}$ spectral range for the three phospholipids are shown in the bottom panels of Figure 6.

The response from the nearby water layers is quite different. For DOPC and DPPC host lipids, we observe that the amplitude of the $\text{Im}\chi^{(2)}$ signal originating from hydrogen-bonded interfacial water molecules in the H-up orientation decreases as the cholesterol content in the monolayer increases. Notably, this change is more pronounced in the case of DOPC, where the area under the curve within the $3100\text{--}3450\text{ cm}^{-1}$ spectral range decreases by 66%, compared to 30% in DPPC as the Chol content increases from 0 to 70 mol % (see Figure 6D and E). The decrease of the $\text{Im}\chi^{(2)}$ response in the OH stretching region with increasing mole fraction of cholesterol, observed for DOPC and DPPC containing monolayers, implies a reduced orientational preference of the membrane-bound water molecules. In SM monolayers, the amplitude of the OH stretch vibration band appears to be virtually insensitive to the cholesterol content (see Figure 6C and F).

The decrease in the interfacial water SFG_{ssp} signal was previously observed in studies involving the zwitterionic deuterated DMPC lipid bilayer upon incorporation of the

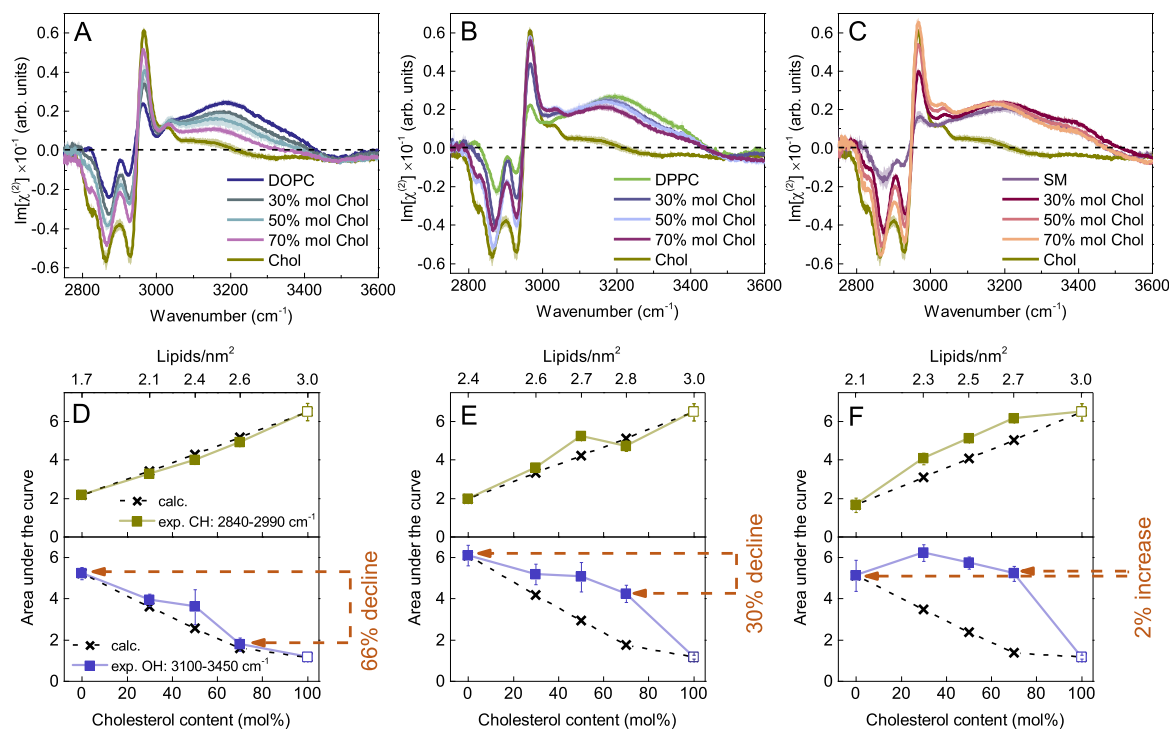


Figure 6. (A–C) $\text{Im}\chi^{(2)}$ spectra of DOPC, DPPC, and SM monolayers on water, respectively, in the absence and presence of cholesterol at molar fractions of 0.3, 0.5, and 0.7 in the CH and OH stretch vibration regions. The $\text{Im}\chi^{(2)}$ spectrum of Chol is shown for reference. Curves represent the mean spectra with shaded areas indicating the standard deviation. (D–F) The corresponding area under the curve in two spectral regions (CH and OH stretching) as a function of cholesterol content (bottom x-axis) in the monolayers with DOPC, DPPC, and SM as host lipids, respectively. The top x-axis indicates lipid densities, calculated using the area per molecule for pure phospholipids and pure cholesterol (at a surface pressure of 40 mN/m), reported in the following references.^{45,46,65} For lipid mixtures, molar fractions were used as weights. The crosses correspond to the spectra calculated as a linear combination of individual components' spectra, multiplied by their molar fraction in the membrane. The lines connecting the points act as a guide to the eye.

cholesterol analogue 6-ketocholestanol.^{69,70} The observed effect was attributed solely to membrane dehydration. While it is plausible that the decrease of the $\text{Im}\chi^{(2)}$ response in the OH stretching region with increasing mole fraction of cholesterol, as observed herein for DOPC and DPPC containing monolayers, may be partially due to membrane dehydration, we consider a reduced orientational preference of the membrane-bound water molecules to be the dominant effect decreasing the water signal. This interpretation is supported by molecular dynamics simulations, which demonstrated a decreased orientational bias of biological water following an increase of the cholesterol content in lipid bilayers composed of PC lipids.^{71,72}

To gain further insight into the effect of cholesterol on interfacial water, we compared the experimental responses of mixed phospholipid/Chol membranes with spectra calculated as a superposition of separate contributions based on their molar fraction in the membrane. The corresponding areas under the curve in two spectral regions (CH and OH stretching) are plotted on the bottom panels of Figure 6 (depicted as black crosses). For a direct visual comparison of the experimentally measured $\text{Im}\chi^{(2)}$ spectrum of the two-component monolayer with the corresponding calculated spectrum, see the Supporting Information. In Figure S3, we provide one exemplary spectral set for each phospholipid.

In the case of DOPC, the measured responses, both from the hydrophobic tails and water, indicate the absence of strong specific interactions between sterol and the unsaturated phospholipid studied (see Figures 6D and S3), consistent with our findings from the carbonyl investigation.

The DPPC/Chol systems show a moderate deviation of the measured response from the hydrophobic tails from the calculated response (13% difference on average). This is likely due to the ordering of phospholipid tails. We also observe that the decrease in the water signal upon adding cholesterol is much less than expected (see Figures 6E and S3). This points at an enhanced orientation of water molecules in the hydration shell of the remaining phospholipid headgroups. We propose that the cholesterol-induced ordering of phospholipid tails entails tighter packing (evidenced also by the cholesterol-induced dehydration of DPPC carbonyl region), resulting in a more vertical and uniform orientation of the lipid terminal methyl groups as well as the headgroups. Collectively, these effects give rise to an increasing signal from oriented water molecules when the Chol concentration increases.

In the case of SM, we observe the highest deviations from the predicted spectra, both in the hydrophobic tails (27% difference on average) and water signals. The amplitude of the OH stretching band does not decline; in fact, it increases slightly (see Figure 6F). It thus appears that in the raft-like SM

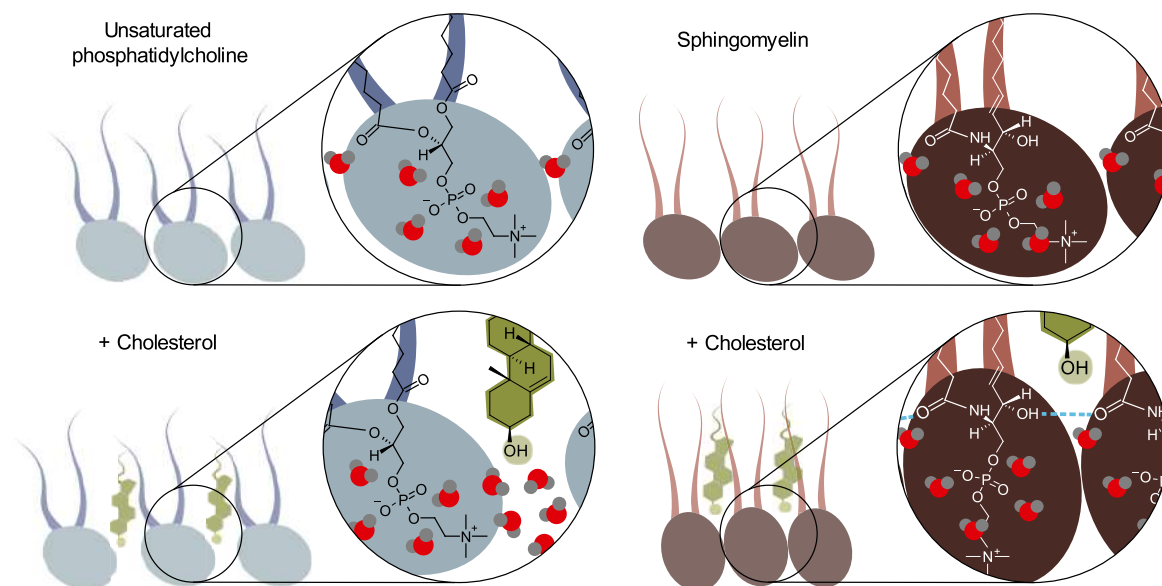


Figure 7. Schematic illustration of the effect of cholesterol on the interlipid interactions and the interfacial water structure. In an unsaturated phosphatidylcholine membrane, cholesterol intercalates into the interfacial region, leading to the protrusion of more bulk-like water molecules between the phosphocholine headgroups. In a sphingomyelin membrane, cholesterol reduces the interlipid distance and facilitates direct intermolecular hydrogen bonding among phospholipids, resulting in the ordering of phosphocholine headgroups and the associated interfacial water molecules.

membrane, the interfacial water remains highly polarized regardless of the cholesterol content. This finding suggests an even more pronounced enhanced packing and a more significant effect of headgroup rearrangement on the orientation of the nearby water molecules, compared to DPPC.

Clearly, our results show that the condensing effect of cholesterol is most pronounced in the case of SM, somewhat weaker in DPPC, and weakest in DOPC systems. In the case of SM, the dilution effect of adding cholesterol appears to be completely absent, which is somewhat unexpected. For glycerophospholipid membranes, the cholesterol hydroxyl group has been recognized to typically reside in the interfacial region of the membrane.^{73–75} For sphingomyelin membranes, the positioning of the sterol OH group might be different. Yasuda et al. demonstrated that the cholesterol-induced lipid tail ordering reaches deeper in the SM membrane when compared to its glycerophospholipid counterpart.⁷⁶ In particular, the rigid fused ring segments of cholesterol were found to be positioned within the central region of the alkyl chains of SM.⁷⁶ The resulting relatively large distance between the hydroxyl group of cholesterol and the amide group of SM would require reorientation of the amide group to enable a direct hydrogen-bonding interaction with the cholesterol hydroxyl group, which was not observed experimentally.⁵¹ Recent experimental studies further hint in this direction, by showing that neither the conformation of the N-linked long acid chain⁵¹ nor the orientation of the carbonyl group⁷⁷ of SM is affected by Chol. These findings suggest that a direct interaction between SM's amide and Chol's hydroxyl group may not exist. Thus, we conclude that the positioning of the Chol's hydroxyl group is well above the SM interfacial region (closer to the hydrophobic core). In this connection, it is important to note that sphingomyelin not only possesses hydrogen-bond acceptor groups but also hydrogen-bond donor

groups (NH and OH) (see the turquoise arrows in Figure 1). Hence, in an SM membrane, intra- and (direct) intermolecular hydrogen-bonding interactions are present, which distinguish it from glycerophospholipid membranes. Owing to the strong condensing effect of cholesterol, the intermolecular van der Waals contacts between SM molecules are maximized, which may also enhance the intermolecular hydrogen-bond network between SM molecules that pushes cholesterol further toward the hydrophobic region of the membrane.⁷⁸ Thus, in addition to the enhanced packing and headgroup ordering, we attribute the nondecreasing water signal to the strong hydrogen-bond network within the SM, which prevents cholesterol from reaching the interfacial region with its hydrophilic hydroxyl group. Instead, cholesterol is anchored deeper in the membrane interior. As a result, the local preferential orientation of interfacial water molecules is preserved even when the SM membrane contains a large fraction of cholesterol.

CONCLUSIONS

We used heterodyne-detected vibrational sum-frequency generation spectroscopy to study the effect of cholesterol on the structure and hydration of monolayers of 1,2-dipalmitoyl-*sn*-glycero-3-phosphocholine (DPPC), 1,2-dioleoyl-*sn*-glycero-3-phosphocholine (DOPC), and egg sphingomyelin (SM) on water. We probed the response of the carbonyl vibrations of the phospholipids, CH vibrations of the phospholipids and cholesterol, and OH vibrations of water molecules hydrating the lipids. We found that the effect of cholesterol strongly depends on the nature of the host zwitterionic phospholipid monolayers.

For the unsaturated phosphatidylcholine DOPC, the responses of the CH and OH vibrations indicate the absence

of strong specific interactions between cholesterol and the unsaturated phospholipid tails. Cholesterol intercalates into the membrane, causing increased separation between adjacent phospholipids. Compared to the cholesterol-free membrane, this results in the decline of the population of oriented water molecules associated with the phospholipid headgroups (see the left side of Figure 7).

For the saturated phosphatidylcholine DPPC, we found that the addition of cholesterol leads to a quite strong increase of the CH signal, which indicates an enhanced ordering of phospholipid tails. We also observe a pronounced relative increase of non-hydrogen-bonded carbonyl groups over hydrogen-bonded carbonyl groups, which indicates that the tighter packing is accompanied by expulsion of part of the water molecules, particularly those located above the headgroup, at the level of the carbonyl groups. We also observe that the decrease in the water signal upon adding cholesterol to the layer is much less than expected from the dilution effect. This points at an enhanced orientation of water molecules in the hydration shell of the remaining phospholipid headgroups. We propose that the cholesterol-induced ordering of phospholipid tails entails tighter packing resulting in a more vertical and uniform orientation of the lipid terminal methyl groups as well as the headgroups.

For SM, we observed an even stronger increase in the response of the CH vibration upon adding cholesterol, indicating an even more pronounced enhanced packing and ordering of the hydrophobic tails than those observed for DPPC. We observe that the amplitude of the OH stretching band does not decrease at all upon adding cholesterol despite the dilution effect of adding cholesterol to the layer. It thus appears that the robust intermolecular hydrogen-bond network of SM anchors cholesterol deeper within the nonpolar membrane interior, limiting its ability to disrupt the orientation of interfacial water molecules. Collectively, the two effects act in tandem to preserve the strong orientational bias of interfacial water molecules in raft-like membranes, even at high cholesterol concentrations (see the right side of Figure 7).

Our findings offer the first experimental evidence that cholesterol influences the alignment of biological water, clearly a phenomenon intricately linked to the membrane's unique composition and the interlipid interactions. The observed strong orientational bias (hence strong membrane dipole potential) in the case of sphingomyelin-rich membranes, even at high cholesterol content conditions, sets sphingomyelin membranes apart from nonraft cell membrane domains and carries potential implications for cellular processes like domain-selective protein binding and membrane fusion events. Membrane dipole potential, originating from the preferential alignment of interfacial water molecules and the anisotropic orientation of lipid dipolar moieties, can reach high values of up to several hundred millivolts,²³ leading to the formation of a strong, local electric field. It is thus of no surprise that such a dipole potential is very effective in modulating the conformation and function of membrane proteins as well as their distribution and binding affinity.^{25,26} It has been shown that the membrane dipole potential is not homogeneous—on the contrary, it is significantly larger in lipid domains enriched in cholesterol, correlating well with the localization of lipid raft markers within the membrane.⁷⁹ Crucially, the spatial heterogeneity of the membrane dipole potential is interwoven with its temporal variation. Recent studies showed strong dependence of the magnitude of the membrane dipole

potential on the stage of the ovary cell (CHO-K1) cycle.⁸⁰ Intriguingly, the measured magnitude of the dipole potential correlated well with the temporal variation of cholesterol in the cell membrane. Our results thus provide a clear molecular-level picture of the origins of composition-specific spatial heterogeneity of the membrane dipole potential, arising from the intricate interactions of cholesterol with membrane lipids and their subsequent effect on the orientational anisotropy of membranes' hydration layer.

This sheds new light on the role of cholesterol in cell membranes' biophysical and biochemical activities and, yet again, manifests the structure–function relationship in lipid membranes. We believe these results lay a strong foundation for future research endeavors, both experimental and computational, to unravel the implications of the interplay between cholesterol and the orientation of membrane-associated water molecules in cellular processes.

■ ASSOCIATED CONTENT

Supporting Information

The Supporting Information is available free of charge at <https://pubs.acs.org/doi/10.1021/jacs.4c00474>.

Exemplary individual $\text{Im}\chi^{(2)}$ spectra of the DOPC–water interface at different lipid surface coverages in the OH stretch vibration region; comparison of the averaged experimentally measured $\text{Im}\chi^{(2)}$ spectra with the calculated ones of SM/Chol monolayers in the C=O stretch vibration region and of DOPC/Chol, DPPC/Chol, and SM/Chol monolayers in the CH and OH stretch vibration regions; description of the origin of the spectral modulation effects; and details of the band assignment in the spectral region 2800–3100 cm^{-1} (PDF)

■ AUTHOR INFORMATION

Corresponding Authors

Hanna Orlikowska-Rzeznik – Faculty of Materials

Engineering and Technical Physics, Poznan University of Technology, 60-965 Poznan, Poland; orcid.org/0000-0003-0697-4781; Email: hanna.orlikowska@put.poznan.pl

Lukasz Piatkowski – Faculty of Materials Engineering and Technical Physics, Poznan University of Technology, 60-965 Poznan, Poland; orcid.org/0000-0002-1226-2257; Email: lukasz.j.piatkowski@put.poznan.pl

Authors

Jan Versluis – AMOLF, Ultrafast Spectroscopy, 1098 XG Amsterdam, The Netherlands

Huib J. Bakker – AMOLF, Ultrafast Spectroscopy, 1098 XG Amsterdam, The Netherlands; orcid.org/0000-0003-1564-5314

Complete contact information is available at: <https://pubs.acs.org/10.1021/jacs.4c00474>

Notes

The authors declare no competing financial interest.

■ ACKNOWLEDGMENTS

This work has been supported by the Polish National Agency for Academic Exchange (NAWA) under the STER programme, Towards Internationalization of Poznan University of Technology Doctoral School (2022–2024). This work was

financed from the budget funds allocated for science in the years 2019–2023 as a research project under the “Diamond Grant” program (decision: 0042/DIA/2019/48). L.P. acknowledges the financial support from the National Science Centre (Poland) 2020/37/B/ST4/01785. H.O.-R. thanks for the experimental and technical support from Alexander A. Korotkevich, Sanghamitra Sengupta, Aswathi Vilangottunjilal, and Hinc Schoenmaker.

REFERENCES

- (1) Cooper, G. M. *The Cell: A Molecular Approach*, Eighth ed.; Sinauer Associates, an imprint of Oxford University Press, 2019.
- (2) Levental, I.; Lyman, E. Regulation of Membrane Protein Structure and Function by Their Lipid Nano-Environment. *Nat. Rev. Mol. Cell Biol.* **2023**, *24*, 107–122.
- (3) Rizo, J. Molecular Mechanisms Underlying Neurotransmitter Release. *Annu. Rev. Biophys.* **2022**, *51*, 377–408.
- (4) Pinke, G.; Zhou, L.; Sazanov, L. A. Cryo-EM Structure of the Entire Mammalian F-Type ATP Synthase. *Nat. Struct. Mol. Biol.* **2020**, *27*, 1077–1085.
- (5) Lu, E.; Cyster, J. G. G-Protein Coupled Receptors and Ligands That Organize Humoral Immune Responses. *Immunol. Rev.* **2019**, *289*, 158–172.
- (6) Sarmiento, M. J.; Llorente, A.; Petan, T.; Khnykin, D.; Popa, I.; Nikolac Perkovic, M.; Konjevod, M.; Jaganjac, M. The Expanding Organelle Lipidomes: Current Knowledge and Challenges. *Cell. Mol. Life Sci.* **2023**, *80* (8), No. 237.
- (7) Paul, B.; Lewinska, M.; Andersen, J. B. Lipid Alterations in Chronic Liver Disease and Liver Cancer. *JHEP Rep.* **2022**, *4* (6), No. 100479.
- (8) Calero, C.; Franzese, G. Membranes with Different Hydration Levels: The Interface between Bound and Unbound Hydration Water. *J. Mol. Liq.* **2019**, *273*, 488–496.
- (9) Zhang, R.; Cross, T. A.; Peng, X.; Fu, R. Surprising Rigidity of Functionally Important Water Molecules Buried in the Lipid Headgroup Region. *J. Am. Chem. Soc.* **2022**, *144* (17), 7881–7888.
- (10) Piatkowski, L.; De Heij, J.; Bakker, H. J. Probing the Distribution of Water Molecules Hydrating Lipid Membranes with Ultrafast Förster Vibrational Energy Transfer. *J. Phys. Chem. B* **2013**, *117* (5), 1367–1377.
- (11) Tielrooij, K. J.; Paparo, D.; Piatkowski, L.; Bakker, H. J.; Bonn, M. Dielectric Relaxation Dynamics of Water in Model Membranes Probed by Terahertz Spectroscopy. *Biophys. J.* **2009**, *97* (9), 2484–2492.
- (12) Wassall, S. R. Pulsed Field Gradient-Spin Echo NMR Studies of Water Diffusion in a Phospholipid Model Membrane. *Biophys. J.* **1996**, *71* (5), 2724–2732.
- (13) Cheng, J. X.; Pautot, S.; Weitz, D. A.; Xie, X. S. Ordering of Water Molecules between Phospholipid Bilayers Visualized by Coherent Anti-Stokes Raman Scattering Microscopy. *Proc. Natl. Acad. Sci. U.S.A.* **2003**, *100* (17), 9826–9830.
- (14) Chen, X.; Hua, W.; Huang, Z.; Allen, H. C. Interfacial Water Structure Associated with Phospholipid Membranes Studied by Phase-Sensitive Vibrational Sum Frequency Generation Spectroscopy. *J. Am. Chem. Soc.* **2010**, *132* (32), 11336–11342.
- (15) Dreier, L. B.; Wolde-Kidan, A.; Bonthuis, D. J.; Netz, R. R.; Backus, E. H. G.; Bonn, M. Unraveling the Origin of the Apparent Charge of Zwitterionic Lipid Layers. *J. Phys. Chem. Lett.* **2019**, *10* (20), 6355–6359.
- (16) Re, S.; Nishima, W.; Tahara, T.; Sugita, Y. Mosaic of Water Orientation Structures at a Neutral Zwitterionic Lipid/Water Interface Revealed by Molecular Dynamics Simulations. *J. Phys. Chem. Lett.* **2014**, *5* (24), 4343–4348.
- (17) Shen, H.; Wu, Z.; Zou, X. Interfacial Water Structure at Zwitterionic Membrane/Water Interface: The Importance of Interactions between Water and Lipid Carbonyl Groups. *ACS Omega* **2020**, *5* (29), 18080–18090.
- (18) Oh, M. I.; Oh, C. I.; Weaver, D. F. Effect of Cholesterol on the Structure of Networked Water at the Surface of a Model Lipid Membrane. *J. Phys. Chem. B* **2020**, *124* (18), 3686–3694.
- (19) Lin, J. H.; Baker, N. A.; Andrew McCammon, J. Bridging Implicit and Explicit Solvent Approaches for Membrane Electrostatics. *Biophys. J.* **2002**, *83* (3), 1374–1379.
- (20) Asawakarn, T.; Cladera, J.; O’Shea, P. Effects of the Membrane Dipole Potential on the Interaction of Saquinavir with Phospholipid Membranes and Plasma Membrane Receptors of Caco-2 Cells. *J. Biol. Chem.* **2001**, *276* (42), 38457–38463.
- (21) Andersen, P. S.; Fuchs, M. Potential Energy Barriers to Ion Transport within Lipid Bilayers. Studies with Tetraphenylborate. *Biophys. J.* **1975**, *15* (8), 795–830.
- (22) Cladera, J.; O’Shea, P.; Hadgraft, J.; Valenta, C. Influence of Molecular Dipoles on Human Skin Permeability: Use of 6-Ketocholestanol to Enhance the Transdermal Delivery of Bacitracin. *J. Pharm. Sci.* **2003**, *92* (5), 1018–1027.
- (23) Zhan, H.; Lazaridis, T. Influence of the Membrane Dipole Potential on Peptide Binding to Lipid Bilayers. *Biophys. Chem.* **2012**, *161*, 1–7.
- (24) Efimova, S. S.; Zakharova, A. A.; Schagina, L. V.; Ostroumova, O. S. Local Anesthetics Affect Gramicidin A Channels via Membrane Electrostatic Potentials. *J. Membr. Biol.* **2016**, *249* (6), 781–787.
- (25) Sarkar, P.; Chattopadhyay, A. Membrane Dipole Potential: An Emerging Approach to Explore Membrane Organization and Function. *J. Phys. Chem. B* **2022**, *126* (24), 4415–4430.
- (26) Kovács, T.; Batta, G.; Hajdu, T.; Szabó, Á.; Váradi, T.; Zákány, F.; Csomós, I.; Szöllosi, J.; Nagy, P. The Dipole Potential Modifies the Clustering and Ligand Binding Affinity of ErbB Proteins and Their Signaling Efficiency. *Sci. Rep.* **2016**, *6* (1), No. 35850.
- (27) Wang, L. Measurements and Implications of the Membrane Dipole Potential. *Annu. Rev. Biochem.* **2012**, *81*, 615–635.
- (28) Cevc, G.; Marsh, D. Hydration of Noncharged Lipid Bilayer Membranes. Theory and Experiments with Phosphatidylethanolamines. *Biophys. J.* **1985**, *47* (1), 21–31.
- (29) Kasson, P. M.; Lindahl, E.; Pande, V. S. Water Ordering at Membrane Interfaces Controls Fusion Dynamics. *J. Am. Chem. Soc.* **2011**, *133* (11), 3812–3815.
- (30) Sardar, A.; Dewangan, N.; Panda, B.; Bhowmick, D.; Tarafdar, P. K. Lipid and Lipidation in Membrane Fusion. *J. Membr. Biol.* **2022**, *255* (6), 691–703.
- (31) Subczynski, W. K.; Pasenkiewicz-Gierula, M.; Widomska, J.; Mainali, L.; Raguz, M. High Cholesterol/Low Cholesterol: Effects in Biological Membranes: A Review. *Cell Biochem. Biophys.* **2017**, *75* (3–4), 369–385.
- (32) Zakany, F.; Kovacs, T.; Panyi, G.; Varga, Z. Direct and Indirect Cholesterol Effects on Membrane Proteins with Special Focus on Potassium Channels. *Biochim. Biophys. Acta, Mol. Cell Biol. Lipids* **2020**, *1865* (8), No. 158706.
- (33) Levental, I.; Levental, K. R.; Heberle, F. A. Lipid Rafts: Controversies Resolved, Mysteries Remain. *Trends Cell Biol.* **2020**, *30* (5), 341–353.
- (34) Kulkarni, R.; Wiemer, E. A. C.; Chang, W. Role of Lipid Rafts in Pathogen-Host Interaction - A Mini Review. *Front. Immunol.* **2022**, *12*, No. 815020.
- (35) Lingwood, D.; Simons, K. Lipid Rafts as a Membrane-Organizing Principle. *Science* **2010**, *327* (5961), 46–50.
- (36) Kucerka, N.; Perlmutter, J. D.; Pan, J.; Tristram-Nagle, S.; Katsaras, J.; Sachs, J. N. The Effect of Cholesterol on Short- and Long-Chain Monounsaturated Lipid Bilayers as Determined by Molecular Dynamics Simulations and X-Ray Scattering. *Biophys. J.* **2008**, *95* (6), 2792–2805.
- (37) Keller, F.; Heuer, A. Chain Ordering of Phospholipids in Membranes Containing Cholesterol: What Matters? *Soft Matter* **2021**, *17* (25), 6098–6108.
- (38) Leftin, A.; Molugu, T. R.; Job, C.; Beyer, K.; Brown, M. F. Area per Lipid and Cholesterol Interactions in Membranes from Separated Local-Field ¹³C NMR Spectroscopy. *Biophys. J.* **2014**, *107* (10), 2274–2286.

- (39) Dahley, C.; Garessus, E. D. G.; Ebert, A.; Goss, K. U. Impact of Cholesterol and Sphingomyelin on Intrinsic Membrane Permeability. *Biochim. Biophys. Acta, Biomembr.* **2022**, *1864* (9), No. 183953.
- (40) Khatibzadeh, N.; Gupta, S.; Farrell, B.; Brownell, W. E.; Anvari, B. Effects of Cholesterol on Nano-Mechanical Properties of the Living Cell Plasma Membrane. *Soft Matter* **2012**, *8* (32), 8350–8360.
- (41) Cheng, C. Y.; Olijve, L. L. C.; Kausik, R.; Han, S. Cholesterol Enhances Surface Water Diffusion of Phospholipid Bilayers. *J. Chem. Phys.* **2014**, *141* (22), No. 22DS13.
- (42) Pyne, S.; Pyne, P.; Mitra, R. K. Addition of Cholesterol Alters the Hydration at the Surface of Model Lipids: A Spectroscopic Investigation. *Phys. Chem. Chem. Phys.* **2022**, *24* (34), 20381–20389.
- (43) Ohto, T.; Backus, E. H. G.; Hsieh, C. S.; Sulpizi, M.; Bonn, M.; Nagata, Y. Lipid Carbonyl Groups Terminate the Hydrogen Bond Network of Membrane-Bound Water. *J. Phys. Chem. Lett.* **2015**, *6* (22), 4499–4503.
- (44) Jurak, M. Surface Gibbs Energy Interaction of Phospholipid/Cholesterol Monolayers Deposited on Mica with Probe Liquids. *Chem. Phys. Lipids* **2014**, *183*, 60–67.
- (45) Ohe, C.; Sasaki, T.; Noi, M.; Goto, Y.; Itoh, K. Sum Frequency Generation Spectroscopic Study of the Condensation Effect of Cholesterol on a Lipid Monolayer. *Anal. Bioanal. Chem.* **2007**, *388* (1), 73–79.
- (46) Shaikh, S. R.; Dumaul, A. C.; Jenki, L. J.; Stillwell, W. Lipid Phase Separation in Phospholipid Bilayers and Monolayers Modeling the Plasma Membrane. *Biochim. Biophys. Acta, Biomembr.* **2001**, *1512* (2), 317–328.
- (47) Moll, C. J.; Versluis, J.; Bakker, H. J. Direct Evidence for a Surface and Bulk Specific Response in the Sum-Frequency Generation Spectrum of the Water Bend Vibration. *Phys. Rev. Lett.* **2021**, *127* (11), No. 116001.
- (48) Moll, C. J. *Bending and Stretching: A Practical Examination of Molecules at Aqueous Interfaces*; University of Amsterdam UvA, Amsterdam, 2022.
- (49) Backus, E. H. G.; Bonn, D.; Cantin, S.; Roke, S.; Bonn, M. Laser-Heating-Induced Displacement of Surfactants on the Water Surface. *J. Phys. Chem. B* **2012**, *116* (9), 2703–2712.
- (50) Miniewicz, A.; Bartkiewicz, S.; Orlikowska, H.; Dradrach, K. Marangoni Effect Visualized in Two-Dimensions Optical Tweezers for Gas Bubbles. *Sci. Rep.* **2016**, *6* (1), No. 34787.
- (51) Li, Y.; Feng, R.; Liu, M.; Guo, Y.; Zhang, Z. Mechanism by Which Cholesterol Induces Sphingomyelin Conformational Changes at an Air/Water Interface. *J. Phys. Chem. B* **2022**, *126* (29), 5481–5489.
- (52) Genova, J.; Petrov, M.; Bivas, I.; Rafailov, P.; Naradikian, H.; Ktranchev, B. Fourier-Transform Infrared and Raman Characterization of Bilayer Membranes of the Phospholipid SOPC and Its Mixtures with Cholesterol. *Colloids Surf., A* **2018**, *557*, 85–93.
- (53) Stevenson, P.; Tokmakoff, A. Ultrafast Fluctuations of High Amplitude Electric Fields in Lipid Membranes. *J. Am. Chem. Soc.* **2017**, *139* (13), 4743–4752.
- (54) Hübner, W.; Blume, A. Interactions at the Lipid–Water Interface. *Chem. Phys. Lipids* **1998**, *96* (1–2), 99–123.
- (55) Dreier, L. B.; Bonn, M.; Backus, E. H. G. Hydration and Orientation of Carbonyl Groups in Oppositely Charged Lipid Monolayers on Water. *J. Phys. Chem. B* **2019**, *123* (5), 1085–1089.
- (56) Yagi, K.; Li, P. C.; Shirota, K.; Kobayashi, T.; Sugita, Y. A Weight Averaged Approach for Predicting Amide Vibrational Bands of a Sphingomyelin Bilayer. *Phys. Chem. Chem. Phys.* **2015**, *17* (43), 29113–29123.
- (57) Mallamace, F.; Corsaro, C.; Mallamace, D.; Vasi, S.; Vasi, C.; Dugo, G. The Role of Water in Protein's Behavior: The Two Dynamical Crossovers Studied by NMR and FTIR Techniques. *Comput. Struct. Biotechnol. J.* **2015**, *13*, 33–37.
- (58) Antila, H. S.; Wurl, A.; Ollila, O. H. S.; Miettinen, M. S.; Ferreira, T. M. Rotational Decoupling between the Hydrophilic and Hydrophobic Regions in Lipid Membranes. *Biophys. J.* **2022**, *121* (1), 68–78.
- (59) Kulig, W.; Jurkiewicz, P.; Olżyńska, A.; Tynkkynen, J.; Javanainen, M.; Manna, M.; Rog, T.; Hof, M.; Vattulainen, I.; Jungwirth, P. Experimental Determination and Computational Interpretation of Biophysical Properties of Lipid Bilayers Enriched by Cholesteryl Hemisuccinate. *Biochim. Biophys. Acta, Biomembr.* **2015**, *1848* (2), 422–432.
- (60) Fritzsching, K. J.; Kim, J.; Holland, G. P. Probing Lipid-Cholesterol Interactions in DOPC/ESM/Chol and DOPC/DPPC/Chol Model Lipid Rafts with DSC and ¹³C Solid-State NMR. *Biochim. Biophys. Acta, Biomembr.* **2013**, *1828* (8), 1889–1898.
- (61) Singh, P. C.; Ahmed, M.; Nihonyanagi, S.; Yamaguchi, S.; Tahara, T. DNA-Induced Reorganization of Water at Model Membrane Interfaces Investigated by Heterodyne-Detected Vibrational Sum Frequency Generation Spectroscopy. *J. Phys. Chem. B* **2022**, *126* (4), 840–846.
- (62) Nojima, Y.; Yamaguchi, S. Heterodyne-Detected Sum Frequency Generation Spectroscopic Study of Weakly Hydrogen-Bonded Water at Charged Lipid Interfaces, Revisited. *J. Phys. Chem. C* **2021**, *125* (42), 23483–23489.
- (63) Nojima, Y.; Suzuki, Y.; Yamaguchi, S. Weakly Hydrogen-Bonded Water Inside Charged Lipid Monolayer Observed with Heterodyne-Detected Vibrational Sum Frequency Generation Spectroscopy. *J. Phys. Chem. C* **2017**, *121* (4), 2173–2180.
- (64) Ohno, P. E.; Wang, H. F.; Geiger, F. M. Second-Order Spectral Lineshapes from Charged Interfaces. *Nat. Commun.* **2017**, *8* (1), No. 1032.
- (65) Miñones, J., Jr.; Pais, S.; Miñones, J.; Conde, O.; Dynarowicz-Łatka, P. Interactions between Membrane Sterols and Phospholipids in Model Mammalian and Fungi Cellular Membranes - A Langmuir Monolayer Study. *Biophys. Chem.* **2009**, *140* (1–3), 69–77.
- (66) Mondal, J. A.; Nihonyanagi, S.; Yamaguchi, S.; Tahara, T. Structure and Orientation of Water at Charged Lipid Monolayer/Water Interfaces Probed by Heterodyne-Detected Vibrational Sum Frequency Generation Spectroscopy. *J. Am. Chem. Soc.* **2010**, *132* (31), 10656–10657.
- (67) Mondal, J. A.; Nihonyanagi, S.; Yamaguchi, S.; Tahara, T. Three Distinct Water Structures at a Zwitterionic Lipid/Water Interface Revealed by Heterodyne-Detected Vibrational Sum Frequency Generation. *J. Am. Chem. Soc.* **2012**, *134* (18), 7842–7850.
- (68) Saak, C.-M.; Dreier, L. B.; Machel, K.; Bonn, M.; G Backus, E. H. Biological Lipid Hydration: Distinct Mechanisms of Interfacial Water Alignment and Charge Screening for Model Lipid Membranes. *Faraday Discuss.* **2024**, *249*, 317–333.
- (69) Ma, S.; Li, H.; Tian, K.; Ye, S.; Luo, Y. In Situ and Real-Time Sfg Measurements Revealing Organization and Transport of Cholesterol Analogue 6-Ketocholestanol in a Cell Membrane. *J. Phys. Chem. Lett.* **2014**, *5* (3), 419–424.
- (70) Ma, S.; Tian, K.; Ye, S. The Dehydration Dynamics of a Model Cell Membrane Induced by Cholesterol Analogue 6-Ketocholestanol Investigated Using Sum Frequency Generation Vibrational Spectroscopy. *Sci. China: Chem.* **2015**, *58* (7), 1176–1186.
- (71) Magarkar, A.; Dhawan, V.; Kallinteri, P.; Viitala, T.; Elmowafy, M.; Róg, T.; Bunker, A. Cholesterol Level Affects Surface Charge of Lipid Membranes in Saline Solution. *Sci. Rep.* **2014**, *4* (1), No. 5005.
- (72) Elola, M. D.; Rodriguez, J. Influence of Cholesterol on the Dynamics of Hydration in Phospholipid Bilayers. *J. Phys. Chem. B* **2018**, *122* (22), 5897–5907.
- (73) Léonard, A.; Escribe, C.; Laguerre, M.; Pebay-Peyroula, E.; Néri, W.; Pott, T.; Katsaras, J.; Dufourc, E. J. Location of Cholesterol in DMPC Membranes. A Comparative Study by Neutron Diffraction and Molecular Mechanics Simulation. *Langmuir* **2001**, *17* (6), 2019–2030.
- (74) Ermilova, I.; Lyubartsev, A. P. Cholesterol in Phospholipid Bilayers: Positions and Orientations inside Membranes with Different Unsaturation Degrees. *Soft Matter* **2019**, *15* (1), 78–93.
- (75) Gater, D. L.; Réat, V.; Czaplicki, G.; Saurel, O.; Milon, A.; Jolibois, F.; Cherezov, V. Hydrogen Bonding of Cholesterol in the Lipidic Cubic Phase. *Langmuir* **2013**, *29* (25), 8031–8038.

(76) Yasuda, T.; Kinoshita, M.; Murata, M.; Matsumori, N. Detailed Comparison of Deuterium Quadrupole Profiles between Sphingomyelin and Phosphatidylcholine Bilayers. *Biophys. J.* **2014**, *106* (3), 631–638.

(77) Matsumori, N.; Yamaguchi, T.; Maeta, Y.; Murata, M. Orientation and Order of the Amide Group of Sphingomyelin in Bilayers Determined by Solid-State NMR. *Biophys. J.* **2015**, *108* (12), 2816–2824.

(78) Matsumori, N.; Yasuda, T.; Okazaki, H.; Suzuki, T.; Yamaguchi, T.; Tsuchikawa, H.; Doi, M.; Oishi, T.; Murata, M. Comprehensive Molecular Motion Capture for Sphingomyelin by Site-Specific Deuterium Labeling. *Biochemistry* **2012**, *51* (42), 8363–8370.

(79) Kovács, T.; Batta, G.; Zákány, F.; Szöllösi, J.; Nagy, P. The Dipole Potential Correlates with Lipid Raft Markers in the Plasma Membrane of Living Cells. *J. Lipid Res.* **2017**, *58* (8), 1681–1691.

(80) Sarkar, P.; Rao, B. D.; Chattopadhyay, A. Cell Cycle Dependent Modulation of Membrane Dipole Potential and Neurotransmitter Receptor Activity: Role of Membrane Cholesterol. *ACS Chem. Neurosci.* **2020**, *11* (18), 2890–2899.

Supporting Information for

Cholesterol Changes Interfacial Water Alignment in Model Cell Membranes

Hanna Orlikowska-Rzeznik,^{1*} Jan Versluis,² Huib J. Bakker,² and Lukasz Piatkowski^{1*}

¹Faculty of Materials Engineering and Technical Physics, Poznan University of Technology, Piotrowo 3, Poznan, Poland

²AMOLF, Ultrafast Spectroscopy, Science Park 104, Amsterdam, The Netherlands

Correspondence: hanna.orlikowska@put.poznan.pl (H. Orlikowska-Rzeznik); lukasz.j.piatkowski@put.poznan.pl
(L. Piatkowski)

Table of Content:

Supplementary Figures S1–S3

Supplementary Notes S1–S2

Supplementary Figures S1–S3

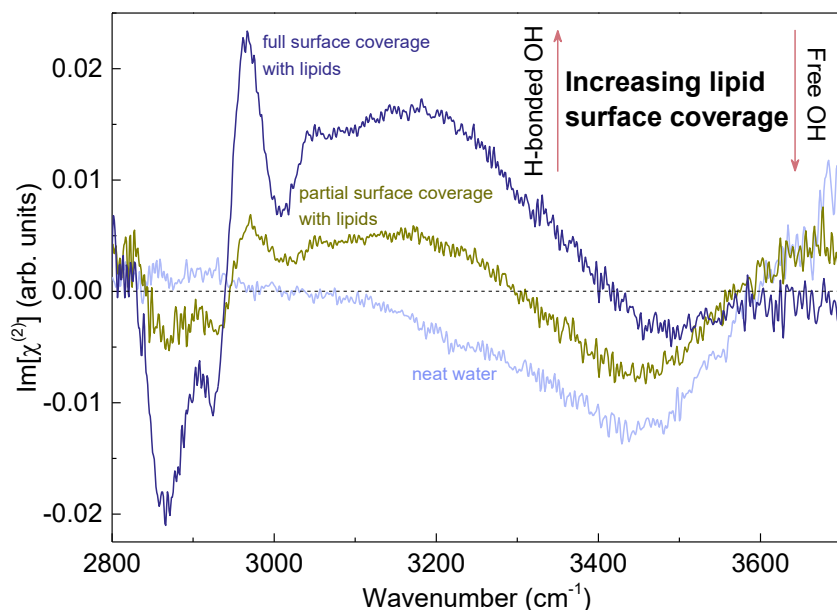


Figure S1. The exemplary $\text{Im}[\chi^{(2)}]$ spectra of neat water and the DOPC-water interface at partial and full lipid surface coverage in the CH and OH stretching vibration region. The chosen (complete) lipid surface coverage corresponds to a surface pressure of around 40 mN/m.

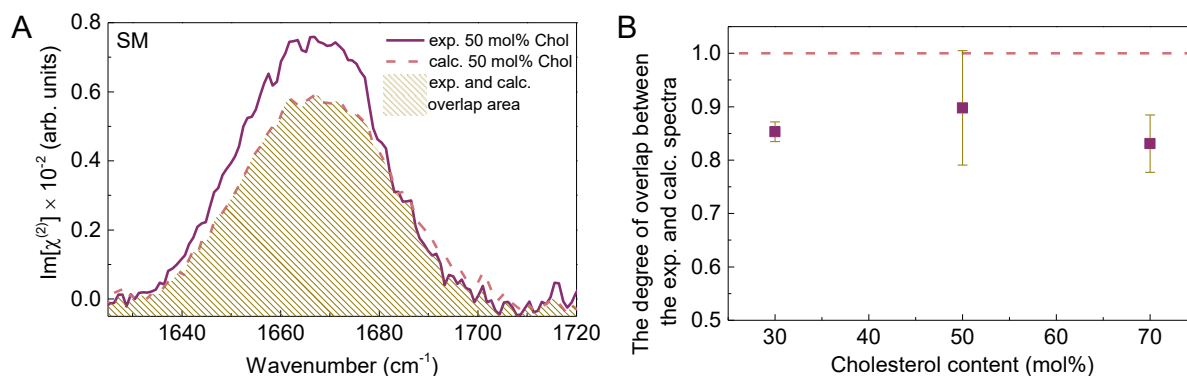


Figure S2. (A) Comparison of averaged experimentally measured $\text{Im}[\chi^{(2)}]$ spectrum with the calculated spectrum for a mixed SM/Chol monolayer at cholesterol molar fraction of 0.5 in the carbonyl stretch vibration region. The calculated spectrum results from a linear combination of separate contributions from pure SM and Chol monolayers at ratios equal to molar fractions of lipids, using averaged spectra of the pure lipids. (B) Mean ratio of the overlap area between individual experimental spectra and their corresponding calculated spectra.

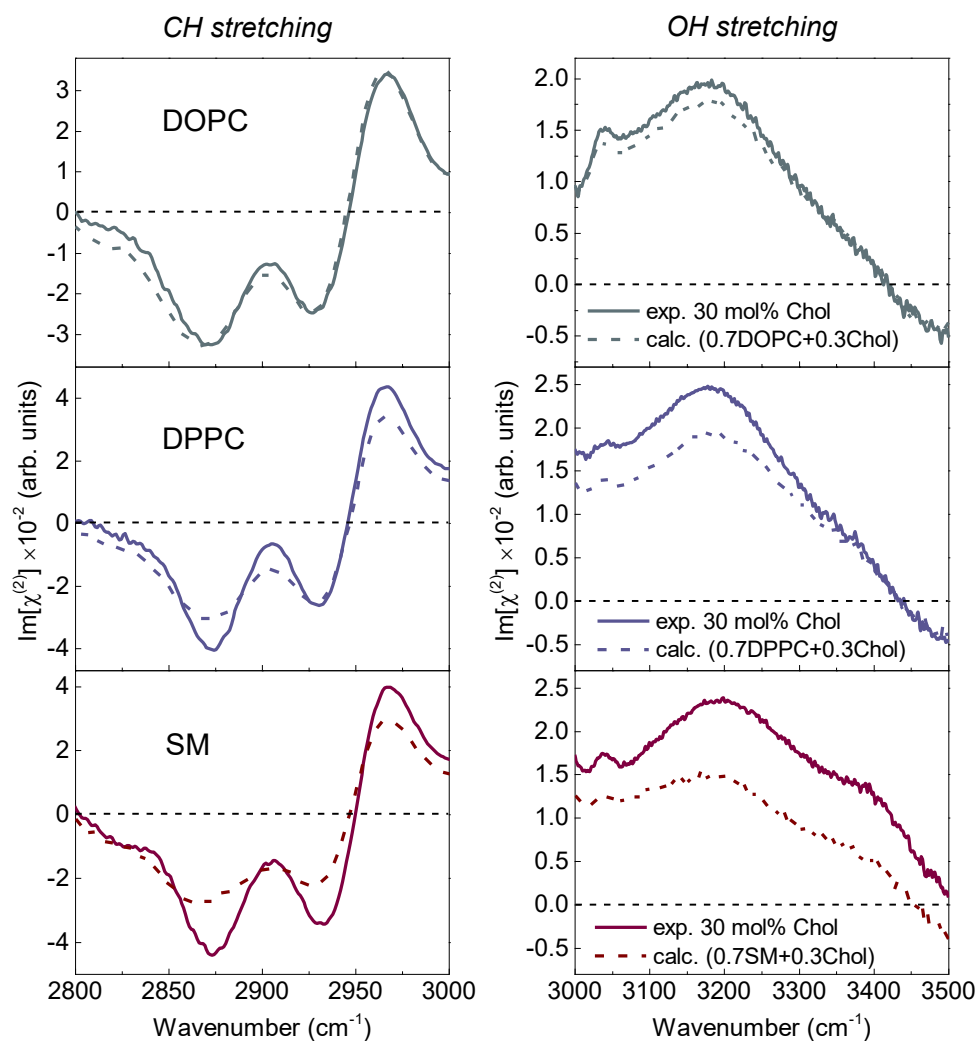


Figure S3. Comparison of the experimentally measured $\text{Im}[\chi^{(2)}]$ spectra of DOPC/Chol, DPPC/Chol, and SM/Chol monolayers at cholesterol molar fraction of 0.3 in the CH (left panels) and OH (right panels) stretch vibration regions with the corresponding calculated spectra as a linear combination of the separate contributions from pure components at their molar fraction. Experimental curves represent the mean spectra. For calculation, the mean spectra of pure DOPC(DPPC) and Chol were used.

Supplementary Notes S1–S2

Note S1

The measured VSG signal is affected by spectral modulation effects resulting from the etaloning effect in a CCD camera. This effect, caused by light waves passing through the camera and reflecting off the camera rear surface, creates interference patterns that degrade the performance of thinned, back-illuminated CCD cameras. Despite advancements in camera technology aimed at reducing this effect and enhancing data quality, complete elimination remains challenging. The etaloning signal mixes with the heterodyne VSG signal and cannot be removed by traditional post-processing methods. The correction procedure with the two quartz orientations largely removes the etaloning effect, thereby strongly enhancing the data quality, particularly in the 6 μm spectral region ($\sim 1600\text{ cm}^{-1}$).^{1,2}

Note S2

For all studied phospholipids (DOPC, DPPC, SM), the $\text{Im}\chi^{(2)}$ spectrum of the lipid membrane in the CH stretching region exhibits the features arising from the vibrations of methyl groups terminating the hydrophobic chains: a negative double-peak feature with maxima at ca. 2870 and 2930 cm^{-1} , assigned to the CH_3 symmetric stretching and the Fermi resonance with its bend overtone, respectively, and a positive band at 2970 cm^{-1} , attributed to the CH_3 asymmetric stretching. The lack of clearly visible signatures from methylene groups (CH_2) is indicative of a well-packed lipid monolayer without isolated gauche defects ($\sim 2820\text{ cm}^{-1}$).³ The region between 3000 and 3080 cm^{-1} covers the vinyl CH stretching vibration from the double bonds in the acyl chains (present only in the case of DOPC).^{4,5} Additionally, it presumably includes the stretching vibrations of the methyl groups on the choline moiety ($\text{N}(\text{CH}_3)_3^+$) weakly interacting with water molecules.⁶ In the Chol spectrum, at around 3040 cm^{-1} , a peak can also be distinguished, which most likely originates from the olefinic CH stretching of the double bond structure ($\text{C}=\text{C}-\text{H}$) in the steroid ring structure.⁷

References

- (1) Moll, C. J.; Versluis, J.; Bakker, H. J. Direct Evidence for a Surface and Bulk Specific Response in the Sum-Frequency Generation Spectrum of the Water Bend Vibration. *Phys. Rev. Lett.* **2021**, *127* (11), 116001.
- (2) Moll, C. J. Bending and Stretching: A Practical Examination of Molecules at Aqueous Interfaces, University of Amsterdam UvA, Amsterdam, 2022.
- (3) Backus, E. H. G.; Bonn, D.; Cantin, S.; Roke, S.; Bonn, M. Laser-Heating-Induced Displacement of Surfactants on the Water Surface. *J. Phys. Chem. B* **2012**, *116* (9), 2703–2712.
- (4) Liljeblad, J. F. D.; Bulone, V.; Tyrode, E.; Rutland, M. W.; Johnson, C. M. Phospholipid Monolayers Probed by Vibrational Sum Frequency Spectroscopy: Instability of Unsaturated Phospholipids. *Biophys. J.* **2010**, *98* (10), L50–L52.
- (5) Maltseva, D.; Gonella, G.; Ruysschaert, J. M.; Bonn, M. Phospholipid Acyl Tail Affects Lipid Headgroup Orientation and Membrane Hydration. *J. Chem. Phys.* **2022**, *156* (23), 234706.
- (6) Genova, J.; Petrov, M.; Bivas, I.; Rafailov, P.; Naradikian, H.; Katranchev, B. Fourier-Transform Infrared and Raman Characterization of Bilayer Membranes of the Phospholipid SOPC and Its Mixtures with Cholesterol. *Colloids Surfaces A Physicochem. Eng. Asp.* **2018**, *557*, 85–93.
- (7) Kodali, D. R.; Small, D. M.; Powell, J.; Krishnan, K. Infrared Micro-Imaging of Atherosclerotic Arteries. *Appl. Spectrosc.* **1991**, *45* (8), 1310–1317.

9

Summary

Biological cell membranes are intricate structures, shaped by interactions among diverse membrane constituents and surrounding water. Biomembranes are widely recognized for their structural and dynamical heterogeneity, evident in both the lipid phase and interfacial water. Despite the fundamental role of cholesterol in regulating the membrane's physicochemical properties, its impact on the interactions between various membrane lipids and their hydration layer has remained elusive. The wide range of molecular species in the membrane, their uneven distribution, and the varying concentrations of lipids and cholesterol, along with the heterogeneity of membrane hydration, underscore their importance for cellular biochemical activity. Thus, unraveling the intricate cholesterol-lipid-water interactions at the molecular level is crucial for understanding the physics and chemistry of life.

To study membrane heterogeneity, researchers commonly use fluorescent environmentally sensitive probes, with Laurdan being the most frequently employed. Any shift in the Laurdan's emission spectrum has been taken as a consequence of alterations in the number and/or mobility of water molecules near the probe's fluorescent moiety. Despite its routine use in cell membrane research for over four decades, the interpretation of data obtained using Laurdan has frequently been incorrect due to lack of direct measures of the effect of membrane hydration levels on Laurdan spectra.

For the first time, I investigated the spectral response of Laurdan to the dehydration of biomimetic cell membranes, directly compared it with the effect of increasing cholesterol content, and elucidated the molecular mechanisms that govern the observed changes. These results, published in the article Orlikowska-Rzeznik et al. *J. Phys. Chem. B* 2023, 127(15), are presented in Chapter 5 of this thesis. I monitored the fluorescence spectrum of Laurdan embedded in solid-supported lipid bilayers as a function of membrane hydration state and confronted them with the spectral changes induced by varying cholesterol content, a major membrane fluidity regulator. This approach allowed me to disentangle the effects of these two stimuli on Laurdan's fluorescence spectral properties. I demonstrated that dehydration-induced changes in Laurdan's emission spectrum involve lipid conformational ordering, hindrance of lipid internal motions, and the slowdown of hydrogen bond network dynamics, collectively impeding dipolar relaxation around the probe's excited state dipole. In contrast, cholesterol incorporation affects the emission mainly by hampering the dynamics of the lipid glycerol backbone and the associated carbonyls. This methodology can be applied to further investigate the molecular mechanisms governing

spectral changes in other environmentally sensitive fluorescent probes. Additionally, by monitoring Laurdan's fluorescence, I discovered that upon perturbation of the interfacial hydration layer, cholesterol undergoes a redistribution within phase-separated lipid membrane between lateral domains, counteracting dehydration-induced extensive changes in fluidity of non-raft membrane regions.

The detailed study of the dehydration-induced intramembranous cholesterol redistribution phenomenon, reported in the article *Orlikowska-Rzeznik et al. J. Phys. Chem. Lett. 2024, 15(16)*, is presented in Chapter 6. Using fluorescence microscopy, I probed cholesterol distribution in the cell membrane under different hydration conditions. I quantified the effect, finding that the affinity for a particular lipid phase (raft-like L_o vs non-raft L_d) reverses as membrane hydration decreases from about 12 to 6 water molecules per lipid. Interestingly, the overall architecture of the membrane, reflected in the size, distribution, and density of L_o phase domains, remains unchanged, implying that cholesterol migration solely reflects its affinity for a specific phase. Complemented by atomistic molecular dynamics simulations, the observations reveal that membrane dehydration causes lipid tails of the L_d phase to straighten, leading to an overall thickening of the L_d phase. This reduces the hydrophobic mismatch between L_o and L_d phases and aligns lipid packing in both phases, facilitating favorable cholesterol interactions with L_d phase lipids. Additionally, dehydration causes phosphocholine (PC) lipids to lose more hydrogen bonds than L_o phase-forming sphingomyelin, prompting cholesterol migration to the L_d phase, where it forms hydrogen bonds with PC lipids, increasing their coordination number.

In the article *Orlikowska-Rzeznik et al. J. Am. Chem. Soc. 2024, 146(19)*, presented in Chapter 7, I report the first direct evidence that cholesterol, by modulating biomimetic cell membrane inter-lipid interactions, alters membrane interfacial water structure. Using broad-band heterodyne-detected sum frequency generation spectroscopy, I probed the vibrational signatures of both lipids and water molecules. This advanced nonlinear optical spectroscopy, which is surface-specific and provides information about the absolute orientation of molecular moieties relative to the interface, revealed that in membranes made from unsaturated phosphatidylcholines (DOPC), cholesterol disrupts the interheadgroup hydration shell, depolarizing water molecules' orientation. In saturated phosphatidylcholines (DPPC) membranes, cholesterol's specific interactions with DPPC lipids increase lipid packing and order lipid headgroups, the so-called condensing effect, limiting the random orientation of membrane-associated water molecules. In sphingomyelin (SM) monolayers, the cholesterol-induced condensing effect is most pronounced, maintaining or even slightly increasing the anisotropic orientation of interfacial water molecules at elevated cholesterol content.

The results of the experimental work presented throughout the thesis unravels the new facets of cholesterol in lipid membranes. First of all, I showed that the affinity of cholesterol towards specific lipid environment is sensitive to the hydration properties of the membrane. This likely provides a regulatory mechanism to prevent excessive fluidity fluctuations that could destabilize the cell membrane and harm the cell. Such behaviour of cholesterol has never been observed before, as studies of lipid membranes under different hydration conditions have remained elusive. The change in cholesterol partitioning is very pronounced even at mild dehydration, a scenario reminiscent of biologically relevant states found in a wide palette of processes, including macromolecule adsorption and all events in which membrane fusion plays a central role. Furthermore, in the thesis, I revealed the important and unique role of cholesterol in modulating the structure of biological water. While the cholesterol-induced condensation effect has been previously extensively studied in the lipid context, I shed light on membrane condensation from the perspective of

interfacial water molecules. This phenomenon is clearly dependent on membrane composition, and as such, it contributes to the spatial, structural heterogeneity, and the dipole potential of the membrane-water interface. Enhanced membrane dipole potential, a property key in ion channels' activity, protein binding, and aggregation, was observed to correlate with membrane cholesterol content and phase separation within the membrane (the abundance of raft-like domains, rich in SM and cholesterol). Thus, my results provide a clear molecular picture of the origin of the composition-specific spatial heterogeneity of the net orientation of molecular moieties at the lipid-water interface. Furthermore, the structure of biological water was theoretically predicted to control membrane fusion dynamics by prior studies. As such, the ordering of interfacial water molecules has potential impact on all processes in which membrane fusion plays a key role.

Overall, my results highlight the intricate role of cholesterol-lipid-water interplay in shaping the architectural and functional heterogeneities in cellular membranes. These studies are particularly insightful for understanding fundamental cellular processes involving membrane fusion, such as neurotransmission, fertilization, exocytosis, intracellular transport, and entry of certain viruses (e.g. HIV, SARS-CoV-2, influenza virus).

10

Scientific achievements

10.1 Education

1. **10.2019 – 09.2024** PhD studies in **Materials Engineering** discipline, Doctoral School of Poznan University of Technology, Poznan University of Technology, Poland.
2. **03.2018 – 06.2019** Master of Science (M.Sc.) in **Technical Physics**, specialization: **Nanotechnology and Functional Materials**, Faculty of Technical Physics, Poznan University of Technology, Poland.
3. **10.2014 – 02.2018** Engineering Studies (B.Eng.) in **Biomedical Engineering**, specialization: **Biomedical Optics**, Faculty of Fundamental Problems of Technology, Wroclaw University of Science and Technology, Poland.

10.2 Internships

1. **09.2022 – 12.2022** (3 months) AMOLF Institute, Ultrafast Spectroscopy, Amsterdam, The Netherlands, group of Prof. Huib. J. Bakker.
Research internship
2. **07.2017 – 08.2017** (2 months) Military Institute of Engineer Technology, Wroclaw, Poland, supervisor: Dr. Krzysztof Bogdanowicz
Student internship
3. **01.2016 – 09.2018** (>2 years) Instrumental Analysis Laboratory, Advanced Materials Engineering and Modelling Group, Faculty of Chemistry, Wroclaw University of Technology, Wroclaw, Poland, supervisor: Prof. Dr. habil. Eng. Stanisław Bartkiewicz.
Student research assistant (full time)

10.3 Publications

1. **H. Orlikowska-Rzeznik***, J. Versluis, H. J. Bakker, L. Piatkowski*. Cholesterol Changes Interfacial Water Alignment in Model Cell Membranes. *Journal of the American Chemical Society* **146**(19), 13151–13162 (2024).
doi: 10.1021/jacs.4c00474. **IF = 15.0**.
2. **H. Orlikowska-Rzeznik***, E. Krok, M. Domanska, P. Setny, A. Lagowska, M. Chattopadhyay, L. Piatkowski*. Dehydration of Lipid Membrane Drives Redistribution of Cholesterol Between Lateral Domains. *The Journal of Physical Chemistry Letters* **15**(16), 4515–4522 (2024).
doi: 10.1021/acs.jpcclett.4c00332. **IF = 5.7**.
3. E. Krok*, H. G. Franquelim, M. Chattopadhyay, **H. Orlikowska-Rzeznik**, P. Schwille, L. Piatkowski*. Nanoscale Structural Response of Biomimetic Cell Membranes to Controlled Dehydration. *Nanoscale* **16**(1), 72–84 (2023).
doi: 10.1039/D3NR03078D. **IF = 6.7**.
4. **H. Orlikowska-Rzeznik***, E. Krok, M. Chattopadhyay, A. Lester, L. Piatkowski*. Laurdan Discerns Lipid Membrane Hydration and Cholesterol Content. *The Journal of Physical Chemistry B* **127**(15), 3382–3391 (2023).
doi: 10.1021/acs.jpcc.3c00654. **IF = 3.5**.
5. M. Chattopadhyay*, E. Krok, **H. Orlikowska-Rzeznik**, L. Piatkowski*. Cooperativity Between Sodium Ions and Water Molecules Facilitates Lipid Mobility in Model Cell Membranes. *Chemical Science* **14**(15), 4002–4011 (2023).
doi: 10.1039/D2SC06836B. **IF = 8.4**.
6. E. Krok*, A. Batura, M. Chattopadhyay, **H. Orlikowska**, L. Piatkowski*. Lateral Organization of Biomimetic Cell Membranes in Varying pH Conditions. *Journal of Molecular Liquids* **345**, 117907 (2022).
doi: 10.1016/j.molliq.2021.117907. **IF = 6.0**.
7. M. Chattopadhyay*, E. Krok, **H. Orlikowska**, L. Piatkowski*. Sensing Hydration of Biomimetic Cell Membranes. *Biosensors* **11**(7), 241 (2021).
doi: 10.3390/bios11070241. **IF = 5.743**.
8. M. Chattopadhyay*, E. Krok, **H. Orlikowska**, P. Schwille, H. G. Franquelim, L. Piatkowski*. Hydration Layer of Only a Few Molecules Controls Lipid Mobility in Biomimetic Membranes. *Journal of the American Chemical Society* **143**(36), 14551–14562 (2021).
doi: 10.1021/jacs.1c04314. **IF = 16.383**.
9. **H. Orlikowska***, L. Piatkowski. Modulation Transfer Microscopy – A Versatile Tool for Ultrafast Nanoscopy. *Acta Physica Polonica A* **139**(3), 288–299 (2021).
doi: 10.12693/APhysPolA.139.288. **IF = 0.725**.
10. **H. Orlikowska***, A. Sobolewska, S. Bartkiewicz. Light-Responsive Surfactants: Photochromic Properties of Water-Soluble Azobenzene Derivatives. *Journal of Molecular*

- Liquids* **316**, 113842 (2020).
doi: 10.1016/j.molliq.2020.113842. **IF** = **6.165**.
11. K. Bujak, **H. Orlikowska**, A. Sobolewska, E. Schab-Balcerzak, H. Janeczek, S. Bartkiewicz, J. Konieczkowska*. Azobenzene vs Azopyridine and Matrix Molar Masses Effect on Photoinduced Phenomena. *European Polymer Journal* **115**, 173–184 (2019).
doi: 10.1016/j.eurpolymj.2019.03.028. **IF** = **3.862**.
12. K. Bujak, **H. Orlikowska**, J. G. Małecki, E. Schab-Balcerzak, S. Bartkiewicz, J. Bogucki, A. Sobolewska, J. Konieczkowska*. Fast Dark Cis-Trans Isomerization of Azopyridine Derivatives in Comparison to Their Azobenzene Analogues: Experimental and Computational Study. *Dyes and Pigments* **160**, 654–662 (2019).
doi: 10.1016/j.dyepig.2018.09.006. **IF** = **4.613**.
13. A. Miniewicz, **H. Orlikowska**, A. Sobolewska*, S. Bartkiewicz. Kinetics of Thermal Cis–Trans Isomerization in Phototropic Azobenzene-Based Single–Component Liquid Crystal in Its Nematic and Isotropic Phases. *Physical Chemistry Chemical Physics* **20**(4), 2904–2913 (2018).
doi: 10.1039/c7cp06820d. **IF** = **3.567**.
14. A. Miniewicz*, C. Quintard, **H. Orlikowska**, S. Bartkiewicz. On the Origin of the Driving Force in the Marangoni Propelled Gas Bubble Trapping Mechanism. *Physical Chemistry Chemical Physics* **19**(28), 18695–18703 (2017).
doi: 10.1039/c7cp01986f. **IF** = **3.906**.
15. **H. Orlikowska**, A. Sobolewska*, A. Miniewicz, S. Bartkiewicz. Application of the Novel Dynamic Thermo-Optical Analysis for Identification of the Sequence of Mesophases in Thermotropic Liquid Crystal. *Liquid Crystals* **44**(7), 1157–1164 (2017).
doi: 10.1080/02678292.2016.1269371. **IF** = **2.636**.
16. A. Miniewicz*, S. Bartkiewicz, **H. Orlikowska**, K. Dradrach. Marangoni Effect Visualized in Two Dimensions: Optical Tweezers for Gas Bubbles. *Scientific Reports* **6**(1), 34787 (2016).
doi: 10.1038/srep34787. **IF** = **4.259**.
17. **H. Orlikowska**, S. Bartkiewicz*. Efektywna metoda rozpoznawania faz ciekłokrystalicznych. *Aparatura Badawcza i Dydaktyczna* **21**(3), 135-140 (2016).
<https://bibliotekanauki.pl/articles/271314.pdf>
18. **H. Orlikowska***. O konwersji światła na energię mechaniczną. In: *Badania i Rozwój Młodych Naukowców w Polsce Nauki techniczne i inżynieryjne, part IV*, Wydawnictwo Młodzi Naukowcy, Poznań, ISBN 978-83-65362-48-3, pp. 63–70 (2017). Chapter in the monograph.

*corresponding author(s)

Total impact factor: **97.159**, h-index: **8**, citations: **227** (self-citations excluded)

10.4 Published, indexed conference materials

1. E. H. G. Backus, G. B. Ari, S. Benaglia, (...), **H. Orlikowska-Rzeznik**, (...), J. Yu. Soft matter–water interface: general discussion. *Faraday Discussions* **249**, 485-520 (2024). doi: 10.1039/d3fd90066e. **IF = 3.4**.
2. X. R. Advincula, E. H. G. Backus, M. Bonn, (...), **H. Orlikowska-Rzeznik**, (...), P. Zhang. Electrified/charged aqueous interfaces: general discussion. *Faraday Discussions* **249**, 381-407 (2024). doi: 10.1039/d3fd90065g. **IF = 3.4**.
3. **H. Orlikowska-Rzeznik**, J. Versluis, H. J. Bakker, L. Piatkowski. Cholesterol’s role in cell membranes is even more multifaceted. *European Biophysics Journal* **52** (Suppl 1):S1–S220, P-429 (2023), conference proceedings. doi: 10.1007/s00249-023-01668-7. **IF = 2.0**.
4. L. Piatkowski, M. Chattopadhyay, E. Krok, **H. Orlikowska-Rzeznik**, P. Schwille, H. G. Franquelim. Lipid-water-ion interactions determine cell membrane structure and dynamics. *European Biophysics Journal* **52** (Suppl 1):S1–S220, O-140 Short talk (2023), conference proceedings. doi: 10.1007/s00249-023-01668-7. **IF = 2.0**.
5. M. Chattopadhyay, E. Krok, **H. Orlikowska-Rzeznik**, L. Piatkowski. Cooperative effort of sodium ions and water molecules facilitates lipid mobility in model cell membranes. *European Biophysics Journal* **52** (Suppl 1):S1–S220, P-331 (2023), conference proceedings. doi: 10.1007/s00249-023-01668-7. **IF = 2.0**.
6. E. Krok, M. Chattopadhyay, **H. Orlikowska-Rzeznik**, H. G. Franquelim, P. Schwille, L. Piatkowski. Impact of water scarcity conditions on the nanoscale structural arrangement of biomimetic cell membranes. *European Biophysics Journal* **52** (Suppl 1):S1–S220, P-395 (2023), conference proceedings. doi: 10.1007/s00249-023-01668-7. **IF = 2.0**.
7. **H. Orlikowska-Rzeznik**, E. Krok, M. Chattopadhyay, A. Lester, L. Piatkowski. Direct effect of biomimetic cell membrane hydration on Laurdan fluorescence. *FEBS Open Bio* **12**, 269, P-04.2-007 (2022), conference proceedings. doi: 10.1002/2211-5463.13440. **IF = 2.6**.
8. E. Krok, M. Chattopadhyay, **H. Orlikowska-Rzeznik**, L. Piatkowski. Decreased hydration causes nanoscale structural rearrangement within biomimetic cell membranes. *FEBS Open Bio* **12**, 27, ShT-04.2-1 (2022), conference proceedings. doi: 10.1002/2211-5463.13442. **IF = 2.6**.
9. L. Piatkowski, M. Chattopadhyay, E. Krok, **H. Orlikowska-Rzeznik**, A. Lester. How the absence of just a few water molecules affects the structure and dynamics of cell membranes. *FEBS Open Bio* **12**, 268, P-04.2-005 (2022), conference proceedings. doi: 10.1002/2211-5463.13440. **IF = 2.6**.
10. M. Chattopadhyay, E. Krok, **H. Orlikowska-Rzeznik**, L. Piatkowski. Sodium ions support lipid mobility in dehydrated biomembranes. *FEBS Open Bio* **12**, 270, P-04.2-009 (2022), conference proceedings. doi: 10.1002/2211-5463.13440. **IF = 2.6**.

10.5 Participation in conferences

Presented talks:

1. **H. Orlikowska-Rzeźnik**, E. Krok, M. Domanska, P. Setny, A. Łągowska, M. Chattopadhyay, L. Piatkowski, Rola cholesterolu i tratw lipidowych w procesie fuzji błonowej, *XXIX Lubelskie Warsztaty Biofizyczne*, 23-24.05.2024, Kazimierz Dolny, Poland.
2. **H. Orlikowska-Rzeźnik**, E. Krok, M. Chattopadhyay, A. Lester, Ł. Piątkowski, Widmo fluorescencji Laurdanu w biomimetycznej błonie lipidowej: wpływ cholesterolu i stopnia nawodnienia błony, *XXVII Lubelskie Warsztaty Biofizyczne*, 26-27.05.2022, Kazimierz Dolny, Poland.
3. **H. Orlikowska**, E. Krok, M. Chattopadhyay, L. Piatkowski, Modulation transfer approach: on the way to routine fluorescence-free imaging of biomimetic membranes, *Early Career Time Resolved Vibrational Spectroscopy Symposium*, 13.06.2021, Ann Arbor, Michigan, United States (online).
4. **H. Orlikowska**, L. Piatkowski, Towards routine fluorescence-free imaging of biomimetic cell membranes, *Single-Molecule Sensors and NanoSystems International Conference*, 9-11.11.2020, Barcelona, Spain, flash (online).
5. **H. Orlikowska**, A. Sobolewska, S. Bartkiewicz, Photochromism in azobenzene-based photo-responsive surfactants, *XI National Conference of Young Scientists in Poland - Research and Development*, 30.03.2020, Poznan, Poland (online).
6. **H. Orlikowska**, E. Krok, M. Chattopadhyay, L. Piatkowski, To see the invisible: stimulated emission microscopy for imaging nonfluorescent components of biomimetic membranes, *4th EMBO Workshop on Computational and Structural Biology and Chemistry*, 28-29.02.2020, Waplewo, Poland, international conference, invited talk.
7. **H. Orlikowska**, Dwuwymiarowa dynamiczna analiza termooptyczna, *II Wroclawskie Akademickie Spotkanie Ambitnych Bioinżynierów*, 17.04.2018, Wrocław, Poland.
8. **H. Orlikowska**, Materio, wiruj! Czyli o optycznym efekcie Marangoniego, *II Ogólnopolska Studencka Fizyczno-Optyczna Konferencja FOKA*, 20–22.10.2017, Szklarska Poreba, Poland.
9. **H. Orlikowska**, Wpływ uporządkowania matrycy na kinetykę reakcji fotochromowej w pochodnej azobenzenu, *Ogólnopolska Konferencja Kryształki Molekularne*, 6–8.09.2017, Warsaw, Poland.
10. **H. Orlikowska**, Mikro-katapulty, nano-szczypce i piko-balony – czyli o tym, jak światło porusza materią, referat ustny, *IV Ogólnokrajowa Konferencja Młodzi Naukowcy w Polsce - Badania i Rozwój*, 21.11.2016, Poznan, Poland.

Poster presentations:

1. **H. Orlikowska-Rzeźnik**, J. Versluis, H. J. Bakker, L. Piatkowski, Cholesterol Modulates the Hydration Properties of Model Cell Membranes in a Lipid Dependent Manner, *Water at Interfaces Faraday Discussion*, 20-22.09.2023, London, England.

2. **H. Orlikowska-Rzeznik**, J. Versluis, H. J. Bakker, L. Piatkowski, Cholesterol's Role in Cell Membranes is Even More Multifaceted, *14th European Biophysical Societies' Association (EBSA) Congress*, 31.07-4.08.2023, Stockholm, Sweden.
3. **H. Orlikowska-Rzeznik**, J. Versluis, H. J. Bakker, L. Piatkowski, Cholesterol Decreases the Orientational Bias of Water Molecules at the Surface of a Model Cell Membrane, *Time Resolved Vibrational Spectroscopy*, 11-16.06.2023, Amsterdam, The Netherlands.
4. **H. Orlikowska-Rzeznik**, E. Krok, M. Chattopadhyay, A. Lester, L. Piatkowski, Lipid Membrane Hydration and Cholesterol Content: Laurdan Sees It Differently, *The #RSCPoster Twitter Conference (Royal Society of Chemistry)*, 28.02-1.03.2023, England (online).
5. **H. Orlikowska-Rzeznik**, E. Krok, M. Chattopadhyay, A. Lester, L. Piatkowski, Direct Effect of Biomimetic Cell Membrane Hydration on Laurdan Fluorescence, *The Biochemistry Global Summit – the 25th IUBMB, 46th FEBS and 15th PABMB Congresses*, 9-14.07.2022, Lisbon, Portugal.
6. **H. Orlikowska-Rzeznik**, E. Krok, M. Chattopadhyay, L. Piatkowski, Fluorescence-Free Detection of Biomimetic Cell Membrane Components Using Modulation Transfer Technique, *The #RSCPoster Twitter Conference (Royal Society of Chemistry)*, 1-2.03.2022, England (online).
7. **H. Orlikowska**, E. Krok, M. Chattopadhyay, L. Piatkowski, Can a Biomimetic Cell Membrane Be Visualized Using a Fluorescence-Free Approach?, *Systems Chemistry Virtual Symposium*, 7-9.07.2021, Strasbourg, France (online).
8. **H. Orlikowska**, E. Krok, M. Chattopadhyay, L. Piatkowski, Modulation Transfer Approach: On the Way to Routine Fluorescence-Free Imaging of Biomimetic Membranes, *Time Resolved Vibrational Spectroscopy*, 14-18.06.2021, Ann Arbor, Michigan, United States (online).
9. **H. Orlikowska**, E. Krok, M. Chattopadhyay, L. Piatkowski, Detection of Model Biomembrane Components Using Fluorescence-Free Modulation Transfer Approach, *Chemical Systems Meeting*, 22-23.03.2021, Valencia, Spain (online).
10. **H. Orlikowska**, E. Krok, M. Chattopadhyay, L. Piatkowski, Detection of Model Biomembrane Components Using Fluorescence-Free Modulation Transfer Approach, *ChemSci2020: Leaders in the Field Symposium*, 7-10.12.2020, Kolkata, India (online).
11. **H. Orlikowska**, M. Kotkowiak, S. Bartkiewicz, P. Skupin-Mrugalska, M. Rojewska, K. Dettlaff, Z. Galewski, Characterization and Liposome Formulation of Photochromic Surfactants, *IV Polish Scientific Networks: Science and Technology*, 19-21.09.2019, Poznan, Poland, international conference.
12. **H. Orlikowska**, S. Bartkiewicz, Z. Galewski, Bistabilne Surfaktanty Fotochromowe, *XXI Ogólnopolska Konferencja Kryształy Molekularne*, 3-7.09.2018, Lodz – Kolumna, Poland.
13. **H. Orlikowska**, S. Bartkiewicz, A. Sobolewska, A. Miniewicz, Z. Galewski, Dynamiczna, Dwuwymiarowa Analiza Termooptyczna – Nowa Metoda Identyfikacji Mezofaz Ciekłokrystalicznych, *XX Ogólnopolska Konferencja Kryształy Molekularne*, 12–16.09.2016, Kazimierz Dolny, Poland.

10.6 Patent activity

Patents:

1. Patent, PL 438733, Poland, 10.07.2024, patent title: *Preparation procedure of lipid membranes with controlled size of laterally separated domains, deposited on a solid substrate/Sposób otrzymywania membran lipidowych o kontrolowanym rozmiarze lateralnie wydzielonych domen, osadzonych na stałym podłożu*, authors: E. Krok, A. Batura, **H. Orlikowska**, M. Chattopadhyay, Ł. Piątkowski.
2. Patent, PL 231877 (B1), Poland, 12.12.2018, patent title: *Air humidity measuring method/Sposób pomiaru wilgotności powietrza*, authors: S. Bartkiewicz, **H. Orlikowska**.
3. Patent, PL 227675 (B1), Poland, 25.07.2017, patent title: *Method of converting light into mechanical energy/Sposób konwersji światła na energię mechaniczną*, authors: S. Bartkiewicz, **H. Orlikowska**, A. Sobolewska, A. Miniewicz.
4. Patent, PL 227673 (B1), Poland, 18.07.2017, patent title: *Handling and supply of small quantities of gases/Sposób przemieszczania i dostarczania małych ilości gazów*, authors: S. Bartkiewicz, A. Miniewicz, K. Dradrach, **H. Orlikowska**.

Patent applications:

1. Patent application, PL437600, Poland, date of registration: 16.04.2021, patent title: *Method of measuring the local hydration of lipid layers in biomimetic and biological systems/Sposób pomiaru lokalnego stopnia nawodnienia warstw lipidowych układów biomimetycznych i biologicznych*, authors: M. Chattopadhyay, E. Krok, **H. Orlikowska**, Ł. Piątkowski.
2. Patent application, PL437601, Poland, date of registration: 16.04.2021, patent title: *Method of measuring the local hydration of lipid layers in biomimetic and biological systems/Sposób pomiaru lokalnego stopnia nawodnienia warstw lipidowych układów biomimetycznych i biologicznych*, authors: M. Chattopadhyay, E. Krok, **H. Orlikowska**, Ł. Piątkowski.

10.7 Scientific grants

Principal investigator in grants:

1. **Preludium-21**, National Science Center, grant number: 2022/45/N/ST4/01442, years: 2023-2026, budget: 209 840 PLN. *Unraveling the effect of steroid hormones on biophysical properties of biomimetic cell membranes.*
2. **Diamentowy Grant**, Ministry of Science and Higher Education, grant number: 0042/DIA/2019/48, years: 2019-2024, budget: 220 000 PLN. *Stimulated emission microscopy for imaging of systems with very low fluorescence efficiency, in particular selected components of model biological membranes.*
3. **SBAD-MK**, Project within the framework of funds allocated from the subvention of the Faculty of Materials Engineering and Technical Physics for the conduct of scientific research

or development works and related tasks for the development of young scientists funded in the internal competition procedure, grant number: 0512/SBAD/6209, year: 2020, budget: 8 200 PLN. *Study of the influence of water molecules on the formation of solid supported lipid bilayers and quantification of their hydration with quartz crystal microbalance.*

Co-investigator in grants:

1. **SBAD-MK**, Projects within the framework of funds allocated from the subvention of the Faculty of Materials Engineering and Technical Physics for the conduct of scientific research or development works and related tasks for the development of young scientists funded in the internal competition procedure in 2022, 2023, and 2024;
 - PI: M. Eng. Anna Łagowska, year: 2024, budget: 12 350 PLN. *Can female sex hormones heal? Determining the interactions of selected steroid hormones with biomimetic cell membranes;*
 - PI: Dr. Eng. Emilia Krok, grant number: 0512/SBAD/6214, year: 2023, budget: 16 265 PLN. *Reverse microengineering - developing functional biomimetic lipid membranes that mimic the biological membranes characteristic of gram-negative and positive bacterial cells;*
 - PI: Dr. Eng. Emilia Krok, grant number: 0512/SBAD/6212, year: 2022, budget: 7 663 PLN. *Biomimetic cell membranes under extreme dehydration - analysis of nanoscopic structural changes.*
2. **Opus-19**, National Science Centre (Poland), grant number: 2020/37/B/ST4/01785, PI: Dr. habil. Eng. Łukasz Piątkowski, Prof. PUT, years: 2021-2025, budget: 1 626 360 PLN. *Seeing the invisible – elucidating the nature of sterol aggregates in biomimetic cell membranes using modulation transfer microscopy.*
3. **Installation Grant**, European Molecular Biology Organization, grant number: IG 4147, PI: Dr. habil. Eng. Łukasz Piątkowski, Prof. PUT, years: 2019-2024, budget: 250 000 EUR *Biological water: the role of hydration in cell membrane organization.*
4. **Opus-8**, National Science Centre (Poland), grant number: 2014/15/B/ST8/00115, PI: Prof. Dr. habil. Eng. Stanisław Bartkiewicz, years: 2015-2018, budget: 896 000 PLN. *Research on new photochromic materials for photonics organized through liquid crystal and polymer structures.*

10.8 Scholarships

1. FNP START scholarship, Foundation for Polish Science (2024).
2. Outgoing scholarship co-funded by the Polish National Agency for Academic Exchange (NAWA) under the STER programme, Towards Internationalization of Poznan University of Technology Doctoral School (2022-2024) for a 3-month internship at AMOLF Institute, Amsterdam, The Netherlands (2022).

3. Scholarship in OPUS-19 grant (National Science Center, Poland) 2020/37/B/ST4/01785, PI: Lukasz Piatkowski, budget: 1 626 360 PLN, in the period: 01.04.2023-31.01.2025.
4. Scholarship of the Minister of Science and Higher Education for outstanding achievements for students:
 - In 2016;
 - In 2017;
 - In 2018.
5. Scholarship of the "100 for 100" program named after Halina Konopacka and Ignacy Matuszewski, funded by the LOTTO Foundation Totalizator Sportowy for students distinguished by their academic achievements and active social attitude on the occasion of the 100th anniversary of Poland's regaining independence (2018).
6. Scholarship of the Rector of the Poznan University of Technology for the best students (2019).
7. Scholarship of the Rector of the Wroclaw University of Science and Technology for the best students:
 - In 2016;
 - In 2017;
 - In 2018.

10.9 Other prizes and awards

1. Poster Prize sponsored by *The Journal of Chemical Physics* for the presentation at Time-Resolved Vibrational Spectroscopy international conference (11-16.06.2023, Amsterdam, The Netherlands).
2. Team Award of the Rector of the Poznan University of Technology for outstanding scientific achievements in 2021: for a series of publications, patent applications, and research grants on the study of the structure and dynamics of biomimetic cell membranes (2022).
3. Nomination to the Polish Intelligent Development Award 2020 in the category *Scientist of the Future*, Center for Intelligent Development (2020).
4. Poster prize for the presentation at the international conference *IV Polish Scientific Networks: Science and Technology* (19-21.09.2019, Poznan, Poland).
5. "Best Diploma of the Year 2018" at Wroclaw University of Science and Technology for first degree graduates, co-organizer: Marshal's Office of the Lower Silesian Voivodeship.
6. Best graduate award of the Wroclaw University of Science and Technology in the academic year 2017/2018.
7. Award of the Rector of the Wroclaw University of Science and Technology for the best student:

- In 2017;
 - In 2018.
8. Presentation prize for the speech at the II Wrocław Academic Meeting of Ambitious Bioengineers (WASABI) (2018).
 9. Special Award of the Rector of the Kielce University of Technology in the 7th edition of the National Competition *Student Inventor* (2017).
 10. First prize for the presentation at the *National Conference of Molecular Crystals in Poland* (2017).
 11. First prize and audience award for the presentation at the *National Student Physical-Optical Conference FOKA* (2017).
 12. Winner of the *I Am a Leader in 2017* competition in the category of science, realized as part of the project *Woman Leader 2017*.
 13. Author of award-winning science photographs entitled: "*Photonic Vortex*," "*Crystal Eye*," and "*Oily Streaks*" presented:
 - at the exhibition "*Not all gold that shines*" as part of the Lower Silesian Science Festival in 2017 and 2016;
 - in the calendar of Wrocław University of Technology (2017).

Bibliography

1. Luo, J., Yang, H. & Song, B.-L. Mechanisms and regulation of cholesterol homeostasis. *Nature Reviews Molecular Cell Biology* **21**, 225–245 (2020).
2. Van Meer, G., Voelker, D. R. & Feigenson, G. W. Membrane lipids: where they are and how they behave. *Nature Reviews Molecular Cell Biology* **9**, 112–124 (2008).
3. Duggan, J. *et al.* Functional imaging of microdomains in cell membranes. *European Biophysics Journal* **37**, 1279–1289 (2008).
4. Levental, I., Levental, K. R. & Heberle, F. A. Lipid rafts: controversies resolved, mysteries remain. *Trends in Cell Biology* **30**, 341–353 (2020).
5. Subczynski, W. K., Pasenkiewicz-Gierula, M., Widomska, J., Mainali, L. & Raguz, M. High cholesterol/low cholesterol: effects in biological membranes: a review. *Cell Biochemistry and Biophysics* **75**, 369–385 (2017).
6. Frallicciardi, J., Melcr, J., Siginou, P., Marrink, S. J. & Poolman, B. Membrane thickness, lipid phase and sterol type are determining factors in the permeability of membranes to small solutes. *Nature Communications* **13**, 1605 (2022).
7. Kovács, T., Batta, G., Zákány, F., Szöllősi, J. & Nagy, P. The dipole potential correlates with lipid raft markers in the plasma membrane of living cells. *Journal of Lipid Research* **58**, 1681–1691 (2017).
8. Wüstner, D. in *Cellular Lipid Metabolism* (ed Ehnholm, C.) 157–190 (Springer Berlin Heidelberg, 2009).
9. Martens, S. & McMahon, H. T. Mechanisms of membrane fusion: disparate players and common principles. *Nature Reviews Molecular Cell Biology* **9**, 543–556 (2008).
10. Su, J. *et al.* Cell–cell communication: new insights and clinical implications. *Signal Transduction and Targeted Therapy* **9**, 196 (2024).
11. Schnaar, R. L. Glycolipid-mediated cell–cell recognition in inflammation and nerve regeneration. *Archives of Biochemistry and Biophysics* **426**, 163–172 (2004).
12. Harding, C. V. & Unanue, E. R. Cellular mechanisms of antigen processing and the function of class I and II major histocompatibility complex molecules. *Cell Regulation* **1**, 499–509 (1990).
13. Le Roux, A.-L., Quiroga, X., Walani, N., Arroyo, M. & Roca-Cusachs, P. The plasma membrane as a mechanochemical transducer. *Philosophical Transactions of the Royal Society B* **374**, 20180221 (2019).
14. Sitia, R. & Meldolesi, J. Endoplasmic reticulum: a dynamic patchwork of specialized subregions. *Molecular Biology of the Cell* **3**, 1067–1072 (1992).

15. Diaz-Rohrer, B., Levental, K. R. & Levental, I. Rafting through traffic: Membrane domains in cellular logistics. *Biochimica et Biophysica Acta (BBA)-Biomembranes* **1838**, 3003–3013 (2014).
16. Korla, K. & Mitra, C. K. Modelling the Krebs cycle and oxidative phosphorylation. *Journal of Biomolecular Structure and Dynamics* **32**, 242–256 (2014).
17. Pinton, P., Giorgi, C., Siviero, R., Zecchini, E. & Rizzuto, R. Calcium and apoptosis: ER-mitochondria Ca²⁺ transfer in the control of apoptosis. *Oncogene* **27**, 6407–6418 (2008).
18. Olzmann, J. A. & Carvalho, P. Dynamics and functions of lipid droplets. *Nature Reviews Molecular Cell Biology* **20**, 137–155 (2019).
19. Wang, C. *et al.* Investigation of endosome and lysosome biology by ultra pH-sensitive nanoprobe. *Advanced Drug Delivery Reviews* **113**, 87–96 (2017).
20. Honsho, M. & Fujiki, Y. Plasmalogen homeostasis–regulation of plasmalogen biosynthesis and its physiological consequence in mammals. *FEBS Letters* **591**, 2720–2729 (2017).
21. Codogno, P. & Meijer, A. J. Autophagy and signaling: their role in cell survival and cell death. *Cell Death & Differentiation* **12**, 1509–1518 (2005).
22. Cui, L. *et al.* Vesicle trafficking and vesicle fusion: mechanisms, biological functions, and their implications for potential disease therapy. *Molecular Biomedicine* **3**, 29 (2022).
23. Rizzoli, S. O. Synaptic vesicle recycling: steps and principles. *The EMBO journal* **33**, 788–822 (2014).
24. Ikon, N. & Ryan, R. O. Cardiolipin and mitochondrial cristae organization. *Biochimica et Biophysica Acta (BBA)-Biomembranes* **1859**, 1156–1163 (2017).
25. Hullin-Matsuda, F., Taguchi, T., Greimel, P. & Kobayashi, T. Lipid compartmentalization in the endosome system. *Seminars in cell & developmental biology* **31**, 48–56 (2014).
26. Stillwell, W. *An introduction to biological membranes: composition, structure and function* (Elsevier, 2016).
27. Casares, D., Escribá, P. V. & Rosselló, C. A. Membrane lipid composition: effect on membrane and organelle structure, function and compartmentalization and therapeutic avenues. *International Journal of Molecular Sciences* **20**, 2167 (2019).
28. Kobayashi, T. & Menon, A. K. Transbilayer lipid asymmetry. *Current Biology* **28**, R386–R391 (2018).
29. Gibson Wood, W., Igbavboa, U., Müller, W. E. & Eckert, G. P. Cholesterol asymmetry in synaptic plasma membranes. *Journal of Neurochemistry* **116**, 684–689 (2011).
30. Daleke, D. L. Regulation of transbilayer plasma membrane phospholipid asymmetry. *Journal of Lipid Research* **44**, 233–242 (2003).
31. Rivel, T., Ramseyer, C. & Yesylevskyy, S. The asymmetry of plasma membranes and their cholesterol content influence the uptake of cisplatin. *Scientific Reports* **9**, 5627 (2019).

32. Bevers, E. M. & Williamson, P. L. Getting to the outer leaflet: physiology of phosphatidylserine exposure at the plasma membrane. *Physiological Reviews* **96**, 605–645 (2016).
33. Ahmadi, D. *et al.* Nanoscale structure and dynamics of model membrane lipid raft systems, studied by neutron scattering methods. *Frontiers in Physics* **10**, 864746 (2022).
34. Konarev, P. V., Gruzinov, A. Y., Mertens, H. D. & Svergun, D. I. Restoring structural parameters of lipid mixtures from small-angle X-ray scattering data. *Journal of Applied Crystallography* **54**, 169–179 (2021).
35. Träger, J., Meister, A., Hause, G., Harauz, G. & Hinderberger, D. Shaping membrane interfaces in lipid vesicles mimicking the cytoplasmic leaflet of myelin through variation of cholesterol and myelin basic protein contents. *Biochimica et Biophysica Acta (BBA)-Biomembranes* **1865**, 184179 (2023).
36. Biswas, B., Shah, D., Cox-Vázquez, S. J. & Vázquez, R. J. Sensing cholesterol-induced rigidity in model membranes with time-resolved fluorescence spectroscopy and microscopy. *Journal of Materials Chemistry B* **12**, 6570–6576 (2024).
37. Van Beekveld, R. A. *et al.* Specific lipid studies in complex membranes by solid-state NMR spectroscopy. *Chemistry—A European Journal* **28**, e202202472 (2022).
38. Okotrub, K., Zaytseva, I., Adichtchev, S. & Surovtsev, N. Raman spectroscopy and DSC assay of the phase coexistence in binary DMPC/cholesterol multilamellar vesicles. *Biochimica et Biophysica Acta (BBA)-Biomembranes* **1863**, 183514 (2021).
39. Flanagan, J. C., Valentine, M. L. & Baiz, C. R. Ultrafast dynamics at lipid–water interfaces. *Accounts of Chemical Research* **53**, 1860–1868 (2020).
40. Maestro, A. & Gutfreund, P. In situ determination of the structure and composition of Langmuir monolayers at the air/water interface by neutron and X-ray reflectivity and ellipsometry. *Advances in Colloid and Interface Science* **293**, 102434 (2021).
41. Pereira, A. R., Shimizu, F. M. & Oliveira Jr, O. N. Cholesterol modulates the interaction between paclitaxel and Langmuir monolayers simulating cell membranes. *Colloids and Surfaces B: Biointerfaces* **205**, 111889 (2021).
42. Chattopadhyay, M. *et al.* Hydration Layer of Only a Few Molecules Controls Lipid Mobility in Biomimetic Membranes. *Journal of the American Chemical Society* **143**, 14551–14562 (2021).
43. Krok, E. *et al.* Nanoscale structural response of biomimetic cell membranes to controlled dehydration. *Nanoscale* **16**, 72–84 (2024).
44. Jaroque, G. N., Sartorelli, P. & Caseli, L. Interfacial vibrational spectroscopy and Brewster angle microscopy distinguishing the interaction of terpineol in cell membrane models at the air-water interface. *Biophysical Chemistry* **246**, 1–7 (2019).
45. Elizondo, E. *et al.* Liposomes and other vesicular systems: structural characteristics, methods of preparation, and use in nanomedicine. *Progress in Molecular Biology and Translational Science* **104**, 1–52 (2011).

46. Akbarzadeh, A. *et al.* Liposome: classification, preparation, and applications. *Nanoscale Research Letters* **8**, 102 (2013).
47. Husen, P., Arriaga, L. R., Monroy, F., Ipsen, J. H. & Bagatolli, L. A. Morphometric image analysis of giant vesicles: a new tool for quantitative thermodynamics studies of phase separation in lipid membranes. *Biophysical Journal* **103**, 2304–2310 (2012).
48. Méléard, P., Bagatolli, L. A. & Pott, T. Giant unilamellar vesicle electroformation: From lipid mixtures to native membranes under physiological conditions. *Methods in Enzymology* **465**, 161–176 (2009).
49. Goodchild, J. A., Walsh, D. L. & Connell, S. D. Nanoscale substrate roughness hinders domain formation in supported lipid bilayers. *Langmuir* **35**, 15352–15363 (2019).
50. Kim, J., Kim, G. & Cremer, P. S. Investigations of water structure at the solid/liquid interface in the presence of supported lipid bilayers by vibrational sum frequency spectroscopy. *Langmuir* **17**, 7255–7260 (2001).
51. Richter, R. P., Bérat, R. & Brisson, A. R. Formation of Solid-Supported Lipid Bilayers: An Integrated View. *Langmuir* **22**, 3497–3505 (2006).
52. Richter, R. P. & Brisson, A. R. Following the formation of supported lipid bilayers on mica: a study combining AFM, QCM-D, and ellipsometry. *Biophysical Journal* **88**, 3422–3433 (2005).
53. Dacic, M. *et al.* Influence of divalent cations on deformation and rupture of adsorbed lipid vesicles. *Langmuir* **32**, 6486–6495 (2016).
54. Ferhan, A. R. *et al.* Solvent-assisted preparation of supported lipid bilayers. *Nature Protocols* **14**, 2091–2118 (2019).
55. Jackman, J. A. & Cho, N.-J. Supported lipid bilayer formation: beyond vesicle fusion. *Langmuir* **36**, 1387–1400 (2020).
56. Mennicke, U. & Salditt, T. Preparation of solid-supported lipid bilayers by spin-coating. *Langmuir* **18**, 8172–8177 (2002).
57. Wood, M. H., Milan, D. C., Nichols, R. J., Casford, M. T. & Horswell, S. L. A quantitative determination of lipid bilayer deposition efficiency using AFM. *RSC Advances* **11**, 19768–19778 (2021).
58. Garg, S., Rühle, J., Lüdtke, K., Jordan, R. & Naumann, C. A. Domain registration in raft-mimicking lipid mixtures studied using polymer-tethered lipid bilayers. *Biophysical Journal* **92**, 1263–1270 (2007).
59. Zhong, Y. & Wang, G. Three-dimensional heterogeneous structure formation on a supported lipid bilayer disclosed by single-particle tracking. *Langmuir* **34**, 11857–11865 (2018).
60. Ho, C. S., Khadka, N. K. & Pan, J. Sub-ten-nanometer heterogeneity of solid supported lipid membranes determined by solution atomic force microscopy. *Biochimica et Biophysica Acta (BBA)-Biomembranes* **1858**, 181–188 (2016).
61. Pedrosa, M., Maldonado-Valderrama, J. & Gálvez-Ruiz, M. J. Interactions between curcumin and cell membrane models by Langmuir monolayers. *Colloids and Surfaces B: Biointerfaces* **217**, 112636 (2022).

-
62. Pereira, A. R. *et al.* Enhanced chitosan effects on cell membrane models made with lipid raft monolayers. *Colloids and Surfaces B: Biointerfaces* **193**, 111017 (2020).
 63. Levental, I. & Lyman, E. Regulation of membrane protein structure and function by their lipid nano-environment. *Nature Reviews Molecular Cell Biology* **24**, 107–122 (2023).
 64. Budin, I. *et al.* Viscous control of cellular respiration by membrane lipid composition. *Science* **362**, 1186–1189 (2018).
 65. Sharma, V. & Mamontov, E. Multiscale lipid membrane dynamics as revealed by neutron spectroscopy. *Progress in Lipid Research* **87**, 101179 (2022).
 66. Morvan, E., Taib-Maamar, N., Grélard, A., Loquet, A. & Dufourc, E. J. Bio-membranes: Picosecond to second dynamics and plasticity as deciphered by solid state NMR. *Biochimica et Biophysica Acta (BBA)-Biomembranes* **1865**, 184097 (2023).
 67. Morvan, E., Taib-Maamar, N., Grélard, A., Loquet, A. & Dufourc, E. J. Dynamic sorting of mobile and rigid molecules in biomembranes by magic-angle spinning ¹³C NMR. *Analytical Chemistry* **95**, 3596–3605 (2023).
 68. Renne, M. F. & Ernst, R. Membrane homeostasis beyond fluidity: control of membrane compressibility. *Trends in Biochemical Sciences* (2023).
 69. Sperotto, M. M. & Ferrarini, A. in *The Biophysics of Cell Membranes: Biological Consequences* (eds Epanand, R. M. & Ruyschaert, J.-M.) 29–60 (Springer, 2017).
 70. Gu, R.-X., Baoukina, S. & Tieleman, D. P. Cholesterol flip-flop in heterogeneous membranes. *Journal of Chemical Theory and Computation* **15**, 2064–2070 (2019).
 71. Ermilova, I. & Lyubartsev, A. P. Cholesterol in phospholipid bilayers: positions and orientations inside membranes with different unsaturation degrees. *Soft Matter* **15**, 78–93 (2019).
 72. Khelashvili, G. & Harries, D. How cholesterol tilt modulates the mechanical properties of saturated and unsaturated lipid membranes. *The Journal of Physical Chemistry B* **117**, 2411–2421 (2013).
 73. Aittoniemi, J. *et al.* Tilt: major factor in sterols' ordering capability in membranes. *The Journal of Physical Chemistry B* **110**, 25562–25564 (2006).
 74. Róg, T. & Pasenkiewicz-Gierula, M. Cholesterol effects on the phosphatidylcholine bilayer nonpolar region: a molecular simulation study. *Biophysical journal* **81**, 2190–2202 (2001).
 75. Róg, T., Pasenkiewicz-Gierula, M., Vattulainen, I. & Karttunen, M. Ordering effects of cholesterol and its analogues. *Biochimica et Biophysica Acta (BBA)-Biomembranes* **1788**, 97–121 (2009).
 76. Ohvo-Rekilä, H., Ramstedt, B., Leppimäki, P. & Slotte, J. P. Cholesterol interactions with phospholipids in membranes. *Progress in lipid research* **41**, 66–97 (2002).
 77. Morrow, M. R., Singh, D., Lu, D. & Grant, C. Glycosphingolipid fatty acid arrangement in phospholipid bilayers: cholesterol effects. *Biophysical journal* **68**, 179–186 (1995).
-

78. Merrill Jr, A. H. *et al.* Sphingolipids—the enigmatic lipid class: biochemistry, physiology, and pathophysiology. *Toxicology and applied pharmacology* **142**, 208–225 (1997).
79. Róg, T. & Pasenkiewicz-Gierula, M. Cholesterol effects on a mixed-chain phosphatidylcholine bilayer: a molecular dynamics simulation study. *Biochimie* **88**, 449–460 (2006).
80. Martinez-Seara, H. *et al.* Interplay of unsaturated phospholipids and cholesterol in membranes: effect of the double-bond position. *Biophysical journal* **95**, 3295–3305 (2008).
81. Hung, W.-C., Lee, M.-T., Chen, F.-Y. & Huang, H. W. The condensing effect of cholesterol in lipid bilayers. *Biophysical journal* **92**, 3960–3967 (2007).
82. Gallová, J., Uhríková, D., Islamov, A., Kuklin, A. & Balgavy, P. Effect of cholesterol on the bilayer thickness in unilamellar extruded DLPC and DOPC liposomes: SANS contrast variation study. *General physiology and biophysics* **23**, 113–128 (2004).
83. McIntosh, T. J. The effect of cholesterol on the structure of phosphatidylcholine bilayers. *Biochimica et Biophysica Acta (BBA)-Biomembranes* **513**, 43–58 (1978).
84. Mielke, S., Sorkin, R. & Klein, J. Effect of cholesterol on the mechanical stability of gel-phase phospholipid bilayers studied by AFM force spectroscopy. *The European Physical Journal E* **46**, 77 (2023).
85. Inoue, T., Yanagihara, S.-i., Misono, Y. & Suzuki, M. Effect of fatty acids on phase behavior of hydrated dipalmitoylphosphatidylcholine bilayer: saturated versus unsaturated fatty acids. *Chemistry and Physics of Lipids* **109**, 117–133 (2001).
86. Cossins, A. R. & Macdonald, A. G. The adaptation of biological membranes to temperature and pressure: fish from the deep and cold. *Journal of Bioenergetics and Biomembranes* **21**, 115–135 (1989).
87. Lönnfors, M., Doux, J. P., Killian, J. A., Nyholm, T. K. & Slotte, J. P. Sterols have higher affinity for sphingomyelin than for phosphatidylcholine bilayers even at equal acyl-chain order. *Biophysical Journal* **100**, 2633–2641 (2011).
88. Roy, A. & Patra, S. K. Lipid raft facilitated receptor organization and signaling: a functional rheostat in embryonic development, stem cell biology and cancer. *Stem Cell Reviews and Reports* **19**, 2–25 (2023).
89. Lingwood, D. & Simons, K. Lipid rafts as a membrane-organizing principle. *science* **327**, 46–50 (2010).
90. Sezgin, E., Levental, I., Mayor, S. & Eggeling, C. The mystery of membrane organization: composition, regulation and roles of lipid rafts. *Nature Reviews Molecular Cell Biology* **18**, 361–374 (2017).
91. Laganowsky, A. *et al.* Membrane proteins bind lipids selectively to modulate their structure and function. *Nature* **510**, 172–175 (2014).
92. Lingwood, D. *et al.* Cholesterol modulates glycolipid conformation and receptor activity. *Nature Chemical Biology* **7**, 260–262 (2011).

-
93. Koyama-Honda, I. *et al.* High-speed single-molecule imaging reveals signal transduction by induced transbilayer raft phases. *The Journal of Cell Biology* **219**, e202006125 (2020).
 94. Varshney, P., Yadav, V. & Saini, N. Lipid rafts in immune signalling: current progress and future perspective. *Immunology* **149**, 13–24 (2016).
 95. Li, X. *et al.* Dependence of SARS-CoV-2 infection on cholesterol-rich lipid raft and endosomal acidification. *Computational and Structural Biotechnology Journal* **19**, 1933–1943 (2021).
 96. Diwaker, D., Mishra, K. P., Ganju, L. & Singh, S. B. Protein disulfide isomerase mediates dengue virus entry in association with lipid rafts. *Viral Immunology* **28**, 153–160 (2015).
 97. Miller, M. E., Adhikary, S., Kolokoltsov, A. A. & Davey, R. A. Ebolavirus requires acid sphingomyelinase activity and plasma membrane sphingomyelin for infection. *Journal of Virology* **86**, 7473–7483 (2012).
 98. Audi, A., Soudani, N., Dbaibo, G. & Zaraket, H. Depletion of host and viral sphingomyelin impairs influenza virus infection. *Frontiers in Microbiology* **11**, 612 (2020).
 99. Campbell, S., Crowe, S. M. & Mak, J. Lipid rafts and HIV-1: from viral entry to assembly of progeny virions. *Journal of Clinical Virology* **22**, 217–227 (2001).
 100. Popik, W., Alce, T. M. & Au, W.-C. Human immunodeficiency virus type 1 uses lipid raft-colocalized CD4 and chemokine receptors for productive entry into CD4+ T cells. *Journal of Virology* **76**, 4709–4722 (2002).
 101. Leung, K. *et al.* HIV-1 assembly: viral glycoproteins segregate quantally to lipid rafts that associate individually with HIV-1 capsids and virions. *Cell Host & Microbe* **3**, 285–292 (2008).
 102. Yang, S.-T., Kiessling, V., Simmons, J. A., White, J. M. & Tamm, L. K. HIV gp41-mediated membrane fusion occurs at edges of cholesterol-rich lipid domains. *Nature Chemical Biology* **11**, 424 (2015).
 103. Sezgin, E. & Schwille, P. Model membrane platforms to study protein-membrane interactions. *Molecular Membrane Biology* **29**, 144–154 (2012).
 104. Heberle, F. A. *et al.* Bilayer thickness mismatch controls domain size in model membranes. *Journal of the American Chemical Society* **135**, 6853–6859 (2013).
 105. Baumgart, T., Hess, S. T. & Webb, W. W. Imaging coexisting fluid domains in biomembrane models coupling curvature and line tension. *Nature* **425**, 821–824 (2003).
 106. Bacia, K., Schwille, P. & Kurzchalia, T. Sterol structure determines the separation of phases and the curvature of the liquid-ordered phase in model membranes. *Proceedings of the National Academy of Sciences* **102**, 3272–3277 (2005).
 107. Sezgin, E. *et al.* Partitioning, diffusion, and ligand binding of raft lipid analogs in model and cellular plasma membranes. *Biophysical Journal* **102**, 296a–297a (2012).
 108. Kaiser, H.-J. *et al.* Order of lipid phases in model and plasma membranes. *Proceedings of the National Academy of Sciences* **106**, 16645–16650 (2009).
-

109. Laage, D., Elsaesser, T. & Hynes, J. T. Water dynamics in the hydration shells of biomolecules. *Chemical Reviews* **117**, 10694–10725 (2017).
110. Huš, M. & Urbic, T. Strength of hydrogen bonds of water depends on local environment. *The Journal of Chemical Physics* **136** (2012).
111. Chaplin, M. F. in *Water And Life: The Unique Properties of H₂O* (eds Lynden-Bell, R. M., Morris, S. C., Barrow, J. D., Finney, J. L. & Harper, C. L.) 87–104 (CRC Press, 2010).
112. Martiniano, H. & Galamba, N. Insights on hydrogen-bond lifetimes in liquid and supercooled water. *The Journal of Physical Chemistry B* **117**, 16188–16195 (2013).
113. Kumar, R., Schmidt, J. & Skinner, J. Hydrogen bonding definitions and dynamics in liquid water. *The Journal of Chemical Physics* **126** (2007).
114. Hubbard, R. E. & Haider, M. K. Hydrogen bonds in proteins: role and strength. *Encyclopedia of life sciences* **1**, 1–6 (2010).
115. Jeffrey, G. A. & Saenger, W. *Hydrogen bonding in biological structures* (Springer Science & Business Media, 2012).
116. Buehler, L. in *Cell Membranes* 141–147 (Garland Science, 2015).
117. Basu Ball, W., Neff, J. K. & Gohil, V. M. The role of nonbilayer phospholipids in mitochondrial structure and function. *FEBS letters* **592**, 1273–1290 (2018).
118. Martelli, F., Calero, C. & Franzese, G. Redefining the concept of hydration water near soft interfaces. *Biointerphases* **16** (2021).
119. Martelli, F., Crain, J. & Franzese, G. Network topology in water nanoconfined between phospholipid membranes. *ACS nano* **14**, 8616–8623 (2020).
120. Bellissent-Funel, M.-C. *et al.* Water determines the structure and dynamics of proteins. *Chemical reviews* **116**, 7673–7697 (2016).
121. Disalvo, E. A., Martini, M. F., Bouchet, A. M., Hollmann, A. & Frías, M. Structural and thermodynamic properties of water–membrane interphases: Significance for peptide/membrane interactions. *Advances in colloid and interface science* **211**, 17–33 (2014).
122. Sarkar, S., Bisoi, A. & Singh, P. C. Understanding of the interaction of biological macromolecules with lipids using vibrational sum-frequency generation spectroscopy. *Journal of Raman Spectroscopy* **53**, 1828–1837 (2022).
123. Watanabe, N., Suga, K., Slotte, J. P., Nyholm, T. K. & Umakoshi, H. Lipid-surrounding water molecules probed by time-resolved emission spectra of laurdan. *Langmuir* **35**, 6762–6770 (2019).
124. Zhang, R., Cross, T. A., Peng, X. & Fu, R. Surprising Rigidity of Functionally Important Water Molecules Buried in the Lipid Headgroup Region. *Journal of the American Chemical Society* **144**, 7881–7888 (2022).
125. Tielrooij, K., Paparo, D., Piatkowski, L., Bakker, H. & Bonn, M. Dielectric relaxation dynamics of water in model membranes probed by terahertz spectroscopy. *Biophysical journal* **97**, 2484–2492 (2009).

-
126. Tristram-Nagle, S. in *Membrane Hydration. Subcellular Biochemistry* (ed Disalvo, E.) 17–43 (Springer, Cham., 2015).
127. Kiselev, M. A. & Lombardo, D. Structural characterization in mixed lipid membrane systems by neutron and X-ray scattering. *Biochimica et Biophysica Acta (BBA)-General Subjects* **1861**, 3700–3717 (2017).
128. Fitter, J., Lechner, R. & Dencher, N. Interactions of hydration water and biological membranes studied by neutron scattering. *The Journal of Physical Chemistry B* **103**, 8036–8050 (1999).
129. Calero, C. & Franzese, G. Membranes with different hydration levels: The interface between bound and unbound hydration water. *Journal of Molecular Liquids* **273**, 488–496 (2019).
130. Re, S., Nishima, W., Tahara, T. & Sugita, Y. Mosaic of water orientation structures at a neutral zwitterionic lipid/water interface revealed by molecular dynamics simulations. *The journal of physical chemistry letters* **5**, 4343–4348 (2014).
131. Shen, H., Wu, Z. & Zou, X. Interfacial water structure at zwitterionic membrane/water interface: the importance of interactions between water and lipid carbonyl groups. *ACS omega* **5**, 18080–18090 (2020).
132. Oh, M. I., Oh, C. I. & Weaver, D. F. Effect of cholesterol on the structure of networked water at the surface of a model lipid membrane. *The Journal of Physical Chemistry B* **124**, 3686–3694 (2020).
133. Binder, H. Water near lipid membranes as seen by infrared spectroscopy. *European Biophysics Journal* **36**, 265–279 (2007).
134. Rosa, A. S., Disalvo, E. A. & Frias, M. Water behavior at the phase transition of phospholipid matrixes assessed by FTIR spectroscopy. *The Journal of Physical Chemistry B* **124**, 6236–6244 (2020).
135. Valentine, M. L., Waterland, M. K., Fathizadeh, A., Elber, R. & Baiz, C. R. Interfacial dynamics in lipid membranes: the effects of headgroup structures. *The Journal of Physical Chemistry B* **125**, 1343–1350 (2021).
136. Chen, X., Hua, W., Huang, Z. & Allen, H. C. Interfacial water structure associated with phospholipid membranes studied by phase-sensitive vibrational sum frequency generation spectroscopy. *Journal of the American Chemical Society* **132**, 11336–11342 (2010).
137. Biswas, B. & Singh, P. C. Signature of the surface hydrated proton and associated restructuring of water at model membrane interfaces: a vibrational sum frequency generation study. *Physical Chemistry Chemical Physics* **23**, 14764–14769 (2021).
138. Mondal, J. A., Nihonyanagi, S., Yamaguchi, S. & Tahara, T. Three distinct water structures at a zwitterionic lipid/water interface revealed by heterodyne-detected vibrational sum frequency generation. *Journal of the American Chemical Society* **134**, 7842–7850 (2012).
139. Piatkowski, L., De Heij, J. & Bakker, H. J. Probing the distribution of water molecules hydrating lipid membranes with ultrafast forster vibrational energy transfer. *The Journal of Physical Chemistry B* **117**, 1367–1377 (2013).
-

140. Wassall, S. R. Pulsed field gradient-spin echo NMR studies of water diffusion in a phospholipid model membrane. *Biophysical journal* **71**, 2724–2732 (1996).
141. Cheng, J.-X., Pautot, S., Weitz, D. A. & Xie, X. S. Ordering of water molecules between phospholipid bilayers visualized by coherent anti-Stokes Raman scattering microscopy. *Proceedings of the National Academy of Sciences* **100**, 9826–9830 (2003).
142. Dreier, L. B. *et al.* Unraveling the origin of the apparent charge of zwitterionic lipid layers. *The journal of physical chemistry letters* **10**, 6355–6359 (2019).
143. Saak, C.-M., Dreier, L. B., Machel, K., Bonn, M. & Backus, E. H. Biological lipid hydration: distinct mechanisms of interfacial water alignment and charge screening for model lipid membranes. *Faraday Discussions* **249**, 317–333 (2024).
144. Chattopadhyay, M., Orlikowska, H., Krok, E. & Piatkowski, L. Sensing hydration of biomimetic cell membranes. *Biosensors* **11**, 241 (2021).
145. Chattopadhyay, M., Krok, E., Orlikowska-Rzeznik, H. & Piatkowski, L. Cooperativity between sodium ions and water molecules facilitates lipid mobility in model cell membranes. *Chemical Science* **14**, 4002–4011 (2023).
146. Malik, S. & Debnath, A. Dehydration induced dynamical heterogeneity and ordering mechanism of lipid bilayers. *The Journal of Chemical Physics* **154** (2021).
147. Mashl, R. J., Scott, H. L., Subramaniam, S. & Jakobsson, E. Molecular simulation of dioleoylphosphatidylcholine lipid bilayers at differing levels of hydration. *Biophysical journal* **81**, 3005–3015 (2001).
148. Sleight, S. B. *et al.* Isolation and proteomic analysis of mouse sperm detergent-resistant membrane fractions: evidence for dissociation of lipid rafts during capacitation. *Biology of reproduction* **73**, 721–729 (2005).
149. Chamberlain, L. H., Burgoyne, R. D. & Gould, G. W. SNARE proteins are highly enriched in lipid rafts in PC12 cells: implications for the spatial control of exocytosis. *Proceedings of the National Academy of Sciences* **98**, 5619–5624 (2001).
150. Aeffner, S., Reusch, T., Weinhausen, B. & Salditt, T. Energetics of stalk intermediates in membrane fusion are controlled by lipid composition. *Proceedings of the National Academy of Sciences* **109**, E1609–E1618 (2012).
151. Tian, Z. *et al.* Biochemical studies of membrane fusion at the single-particle level. *Progress in lipid research* **73**, 92–100 (2019).
152. Witkowska, A., Heinz, L. P., Grubmüller, H. & Jahn, R. Tight docking of membranes before fusion represents a metastable state with unique properties. *Nature communications* **12**, 3606 (2021).
153. Rizo, J. Molecular mechanisms underlying neurotransmitter release. *Annual Review of Biophysics* **51**, 377–408 (2022).
154. Jablonski, A. Efficiency of Anti-Stokes Fluorescence in Dyes. *Nature* **131**, 839–840 (1933).
155. Sauer, M., Hofkens, J. & Enderlein, J. in *Handbook of Fluorescence Spectroscopy and Imaging* (John Wiley & Sons, Ltd, 2011).

-
156. Lewis, G. N. & Kasha, M. Phosphorescence and the Triplet State. *Journal of the American Chemical Society* **62**, 2100–2116 (1944).
 157. Stokes, G. G. On the change of refrangibility of light. *Philosophical Transactions of the Royal Society of London* **142**, 463–562 (1852).
 158. Scollo, F. *et al.* What does time-dependent fluorescence shift (TDFS) in biomembranes (and proteins) report on? *Frontiers in Chemistry* **9**, 738350 (2021).
 159. Marvin, M. *Microscopy apparatus* US Patent US3013467A, Dec. 19, 1961.
 160. Fu, Y. & Finney, N. S. Small-molecule fluorescent probes and their design. *RSC advances* **8**, 29051–29061 (2018).
 161. Lovell, T. C., Branchaud, B. P. & Jasti, R. An Organic Chemist’s Guide to Fluorophores—Understanding Common and Newer Non-Planar Fluorescent Molecules for Biological Applications. *European Journal of Organic Chemistry* **27**, e202301196 (2024).
 162. Gupta, U., Singh, V. K., Kumar, V. & Khajuria, Y. Spectroscopic studies of cholesterol: fourier transform infra-red and vibrational frequency analysis. *Materials Focus* **3**, 211–217 (2014).
 163. Boldyrev, I. A. *et al.* New BODIPY lipid probes for fluorescence studies of membranes. *Journal of Lipid Research* **48**, 1518–1532 (2007).
 164. Hölttä-Vuori, M. *et al.* BODIPY-cholesterol: a new tool to visualize sterol trafficking in living cells and organisms. *Traffic* **9**, 1839–1849 (2008).
 165. Marks, D. L., Bittman, R. & Pagano, R. E. Use of Bodipy-labeled sphingolipid and cholesterol analogs to examine membrane microdomains in cells. *Histochemistry and Cell Biology* **130**, 819–832 (2008).
 166. Eggeling, C. *et al.* Direct observation of the nanoscale dynamics of membrane lipids in a living cell. *Nature* **457**, 1159–1162 (2009).
 167. Tyteca, D. *et al.* Three unrelated sphingomyelin analogs spontaneously cluster into plasma membrane micrometric domains. *Biochimica et Biophysica Acta (BBA)-Biomembranes* **1798**, 909–927 (2010).
 168. Baumgart, T., Hunt, G., Farkas, E. R., Webb, W. W. & Feigenson, G. W. Fluorescence probe partitioning between Lo/Ld phases in lipid membranes. *Biochimica et Biophysica Acta (BBA)-Biomembranes* **1768**, 2182–2194 (2007).
 169. Klymchenko, A. S. & Kreder, R. Fluorescent Probes for Lipid Rafts: From Model Membranes to Living Cells. *Chemistry & Biology* **21**, 97–113 (2014).
 170. Sengupta, P., Hammond, A., Holowka, D. & Baird, B. Structural determinants for partitioning of lipids and proteins between coexisting fluid phases in giant plasma membrane vesicles. *Biochimica et Biophysica Acta (BBA) - Biomembranes* **1778**, 20–32 (2008).
 171. Baumgart, T., Hess, S. & Webb, W. Imaging coexisting fluid domains in biomembrane models coupling curvature and line tension. *Nature* **825**, 821–824 (2003).
-

172. Dietrich, C. *et al.* Lipid rafts reconstituted in model membranes. *Biophysical Journal* **80**, 1417–1428 (2001).
173. Jin, L., Millard, A. C., Wuskell, J. P., Clark, H. A. & Loew, L. M. Cholesterol-enriched lipid domains can be visualized by di-4-ANEPPDHQ with linear and nonlinear optics. *Biophysical Journal* **89**, L04–L06 (2005).
174. Ragaller, F. *et al.* Dissecting the mechanisms of environment sensitivity of smart probes for quantitative assessment of membrane properties. *Biophysical Journal* **122**, 224a (2023).
175. Sezgin, E., Sadowski, T. & Simons, K. Measuring lipid packing of model and cellular membranes with environment sensitive probes. *Langmuir* **30**, 8160–8166 (2014).
176. Park, S. J., Juvekar, V., Jo, J. H. & Kim, H. M. Combining hydrophilic and hydrophobic environment sensitive dyes to detect a wide range of cellular polarity. *Chemical Science* **11**, 596–601 (2020).
177. Shynkar, V. V., Klymchenko, A. S., Duportail, G., Demchenko, A. P. & Mély, Y. Two-color fluorescent probes for imaging the dipole potential of cell plasma membranes. *Biochimica et Biophysica Acta (BBA)-Biomembranes* **1712**, 128–136 (2005).
178. Colom, A. *et al.* A fluorescent membrane tension probe. *Nature chemistry* **10**, 1118–1125 (2018).
179. Amaro, M., Reina, F., Hof, M., Eggeling, C. & Sezgin, E. Laurdan and Di-4-ANEPPDHQ probe different properties of the membrane. *Journal of Physics D: Applied Physics* **50**, 134004 (2017).
180. Boyd, R. W. *Nonlinear Optics (Second Edition)* (Academic Press, 2003).
181. Morita, A. *Theory of sum frequency generation spectroscopy* (Springer, 2018).
182. Mukamel, S. *Principles of Nonlinear Optical Spectroscopy* 1995.
183. Shen, Y. R. *Fundamentals of sum-frequency spectroscopy* (Cambridge University Press, 2016).
184. Lambert, A. G., Davies, P. B. & Neivandt, D. J. Implementing the theory of sum frequency generation vibrational spectroscopy: A tutorial review. *Applied Spectroscopy Reviews* **40**, 103–145 (2005).

Declarations of the co-authors

**POLITECHNIKA POZNAŃSKA**

FACULTY OF MATERIALS ENGINEERING AND TECHNICAL PHYSICS

Institute of Physics

Piotrowo 3, 61-138 Poznań

www.put.poznan.pl



Poznań, date: 11.09.2024

Dr. habil. Eng. Łukasz Piątkowski, Prof. PUT
Poznan University of Technology,
Faculty of Materials Engineering and Technical Physics
Institute of Physics
email: lukasz.j.piatkowski@put.poznan.pl

Declaration of Co-Authorship

I declare that according to the CRediT author statement, in the following publications:

1. *Laurdan discerns lipid membrane hydration and cholesterol content*
Hanna Orlikowska-Rzeźnik, Emilia Krok, Madhurima Chattopadhyay, Agnieszka Lester, Lukasz Piątkowski
The Journal of Physical Chemistry B (2023), volume 127, issue 15, pages 3382–3391
2. *Dehydration of lipid membrane drives redistribution of cholesterol between lateral domains*
Hanna Orlikowska-Rzeźnik, Emilia Krok, Maria Domanska, Piotr Setny, Anna Lagowska, Madhurima Chattopadhyay, Lukasz Piątkowski
The Journal of Physical Chemistry Letters (2024), volume 15, issue 16, pages 4515–4522
3. *Cholesterol changes interfacial water alignment in model cell membranes*
Hanna Orlikowska-Rzeźnik, Jan Versluis, Huib J. Bakker, Lukasz Piątkowski
Journal of the American Chemical Society (2024), volume 146, issue 19, pages 13151–13162, 2024

my contribution was: conceptualization (1-2), formal analysis (1), software (1), data curation (1), funding acquisition (1-3), investigation (1-2), methodology (1-3), project administration (1-3), resources (1-3), supervision (1-3), validation (1-2), writing–review and editing (1-3)

I agree to submit the above work by **M. Eng. Hanna Orlikowska-Rzeźnik**, as a part of her PhD dissertation titled: “*On discovering new facets of cholesterol in model cell membranes: the molecular interplay with biological water*” in the form of a collection of published and thematically related scientific articles.

Lukasz Piątkowski



POLITECHNIKA POZNAŃSKA

FACULTY OF MATERIALS ENGINEERING AND TECHNICAL PHYSICS

Institute of Physics

Piotrowo 3, 61-138 Poznań

www.put.poznan.pl



Poznań, date: 11.09.2024

Dr. Eng. Emilia Krok
Poznan University of Technology
Faculty of Materials Engineering and Technical Physics
Institute of Physics
email: emilia.krok@put.poznan.pl

Declaration of Co-Authorship

I declare that according to the CRediT author statement, in the following publications:

1. *Laurdan discerns lipid membrane hydration and cholesterol content*
Hanna Orlikowska-Rzeźnik, Emilia Krok, Madhurima Chattopadhyay, Agnieszka Lester, Lukasz Piatkowski
The Journal of Physical Chemistry B (2023), volume 127, issue 15, pages 3382–3391
2. *Dehydration of lipid membrane drives redistribution of cholesterol between lateral domains*
Hanna Orlikowska-Rzeźnik, Emilia Krok, Maria Domanska, Piotr Setny, Anna Łągowska, Madhurima Chattopadhyay, Lukasz Piatkowski
The Journal of Physical Chemistry Letters (2024), volume 15, issue 16, pages 4515–4522

my contribution was: conceptualization (1-2), methodology (1), investigation (1-2), validation (2), writing–review and editing (1-2).

I agree to submit the above work by **M. Eng. Hanna Orlikowska-Rzeźnik**, as a part of her PhD dissertation titled: *“On discovering new facets of cholesterol in model cell membranes: the molecular interplay with biological water”* in the form of a collection of published and thematically related scientific articles.

Emilia Krok



POLITECHNIKA POZNAŃSKA

FACULTY OF MATERIALS ENGINEERING AND TECHNICAL PHYSICS
Institute of Physics
Piotrowo 3, 61-138 Poznań
www.put.poznan.pl



Poznań, date: 11.09.2024

M. Eng. Anna Lagowska
Poznan University of Technology,
Faculty of Materials Engineering and Technical Physics
Institute of Physics
email: anna.lagowska@doctorate.put.poznan.pl

Declaration of Co-Authorship

I declare that according to the CRediT author statement, in the following publication:

Dehydration of lipid membrane drives redistribution of cholesterol between lateral domains
Hanna Orlikowska-Rzeźnik, Emilia Krok, Maria Domanska, Piotr Setny, Anna Lagowska, Madhurima Chattopadhyay, Lukasz Piatkowski
The Journal of Physical Chemistry Letters (2024), volume 15, issue 16, pages 4515–4522

my contribution was: data curation, formal analysis, investigation, writing–review and editing.

I agree to submit the above work by **M. Eng. Hanna Orlikowska-Rzeźnik**, as a part of her PhD dissertation titled: *“On discovering new facets of cholesterol in model cell membranes: the molecular interplay with biological water”* in the form of a collection of published and thematically related scientific articles.

Anna Lagowska



POLITECHNIKA POZNAŃSKA

FACULTY OF MATERIALS ENGINEERING AND TECHNICAL PHYSICS
Institute of Physics
Piotrowo 3, 61-138 Poznań
www.put.poznan.pl



Poznań, date: 11.09.2024

M. Eng. Agnieszka Lester
Poznan University of Technology,
Faculty of Materials Engineering and Technical Physics
Institute of Physics
email: agnieszka.lester@doctorate.put.poznan.pl

Declaration of Co-Authorship

I declare that according to the CRediT author statement, in the following publication:

Laurdan discerns lipid membrane hydration and cholesterol content

Hanna Orlikowska-Rzeźnik, Emilia Krok, Madhurima Chattopadhyay, Agnieszka Lester, Lukasz Piatkowski
The Journal of Physical Chemistry B (2023), volume 127, issue 15, pages 3382–3391

my contribution was: investigation, writing – review and editing.

I agree to submit the above work by **M. Eng. Hanna Orlikowska-Rzeźnik**, as a part of her PhD dissertation titled:
“*On discovering new facets of cholesterol in model cell membranes: the molecular interplay with biological water*”
in the form of a collection of published and thematically related scientific articles.

Agnieszka Lester

UT Southwestern
Medical Center

Dallas, Texas, USA
September 5, 2024

Madhurima Chattopadhyay, Ph.D.
Post-doctoral researcher
Department of Biophysics
University of Texas Southwestern Medical Center
email: Madhurima.Chattopadhyay@UTSouthwestern.edu

Declaration of Co-Authorship

I declare that according to the CRediT author statement, in the following publication:

1. *Laurdan discerns lipid membrane hydration and cholesterol content*
Hanna Orlikowska-Rzeznik, Emilia Krok, Madhurima Chattopadhyay, Agnieszka Lester, Lukasz Piatkowski
The Journal of Physical Chemistry B (2023), volume 127, issue 15, pages 3382–3391
2. *Dehydration of lipid membrane drives redistribution of cholesterol between lateral domains*
Hanna Orlikowska-Rzeznik, Emilia Krok, Maria Domanska, Piotr Setny, Anna Lagowska, Madhurima Chattopadhyay, Lukasz Piatkowski
The Journal of Physical Chemistry Letters (2024), volume 15, issue 16, pages 4515–4522

my contribution was: conceptualization (2), methodology (1-2), investigation (2), writing – review and editing (1).

I agree to submit the above work by **M. Eng. Hanna Orlikowska-Rzeznik**, as a part of her PhD dissertation titled: *"On discovering new facets of cholesterol in model cell membranes: the molecular interplay with biological water"* in the form of a collection of published and thematically related scientific articles.

Madhurima Chattopadhyay



M. Eng. Hanna Orlikowska-Rzeźnik

Ref: HB/2024-41
Ext.: + 31 20 7547100
Email: h.bakker@amolf.nl

Amsterdam, 11 September 2024

Re: **Declaration of Co-Authorship**

I declare that according to the CRediT author statement, in the following publication:

Cholesterol changes interfacial water alignment in model cell membranes

Hanna Orlikowska-Rzeźnik, Jan Versluis, Huib J. Bakker, Lukasz Piatkowski

Journal of the American Chemical Society (2024), volume 146, issue 19, pages 13151–13162, 2024

my contribution was: funding acquisition, methodology, project administration, resources, supervision, validation, writing – review, and editing.

I agree to submit the above work by **M. Eng. Hanna Orlikowska-Rzeźnik**, as a part of her PhD dissertation titled: *“On discovering new facets of cholesterol in model cell membranes: the molecular interplay with biological water”*, in the form of a collection of published and thematically related scientific articles.

Yours sincerely,

A handwritten signature in blue ink, appearing to read 'H.J. Bakker', is written over a light blue circular stamp or watermark.

Prof. dr. H.J. Bakker
Director AMOLF

Mailing address

P.O. Box 41883
1009 DB Amsterdam
The Netherlands

Visitors

Science Park 104
1098 XG Amsterdam
The Netherlands

Phone +31 (0)20 754 7100

E-mail info@amolf.nl

Web www.amolf.nl

twitter.com/_amolf

IBAN NL78 ABNA 0642 3835 96

BIC ABNANL2A

BTW NL 002882243B01

KvK 41150068

AMOLF is an institute of the Netherlands Foundation of Scientific Research Institutes (NWO-I).



Amsterdam, date: 05.09.2024

Ref: Jan Versluis
Ext.: + 31 20 [Phone number]
Email: versluis@amolf.nl

Declaration of Co-Authorship

I declare that according to the CRediT author statement, in the following publication:

Cholesterol changes interfacial water alignment in model cell membranes
Hanna Orlikowska-Rzeznik, Jan Versluis, Huib J. Bakker, Lukasz Piatkowski
Journal of the American Chemical Society (2024), volume 146, issue 19, pages 13151–13162, 2024

my contribution was: methodology, software, supervision, validation, writing – review and editing.

I agree to submit the above work by **M. Eng. Hanna Orlikowska-Rzeznik**, as a part of her PhD dissertation titled: "*On discovering new facets of cholesterol in model cell membranes: the molecular interplay with biological water*" in the form of a collection of published and thematically related scientific articles.

Jan Versluis

A handwritten signature in blue ink, appearing to read "Jan Versluis", is written over a light blue circular stamp.

Mailing address

P.O. Box 41883
1009 DB Amsterdam
The Netherlands

Visitors

Science Park 104
1098 XG Amsterdam
The Netherlands

Phone +31 (0)20 754 7100

E-mail info@amolf.nl
Web <https://amolf.nl>
Twitter [_amolf](#)

IBAN NL11ABNA0100025501

BIC ABNANL2A
BTW NL 002882243B01
KvK 41150068

AMOLF is part of the Foundation for Dutch Scientific Research Institutes (NWO-I)



UNIVERSITY
OF WARSAW

CeNT CENTRE
OF NEW
TECHNOLOGIES

Warsaw, 05.09.2024

Dr. Piotr Setny,
Centre of New Technologies,
University of Warsaw,
p.setny@cent.uw.edu.pl

Declaration of Co-Authorship

I declare that according to the CRediT author statement, in the following publication:

Dehydration of lipid membrane drives redistribution of cholesterol between lateral domains
Hanna Orlikowska-Rzeźnik, Emilia Krok, Maria Domanska, Piotr Setny, Anna Łagowska, Madhurima Chattopadhyay, Lukasz Piatkowski
The Journal of Physical Chemistry Letters (2024), volume 15, issue 16, pages 4515–4522

my contribution was: data curation, formal analysis, investigation, methodology, software, resources, validation, writing–original draft, writing–review and editing.

I agree to submit the above work by **M. Eng. Hanna Orlikowska-Rzeźnik**, as a part of her PhD dissertation titled: “*On discovering new facets of cholesterol in model cell membranes: the molecular interplay with biological water*” in the form of a collection of published and thematically related scientific articles.

city, date: Warsaw, 5.09.2024

Maria Domańska

Declaration of Co-Authorship

I declare that according to the CRediT author statement, in the following publication:

Dehydration of lipid membrane drives redistribution of cholesterol between lateral domains

Hanna Orlikowska-Rzeźnik, Emilia Krok, Maria Domanska, Piotr Setny, Anna Lagowska, Madhurima Chattopadhyay, Lukasz Piatkowski

The Journal of Physical Chemistry Letters (2024), volume 15, issue 16, pages 4515–4522

my contribution was: data curation, formal analysis, investigation, software, writing-review and editing.

I agree to submit the above work by **M. Eng. Hanna Orlikowska-Rzeźnik**, as a part of her PhD dissertation titled: *“On discovering new facets of cholesterol in model cell membranes: the molecular interplay with biological water”* in the form of a collection of published and thematically related scientific articles.

Maria Domańska

Acknowledgments

The research undertaken over the past five years forms the essence of this doctoral thesis. However, this journey extends far beyond the realm of scientific work and reaches back to earlier years. Along the way, I have been fortunate to encounter many insightful and encouraging companions. Now, I would like to take a moment to step away from the world of membranes and express my heartfelt gratitude to everyone who made this doctoral thesis possible, and to those who made this journey more enjoyable.

Special thanks are owed to my loved ones. I would like to thank Miłosz, my husband, for bringing his humor into my life—something I deeply appreciated while writing this thesis. Thank you for easing me through challenging emotional moments, for your understanding, and for your patience. You always knew how to lift my spirits and help me see things from a different perspective, especially when facing issues that seemed hopeless in my work. Our awesome journey—starting from the Fred Again concert in Amsterdam, through exploring the southern coast of England, and culminating with the Faraday Discussion conference in London, will always remind me of the PhD time.

Mom and Dad, I am endlessly grateful for your constant support, and your hard work, which made it possible for me to move to Wrocław and pursue my studies. You have created a home filled with love and understanding, which has been a safe haven for our whole family. Mom, you are the most selfless person I know, with infinite reserves of goodness. Dad, you are a man of action and initiative; without you, everything would go so slowly. I think I have become a decent person thanks to you.

My dear sisters, Agata and Marta, my clever, beautiful souls, I cannot imagine this journey without you. Your unwavering support, laughter, and wonderfully quirky craziness have kept me grounded throughout this process. Whether it was sharing a silly moment or offering words of encouragement, you both brought joy and lightness when I needed it most. To my brothers-in-law, I couldn't be luckier to have you alongside me during family time. Thank you for always being ready to lend a hand, for our thoughtful discussions, and, of course, for adding your own unique traits to our family—Norbert, for a lot of blonde, and Filip, for finally bringing some much-needed height! And to Laura, Liwia, Oliwier, and Kazik, my little, brilliant pixies—you bring so much light, laughter, and joy into my life. It's truly fascinating to watch you grow, each of you with your boundless curiosity, creativity, and unique spark.

I wish to extend my gratitude to my mother-in-law, Beata; my sister-in-law, Michalina; my honorary grandmothers, Halina, Czesia, and Krystyna; my uncles and aunts, particularly Edziu and Irena; my cousins, especially Sylwia and Marcin; as well as Ania, Mirek, Marcel, and Dorota, for always cheering me on.

ACKNOWLEDGMENTS

I couldn't forget about my friends outside of work—especially Karolina, Kaja, Tamara, Chudy, Marysia, Jagoda, Kasia, Piotrek G., Marta, Ola, Kosa, Aleks, Jakub, Michał C., and Robert. Thank you for all the adventures, trips, outings, and parties, and for reminding me that there's so much more to life than work.

Moving to my work family, I would like to extend my deepest thanks to my supervisor, Łukasz, whose life path crossed with mine at the Institute at just the right time. I'm incredibly grateful that you accepted me into the team and gave me the opportunity to be one of your first three formal PhD students. It has been an honor to start everything from scratch alongside you. I have learned so much from your scientific mind, and growing as a scientist side by side with you has greatly boosted my creativity and curiosity. Thank you for your supportive and motivating leadership, which gave me the confidence to spread my wings and aim higher. Your guidance has been invaluable, from working in the lab to writing projects, and especially in handling those tricky reviewer comments. I am particularly grateful for your support during my internship at AMOLF—the few days you accompanied me were truly appreciated. I admire how you manage so many things at once and yet always made time for me. Whether it was reviewing an article, a grant proposal, a report, or checking over this thesis, you dedicated your time—even outside of office hours—to help me. Thank you for every discussion (scientific or otherwise) over a cup of coffee, and for helping to break down what felt like huge problems into manageable tasks. I also want to thank you for making the work environment enjoyable with your humor, especially when combined with Emilka's—sometimes to the point of being overwhelming! Lastly, I apologize for my teasing about your food choices—I only do it out of sympathy and concern. But, I am sure you're eagerly awaiting the reopening of the cafeteria on the ground floor to buy drożdżówka :)

Emilia and Madhurima, my smart and awesome doctors, it's finally my turn to complete the thesis. It has been an absolute pleasure to share an office with you for four years (and yes, Emi, even longer for us—there truly seems to be no end in sight!). I cannot imagine better companions for this PhD journey. Without you, it wouldn't have been nearly as enjoyable. Madhu, thank you for being there from the beginning. We shared our first days in the lab with the challenge of creating our first good-looking supported lipid bilayer with domains. It was an exciting yet demanding time, but it was easier with you by my side. I'm grateful for all our desk-to-desk scientific discussions, as well as the quirky conversations that I'm sure I wouldn't have had with anyone else. Our time spent in Lisbon and Stockholm for conferences was super nice, especially our dance in the Golden Hall, where we got a small taste of the Nobel Laureates' banquet experience. Your kindness, enthusiasm, and dedication to research are truly inspiring. I hope you will achieve all your dreams, both in science and in your personal life.

Emi, oh Emi! My loyal, never-abandoning companion. I am beyond grateful to the universe for placing you on my PhD path. You are the funniest, smartest, and most helpful colleague I could have wished for. You were always ready to lend a hand or simply be there, and I cannot thank you enough for all the support. I'll never forget the countless hours we spent on the Laurdan project, working in the darkness but always cheered up by candy bars. You also made the cholesterol migration project so much more enjoyable—because data collection with you was always a blast. Just recently, as I was preparing a sample, I looked around the lab and noticed that everything on the benchtop was organized by you. You've made our lab a better place. And I will never forget how we shared frustration in Lisbon when the hotel staff kept tucking the duvet between the mattress and bed frame, just to irritate us! Besides, we definitely deserve an award for our incredible past PowerPoint illustrations, and I'm still waiting for that recognition!

Additionally, thank you for helping me build resilience to uncomfortable situations—first with Campari, and then with this crazy dummy Denver. Thank you also for all those funny moments in the office, when our brains were refusing to cooperate. Since I know you're a fan of cheesy poems, let me sum up our moments of mental fatigue with a meme-inspired verse: *'Roses are red, the sun is shining, my mental health is rapidly declining.'*

Agnieszka, thank you for keeping my blood sugar level high with your delicious baked goods! You're a wonderful listener, and I always felt truly understood when talking to you. I particularly cherish the time we spent in Portugal at the conference. We were so determined to swim in the ocean, even though no one else wanted to join us. Do you remember how difficult it was to get there—no trains due to protests, a long walk, a ferry ride—but in the end, it was worth it! Now, I wish you a fantastic and fruitful time in Germany.

Aniunia, my lovely, funny sunshine—I am so happy you joined our team! You truly share my vibe and bring such a refreshing energy, along with an artistic spirit. You're a wonderful, creative, and honest person, and I am so grateful for the beautiful bead necklaces you gift me with (they are my favorite jewelry now). Thanks to you, we finally have some music in the lab and pastel keyboards that together brings more joy during experimental struggles. Thank you for all the time we spent side by side next to the optical table, and for respecting my precious beam paths. I know your PhD journey hasn't had the smoothest start, with everything seeming to fall apart lately, but I promise it won't last long. Soon, things will start coming together, and we'll achieve great things that will make you proud.

Ania Piechowiak, I couldn't have been luckier to have you managing the finances of my projects. Thank you for handling countless tasks, many of which I'm sure I never even knew about. Your support and creativity were invaluable in solving every problem that came our way. More importantly, you've become a true friend. Your wild sense of humor lifted my spirits, even on the toughest days. And, of course, we'll always treasure our *kaszanka* experience in Lublin—forever in our hearts and minds. I also want to extend my thanks to others from the administrative staff. Joanna Buszkiewicz, thank you for all your support with the Diamond Grant—I could always count on you. Madzia, thank you for our brief but always pleasant chats, and for sharing those little moments during busy days in the office. Mrs. Lidka, thank you for inspiring me with your femininity and for all our conversations about makeup foundations and cheek blushes.

I'd also like to thank Michał, whom I first met six years ago at a conference in Łódź. Your fantastic energy brought me immediately to PUT, and you eventually became my daily supervisor during my Master studies. Thank you for organizing the measurements at different facilities of various universities in Poznań. Thank you for all the time you spent to accompany me—I guess now, with Olga is this world, it wouldn't be that easy. Your belief in me and your well-wishes meant a lot. Thanks for all the help at work, especially at so important things, such as hanging journal covers in the office. Thank you for being the only one to celebrate Woman's Day with us.

Andrzej, thank you for always being there to lend a hand. Thank you for all our discussions about bikes, sports, trips, flat renovations, just to mention a few. So many times, my coffee never made it to my desk because we couldn't stop chatting in the corridor. You're a unique person, and my daily life at PUT wouldn't have been the same without you.

Marta, thank you for your kindness and positivity, and for your birthday barbecue. It was a much-needed break during a challenging time, and I truly enjoyed the chance to relax and

ACKNOWLEDGMENTS

chat with everyone. Semir, I appreciate our conversations and the humor you always bring, even though I'm still a bit hurt over you eating my piece of delicious cake. You promised me a sweet surprise, and I'm still waiting! Iza, your constant willingness to share gummy candies has been greatly appreciated. Paulina, thank you for your help in the lab at fifth floor when I first joined PUT during my Master's. Ania Martin, your random sweet treats in room 524 were always a delightful surprise and are greatly appreciated.

I'd also like to thank Alicja, Kamil, and Karol, my fifth-floor mates, for the many enjoyable conversations and for tolerating the aromas of my lunches, especially the fish. Karol, your dry humor has been a refreshing (hehs) part of my workday. Kamil, I appreciate our small but always funny chats and your help with technical and equipment issues. Alicja, I'm especially grateful for our conversations by the Warta River during Marta's birthday barbecue.

I also wish to extend my thanks to the team from Lublin, especially Rafał, Wojtek, Monika, and Prof. Gruszecki, for welcoming us into the Polish biophysical family. Your vibrant and positive nature radiates marvelous energy and warmth. I deeply appreciate all the laughter and the stories you shared, whether around the fireplace or elsewhere.

Next, I would like to thank Piotr and Marysia for their significant contributions to the content of Chapter 7. Working with you has been pleasant and seamless experience, and I am glad that our collaboration continues.

Here, I wish to return to my scientific roots and express my deepest gratitude to those who have been instrumental in my journey. First and foremost, I want to thank Prof. Stanisław Bartkiewicz, without whom the idea of me doing PhD would probably never arise. You are incredibly inspiring person, with never-ending stories to share. You provided me with the opportunity to develop my scientific skills, transforming the time spent in study into meaningful success. The many conversations with you have significantly contributed to my growth as a mature individual. I am also profoundly grateful to Prof. Andrzej Miniewicz and Prof. Anna Sobolewska for all our scientific discussions over coffee (and green tea, in Prof. Sobolewska's case). Your kindness and support have been invaluable.

My sincere thanks extend to the exceptional Dean, Prof. Mirosław Szybowicz, who greatly facilitated my transfer from studies in Wrocław to Poznań mid-semester. Your help have been invaluable. I also appreciate your generous doses of humor whenever I needed to handle something on the second floor. My further thanks go to Prof. Alina Dudkowiak, who welcomed me into the Molecular Physics department and whose intuition guided me to Łukasz. Additionally, I want to thank Prof. Ryszard Czajka for his kind and supportive words and Arek for supporting all my expensive ideas.

Last but not least, I wish to extend my heartfelt thanks to everyone I had the pleasure of interacting with at AMOLF. Though my time there was brief—just three months—it became a deeply significant and cherished part of my PhD journey. The experience was so intense and eventful that it felt like it could have easily spanned three years. Reflecting on my time in Amsterdam always brings me immense joy. Jan, you were the first person I met at AMOLF. Thank you for taking me under your wings, sharing your office, and offering your expert technical assistance. Your unwavering support was crucial to the successful completion of my SFG project. Huib, thank you for hosting me at AMOLF and for the experience of hearing your delightful Christmas story. Your help with restructuring and enhancing the article included in the last chapter of this thesis was invaluable. Balazs, you are truly one of a kind. Thank you for enriching

my days with your countless thoughts and fast talking, I often struggled to follow. Sanghamitra, I've never met anyone quite like you (and I mean that in the most fantastic way, of course). Your positive energy filled every corner of the room. Thank you for all the parties, drinks, and the unforgettable moments, like our collective, high-spirited singing and dancing at your party or your vibrant, joyful dance with Dhawal. Your open-hearted and caring nature, along with your support in the lab during late hours when things seemed to fall apart, were immensely comforting. Kris, thank you for all the coffee breaks, pleasant chats, and for sharing your charming and creative personality. Hincó, thank you for your help with the rotating table for the SFG experiments, for sharing your extraordinary array of nautical sayings, and, of course, for our Titanic-like photo. I'll never forget the experience of sleeping in your beautiful boat home. Finally, Ash, Alex, Jan, and Hincó—thank you for being part of the best 'Hannah Montana' team during the AMOLF outing. We may have been terrible at farmers' golf, but anyway we were awesome and somehow we still won. Dhawal, your bike loan was greatly appreciated.

Aswathi and Alex, you are my *'hey, you know what happened today?'* people. The text Ash sent me (with slight adjustment) when I left AMOLF perfectly captures what I felt during our early days together. You both made my time in Amsterdam exceptionally joyful. Thank you for all the hugs, and the small and big talks. The perfect blend of light and darkness in your souls was something that particularly drew me in. We shared some truly magical moments, especially when I returned to Amsterdam for the conference in the summer. Alex, my Slavic soulmate, I first met you several times as you kept changing your appearance, but it was always a pleasure. Thank you for always being there for me, for our conversations, walks, and dances in the lab. Я находил радость в наших беседах и утешение в тихих моментах, Саша. Aswathi, my girl, you were the person with whom I explored the oceans and forests of everyday life at AMOLF. With you, everything felt easier and more joyful (even the never-ending process of cleaning the troughs). We navigated through every emotional shade together. It brings me great joy to watch your endeavors with Athul on YouTube; it's a comforting pleasure, even though I don't understand a word in Malayalam. The words of a poet I found on Instagram elegantly mirror what I wish to express: *'I'm proud of you. Proud of every step you're taking forward, especially the ones that are too small for the world to notice. I'm proud of them all.'* You are my best friend, Ash, and I miss you so much.